ACS SYMPOSIUM SERIES 1091

Petite and Sweet: Glyco-Nanotechnology as a Bridge to New Medicines

EDITED BY

Xuefei Huang and
Joseph J. Barchi, Jr.

Petite and Sweet: Glyco-Nanotechnology as a Bridge to New Medicines

Downloaded by 89.163.35.42 on June 2, 2012 | http://pubs.acs.org
Publication Date (Web): December 13, 2011 | doi: 10.1021/bk-2011-1091.fw001

Downloaded by 89.163.35.42 on June 2, 2012 | http://pubs.acs.org
Publication Date (Web): December 13, 2011 | doi: 10.1021/bk-2011-1091.fw001

ACS SYMPOSIUM SERIES **1091**

Petite and Sweet: Glyco-Nanotechnology as a Bridge to New Medicines

Xuefei Huang, Editor
Michigan State University
East Lansing, Michigan

Joseph J. Barchi, Jr., Editor
National Cancer Institute at Frederick
Frederick, Maryland

Downloaded by 89.163.35.42 on June 2, 2012 | http://pubs.acs.org
Publication Date (Web): December 13, 2011 | doi: 10.1021/bk-2011-1091.fw001

Sponsored by the
ACS Division of Carbohydrate Chemistry

American Chemical Society, Washington, DC

Distributed in print by Oxford University Press, Inc.

Downloaded by 89.163.35.42 on June 2, 2012 | http://pubs.acs.org
Publication Date (Web): December 13, 2011 | doi: 10.1021/bk-2011-1091.fw001

Library of Congress Cataloging-in-Publication Data

Petite and sweet : glyco-nanotechnology as a bridge to new medicines / Xuefei Huang, Joseph J. Barchi, Jr., editor[s] ; sponsored by the ACS Division of Carbohydrate Chemistry.
p. cm. -- (ACS symposium series ; 1091)
Includes bibliographical references and index.
ISBN 978-0-8412-2688-3 (alk. paper)
1. Nanotechnology. 2. Biotechnology. 3. Glycoconjugates. 4. Drug development. I. Huang, Xuefei. II. Barchi, Joseph J. III. American Chemical Society. Division of Carbohydrate Chemistry.
TP248.25.N35P48 2011
615.1′901--dc23
2011046249

The paper used in this publication meets the minimum requirements of American National Standard for Information Sciences—Permanence of Paper for Printed Library Materials, ANSI Z39.48n1984.

Copyright © 2011 American Chemical Society

Distributed in print by Oxford University Press, Inc.

All Rights Reserved. Reprographic copying beyond that permitted by Sections 107 or 108 of the U.S. Copyright Act is allowed for internal use only, provided that a per-chapter fee of $40.25 plus $0.75 per page is paid to the Copyright Clearance Center, Inc., 222 Rosewood Drive, Danvers, MA 01923, USA. Republication or reproduction for sale of pages in this book is permitted only under license from ACS. Direct these and other permission requests to ACS Copyright Office, Publications Division, 1155 16th Street, N.W., Washington, DC 20036.

The citation of trade names and/or names of manufacturers in this publication is not to be construed as an endorsement or as approval by ACS of the commercial products or services referenced herein; nor should the mere reference herein to any drawing, specification, chemical process, or other data be regarded as a license or as a conveyance of any right or permission to the holder, reader, or any other person or corporation, to manufacture, reproduce, use, or sell any patented invention or copyrighted work that may in any way be related thereto. Registered names, trademarks, etc., used in this publication, even without specific indication thereof, are not to be considered unprotected by law.

PRINTED IN THE UNITED STATES OF AMERICA

Downloaded by 89.163.35.42 on June 2, 2012 | http://pubs.acs.org
Publication Date (Web): December 13, 2011 | doi: 10.1021/bk-2011-1091.fw001

Foreword

The ACS Symposium Series was first published in 1974 to provide a mechanism for publishing symposia quickly in book form. The purpose of the series is to publish timely, comprehensive books developed from the ACS sponsored symposia based on current scientific research. Occasionally, books are developed from symposia sponsored by other organizations when the topic is of keen interest to the chemistry audience.

Before agreeing to publish a book, the proposed table of contents is reviewed for appropriate and comprehensive coverage and for interest to the audience. Some papers may be excluded to better focus the book; others may be added to provide comprehensiveness. When appropriate, overview or introductory chapters are added. Drafts of chapters are peer-reviewed prior to final acceptance or rejection, and manuscripts are prepared in camera-ready format.

As a rule, only original research papers and original review papers are included in the volumes. Verbatim reproductions of previous published papers are not accepted.

ACS Books Department

Preface

Over the past decade, diagnostics and therapeutics research has evolved towards the use of more specific and targeted approaches. A most profound impact has been observed in the nanotechnology sectors, where an explosion in directing molecules to specific biomarkers has illustrated great potential not only in detection but also in targeted therapy. As some of the most common cell-surface ligands, carbohydrates and glyco-conjugates are known to play crucial roles in many medicinally important physiological processes, including inflammatory and immunological responses, tumor metastasis, cell-cell signaling, apoptosis, cell adhesion, bacterial and viral recognition, and anticoagulation. Glyco-nanotechnology, the interfacing of glycoscience and nanotechnology, is an exciting new field to translate basic discoveries into important clinical applications.

In order to highlight the potential of glyco-nanotechnology and to stimulate discussion and collaboration, a symposium titled "**Petite and Sweet: Glyco-Nanotechnology as a Bridge to New Medicines**" was organized at the 240th American Chemical Society (ACS) National Meeting in Boston, Massachusetts, where we brought together experts from around the world to present the latest results in recruiting sugar-functionalized nanocomposites for biological and biomedical applications. A great deal of excitement was generated from this symposium. To share the information with a broader audience and to attract more researchers to this rapidly advancing field, we assembled this ACS Symposium Series book.

This book describes the current progress in the glyco-nanotechnology field. Chapters 1 and 2 give a general overview of glyco-nanomaterial applications. In Chapter 1, Davis and coworkers provide a summary of recent developments of glyco-nanomaterials according to the core composition. Chapter 2 by Lin and colleagues introduces applications of glyconanoparticles toward protein recognition and detection, cell targeting and imaging, and the immobilization of carbohydrate modifying enzymes on nanoparticles.

Following the overview on applications, Thygesen and Jensen discuss methods to fabricate glyconanoparticles in Chapter 3, with a particular focus on the development of highly chemoselective reactions. Chapter 4 by Yan, Ramström, and coworkers introduces a novel strategy utilizing light initiated nitrene formation to conjugate carbohydrates onto a wide variety of nanomaterials. With the synthetic methodologies established, Chapter 5 dedicates itself to describe methods to characterize glyco-nanomaterial, which is another important aspect of glyco-nanotechnology research. Thorough characterization of the materials synthesized is critical to ensure the quality of nanoparticles and the reproducibility

Downloaded by 89.163.35.42 on June 2, 2012 | http://pubs.acs.org
Publication Date (Web): December 13, 2011 | doi: 10.1021/bk-2011-1091.pr001

Downloaded by 89.163.35.42 on June 2, 2012 | http://pubs.acs.org
Publication Date (Web): December 13, 2011 | doi: 10.1021/bk-2011-1091.pr001

of their biological functions. In this chapter, Morasso, Prosperi, and colleagues review the most common analytical techniques used to characterize the saccharide portion of glyco-nanomaterials. The pros and cons of these methods are analyzed.

Glyco-nanomaterials can have many types of core structures. In Chapters 6, 7, and 8, discussions on several common cores are provided. In Chapter 6, Pieters summarizes the latest development in the attachment of carbohydrates onto various dendritic scaffolds, and how these glyco-dendrimers could enhance the inhibition of carbohydrate-protein interactions by taking advantage of multivalency effects. This is followed by Chapter 7, where Weingart and Sun report on the functionalization of quantum dots with carbohydrates and the biological applications of these glyco-quantum dots. In Chapter 8, Sun and coworkers discuss the synthesis and characterization of carbohydrate immobilized carbon nanotubes, and provide interesting examples of their applications in cell recognition and adhesion.

The last section of the book deals with more specific applications of glyco-nanomaterials. In Chapter 9, Field et. al. describe how to use glyco-nanoparticles fashioned from synthetic carbohydrates and glycoconjugates to decipher the role carbohydrates play in host infection by the parasite *Trypanosoma cruzi*. In Chapter 10, Barchi focuses on the potential utilities of glyco-nanotechnology for tumor detection and treatment. Features of cancer cells that can be exploited for nano-therapeutic intervention and applications in imaging and radio-sensitization, drug delivery and immunology/vaccine design are highlighted. In Chapter 11, El-Dakdouki and Huang summarize the recent biological applications of hyaluronic acid functionalized nanomaterials, ranging from metallic nanoparticles to glyco-polymers and liposomes. These glyco-materials offer an attractive platform for many interesting applications including molecular imaging, targeted drug delivery, tissue repair and regeneration.

We hope this book can provide the readers with knowledge of the current status of glyco-nanotechnology research and kindle additional interests in this field. There are tremendous opportunities in biomedical applications of glyco-nanomaterials and we have just begun to uncover them. Please join us in this exciting journey!

Acknowledgments

We are grateful for the generous financial support from GP BioSciences, Omicron and the ACS Division of Carbohydrate Chemistry. We would like to thank all the symposium speakers, meeting participants, and especially authors and peer previewers for their time and contributions. The expert help from staff members of ACS Books is gratefully acknowledged. Without their efforts and dedication, this book would not have been possible.

Dr. Xuefei Huang

Department of Chemistry
Michigan State University
East Lansing, Michigan 48824
xuefei@chemistry.msu.edu (e-mail)

Dr. Joseph J. Barchi, Jr.

Chemical Biology Laboratory
National Cancer Institute at Frederick
376 Boyles Street, P.O. Box B
Frederick, Maryland 21702
barchi@helix.nih.gov (e-mail)

Downloaded by 89.163.35.42 on June 2, 2012 | http://pubs.acs.org
Publication Date (Web): December 13, 2011 | doi: 10.1021/bk-2011-1091.pr001

Downloaded by OHIO STATE UNIV LIBRARIES on June 3, 2012 | http://pubs.acs.org
Publication Date (Web): December 13, 2011 | doi: 10.1021/bk-2011-1091.ot001

Editors’ Biographies

Xuefei Huang

Xuefei Huang received his undergraduate education from the University of Science and Technology of China. In 1994, he came to the U.S. and joined the group of Prof. Koji Nakanishi at Columbia University, where he worked on the development of circular dichroism methods for absolute configurational assignments and bio-organic studies of neurotoxins. Upon receiving his Ph.D. degree in 1999, he joined Prof. Chi-Huey Wong’s group at the Scripps Research Institute as a postdoctoral researcher, where he was exposed to the wonderful world of glyco-chemistry and glycobiology. After another postdoc stint back to Columbia University, he started his independent research career at the University of Toledo in 2002. He was promoted to associate professor in 2006 with tenure and in 2008 he moved to Michigan State University. His research interests are in several areas including the development of glyco-nanoparticles for biological applications, total synthesis of complex oligosaccharides and glycoconjugates, and the development of carbohydrates based anti-cancer vaccines.

Joseph J. Barchi, Jr.

Joe Barchi was born in and raised in New Jersey and received an AB in chemistry from Rutgers University. While at Rutgers he performed research in the laboratory of Spencer Knapp and graduated a Henry Rutger’s Scholar. He went on to receive his Ph.D. in Synthetic Organic and Marine Natural Products Chemistry from the University of Hawaii with Professor Richard E. Moore which was followed by a 2 years postdoctoral fellowship at Duke University with Bert Fraser-Reid. He then joined the National Cancer Institute as a staff fellow in the Laboratory of Medicinal Chemistry 1988. He subsequently was promoted to permanent Staff Scientist in 1995. He currently holds the position of Senior Scientist/Investigator and is the NMR Facility Head at the LMC. His main research interests are in synthetic medicinal chemistry as it relates to carbohydrate-based drug design, the development of novel sugar-conjugated nanoparticles and the high-resolution structural analysis of sugars, glycopeptides, nucleosides and small molecule drug candidates by NMR spectroscopy.

In Petite and Sweet: Glyco-Nanotechnology as a Bridge to New Medicines; Huang, X., et al.;
ACS Symposium Series; American Chemical Society: Washington, DC, 2011.

Downloaded by 89.163.35.42 on June 2, 2012 | http://pubs.acs.org
Publication Date (Web): December 13, 2011 | doi: 10.1021/bk-2011-1091.ch001

Chapter 1

Recent Biotechnological Applications of Glyco-Nanomaterials

Sung You Hong,*,1,2 Malcolm L. H. Green,*,3 and Benjamin G. Davis*,1

**[1]Department of Chemistry, Chemistry Research Laboratory,
University of Oxford, Mansfield Road, Oxford, OX1 3TA, U.K.
[2]School of Nano-Bioscience and Chemical Engineering,
Ulsan National Institute of Science and Technology (UNIST),
Ulsan 689-798, South Korea
[3]Department of Chemistry, Inorganic Chemistry Laboratory,
University of Oxford, South-Parks Road, Oxford, Ox1 3QR, U.K.
*E-mails: syhong@unist.ac.kr; malcolm.green@chem.ox.ac.uk;
ben.davis@chem.ox.ac.uk**

Thanks to the chemically tunable sizes and physical (e.g. electronic, photonic and magnetic) properties, nanomaterials are recently being applied as imaging agents or spectroscopic tools to monitor cellular or biological systems. However, unfunctionalized nanomaterials have a perceived, potential risk of cytotoxicity and a typical lack of cell-specific function. Given the distinct roles of glycans in nature, aqueous solubility/dispersability, biocompatibility, and as endogenous ligands, the properties of nanomaterials can be improved and directed by constructing glycosylated hybrids. In this mini-review, recent developments of glyco-nanomaterials including carbon-based nanomaterials, magnetic nanoparticles, and gold nanoparticles will be discussed.

In Petite and Sweet: Glyco-Nanotechnology as a Bridge to New Medicines; Huang, X., et al.;
ACS Symposium Series; American Chemical Society: Washington, DC, 2011.

Downloaded by 89.163.35.42 on June 2, 2012 | http://pubs.acs.org
Publication Date (Web): December 13, 2011 | doi: 10.1021/bk-2011-1091.ch001

1. Importance of Glyco-Conjugates

Biomolecules often display specific complementary interactions such as antigen-antibody, hormone-receptor and protein-protein/nucleic acid-nucleic acid/nucleic acid-protein interactions (*1*). It has become clear that glycoproteins or glycolipids, the natural hybrid forms of carbohydrates and proteins or lipids, take part in cellular communication, inflammation and immune responses using the carbohydrate-protein or carbohydrate-carbohydrate interactions (*2*, *3*). Moreover, certain glycan patterns have been reported to be characteristic chemical markers of disease states such as cancer, asthma and diabetes (*4*, *5*).

Despite their importance in these specific recognition processes, individual protein-carbohydrate interactions often are of low affinity and broad specificity (*6*). Nature overcomes this weak affinity by utilizing multivalent interactions (*6*, *7*). The number of carbohydrate residues and the associated branching mode are major determinants of binding avidity of ligands to cell surface receptors (*7*).

Recently, neoglycoconjugates bearing multiple copies of carbohydrate residues such as glyco-dendrimers or glyco-polymers have been introduced to study carbohydrate-protein interactions (*6*–*9*). Nanomaterials with inherent high surface/volume ratio can allow a greater contact surface area to improve multivalency (or the so-called glycosidic cluster) effects. Integration of nanomaterials with biomolecules, especially carbohydrates, can allow biomedical applications such as drug delivery systems, imaging agents, diagnostic platforms, or precise sensing tools.

2. Recent Development of Glyco-Nanomaterials

2. 1. Carbon-Based Nanomaterials

Elemental carbon has several allotropes including tetravalent diamond and trivalent graphitic structures. While diamond is made of an sp^3 carbon network (cubic crystal structure with face centered lattice), graphite has two-dimensional (2D) layers of hexagonally arrayed sp^2 carbon atoms with the interlayer spacing of 0.34 nm. Due to delocalized pi-electrons, graphite is an efficient conducting material (*10*).

In 1985, a new class of carbon allotropes, so called buckminsterfullerene, having chemical formula C_{60} based on the 2D graphitic structure was reported by Kroto and coworkers (*11*). Once the size of graphene-like sheets becomes nano-scale, the ratio of boundary carbon atom/inner carbon atom increases. To remove ‘dangling’ bonds, the whole structure rolls up to produce hollow closed structures (*12*).

Since the geometrical curved structures should satisfy Euler’s theorem, C_{60} is composed of 20 hexagons and 5 pentagons making a truncated icosahedron structure (*11*, *13*). The theorem can be extended to one-dimensional (1D) elongated fullerenes, named carbon nanotubes (CNTs).

Downloaded by 89.163.35.42 on June 2, 2012 | http://pubs.acs.org
Publication Date (Web): December 13, 2011 | doi: 10.1021/bk-2011-1091.ch001

2.1.1. *[60]Fullerene*

To improve the aqueous solubility and biocompatibility, surface modification of carbon-based nanomaterials including C_{60} and CNTs is essential. Fullerene derivatives have been reported to exhibit a wide range of biochemical roles such as enzyme inhibition (e.g. of cysteine proteinases and serine proteinases), antiviral/ antibacterial activity, DNA cleavage, neuroprotection and antiapoptotic activity (*14*, *15*). Polyhydroxylated fullerenes, so called fullerenols, are highly water-soluble (*16*) and can act as radical scavengers and were also applied as magnetic resonance agents by encapsulating Gd inside hollow core (Gd@fullerenols) (*17*).

In 2001, Kato et al. reported the synthesis of α-D-mannosyl [60]fullerenes and fullerenols through the thermal coupling between 2-azidoethyl α-D-mannoside and aromatic C=C bonds on the surface of [60]fullerene (see Figure 1) (*18*). The blocking activity of such glyco-fullerenols was tested in lectin-induced hemagglutination assay; it was found that the mannosyl linkage reduced erythrocyte aggregation activity. Nierengarten et al. reported the synthesis of fullerene ‘sugar balls’ having hexakis-adducts to provide a spherical platform while avoiding excessive amphiphilic character (*19*). The terminal alkyne groups were introduced via the Bingel reaction, and then azido sugars were coupled through Cu(I)-catalyzed azide-alkyne cycloaddition (CuAAC).

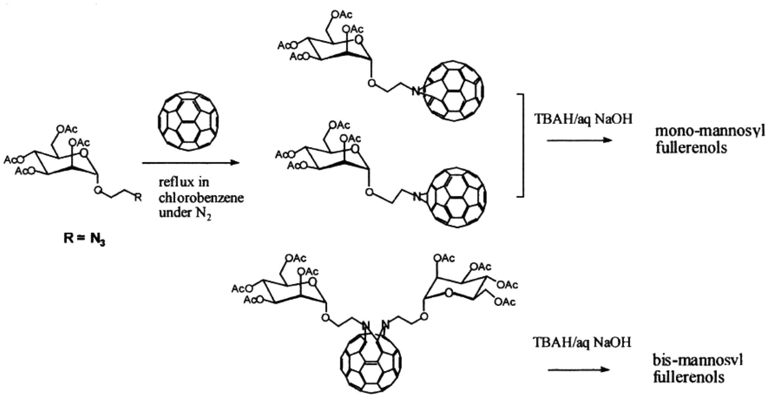

Figure 1. Synthesis of mono- or bis-adducts of α-D-mannosyl [60]fullerenols. Adapted from reference (18). Journal Permission.

2.1.2. *Carbon Nanotubes*

Depending on the number of the sidewalls (or graphene-like sheets), CNTs can be classified into single-walled carbon nanotubes (SWCNTs) or multi-walled carbon nanotubes (MWCNTs) (*12*). The lengths of CNTs are from tens of nanometers to tens of micrometers (or longer) depending on the synthetic methods and the purification conditions. The diameter of SWCNTs is typically 1-2 nm, and that of MWCNTs is 2-25 nm. Since CNTs are basically a closed form of the graphene-like sheet, they contain 1D nanopores. Thanks to their inner hollow space and outer surface, functionalized CNTs (f-CNTs) have become a potential candidate for delivery systems. Moreover, SWCNTs exhibit characteristic Raman peak as well as photoluminescence in NIR range. These intrinsic optical properties are being used for the non-labeled imaging and spectroscopy. However, the major obstacles of CNTs for biomedical applications come from their suggested cytotoxicity and observed insolubility (*20*, *21*). It has been shown that surface functionalization can reduce perceived cytotoxicity and improve the aqueous solubility (or dispersibility) by either covalent (*22*, *23*) or non-covalent (*24*, *25*) methods.

Non-covalent modification of CNTs is conducted by physical mixing (such as sonication) of CNTs with surfactants or polymers (*26*). Since the conjugated pi-scaffolding of graphene-like sheets is preserved, the unique physical properties including Raman peaks and photoluminescence are often also retained. For this reason, such non-covalent modification has proven a popular method for exploiting CNTs' intrinsic optical properties for example in biomedical imaging applications. There are a number of amphiphiles to disperse either SWCNTs or MWCNTs including SDS, Triton X-100, Tween-20, and PEGylated phospholipids. Remarkably, aromatic molecules like pyrene derivatives can disperse CNTs by π-π stacking with graphene-like sidewalls of CNTs. However, non-covalent type modifications have the clear potential risk of losing their coating materials once introduced into a biological milieu and, at present, the ultimate fate of such non-covalent f-CNTs (following e.g. loss of surfactant molecules that might interact with cell membranes) is unclear.

Covalent modification of CNTs uses the surface functionality of CNTs. For such functionalization, it is worth noting that tip sites are more reactive than sidewall sites. Since the tips have similar structure of fullerene hemisphere, the density of π orbitals (as indicated by reactive coefficients) shifts from the concave surface to the convex surface, resulting in an increased chemical reactivity on the convex side (*27*).

Oxidation to introduce carboxylic acid groups on the surface of CNTs is commonly used. These treatments using nitric acid or nitric/sulfuric acid mixture induce tip opening and the formation of defect sites on the sidewalls (*12*, *28*). The acid-cut CNTs can be further functionalized with alcohol or amine to provide esters or amides. In 1998, seminal work was independently reported from two groups led by Prof. Richard E. Smalley (1996 Nobel Prize Winner in Chemistry) and Prof. Robert C. Haddon. Whereas the Smalley group chose to visualize amide bond formation using gold nanoparticle tagging, the Haddon lab demonstrated amide bond formation using FT-IR (*29*, *30*).

In 1993, Italian chemists M. Prato, G. Scorrano, M. Maggini applied 1,3-dipolar cycloaddition strategies, one of the most useful methods to afford heterocyclic structures, on [60]fullerene to produce C_{60}-pyrrolidine derivatives (*31*, *32*). Azomethine ylide was generated *in situ* through iminium salt formation of α-amino acid and aldehyde followed by decarboxylation. The reaction is site-selective with the *syn* addition of azomethine ylide across a [6,6] ring junction of the [60]fullerene as shown in Figure 2. The method, the so-called

Downloaded by 89.163.35.42 on June 2, 2012 | http://pubs.acs.org
Publication Date (Web): December 13, 2011 | doi: 10.1021/bk-2011-1091.ch001

Prato reaction, was later extended to CNTs to introduce pyrrolidine rings along the sidewalls as well as tip sites of CNTs, and has become one of the most useful approaches for surface modification of CNTs without cutting tubes (*33*).

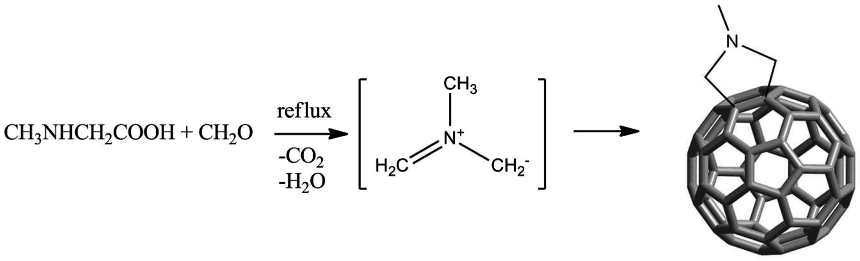

Figure 2. Reaction mechanism of the Prato reaction on [60]fullerene. Adapted from reference (32). Journal Permission.

Downloaded by 89.163.35.42 on June 2, 2012 | http://pubs.acs.org
Publication Date (Web): December 13, 2011 | doi: 10.1021/bk-2011-1091.ch001

2.1.3. Glyco-CNTs

To mimic mucin-like glyco-conjugates, Bertozzi and coworkers (*34*, *35*) reported a non-covalent approach using CNTs coated with glyco-polymers (C_{18}-α-MM): use of a C18-lipid tail allowed wrapping of the CNT surface through hydrophobic interactions and α-*N*-acetylgalactosamine (α-GalNAc) was added as the cell-surface carbohydrate counterpart. While pristine (non-glycosylated) CNTs induced cell death, the C_{18}-α-MM coated CNTs were found to be nontoxic in *in vitro* cell studies. Later, the same group developed glyco-dendrimers that can allow uniform coating of CNTs (*36*). The dendrimers were synthesized using copper(I)-catalyzed chemistry between azide-functionalized pyrenes (used as the CNT-interacting group) and sugar units having alkyne termini; this overcame some of the polydispersity problems (>1.7) associated with use of C_{18}-α-MM. However, surfactant-type coatings in such molecules may eventually dissipate leaving potentially cytotoxic pristine CNTs inside biological systems (*37*). Therefore, covalent type surface glycosylation of CNTs might provide a useful alternative strategy for applications requiring *in vivo* biological probes.

Pempeo and Resasco (*38*) demonstrated a covalent approach of glyco-CNTs by coupling glucosamine on carboxylic acid groups on the oxidized CNTs via a carbodiimide activation route. Using a similar method, Sun and coworkers (*39*) reported the use of galactosylated-SWCNTs for capturing pathogenic *E. coli* O157:H7. SEM image suggested that each cell strongly bound to glycosylated nanotubes (see Figure 3). Thanks to the high aspect ratio & surface area/volume ratio of such CNTs, sugar copies can be efficiently displayed to provide improved multivalency effect.

Downloaded by 89.163.35.42 on June 2, 2012 | http://pubs.acs.org
Publication Date (Web): December 13, 2011 | doi: 10.1021/bk-2011-1091.ch001

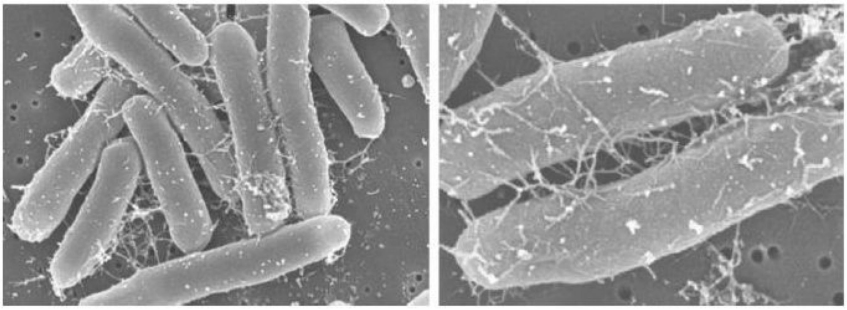

Figure 3. SEM images of Gal-SWNTs capturing E. coli O157:H7. Adapted from reference (39). Journal Permission.

Glycoproteins can largely be divided into two main classes depending on the glycopeptidic linkage: *N*-linked glycans (often large and complex oligosaccharides) contain *N*-acetylglucosamine (GlcNAc) β-linked to asparagine (Asn) via an amide bond (*2*). *O*-linked glycans are usually shorter and less complex and attached to serine or threonine. The Davis lab has previously developed a one-pot glycosylation method based on the Staudinger ligation to afford *N*-linked glycopeptides: the direct coupling of deprotected azido sugar allowed good control of resulting stereochemistry (*40*). This ligation method, first developed for glycopeptide synthesis, was subsequently applied to CNT glycosylation. After pre-activation of the carboxylic acid groups on CNTs, *in situ* generated aza-ylide of GlcNAc motif was conjugated (*41*, *42*). After this first chemical glycosylation step, enzymatic glycosylation using β1,4-galactosyltransferase was then carried out to regio- and stereo-selectively elaborate this monosaccharide attachment to disaccharide *N*-acetyl-lactosamine (LacNAc).

Since sugars bear a number of hydroxyl groups these could, in principle, be used as tagging sites to couple the heavy element containing molecules, which could be visualized via transmission electron microscopy. To test this hypothesis, 2,3,5-triiodobenzoyl (TIBz) groups was selected as suitable tagging agents for a number of reasons. First of all, the localization of three iodides within in a single phenyl ring might allow maximization of scattering signal. Secondly, 2,3,5-triiodobenzoic acid (TIBA) is readily available. Finally, the benzoyl (Bz) group is one of the most commonly used protecting groups in carbohydrate chemistry. STEM following TIBz-tagging revealed clear contrast differences arising from the atomic number differences between iodine (Z=53) and carbon (Z=6), and allowed the imaging of more functionalized regions of CNTs, which showed higher contrast (see Figure 4).

Downloaded by 89.163.35.42 on June 2, 2012 | http://pubs.acs.org
Publication Date (Web): December 13, 2011 | doi: 10.1021/bk-2011-1091.ch001

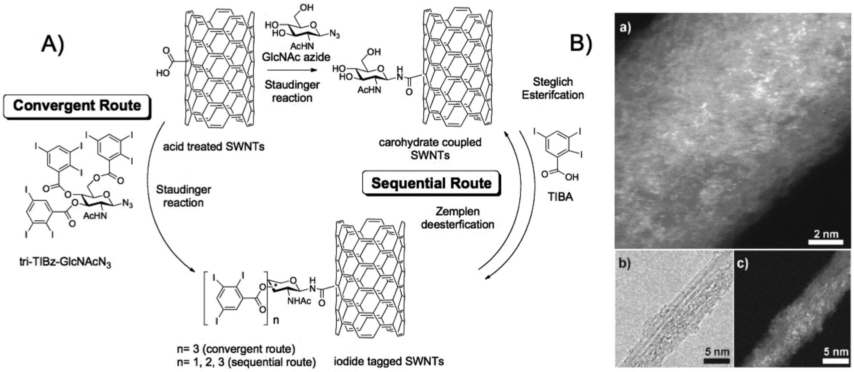
A)
Convergent Route
acid treated SWNTs
GlcNAc azide
Staudinger reaction
carohydrate coupled SWNTs
Sequential Route
Staudinger reaction
tri-TIBz-GlcNAcN3
Zemplen deesterfication
Steglich Esterifcation
TIBA
n= 3 (convergent route)
n= 1, 2, 3 (sequential route)
iodide tagged SWNTs
B)
a)
2 nm
b)
5 nm
c)
5 nm

Figure 4. A) Synthesis of glyco-SWNTs; B) STEM images of iodide tagged SWNTs. Adapted from reference (41). Journal Permission.

The structural uniqueness of nanotubular structures compared with other nanomaterials comes from the 1D hollow pores and their capillarity (*43*). Molten phase salts or solutions can be encapsulated inside CNTs through capillary action once the surface tension is below ~180 mN/m (*44*). Because of the small diameter of SWCNTs (typically 1-2 nm), several encapsulated inorganic salts like KI (*45*), BaI_2 (*46*), and CoI_2 (*47*) have been reported to have different crystal structures compared with their bulk form. In molten phase filling methods, a mixed powder of purified SWCNTs and guest materials (GM) are heated together *in vacuo* above the melting point of the GM. During the annealing step molten phase GM moves into the nanopores of SWCNTs. On cooling, the internal GM becomes solidified and the tip sites of SWCNTs are closed to remove the dangling bonds (*43*).

Despite independent progress in the surface functionalization of CNTs and in filling methods, the covalent surface modification of the filled/closed SWCNTs had not until recently been realized. To introduce carboxylic acid groups onto the surface of CNTs, oxidative methods (standard protocols: nitric acid or nitric/sulfuric acid mixture with reflux or sonication, see above) are required. However, acid-cut CNTs are produced under the reaction conditions in which tip sites are re-opened, and as results any 'filling' materials become released during such treatments. To avoid destructive oxidation methods, mild 1,3-dipolar cycloaddition using azomethine ylides have been combined by us in the creation of filled-closed-funcitionalized CNTs (see Figure 5). In one example, after encapsulation of radioemitter $Na^{125}I$ inside the nanopores, the surface of these radioactive material filled SWCNTs was glycosylated to improve both water solubility and biocompatibility. This allowed the development of an alternative type of radio-tracer system with remarkably high radioisotope-loading capacity and hence high sensitivity and was the first example of *in vivo* application of filled-and-functionalized CNTs (*42*, *48*).

Downloaded by 89.163.35.42 on June 2, 2012 | http://pubs.acs.org
Publication Date (Web): December 13, 2011 | doi: 10.1021/bk-2011-1091.ch001

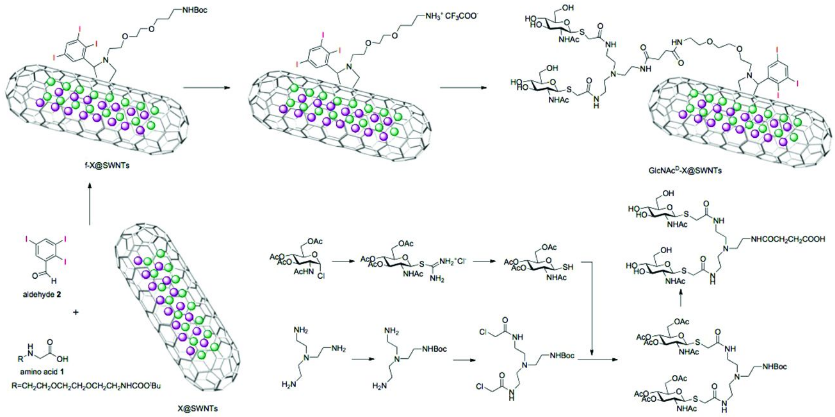

Figure 5. Synthesis of filled and functionalized SWNTs. Adapted from reference (48). Journal Permission.

2.2. Glyco-Magnetic Nanoparticles

Since the late 1980s, magnetic nanoparticles (MNPs) including iron oxide- and manganese oxide-NPs have been of particular interest as contrast agents for magnetic resonance imaging (MRI) (*49*). MRI can be used to generate internal tomographic tissue images by using of the hydrogen nuclei relaxation from water molecules under a radio frequency (RF)-induced electromagnetic field. When the RF pulse is removed, the excited state goes back to the stable state via longitudinal (T1) and transverse (T2) relaxation. In this way, whilst T1 weighted MRI gives ‘whitened’ contrast, T2 weighted MRI affords ‘dark’ contrast. In clinical practice, gadolinium complexes are more commonly used as contrast agents. However, MNP-biomolecule hybrids have strong potential due to their sensitivity, receptor targeting, and multimodal imaging power (*50*).

For their biomedical imaging application, MNPs should satisfy the following requirements: (i) a uniform/stable and high superparamagnetism, (ii) aqueous solubility/dispersibility under the physiological condition, (iii) low cytotoxicity/biocompatibility, (iv) ‘stealthing’ effects from the reticuloendothelial system (RES), (v) surface ligand (targeting molecule) display for receptor binding with high avidity.

To attain condition (i), MNPs need to be monodisperse and the composition should be controlled. The general synthetic approach for the monodisperse nanoparticles is a short burst of nucleation and slow controlled growth (the LaMer model) (*51*). One of the most well-known synthetic methods is “hot injection” method introduced by Bawendi and his colleagues for the synthesis of semi-conducting nanocrystals (or so-called quantum dots) (*52*). The fast homogenous nucleation and the diffusion-controlled crystal growth allow the formation of nanoparticles with narrow size distribution, since heterogeneous nucleation will give broad size distribution via the Ostwald ripening process.

To achieve the conditions (ii-v), surface functionalization with appropriate ligand is the key. While antibodies are frequently used thanks to their specificity, they suffer from high cost, short life time/thermal stability, and potential immunogenicity. Structurally-defined organic molecules as ligands provide a valuable alternative solution.

Designed glyco-MNPs have been shown recently to allow detection by successfully mimicking leukocyte recruitment during inflammation (see Figure 6) (*53*). Because of the high surface/volume ratio, glyco-MNPs can display multiple copies of oligosaccharides maximizing cluster glycoside effects. Tetrasaccharide sialyl-Lewis X (sLe^X)-functionalized MNPs successfully targeted E-/P-selectins. Remarkably, sLe^X-MNPs detected inflammation events, both *in vitro* and *in vivo*. Studies inside the brain of mouse models of stroke allowed detection by specifically binding to the activated endothelium of blood vessels running through diseased tissue. It is worth noting that cross-species effects that are possible with such sugars are harder to achieve with antibody-type ligand systems; in this way such glyco-MNPs may prove more readily translated. Moreover, sLe^X-MNPs did not show any significant signs of cytotoxicity.

Downloaded by 89.163.35.42 on June 2, 2012 | http://pubs.acs.org
Publication Date (Web): December 13, 2011 | doi: 10.1021/bk-2011-1091.ch001

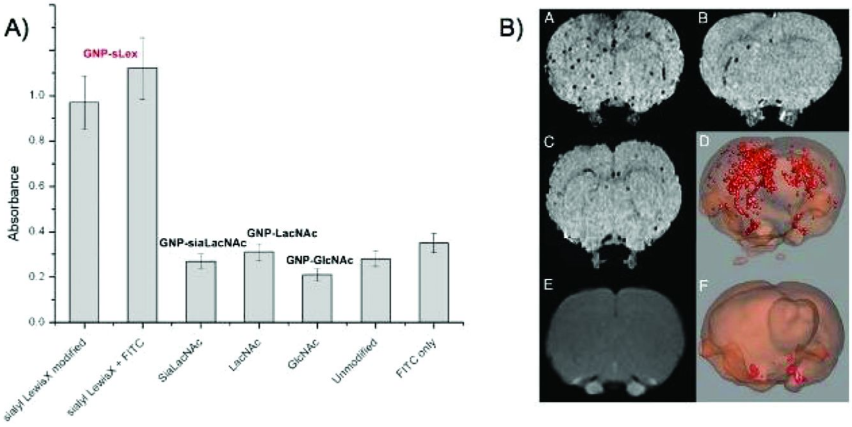

Figure 6. A) in vitro binding studies using sLe^X-MNPs to rat E-selectin; B) MRI imaging and their 3D reconstruction of sLe^X-MNPs. Adapted from reference (53). Journal Permission.

2.3. Gold Nanoparticles

The unique opto-electronic properties, high aqueous solubility, biocompatibility, and facile chemical modification make gold nanoparticles (AuNPs) a useful tool to study or monitor biological binding events (*54–56*). For example, the Mirkin lab at Northwestern University has introduced the notion of colorimetric DNA detection method using oligonucleotide-modified gold nanoparticles (*57*). Color changes of these nanoparticles are strongly correlated with the resonance between a collective oscillation of electrons (plasmons) and the incident electromagnetic radiation, called localized surface plasmon resonance (LSPR). Resonance frequencies or surface plasmon bands of gold lie in the visible region (400-750 nm). The high surface area/volume ratio of AuNPs allows enhanced LSPR sensitivity and colorimetric changes (*56*).

The basic concepts used to synthesize AuNPs focus on the treatment of gold salts with mild reducing agents and the capping agents. By changing reaction conditions, the size, shape and morphology of NPs can be tuned, which can influence LSPR properties. The traditional but still widely used synthesis is the Turkevich method, reduction of gold (III) chloride hydrate ($HAuCl_4$) by citric acid in hot water to afford highly water-soluble gold particles (ca. 16 nm) (*58*). The Xia group at Washington University is a leading group for the synthesis of size and shape controlled AuNPs (*59*); in this way the LSPR of AuNPs could be modified. For example, the typical AuNPs produced from the Turkevich method have an LSPR peak around 520 nm, but those of so-called 'gold nanocages' shift to NIR ranges. Recently AuNPs are being developed as unified platforms in various biomedical areas such as LSPR-based sensing, photo-acoustic imaging, photo-thermal therapy and diagnostics (*60*).

In 1992, a carbohydrate analog-AuNP hybrid system was designed by Bertozzi and Bednarski (*61*). As the attachment of antibodies to bacterial cells is necessary to activate host defense mechanisms such as macrophage opsonization via antibody recognition, a system based on a mannose-analog bound to an avidin/anti-avidin antibody conjugate was developed. These conjugates could recognize and bind to mannose receptors on the type 1 pili of *E. coli*. The carbohydrate-protein interaction was visualized via transmission electron microscopy (TEM) aided by gold colloid tagging: i.e. AuNPs could be easily seen at the pili due to their strong scattering power (gold Z=79). Control samples lacking the mannosyl units did not show binding. In addition to aiding in TEM visualization, AuNPs with mannose immobilized on the surface were used to detect the *E. coli* expressing mannose-specific receptors in type 1 pili. For more details, see the chapter by Chun-Cheng Lin and coworkers in this book.

In 2001, Kataoka and coworkers reported carbohydrate-lectin binding measurements using LSPR of AuNPs and the colorimetric assay (*62*). AuNPs (1-10 nm) were prepared by *in situ* reduction of $HAuCl_4$ with $NaBH_4$ in the presence of a poly(ethylene glycol) and in this way, coated onto the surface of AuNPs through gold-thiolate interaction. Lactose (Lac) was then coupled to PEG terminal aldehyde through reductive amination. Lac-AuNPs exhibited aggregation when the lectin *Ricinus communis* agglutinin (RCA_{120}), which recognizes β-D-galactosyl linkages, was added inducing a reversible color change. Russell, Field and coworkers (*63*) have used similar colorimetric changes for pathogen detection. A subunit of Cholera toxin CTB binds to lactosyl unit and induce color changes of lactose-AuNPs by aggregation, which allowed the AuNP-based sensor to detect Cholera toxin within 10 min.

Downloaded by 89.163.35.42 on June 2, 2012 | http://pubs.acs.org
Publication Date (Web): December 13, 2011 | doi: 10.1021/bk-2011-1091.ch001

3. Conclusions

Recently, various types of glyco-nanomaterials have been introduced with technological applications ranging from pathogen detectors to diagnostic agents. Given the various (often highly specific) roles of endogenous cellular glyco-conjugates, glyco-nanomaterials are useful in providing chemical platforms to help and exploit the understanding of carbohydrate-mediated biological events. This may have particular utility in the area of biomedical imaging, where multimodal imaging techniques such as fluorescence/MRI or PET/MRI probes based on glyco-NPs can be envisaged that might provide improved signal sensitivity and spatial resolution. By taking advantage of the often unique physical properties and inducible sizes, the authors expect that such biomedical glyco-nanotechnology will extend the scope of carbohydrate chemistry and glycobiology and in this way provide an alternative basis for studying systems biology and associated events (both in healthy and diseased organisms) in a way that expands and complements traditional approaches based on, for example, antibody and peptide ligands.

Downloaded by 89.163.35.42 on June 2, 2012 | http://pubs.acs.org
Publication Date (Web): December 13, 2011 | doi: 10.1021/bk-2011-1091.ch001

References

1. Katz, E.; Willner, I. *Angew. Chem., Int. Ed.* **2004**, *43*, 6042–6108.
2. Dwek, R. A. *Chem. Rev.* **1996**, *96*, 683–720.
3. Varki, A. *Glycobiology* **1993**, *3*, 97–130.
4. Dube, D. H.; Bertozzi, C. R. *Nat. Rev. Drug Discovery* **2005**, *4*, 477–488.
5. Ohtsubo, K.; Marth, J. D. *Cell* **2006**, *126*, 855–867.
6. Lundquist, J. J.; Toone, E. J. *Chem. Rev.* **2002**, *102*, 555–578.
7. Kiessling, L. L.; Gestwicki, J. E.; Strong, L. E. *Angew. Chem., Int. Ed.* **2006**, *45*, 2348–2368.
8. Lee, Y. C.; Townsend, R. R.; Hardy, M. R.; Lönngren, J.; Arnarp, J.; Haraldsson, M.; Lönn, H. *J. Biol. Chem.* **1983**, *258*, 199–202.
9. Mammen, M.; Choi, S.-K.; Whitesides, G. M. *Angew. Chem., Int. Ed.* **1998**, *37*, 2754–2794.
10. Smart, L.; Moore, E. *Solid State Chemistry: An Introduction*, 2nd ed.; Chapman & Hall: London, 1995.
11. Kroto, H. W.; Heath, J. R.; O'Brien, S. C.; Curl, R. F.; Smalley, R. E. *Nature* **1985**, *318*, 162–163.
12. Ajayan, P. M. *Chem. Rev.* **1999**, *99*, 1787–1800.
13. Kroto, H. W. *Science* **1988**, *242*, 1139–1145.
14. Jensen, A. W.; Wilson, S. R.; Schuster, D. I. *Bioorg. Med. Chem.* **1996**, *4*, 767–779.
15. Bosi, S.; Da Ros, T.; Spalluto, G.; Prato, M. *Eur. J. Med. Chem.* **2003**, *38*, 913–923.
16. Chiang, L. Y.; Upasani, R. B.; Swirczewski, J. W. *J. Am. Chem. Soc.* **1992**, *114*, 10154–10157.
17. Mikawa, M.; Kato, H.; Okumura, M.; Narazaki, M.; Kanazawa, Y.; Miwa, N.; Shinohara, H. *Bioconjugate Chem.* **2001**, *12*, 510–514.

Downloaded by 89.163.35.42 on June 2, 2012 | http://pubs.acs.org
Publication Date (Web): December 13, 2011 | doi: 10.1021/bk-2011-1091.ch001

18. Kato, H.; Yashiro, A.; Mizuno, A.; Nishida, Y.; Kobayashi, K.; Shinohara, H. *Bioorg. Med. Chem. Lett.* **2001**, *11*, 2935–2939.
19. Nierengarten, J.-F.; Iehl, J.; Oerthel, V.; Holler, M.; Illescas, B. M.; Muñoz, A.; Martín, N.; Rojo, J.; Sánchez-Navarro, M.; Cecioni, S.; Vidal, S.; Buffet, K.; Durka, M.; Vincent, S. P. *Chem. Commun.* **2010**, *46*, 3860–3862.
20. Prato, M.; Kostarelos, K.; Bianco, A. *Acc. Chem. Res.* **2008**, *41*, 60–68.
21. Bianco, A.; Kostarelos, K.; Partidos, C. D.; Prato, M. *Chem. Commun.* **2005**, 571–577.
22. Lacerda, L.; Bianco, A.; Prato, M.; Kostarelos, K. *Adv. Drug Delivery Rev.* **2006**, *58*, 1460–1470.
23. Singh, R.; Pantarotto, D.; Lacerda, L.; Pastorin, G.; Klumpp, C.; Prato, M.; Bianco, A.; Kostarelos, K. *Proc. Natl. Acad. Sci. U.S.A.* **2006**, *103*, 3357–3362.
24. Kam, N. W. S.; Dai, H. *J. Am. Chem. Soc.* **2005**, *127*, 6021–6026.
25. Kam, N. W. S.; O'Connell, M.; Dai, H. *Proc. Natl. Acad. Sci. U.S.A.* **2005**, *102*, 11600–11605.
26. Liu, Z.; Tabakman, S.; Welsher, K.; Wisdom, J. A.; Dai, H. *Nano Res.* **2009**, *2*, 85–120.
27. Haddon, R. C. *Science* **1993**, *261*, 1545–1550.
28. Hirsch, A. *Angew. Chem., Int. Ed.* **2002**, *41*, 1853–1859.
29. Liu, J.; Rinzler, A. G.; Dai, H.; Hafner, J. H.; Bradley, R. K.; Boul, P. J.; Lu, A.; Iverson, T.; Shelimov, K.; Huffman, C. B.; Rodriguez-Macias, F.; Shon, Y. S.; Lee, T. R.; Colbert, D. T.; Smalley, R. E. *Science* **1998**, *280*, 1253–1256.
30. Chen, J.; Hamon, M. A.; Hu, H.; Chen, Y.; Rao, A. M.; Eklund, P. C.; Haddon, R. C. *Science* **1998**, *282*, 95–98.
31. Maggini, M.; Scorrano, G.; Prato, M. *J. Am. Chem. Soc.* **1993**, *115*, 9798–9799.
32. Prato, M.; Maggini, M. *Acc. Chem. Res.* **1998**, *31*, 519–526.
33. Georgakilas, V.; Tagmatarchis, N.; Pantarotto, D.; Bianco, A.; Briand, J. P.; Prato, M. *Chem. Commun.* **2002**, 3050–3051.
34. Chen, X.; Lee, G. S.; Zettle, A.; Bertozzi, C. R. *Angew. Chem., Int. Ed.* **2004**, *43*, 6111–6116.
35. Chen, X.; Tam, U. C.; Czlapinski, J. C.; Lee, G. S.; Rabuka, D.; Zettle, A.; Bertozzi, C. R. *J. Am. Chem. Soc.* **2006**, *128*, 6292–6293.
36. Wu, P.; Chen, X.; Hu, N.; Tam, U. C.; Blixt, O.; Zettle, A.; Bertozzi, C. R. *Angew. Chem., Int. Ed.* **2008**, *47*, 5022–5025.
37. Chen, X.; Wu, P.; Rousseas, M.; Okawa, D.; Gartner, Z.; Zettle, A.; Bertozzi, C. R. *J. Am. Chem. Soc.* **2009**, *131*, 890–891.
38. Pompeo, F.; Resasco, D. E. *Nano Lett.* **2002**, *2*, 369–373.
39. Gu, L.; Elkin, T.; Jiang, X.; Li, H.; Lin, Y.; Qu, L.; Tzeng, T.-R. J.; Joseph, R.; Sun, Y.-P. *Chem. Commun.* **2005**, 874–876.
40. Doores, K. J.; Mimura, Y.; Dwek, R. A.; Rudd, P. M.; Elliott, T.; Davis, B. G. *Chem. Commun.* **2006**, 1401–1403.
41. Hong, S. Y.; Tobias, G.; Ballesteros, B.; El Oualid, F.; Errey, J. C.; Doores, K. J.; Kirkland, A. I.; Nellist, P. D.; Green, M. L. H.; Davis, B. G. *J. Am. Chem. Soc.* **2007**, *129*, 10966–10967.

42. Hong, S. Y. DPhil thesis, University of Oxford: Oxford, 2009.
43. Hong, S. Y.; Kreizman, R.; Rosentsveig, R.; Zak, A.; Sloan, J.; Enyashin, A. N.; Seifert, G.; Green, M. L. H.; Tenne, R. *Eur. J. Inorg. Chem.* **2010**, *2010*, 4233−4243.
44. Dujardin, E.; Ebbesen, T. W.; Hiura, H.; Tanigaki, K. *Science* **1994**, *265*, 1850–1852.
45. Meyer, R. R.; Sloan, J.; Dunin-Borkowski, R. E.; Kirkland, A. I.; Novotny, M. C.; Bailey, S. R.; Hutchison, J. L.; Green, M. L. H. *Science* **2000**, *289*, 1324–1326.
46. Sloan, J.; Grosvernor, S. J.; Friedrichs, S.; Kirkland, A. I.; Hutchison, J. L.; Green, M. L. H. *Angew. Chem., Int. Ed.* **2002**, *41*, 1156–1159.
47. Philp, E.; Sloan, J.; Kirkland, A. I.; Meyer, R. R.; Friedrichs, S.; Hutchison, J. L.; Green, M. L. H. *Nat. Mater.* **2003**, *2*, 788–791.
48. Hong, S. Y.; Tobias, G.; Al-Jamal, K. T.; Ballesteros, B.; Ali-Boucetta, H.; Lozano-Perez, S.; Nellist, P. D.; Sim, R. B.; Finucane, C.; Mather, S. J.; Green, M. L. H.; Kostarelos, K.; Davis, B. G. *Nat. Mater.* **2010**, *9*, 485–490.
49. Jun, Y.-W.; Seo, J.-W.; Cheon, J. *Acc. Chem. Res.* **2008**, *41*, 179–189.
50. Na, H. B.; Song, I. C.; Hyeon, T. *Adv. Mater.* **2009**, *21*, 2133–2148.
51. LaMer, V. K.; Dinegar, R. H. *J. Am. Chem. Soc.* **1950**, *72*, 4847–4854.
52. Murray, C. B.; Norris, D. J.; Bawendi, M. G. *J. Am. Chem. Soc.* **1993**, *115*, 8706–8715.
53. van Kasteren, S. I.; Campbell, S. J.; Serres, S.; Anthony, D. C.; Sibson, N. R.; Davis, B. G. *Proc. Natl. Acad. Sci. U.S.A.* **2009**, *106*, 18–23.
54. Rosi, N. L.; Mirkin, C. A. *Chem. Rev.* **2005**, *105*, 1547–1562.
55. Skrabalak, S. E.; Chen, J. Y.; Sun, Y. G.; Lu, X. M.; Au, L.; Cobley, C. M.; Xia, Y. N. *Acc. Chem. Res.* **2008**, *41*, 1587–1595.
56. Murphy, C. J.; Gole, A. M.; Stone, J. W.; Sisco, P. N.; Alkilany, A. M.; Goldsmith, E. C.; Baxter, S. C. *Acc. Chem. Res.* **2008**, *41*, 1721–1730.
57. Mirkin, C. A.; Letsinger, R. L.; Mucic, R. C.; Storhoff, J. J. *Nature* **1996**, *382*, 607–609.
58. Enüstün, B. V.; Turkevich, J. *J. Am. Chem. Soc.* **1963**, *85*, 3317–3328.
59. Xia, Y.; Xiong, Y.; Lim, B.; Skrabalak, S. E. *Angew. Chem., Int. Ed.* **2009**, *48*, 60–103.
60. Cobley, C. M.; Chen, J.; Cho, E. C.; Wang, L. V.; Xia, Y. *Chem. Soc. Rev.* **2011**, *40*, 44–56.
61. Bertozzi, C. R.; Bednarski, M. D. *J. Am. Chem. Soc.* **1992**, *114*, 2242–2245.
62. Otsuka, H.; Akiyama, Y.; Nagasaki, Y.; Kataoka, K. *J. Am. Chem. Soc.* **2001**, *123*, 8226–8230.
63. Schofield, C. L.; Field, R. A.; Russell, D. A. *Anal. Chem.* **2007**, *79*, 1356–1361.

Downloaded by 89.163.35.42 on June 2, 2012 | http://pubs.acs.org
Publication Date (Web): December 13, 2011 | doi: 10.1021/bk-2011-1091.ch001

Chapter 2

Functionalized Glyconanoparticles for the Study of Glycobiology

**Wei-Ting Chien,[1] Ching-Ching Yu,[1] Chien-Fu Liang,[1]
Chian-Hui Lai,[1] Po-Chiao Lin,[*,2] and Chun-Cheng Lin[*,1]**

**[1]Department of Chemistry, National Tsing Hua University,
101 Sec. 2 Kuang-Fu Rd., Hsinchu 30013, Taiwan
[2]Department of Chemistry, National Sun Yat-sen University,
No. 70, Lienhai Rd., Kaohsiung 80424, Taiwan
[*]E-mails: cclin66@mx.nthu.edu.tw; pclin@mail.nsysu.edu.tw**

Glyconanoparticles (glyco-NPs), defined as nanocarriers that display synthetic carbohydrate molecules, present multiple carbohydrate ligands on their surfaces and enhance the weak interactions of carbohydrate ligands with receptor biomolecules through multivalent effects. Because of the highly specific and structurally modulable nature of synthetic carbohydrate molecules, various glyco-NPs have been developed to accelerate the study of glycobiology. Herein, we briefly introduce recent applications of glyco-NPs toward protein recognition and detection, cell targeting and imaging, and carbohydrate-active enzyme immobilization.

I. Introduction

Glycosylation is an important biological modification that diversifies the functionality of biomolecules such as proteins and lipids, thereby endowing them with biological activity (*1*). Complex carbohydrates that are attached to glycoproteins, proteoglycans, and glycosphingolipids are termed glycans. These molecules are major components of the cellular membrane and are known to mediate cell-cell and cell-extracellular matrix interactions (*2*). Glycan sequences are considered to be information codes that are involved in a wide range of biological processes, such as molecular recognition, cell adhesion, molecular trafficking and clearance, and signal transduction (*3*, *4*). The expression of glycans

In Petite and Sweet: Glyco-Nanotechnology as a Bridge to New Medicines; Huang, X., et al.;
ACS Symposium Series; American Chemical Society: Washington, DC, 2011.

with particular structures regulates the maintenance of living organisms. On the other hand, the aberrant expression of glycans is believed to be the universal hallmark of malignant transformation, cancer metastasis, and tumor progression (*5*). The lack of expression or excessive expression of certain glycans and altered glycan structures have been found to relate closely to abnormal molecular recognition events such as cell migration and metastasis. The study of the relationship between glycan structures and their specific functions may provide more insights into the molecular level mechanisms of many diseases (*6*, *7*). However, a systematic study of the functions of glycans has been limited because of the weak binding affinities (K_a = 10^3-10^4 M^{-1}) of carbohydrate-mediated interactions. In nature, the multivalent presentation of receptors and ligands overcomes the low affinity of monomeric interactions (*8*). The high density of both receptors and ligands leads to multiple interaction sites, resulting in a significant enhancement of binding affinities and specificities.

Various scaffolds have been formulated as a way to present multivalent ligands, including dendrimers (*9*), polymers (*10*), liposomes (*11*), and engineered molecular scaffolds (*12*). Assembling synthetic carbohydrate molecules on a multivalent scaffold has been shown to be effective in presenting multiple ligands. Recently, nanotechnology has provided new materials with high ligand loading capacities for the study of weak biomolecular interactions (*13*). The unique quantum properties of nanoscale materials have great promise in the design of highly sensitive and innovative biosensing devices, machines, and self-assemblies (*14–16*). Metals (*17*) (e.g., Au, Ag, and iron oxides) and semiconductors (*18–22*) (e.g., PbS, Ag_2S, CdS, CdSe, and TiO_2) are attractive carriers for multivalent ligands. Among these types of metal nanoparticles (NPs), gold nanoparticles (AuNPs) are the most studied. The easy formation of Au-S bonds provides a straightforward chemical strategy for surface modification. In addition, the unique surface plasmon resonance of AuNPs has been widely used in diverse applications, especially in studies of biomolecular interactions. Moreover, the tunable fluorescent emission of semiconductor nanoparticles (e.g., quantum dots (QDs)), makes them ideal fluorescent tags in many biomedical applications (*23*). Therefore, various functionalized QDs have been used to track target proteins in complicated biological environments (*24*). Recently, magnetic nanoparticles (MNPs), such as iron oxide (Fe_3O_4) and FePt nanoalloys, have been more frequently used in biomedical applications. Because of their unique superparamagnetic properties and water solubility, MNPs can be used to separate biomolecules by an external magnetic field, preventing contamination and sample degradation from tedious desalting and purification processes.

Because of the high surface-area to volume ratio of NPs, the surface-bound ligand density can be increased to satisfy the requirement of the "multivalent effect (*25*)," resulting in significantly enhanced binding affinity. However, the appropriateness of the conjugation method used in the surface modification plays a crucial role in achieving ligand assembly. In the case of QDs, organic ligands can be assembled onto the surface by hydrophobic interaction, followed by ligand exchange to transfer the NPs into an aqueous solution (*23*). Additionally, covalent chemical bond formation via amide bond coupling reactions, Cu(I)-catalyzed

1,2,3-triazole cycloadditions, and Michael additions have been successfully used for the surface modification of iron oxide MNPs (*26–28*).

By taking advantage of the multivalent effect, the combination of NPs and synthetic carbohydrates can be a powerful platform for the study of interactions involving complex carbohydrates. In 2001, Penadés *et al.* first reported the use of carbohydrate (lactose and Le^X)-modified AuNPs (glycol-AuNPs) in the study of carbohydrate-carbohydrate interactions (*29*). The results demonstrated that glyco-AuNPs can successfully mimic the glycocalyx on the cell surface. In the last decade, hundreds of glyco-NP-related articles have been published to accelerate our understanding of glycobiology. This article provides a brief overview of the applications of glyco-NPs and our own contributions to the field of carbohydrate-based molecular recognition, cell targeting and imaging, and carbohydrate-active enzyme immobilization.

II. Glyconanoparticles for Protein Detection

Glyco-NPs have diverse applications, such as sensing, cellular targeting and imaging, and carbohydrate-based diagnosis and therapy (*30*). In recent decades, a variety of glyco-NPs, such as glyco-AuNPs, glyco-quantum dots (glyco-QDs), and glyco-magnetic nanoparticles (glyco-MNPs), have been designed and used in the study of carbohydrate-mediated biomolecular interactions (*31*, *32*). Thus, the combination of glyco-NPs with various analytical techniques such as transmission electron microscopy (TEM), colorimetric assays, and surface plasmon resonance (SPR), can provide the sensitive detection of target proteins.

In TEM imaging, the scattering of electrons from the sample at the condense system of the TEM is closely related to the thickness and composition of the material, enabling the user to observe molecular interactions. Penadés and co-workers were the first to use TEM to monitor the aggregation of Le^x-AuNPs in the presence of Ca^{2+} ions (*29*). Similarly, Kamerling *et al.* have prepared a series of glucose (Glc)-, maltose (Mal)-, maltohexaose-, mannose (Man)-, mannotriose-, and mannopentaose-containing AuNPs by the reductive amination of the saccharide with trityl-protected cysteamine, followed by detritylation and assembly onto the AuNP. The multivalent interactions between these glyco-AuNPs and concanavalin A (Con A) were validated by TEM (*33*), as shown in Figure 1.

The color changes associated with the aggregation of metal nanoparticles have led to the development of colorimetric-based assays for a variety of target species. Kataoka *et al.* (*34*) have proposed a reversible aggregation-dispersion assay using lactose (Lac)-PEGylated AuNPs via the sequential addition of RCA_{120} lectin, and galactose (Gal) to generate color changes (red→purple→red), as shown in Figure 2. Subsequently, Chen *et al.* (*35*) developed a AuNP-based competitive colorimetric assay by utilizing several proteins to dissociate the aggregation of the Man-AuNP/Con A complex, resulting in a color change from blue to burgundy to indicate that some proteins were able to compete with Man-AuNP to bind with Con A and disrupt the agglomeration of the particles. The color change can be detected by the naked eye within 2 min, and the detection limit can be as low as 5 nM. Furthermore, Russell *et al.* (*36*) have shown that mannose-stabilized silver nanoparticles (Man-AgNP, at 3 nM) can be used to detect Con A at concentrations between 0.08 and 0.26 μM; additionally, these nanoparticles react faster than the Man-AuNPs. However, the detection sensitivity of Man-AuNPs is optimal at a Con A concentration of 0.04 μM, while that for Man-AgNPs is only at 0.1 μM. The specificity of this bioassay was demonstrated by the addition of a lectin (RCA_{120} or Con A) to induce selective aggregation of the mixed glyco-NPs (Lac-AuNP and Man-AgNP). Recently, small Au nanoclusters capped with ligands on the surface were found to possess luminescence at different wavelengths with significant quantum yields (*37*). Alkanethiol (RSH)-capped fluorescent AuNPs (diameter < 2 nm) are called Au nano-dots (AuND). Chang *et al.* assembled mannose-SH on the surface of AuNDs to create Man-AuNDs with a diameter of 1.8 nm and a quantum yield of 8.6%. The limit of detection for Con A was determined to be 75 pM, based on an assay in which Man-AuND/Con A aggregates are formed, followed by the addition of mannose to dissociate the aggregate (*38*).

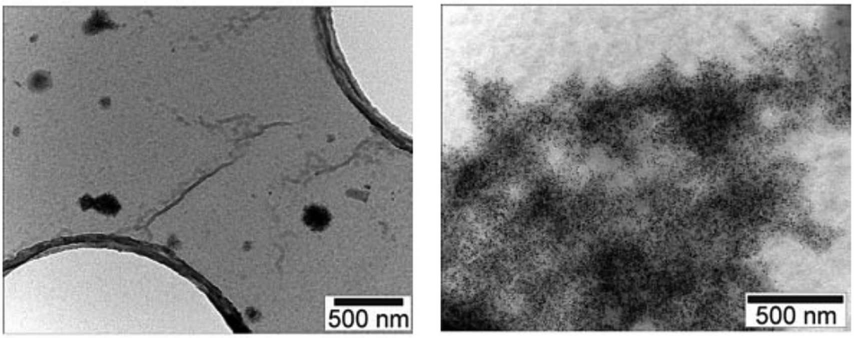

Figure 1. TEM images of the aggregation of Mal-AuNP and Man-AuNP with Con A. Left: Mal-AuNP incubated overnight with Con A in HEPES buffer (pH 7.4), containing 10 mM $CaCl_2$ (500 nm). Right: Man-AuNP incubated overnight with ConA in HEPES buffer (pH 7.4), containing 10 mM $CaCl_2$ (500 nm). Reprinted with permsision from ref (33). Copyright 2005 John Wiley and Sons.

In general, the glyco-NPs are synthesized by first coupling the thiol-containing linkers with saccharides, after which the resulting ligands are assembled onto the NPs. This process involves many manipulation steps and is thus tedious and time-consuming. Methods that enable the assembly of unprotected carbohydrates on AuNPs without laborious glycosylation and protecting-group chemistry are highly desirable. Jensen *et al.* (*39*) used a bifunctional linker, as shown in Figure 3, to couple unprotected glycans via oxime formation. Because of the lipophilic trityl tag, the resulting products were easily purified. After removal of the trityl group, the thio-glycans were assembled onto the AuNP. Although two oxime-tautomers (the open-chain and the N-glycosyl oxy-amine) were formed, the cyclic ring-chain tautomer was the predominant one (60%) and retained its binding activity toward the corresponding lectin (Figure 3). Moreover, Yan *et al.* (*40*) applied photocoupling chemistry to attach saccharides onto perfluorophenyl azide (PFPAs)-functionalized AuNPs. Upon light activation, the azide moieties were converted to highly reactive nitrenes, which then inserted into CH and NH bonds, creating highly robust covalent linkages (Figure 4). Although the insertion of the nitrene into the saccharide was not done in a regio-controlled manner, the resulting glyco-AuNPs showed an enhancement in their affinity to the target lectin.

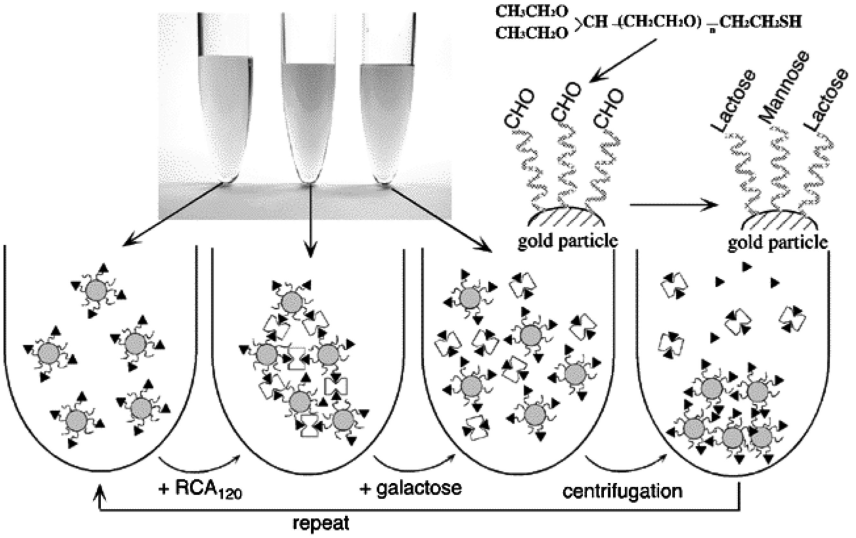

Figure 2. Schematic representation of the reversible aggregation-dispersion behavior of lactose Au-NPs by sequential addition of RCA$_{120}$ lectin, and galactose with concomitant change in color from pinkish-red to purple to pinkish-red. Reprinted with permsision from ref (34). Copyright 2001 American Chemical Society.

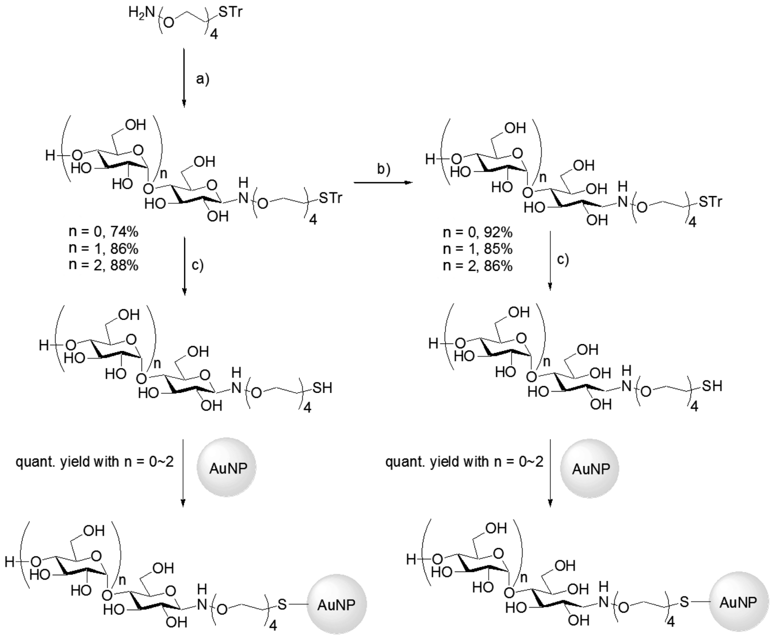

Figure 3. (a) Glucose/maltose/maltotriose (1.1 equiv.), MeCN, H_2O, HOAc, 16 h; (b) $NaBH_3CN$ (2 equiv.), HOAc, 2 h; c) TFA, triethylsilane (TES), CH_2Cl_2, 5 min.

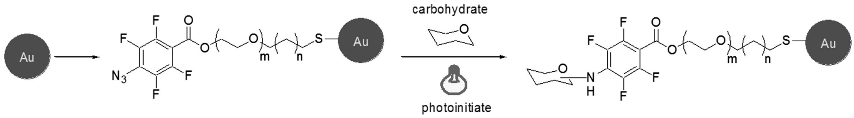

Figure 4. Functionalization of AuNPs with PFPA-Thiol and the subsequent coupling of carbohydrates. Reprinted with permission from ref (40). Copyright 2010 American Chemical Society.

The recent automation of SPR technology, which can be used to quantify the binding affinities and subsequently determine the kinetic data of biomolecular interactions (*41*), facilitates the analysis of the binding affinity of glyco-NPs with their target proteins. The SPR technique has been used to quantitatively analyze the affinities of Man-, Glc-, and Gal-AuNPs with Con A (*42*). Furthermore, we have discussed the effect of NP size and linker length on the affinity enhancement using SPR competition assays and a system composed of globotriose (P^k ligand)-functionalized AuNPs (P^k-AuNPs) and the B_5 subunit of Shiga-like toxin (B-Slt) (*43*). The P^k-AuNP with a size of 20 nm and a longer linker length had the greatest affinity enhancement (up to 10^8-fold compared to the P^k monomer). Field *et al.* (*44*) found that the thioctic acid amide linker, **1b**, formed better ordered monolayers on planar and global gold surfaces than did the 2-thioethyl linker, **1a,** as shown in Figure 5. The well-ordered and self-assembled monolayer on the surface of the AuNPs resulted in the suppression of non-specific protein binding and an increase in the stability of the glyco-AuNPs.

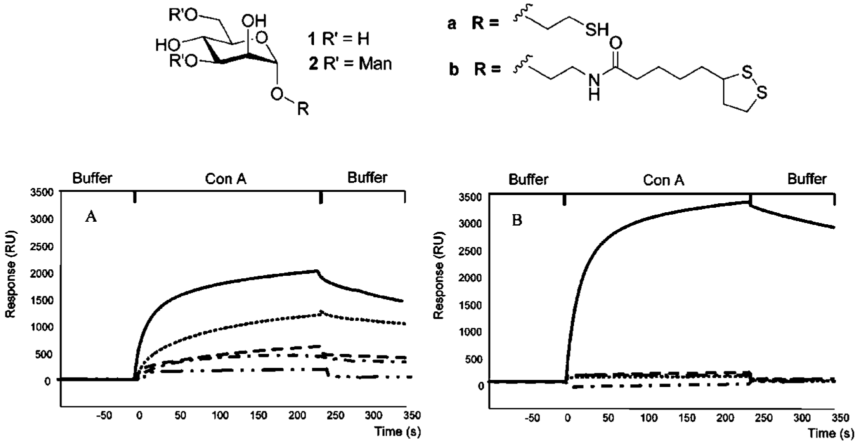

*Figure 5. Comparison of SPR responses after injection of 10 μg Con A (solid), 20 μg RCA_{120} (dash-dot-dot), 20 μg TPL (dash-dot), 20 μg fibrinogen (dot), and 20 μg cytochrome c (dash) over gold surfaces modified with (a) trimannoside **2a** or (b) trimannoside **2b**. Reprinted with permission from ref (44). Copyright 2005 The Royal Society of Chemistry.*

Aside from the common analytical methods of TEM, colorimetric assays, and SPR, there are several other methods that have been used to study glyco-NP-protein interactions. Recently, Joshi *et al.* (*45*) used electrochemical impedance spectroscopy (EIS) as a reliable, label-free method to detect glycan-lectin interactions. Galactose-binding agglutinin (PNA) and sialic acid-binding agglutinin (SNA) were covalently immobilized on layered Cu/Ni/Au printed circuit board (PCB) electrodes. The AuNPs were encapsulated with TF-antigen, asialofetuin (ASF) containing both LacNAc and TF-antigen, or fetuin (FET) containing sialylated glycoform. These glyco-AuNPs were run separately on PNA- and SNA-immobilized PCB electrodes, providing rapid and reliable detection. The detection sensitivity was 1 pg/mL for TF-AuNP and 10 pg/mL for ASF- and FET-AuNPs. Further expansion of this technology into novel, electrochemically driven lectin arrays may find application in the diagnosis of cancer and other diseases with multiple glycobiomarkers or as a rapid, low-cost, bioanalytical tool for glycoproteome analyses. In another study, Narain *et al.* (*46*) applied reversible addition-fragmentation chain transfer (RAFT) polymerization using *N*-(8-((+)-biotinamido)-3,6-dioxaoctyl)-2-((2-phenyl-1-thioxo) thio)-4-cyano-pentanoate (BCBDBA), a new biotinylated RAFT agent, to synthesize biotinylated glyco-polymers containing *N*-acetyl-glycosamine (GlcNAc) or Man residues. Next, functionalized monodisperse gold colloids bearing carbohydrate and biotin moieties on the surface were prepared using photochemical reduction in the presence of the glycopolymer, Irgacure-2959, $HAuCl_4$, and PEG-SH. The resulting biotinylated GlcNAc- or Man-AuNPs were then immobilized on avidin-coated dotLab sensor chips through the strong affinity between biotin and avidin. These avidin-conjugated glyco-AuNPs could serve as probes for the studies of the specific recognitions with Con A or WGA. Barboiu *et al.* (*47*) have also presented an effective system that uses glyco-AuNPs as quartz crystal microbalance (QCM) amplifiers in their studies of carbohydrate interactions. In this system, Con A was immobilized on QCM quartz crystals by a combination of non-specific hydrophobic interactions and the recognition of mannan. Glyco-AuNPs were then used as QCM amplifiers to interact with the immobilized Con A. This system showed highly specific recognition based on sugar structure; the avidity constants with Con A found for Man- and Mal-AuNPs were $1.6 \times 10^7\ M^{-1}$ and $7.2 \times 10^7\ M^{-1}$, respectively.

III. Glyco-NPs for Cell Targeting, Imaging, and Separation

Because of the substantial progress in the development of biocompatible nanomaterials, a variety of biomolecule-functionalized nanomaterials have been prepared. Their superior performance in protein-level interactions has been successfully demonstrated, as discussed in the preceeding section. To expand the detection target from proteins to cells, glyco-NPs can also act as carbohydrate-carriers to mimic the glycocalyx on the cell surface and reduce the complexity in real carbohydrate-cell interactions. A major challenge in the development of glyco-AuNPs for the study of cellular interactions is to span the cellular membrane, which is made up of a negatively charged surface and a hydrophobic lipid bilayer. To address this issue, NPs carrying positive charges are required. Thus, a cationic glycopolymer-coated AuNP was synthesized via the RAFT process (*48*). Because of the cationic character of the nanoparticle surface, it can undergo endocytosis through electrostatic interactions, followed by vesicular escape. Due to the ability of this new type of AuNP to disrupt endocytotic vesicles, it can be further used as a gene transfect carrier.

Additionally, a convenient and label-free scanometric method has been developed for *in situ* cell surface carbohydrate detection (*49*). It was found that the Con A-induced aggregation of Man-AuNPs could be inhibited by the specific binding of Con A to the cell surface mannose, resulting in a decreasing concentration of free Con A in solution and a decrease in the aggregation of Man-AuNPs. The aggregated Man-AuNPs provide fewer seeds for silver precipitation than do the dispersed Man-AuNPs; thus, with an increase in cell number, a strong silver signal can be observed, as shown in Figure 6.

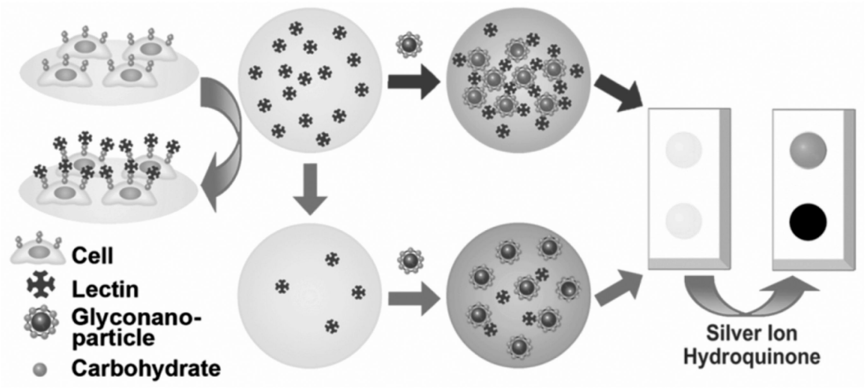

Figure 6. Scheme of the scanometric strategy for the in situ detection of mannose groups on living cells. Reprinted with permsision from ref (49). Copyright 2010 American Chemical Society.

The need for an assay for the rapid detection and separation of bacterial pathogens has emerged to assist in the correct treatment of infections. Because of their crucial role in cell-cell communication, the unique structures of carbohydrates promise a high specificity for the recognition of the corresponding receptor on the cell surface. Thus, carbohydrates may be used as probes to detect specific cells. In 2002, we first used Man-AuNPs to demonstrate the applicability of glyco-NPs in cellular recognition via carbohydrate-receptor interactions. Type 1 pili are widely distributed on enteric bacteria, and their structure and assembly are well characterized. A type 1 pilus is composed of FimA, FimF, FimG, and FimH proteins. FimH is uniquely responsible for the binding of D-mannose. Man-AuNPs bind specifically to the FimH adhesins of bacterial type 1 pili of *Escherichia coli* (*E. Coli*), strain ORN178; the ORN208 strain is deficient of the FimH gene, resulting in the expression of abnormal type 1 pili that fail to mediate D-mannose-specific binding. The capture of Man-AuNPs by a bacterium was illustrated by TEM (*50*), as shown in Figure 7.

Alternatively, MNPs can be used in place of AuNPs in the same concept (*51*). There are two major advantages of using MNPs for this purpose: high surface area/volume ratio and the high magnetization via their superparamagnetic properties. The sizes of MNPs are typically about two orders of magnitude smaller than those of bacteria, which allows for the attachment of multiple NPs onto a bacterial cell, rendering easy and magnet-mediated separation. The multivalent presentation of carbohydrates on glyco-MNPs produces multivalent interactions with receptors on the cell surface, resulting in strong binding. Fluorescence microscopy can then be used for detection and enumeration. Through multivalent interaction followed by magnetic separation, this method can achieve a detection limit of 10^4 bacteria per mL. The rapid magnetic separation considerably reduces the operation time and prevents the contamination that is common with conventional separation processes, such as centrifugation or affinity column chromatography. High capture efficiencies of up to 88% have been achieved with 45 min incubations, as shown in Figure 8.

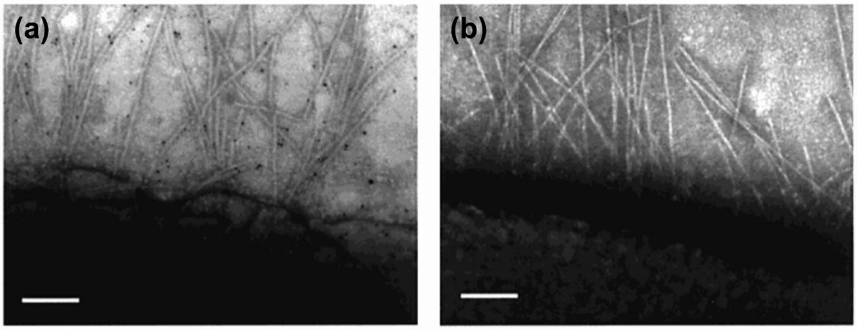

Figure 7. Typical TEM images of sectioned areas of (a) pili of E. coli strain ORN178 bound with Man-AuNPs and (b) the E. coli strain ORN208, deficient in the FimH gene without Man-AuNP binding. The experiments were performed in LB at room temperature. Scale bar = 100 nm. Reprinted with permsision from ref (50). Copyright 2002 American Chemical Society.

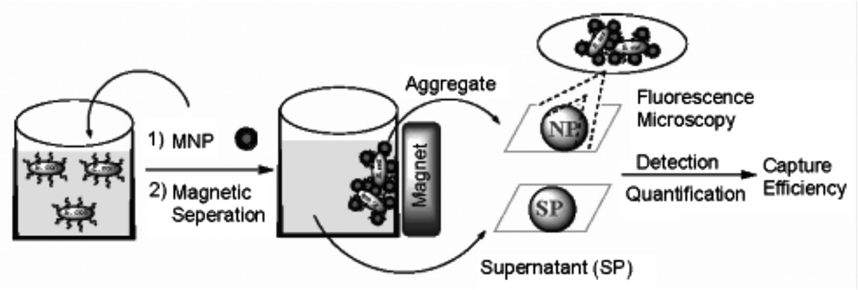

Figure 8. Schematic demonstration of pathogen detection by MNPs. Reprinted with permsision from ref (51). Copyright 2007 American Chemical Society.

MNPs have been also integrated into cell sorter microsystems, in which specific cells can be separated from complicated mixtures (*52*). By taking advantage of the small Reynolds number, the integrated electromagnet microfluidic device can absorb the MNP-bound bacteria with a magnet to cross the stream boundary and traverse into the neighboring sorting stream. Optimization of the flow rate and the ratio of NPs to bacteria can improve the sorting efficiency. The results of this study indicated that the microfluidic system was capable of sorting up to 1000 bacterial cells within 1 min, with a greater than 70% sorting efficiency, as shown in Figure 9.

Phosphate-containing perfluorophenyl azides have been used to modify the surface of MNPs via photochemically induced CH insertion (*53*). This chemical transformation allows for monosaccharides to be immobilized without chemical derivatization while retaining their recognition abilities, as demonstrated by the strong affinity they retain with their corresponding carbohydrate-binding proteins (mannose and Con A) and bacteria (mannose and FimH-containing *E. coli*). Thus, the results of NP-directed cell targeting can potentially provide a rapid and specific platform for clinical diagnosis, decontamination, and biomedical applications.

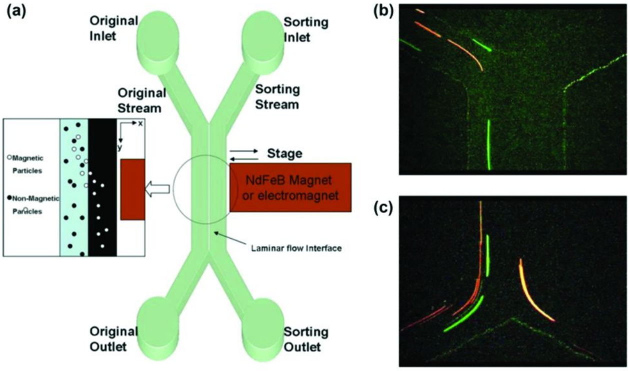

Figure 9. (a) (Color online) Schematic for the integrated microfluidic cell sorting system. (b) (Color online) A mixture of the DsRed-expressing E. coli ORN178 (red), GFP-expressing E. coli ORN208 (green), and mannose-coated magnetic nanoparticles were injected into the left inlet. (c) With an applied magnetic field, the DsRed-expressing E. coli ORN178 (red), which were bound to the mannose-coated magnetic nanoparticles, moved to the right side of the microchannel. Reprinted with permission from ref (52). Copyright 2008, American Institute of Physics. (see color insert)

Monitoring cell trafficking and distinguishing cellular adhesion and recognition *in vivo* are key issues in the development of cellular-based therapy (*54*). Although various types of small molecule bioprobes are available, their weak receptor binding affinities and the ease of photo-bleach limit their applications in biological systems. Because NPs are 100 to 1000 times smaller than human cells and of a similar size as biomolecules, NPs can potentially be used in biosystems to provide a nanoplatform to mimic cellular interactions, overcome biomedicinal barriers (*32*), and probe the mechanisms of biological processes (*32*, *55*). Fluorescence microscopy (*56–66*), magnetic resonance imaging (MRI) (*67–71*), and TEM (*50*, *51*, *53*) have been used with glyco-NPs to image specific cell targeting.

The asialoglycoprotein receptor (ASGP-R), found on liver cell surfaces and especially on liver cancer cell surfaces (*56–59*), recognizes Gal or *N*-acetyl-galactosamine (GalNAc) residues on the nonreducing end of glycoproteins, particularly desialyated tri- or tetra-antennary *N*-link glycans, via multivalent interaction; the resulting interaction then triggers receptor-mediated endocytosis to intake glycoproteins into the cell (*72–75*). As such, this recognition model can be used to study the interaction of Gal-NPs with liver cells *in vivo* and *in vitro* (*56–59*). Because QDs have a wide absorption spectrum and narrow emission spectrum with high luminescence and low photobleaching, they are ideal optical probes (*76*). Figure 10 (a) shows a specifically labeled tri-antennary Gal-QD, synthesized by click chemistry as the key conjugation chemistry, with ASGP-R on an A549 lung cancer cell surface, demonstrating that the nanohybrid can be selectively delivered into ASGP-R-enriched lung cancer cells without causing cell damage (*56*). Furthermore, as shown in Figure

10 (b), PEGylated QDs with capped Man, Gal, and GalNAc were synthesized. These glyco-QDs were exploited to study the specific carbohydrate−protein interactions on hepatocytes *in vitro* and *in vivo* (*58*). In addition to QDs, MNPs with fluorescent and magnetic characteristics are also ideal non-invasive imaging probes because of the ease with which they can be observed by both fluorescence emission and MRI. Incorporation of stable fluorescent dyes onto MNPs could provide a cost-effective and sensitive probe for biological imaging with a reduced concern for cytotoxicity. Because of the presence of the fluorescent dye, fluorescent MNPs can be easily tracked by optical methods, offering a better spatial resolution than those by MRI. As shown in Figure 10.(c), a well-designed, multifunctional MNP with fluorescent, magnetic, and targeting properties was used to specifically target ASGP-R on the surface of HepG2 cells (*57*). The results revealed for the first time that the spatial orientation of the pre-assembled multivalent galactosyl ligand influences MNP uptake by HepG2 cells. Because of the ease of surface functionalization and of the non-cytotoxic nature of the multifunctional MNPs, they can serve as potential probes in both imaging and drug delivery bioapplications. Glyco-QDs have also been applied to probe lectins on mouse sperm (*62*); to study polyvalent interactions with live leukocytes (*63*); and to label macrophages (*64*), bacteria (*65*), and other cell types (*60*, *66*).

In addition to glyco-MNPs, carbohydrate-based MRI nanoprobes have been also developed (*67–69*). In these MNP systems, the unique property of superparamagnetism serves as a good contrast-enhancing probe (*61*). Davis and co-workers reported the use of sialyl Lewis^X-coated MNPs (sLe^X-MNPs) to allow for pre-symptomatic *in vivo* imaging of brain disease by MRI (*67*). By using the S-cyanomethyl (SCM) precursor group at the reducing end of the saccharides, the carbohydrates could be immobilized easily on the amino MNPs. The sLe^X-MNPs allowed for the direct detection of an endothelial marker, E-selectin, in a model of acute inflammation, providing high binding selectivity and selective T_2 contrast in the brain of a rat. As shown in Figure 11 (a), Huang and co-workers used five kinds of glycol-MNPs, Man-, Gal-, Fuc-(fucose), Sia-(sialic acid), and GlcNAc-MNPs, to interact with various lectins and *E. coli* strains, demonstrating that the glyco-MNPs retain their own natural recognition and binding specificities (*68*). Ten cell lines, including normal and cancer cells, were then examined with these five glyco-MNPs and analyzed by MRI. The statistical analysis of the MRI data indicated that the glyco-MNPs could provide a qualitative and quantitative profile of the characteristics of the cancer cells. Thus, glyco-MNP-based MRI detection can allow for the differentiation of related isogenic cancer cell subtypes or cells with different metastatic potencies. The anti-adhesive properties of glyco-MNPs were also used to develop potential anti-adhesive cancer agents. In addition, the use of carbohydrates as recognition elements on NPs has been shown to provide functional information as a glyco-code for lectins active on the cell surface (*68*).

Recently, a new method was developed for the synthesis of glyco-MNPs by pH-driven disassembly/assembly of horse spleen apoferritin on the surface of MNPs, followed by conjugation with vinyl sulfonyl saccharides (*69*). Moreover, paramagnetic glyco-AuNPs were prepared by reducing a gold salt in the presence of a mixture of sugar ligand and a tetraazacyclododecane triacetic acid (DO3A)-Gd complex to form a new type of carbohydrate-based MRI nanoprobe. In Figure 11 (b), the surface carbohydrates are demonstrated to protect the magnetic nanocrystals from aggregation and nonspecific biomolecular interactions in a manner better than other ligands (*70*). The carbohydrates also conferred the glyco-ferrites with high solubility and stability under physiological conditions, low cytotoxicity, and a lack of immunogenicity (*71*).

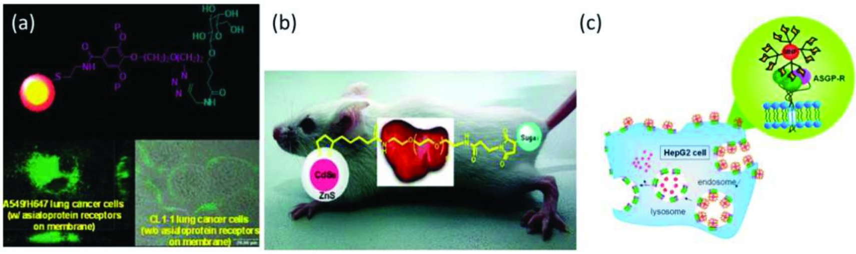
(a)
A549/H647 lung cancer cells (w/ asialoprotein receptors on membrane)
CL1-1 lung cancer cells (w/o asialoprotein receptors on membrane)
(b)
CdSe
ZnS
Sugar
(c)
ASGP-R
HepG2 cell
endosome
lysosome

Figure 10. The glyco-NPs were applied for bio-imaging through the use of fluorescence microscopy. For example, (a) a tri-antennary Gal-QD was selectively delivered into ASGP-R-enriched A549 lung cancer cells. Reprinted with permsision from ref (56). Copyright 2008 John Wiley and Sons. (b) PEGylated Gal-QD was used to study the specific carbohydrate−protein interactions on hepatocytes in vitro and in vivo. Reprinted with permsision from ref (58). Copyright 2009 American Chemical Society. (c) The well-defined multifunctional fluorescent Gal-MNP was used to specifically target HepG2 cells. Reprinted with permsision from ref (57). Copyright 2010 John Wiley and Sons. (see color insert)

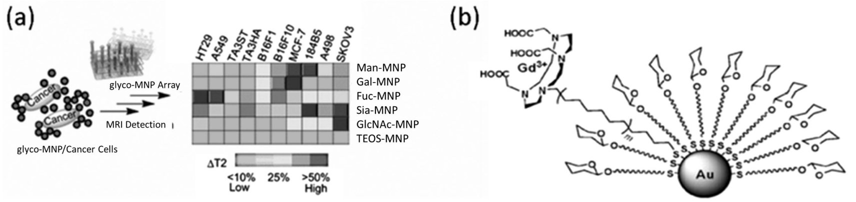

Figure 11. Applications of glyco-NPs in MRI imaging. (a) To profile cancer cell characteristics, different kinds of glyco-MNPs were incubated with cancer cells to provide different T_2 relaxation times. Reprinted with permsision from ref (68). Copyright 2010 American Chemical Society. (b) DO3A-Gd complexes serve as T_1-contrast agents for MRI imaging. Reprinted with permission from ref (70). Copyright 2009 The Royal Society of Chemistry.

IV. Immobilization of Carbohydrate-Active Enzymes

In addition to the use as MRI probes, MNPs are also attractive materials to serve as supports for enzyme immobilization and facilitate separations by applying an external magnetic field; this could facilitate the recycling of enzymes and broaden their applications in organic synthesis. In this section, the strategy for carbohydrate-active enzyme imobilization, especially on MNP, will be discussed.

The application of carbohydrates in modern medicine has been limited by the high cost of the synthesis of biologically important glycoconjugates. It is generally recognized that the enzymatic synthesis of oligosaccharides using glycosyltransferases is a promising practical alternative to chemical synthesis because enzyme-based synthesis has produced highly stereo- and regio-selective glycosylation without tedious multi-step protection and deprotection steps. With the increasing availability of recombinant glycosyltransferases in recent years, it can be expected that more researchers will use these enzymes to construct various glycoconjugates. However, these recombinant enzymes are either expensive or unstable as versatile reagents in chemoenzymatic synthesis and cannot be recovered from the reaction mixture by common work-up processes.

To reduce the cost of using enzymes in the synthesis of complex carbohydrates, immobilization of the enzymes provides for facile separation and reuse of costly biocatalysts as well as the potential for improved operational stability. Generally, enzymes are immobilized on micro-scale solid supports by random covalent linkages. For example, Nishimura *et al.* covalently immobilized recombinant β-1,4-galactosyltransferase and α-2,6-sialyltransferase on Sepharose beads by random amide bond formation and employed this system in the synthesis of a trisaccharide derivative (*77*). However, random immobilization of an enzyme may result in a significant loss of enzyme activity.

To allow for the immobilized enzyme to retain the higher enzyme activity of the free enzyme, oriented/site-specific immobilization techniques have been developed. Augé and co-workers first reported the oriented and non-covalent immobilization of recombinant α-1,3/4-galactosyltransferase (FucT-III) and α-2,3-sialyltransferase (ST3Gal-III) on agarose beads by an interaction between Ni^{2+}-NTA and a His-tag at the C-terminus or N-terminus; these immobilized enzymes were highly stable (*78*, *79*). Furthermore, using a similar approach, Wang and co-workers developed a system involving many immobilized enzymes in the synthesis of sugar nucleotides (*80*, *81*), as shown in Figure 12. In this study, UDP-Gal was generated by an amalgamation of the immobilized recombinant enzymes that are involved in the biosynthetic pathway of UDP-Gal. In conjunction with galactosyltransferase either on a bead or in solution, this system can be used as a common reagent for the synthesis of various oligosaccharides.

Most glycosyltransferases are membrane-bound enzymes containing a hydrophobic tail, which often causes protein insolubility and subsequent precipitation. To solve this problem, Nishimura and co-workers immobilized the full-length α1,3-fucosyltransferase of *Helicobacter pylori* (*H. pylori*) onto a magnetic microbead coated with 11-mercaptoundecylphosphocholine. They discovered that the formation of an α-helical structure of the C-terminus amphipathic peptide of *H. pylori* α-1,3/α-1,4-FucTs was induced by interaction

In Petite and Sweet: Glyco-Nanotechnology as a Bridge to New Medicines; Huang, X., et al.;
ACS Symposium Series; American Chemical Society: Washington, DC, 2011.

with the surface zwitterionic phosphorylcholine motif, resulting in reduced precipitation (*82*). In general, site-specific (oriented) enzyme immobilization should retain higher enzyme activity than random immobilization.

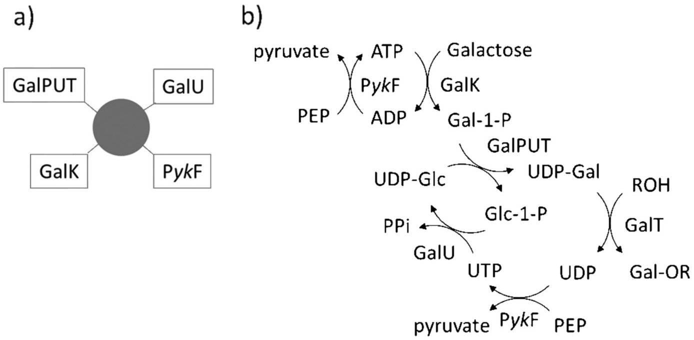

Figure 12. Immobilized enzymes in sugar nucleotide synthesis. (a) UDP-Gal regeneration beads. Reprinted with permsision from ref (80). Copyright 2001 American Chemical Society. (b) Biosynthetic pathway for galactosides with regeneration of UDP-Gal.

Although site-specific (oriented) enzyme immobilization can be achieved by non-covalent interactions via the C or N termini, the non-covalently immobilized enzyme may potentially dissociate from the solid surface during long-term storage or recycling. Thus, many recent efforts have focused on the site-specific, covalent immobilization of proteins onto solid supports. One of the most popular approaches used to achieve this goal is the fusion of a protein of interest with a tagged peptide that reacts with a substrate immobilized on a solid support to form a covalent adduct, catalyzed by enzymes such as PPTase (*83*), FTase (*84*, *85*), SrtA (*86*), and TGase (*87*), as shown in Figure 13. For example, Nishimura and co-workers immobilized recombinant glycosyltransferases onto commercially available solid supports through a transpeptidase reaction catalyzed by sortase A of *Staphylococcus aureus* (*86*), as shown in Figure 14 (c). This method allowed for the highly specific conjugation of recombinant human β-1,4-galactosyltranseferase and recombinant *H. pylori* α-1,3-fucosyltransferase with simple aliphatic amino groups displayed on the surface of solid materials via the designated C-terminus signal peptide moiety of the target enzyme. This approach provides a highly efficient and covalent immobilization of the typically unstable, membrane-bound enzymes, and causes minimal impact on the protein conformation. While this approach works well, the efficiency of the enzyme-catalyzed transformation could be jeopardized by the location of the tag and the substrate on the solid support, due to steric effects. To circumvent this problem, an array of bioorthogonal ligation chemistries has been developed, including click chemistry, the Staudinger ligation (*88*, *89*), the Diels-Alder reaction (*90*), and native chemical ligation (NCL) (*91*, *92*). We have focused on the site-specific and covalent immobilization of proteins on glass slides and magnetic nanoparticles (MNPs) by combining intein protein over-expression technology and NCL. We showed that the orientation of the immobilized protein on a solid support is crucial for its activity (*27*, *93*, *94*). Via incubation of a cysteine-modified MNP with CMP-sialic acid synthetase (CSS) expressed as intein fusion protein in the presence of sodium mercaptoethane sulfonate, CSS was covalently immobilized on MNPs by NCL without tedious protein purification procedures (*95*). Because of their nano-scale size, these MNPs provide the maximal surface area per unit volume for enzyme immobilization and were shown to retain 75% of the activity of the free enzyme, while the same enzyme immobilized on microbeads or randomly immobilized on MNPs only provides 35% of the activity of the free enzyme, as shown in Figure 14. The immobilized CSS can be easily recovered from the aqueous suspension by applying a magnetic field. In addition, the immobilized enzyme retains almost 100% of its original immobilized activity after storage at 4 °C for 7 months or reuse in at least ten consecutive enzyme assays. Furthermore, the immobilized CSS was used to synthesize 500 mg CMP-sialic acids, with satisfactory yield and purity.

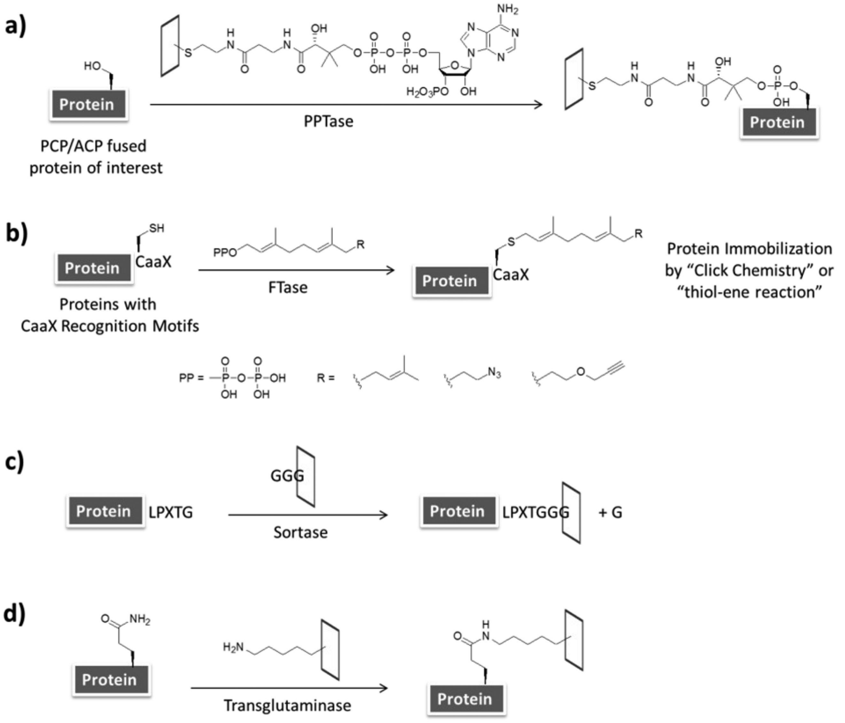
a)
HO
Protein
PCP/ACP fused
protein of interest
PPTase
Protein
b)
SH
Protein
CaaX
Proteins with
CaaX Recognition Motifs
PPO
R
FTase
Protein
CaaX
Protein Immobilization
by "Click Chemistry" or
"thiol-ene reaction"
PP =
R =
c)
Protein
LPXTG
GGG
Sortase
Protein
LPXTGGG
+ G
d)
Protein
Transglutaminase
Protein

Figure 13. Site-specific protein immobilization by enzymatic reactions. (a) PPTase, (b) FTase, (c) Sortase (SrtA), and (d) TGase.

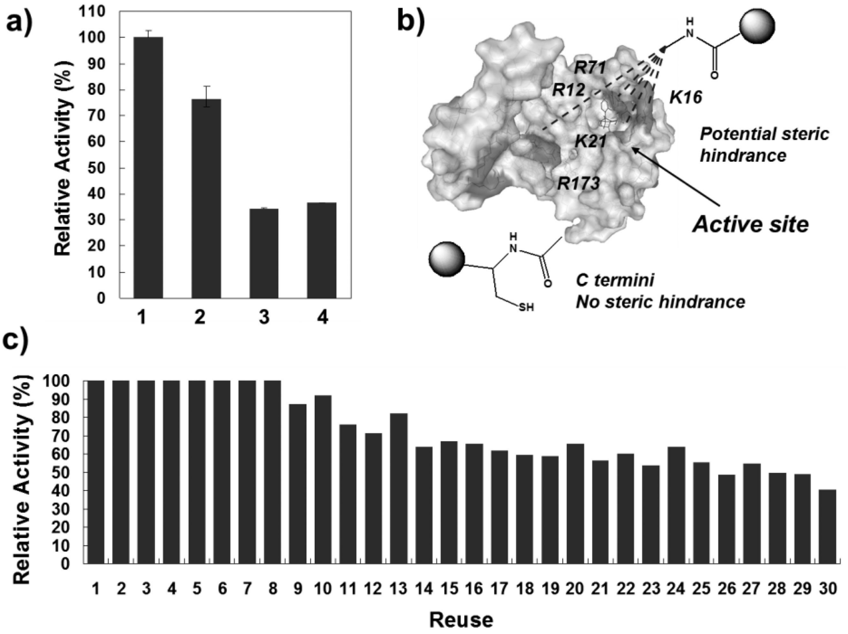

Figure 14. CSS-MNP activity affected by the immobilization method. (a) Relative activity of CSS. Column 1: native CSS, column 2: site-specific immobilized CSS, column 3: random immobilized CSS, column 4: site-specific immobilized CSS on microbeads. (b) Elucidation of steric effects by CSS X-ray structure. (c) Enzymatic activity of CSS-MNP upon repetitive use in the enzyme assay. Reprinted with permission from ref (95). Copyright 2008 The Royal Society of Chemistry.

To broaden the applications of immobilized enzymes in the synthesis of carbohydrates, we immobilized glucose-1-phosphate thymidylyltransferase (RmlA, from *Aneurinibacillus thermoaerophilus* DSM 10155) (*96*) on a MNP by NCL and used it to synthesize UDP-galactose, a galactose donor for galactosyltransferase. The broad substrate tolerance of RmlA made it possible to prepare UDP-galactose on a 100 mg scale in one attempt. By combination with β-1,4-galactosyltransferase, *N*-acetyllactosamine could also be obtained easily on a 100 mg scale in a one-pot, two enzyme synthesis. To investigate the details of enzyme immobilization on MNPs, we developed methods for the immobilization of water-soluble and membrane-bound enzymes by NCL and streptavidin-biotin interaction. Sialyltransferase PmST1 (from *Pasteurella multocida*) and CSS were chosen as water-soluble enzymes while sialyltransferase NgST (from *Neisseria gonorrhoeae*) was chosen as the membrane-bound enzyme. Using a streptavidin-biotin interaction, we were able to immobilize NgST on a solid support under mild ligation conditions, which prevented the enzyme from decomposing at high temperatures and provided an approximately two-fold increase in activity compared to other immobilization methods. Finally, the ganglioside GM3-derivative (sialyl-lactose derivative) was synthesized in a one-pot system by combining immobilized PmST1 and CSS. The enzymes retained 50% activity after being reused ten times. Furthermore, the results obtained using the one-pot, two-immobilized-enzyme system demonstrated that immobilized enzymes can be applied on large-scale synthesis with moderate yields and purities. The works mentioned above will be published soon.

V. Conclusion

Because of their powerful affinity enrichment properties, glyco-NPs offer a promising platform for the study of carbohydrate-mediated interactions. The combination of glyco-NPs with various analytical instruments can be successfully applied to the qualitative or quantitative analysis of carbohydrate-carbohydrate and carbohydrate-protein interactions. The tailored structures of synthetic carbohydrate ligands on the surface of NPs can mimic the glycocalyx on cell surfaces and thus can be used to study significant cell-cell and cell-extracellular matrix interactions. In this way, cell recognition, targeting, and imaging can be achieved. Moreover, carbohydrate-active enzymes such as glycosynthase, glycosyltransferases, and glycosidases hold key positions in the study of glycobiology. Modern chemical strategies for the site-specific immobilization of proteins have been demonstrated to be an important technique in carbohydrate-active enzyme immobilization on NPs. The resulting enzyme-NP complexes were successfully applied to the preparation of glycans, especially those with complicated sequences. However, considerable improvement in NP function remains to be realized, particularly in the domains of recognition specificity and sensitivity. Efforts are therefore ongoing to develop new strategies, particularly for the synthesis of NPs with high ligand loading capacity, and ligand diversity and the application of glyco-NPs in the contexts of proteomic and biomarker discovery.

References

1. Dwek, R. A. *Chem. Rev.* **1996**, *96*, 683–720.
2. Li, M.; Song, L.; Qin, X. *J. Biosci.* **2010**, *35*, 665–673.
3. Ohtsubo, K.; Marth, J. D. *Cell* **2006**, *126*, 855–667.
4. Reis, C. A.; Osorio, H.; Silva, L.; Gomes, C.; David, L. *J. Clin. Pathol.* **2010**, *63*, 322–329.
5. Varki, A.; Chrispeels, M. J. *Essentials of Glycobiology*; Cold Spring Harbor Laboratory Press: Cold Spring Harbor, NY, 1999; pxvii.
6. Freeze, H. H.; Aebi, M. *Curr. Opin. Struct. Biol.* **2005**, *15*, 490–498.
7. Peracaula, R.; Barrabes, S.; Sarrats, A.; Rudd, P. M.; de Llorens, R. *Dis Markers* **2008**, *25*, 207–218.
8. Mammen, M.; Choi, S. K.; Whitesides, G. M. *Angew. Chem., Int. Ed.* **1998**, *37*, 2755–2794.
9. Roy, R.; Kim, J. M. *Angew. Chem., Int. Ed.* **1999**, *38*, 369–372.
10. Disney, M. D.; Zheng, J.; Swager, T. M.; Seeberger, P. H. *J. Am. Chem. Soc.* **2004**, *126*, 13343–13346.

11. Kingerywood, J. E.; Williams, K. W.; Sigal, G. B.; Whitesides, G. M. *J. Am. Chem. Soc.* **1992**, *114*, 7303–7305.
12. Clemons, P. A. *Curr. Opin. Chem. Biol.* **1999**, *3*, 112–115.
13. Katz, E.; Willner, I. *Angew. Chem., Int. Ed.* **2004**, *43*, 6042–108.
14. Niemeyer, C. M. *Angew. Chem., Int. Ed.* **2001**, *40*, 4128–4158.
15. Alivisatos, P. *Nat. Biotechnol.* **2004**, *22*, 47–52.
16. Rosi, N. L.; Mirkin, C. A. *Chem. Rev.* **2005**, *105*, 1547–1562.
17. Murali, K. R. *Metal Nano Particles: Synthesis, Characterization and Applications*; Feldman, D. I., Foss, C. A., Eds; Marcel Dekker: New York, 2002; Vol. 18, pp 565−566.
18. Meldrum, F. C.; Flath, J.; Knoll, W. *Langmuir* **1997**, *13*, 2033–2049.
19. Stathatos, E.; Lianos, P.; DelMonte, F.; Levy, D.; Tsiourvas, D. *Langmuir* **1997**, *13*, 4295–4300.
20. Rizza, R.; Fitzmaurice, D.; Hearne, S.; Hughes, G.; Spoto, G.; Ciliberto, E.; Kerp, H.; Schropp, R. *Chem. Mater.* **1997**, *9*, 2969–2982.
21. Klein, D. L.; Roth, R.; Lim, A. K. L.; Alivisatos, A. P.; McEuen, P. L. *Nature* **1997**, *389*, 699–701.
22. Spanhel, L.; Weller, H.; Fojtik, A.; Henglein, A. *Ber. Bunsenges. Phys. Chem.* **1987**, *91*, 88–94.
23. Hammer, N. I.; Emrick, T.; Barnes, M. D. *Nanoscale Res. Lett.* **2007**, *2*, 282–290.
24. Kim, B. Y. S.; Jiang, W.; Oreopoulos, J.; Yip, C. M.; Rutka, J. T.; Chan, W. C. W. *Nano Lett.* **2008**, *8*, 3887–3892.
25. Gestwicki, J. E.; Cairo, C. W.; Strong, L. E.; Oetjen, K. A.; Kiessling, L. L. *J. Am. Chem. Soc.* **2002**, *124*, 14922–14933.
26. Gupta, A. K.; Gupta, M. *Biomaterials* **2005**, *26*, 3995–4021.
27. Lin, P.-C.; Ueng, S.-H.; Yu, S.-C.; Jan, M.-D.; Adak, A. K.; Yu, C.-C.; Lin, C.-C. *Org. Lett.* **2007**, *9*, 2131–2134.
28. Lin, P.-C.; Chou, P.-H.; Chen, S.-H.; Liao, H.-K.; Wang, K.-Y.; Chen, Y.-J.; Lin, C.-C. *Small* **2006**, *2*, 485–489.
29. de la Fuente, J. M.; Barrientos, A. G.; Rojas, T. C.; Rojo, J.; Canada, J.; Fernandez, A.; Penades, S. *Angew. Chem., Int. Ed.* **2001**, *40*, 2258–2261.
30. de la Fuente, J. M.; Penades, S. *Glycoconjugate J.* **2004**, *21*, 149–163.
31. Wang, X.; Liu, L. H.; Ramstrom, O.; Yan, M. *Exp. Biol. Med.* **2009**, *234*, 1128–1139.
32. de la Fuente, J. M.; Penades, S. *Biochim. Biophys. Acta* **2006**, *1760*, 636–651.
33. Halkes, K. M.; de Souza, A. C.; Maljaars, C. E. P.; Gerwig, G. J.; Kamerling, J. P. *Eur. J. Org. Chem.* **2005**, *2005*, 3650–3659.
34. Otsuka, H.; Akiyama, Y.; Nagasaki, Y.; Kataoka, K. *J. Am. Chem. Soc.* **2001**, *123*, 8226–8230.
35. Tsai, C. S.; Yu, T. B.; Chen, C. T. *Chem. Commun.* **2005**, 4273–4275.
36. Schofield, C. L.; Haines, A. H.; Field, R. A.; Russell, D. A. *Langmuir* **2006**, *22*, 6707–6711.
37. Zheng, J.; Nicovich, P. R.; Dickson, R. M. *Annu. Rev. Phys. Chem.* **2007**, *58*, 409–431.

38. Huang, C.-C.; Chen, C.-T.; Shiang, Y.-C.; Lin, Z.-H.; Chang, H.-T. *Anal. Chem.* **2009**, *81*, 875–882.

39. Thygesen, M. B.; Sauer, J.; Jensen, K. J. *Chem. Eur. J.* **2009**, *15*, 1649–1660.

40. Wang, X.; Ramstrom, O.; Yan, M. *Anal. Chem.* **2010**, *82*, 9082–9089.

41. Mann, D. A.; Kanai, M.; Maly, D. J.; Kiessling, L. L. *J. Am. Chem. Soc.* **1998**, *120*, 10575–10582.

42. Lin, C. C.; Yeh, Y. C.; Yang, C. Y.; Chen, G. F.; Chen, Y. C.; Wu, Y. C.; Chen, C. C. *Chem. Commun.* **2003**, *39*, 2920–2921.

43. Chien, Y.-Y.; Jan, M.-D.; Adak, A. K.; Tzeng, H.-C.; Lin, Y.-P.; Chen, Y.-J.; Wang, K.-T.; Chen, C.-T.; Chen, C.-C.; Lin, C.-C. *ChemBioChem* **2008**, *9*, 1100–1109.

44. Karamanska, R.; Mukhopadhyay, B.; Russell, D. A.; Field, R. A. *Chem. Commun.* **2005**, *41*, 3334–3336.

45. La Belle, J. T.; Gerlach, J. Q.; Svarovsky, S.; Joshi, L. *Anal. Chem.* **2007**, *79*, 6959–6964.

46. Jiang, X.; Housni, A.; Gody, G.; Boullanger, P.; Charreyre, M. T.; Delair, T.; Narain, R. *Bioconjugate Chem.* **2010**, *21*, 521–530.

47. Mahon, E.; Aastrup, T.; Barboiu, M. *Chem. Commun.* **2010**, *46*, 5491–5493.

48. Ahmed, M.; Deng, Z.; Liu, S.; Lafrenie, R.; Kumar, A.; Narain, R. *Bioconjugate Chem.* **2009**, *20*, 2169–2176.

49. Ding, L.; Qian, R.; Xue, Y.; Cheng, W.; Ju, H. *Anal. Chem.* **2010**, *82*, 5804–5809.

50. Lin, C.-C.; Yeh, Y.-C.; Yang, C.-Y.; Chen, C.-L.; Chen, G.-F.; Chen, C.-C.; Wu, Y.-C. *J. Am. Chem. Soc.* **2002**, *124*, 3508–3509.

51. El-Boubbou, K.; Gruden, C.; Huang, X. *J. Am. Chem. Soc.* **2007**, *129*, 13392–13393.

52. Shih, P.-H.; Shiu, J.-Y.; Lin, P.-C.; Lin, C.-C.; Veres, T.; Chen, P. *J. Appl. Phys.* **2008**, *103*, 07A316/1–07A316/3.

53. Liu, L. H.; Dietsch, H.; Schurtenberger, P.; Yan, M. *Bioconjugate Chem.* **2009**, *20*, 1349–1355.

54. Weissleder, R.; Mahmood, U. *Radiology* **2001**, *219*, 316–333.

55. Won, J.; Kim, M.; Yi, Y. W.; Kim, Y. H.; Jung, N.; Kim, T. K. *Science* **2005**, *309*, 121–125.

56. Chen, C.-T.; Munot, Y. S.; Salunke, S. B.; Wang, Y.-C.; Lin, R.-K.; Lin, C.-C.; Chen, C.-C.; Liu, Y.-H. *Adv. Funct. Mater.* **2008**, *18*, 527–540.

57. Lai, C.-H.; Lin, C.-Y.; Wu, H.-T.; Chan, H.-S.; Chuang, Y.-J.; Chen, C.-T.; Lin, C.-C. *Adv. Funct. Mater.* **2010**, *20*, 3948–3958.

58. Kikkeri, R.; Lepenies, B.; Adibekian, A.; Laurino, P.; Seeberger, P. H. *J. Am. Chem. Soc.* **2009**, *131*, 2110–2112.

59. Yang, Y.; Zhao, Y.-T.; Yan, T.-T.; Yu, M.; Sha, Y.-L.; Zhao, Z.-H.; Li, Z.-J. *Tetrahedron Lett.* **2010**, *51*, 4182–4185.

60. Yang, Y.; Yu, M.; Yan, T.-T.; Zhao, Z.-H.; Sha, Y.-L.; Li, Z.-J. *Bioorgan. Med. Chem.* **2010**, *18*, 5234–5240.

61. Jun, Y. W.; Lee, J. H.; Cheon, J. *Angew. Chem., Int. Ed.* **2008**, *47*, 5122–5135.

62. Robinson, A.; Fang, J.-M.; Chou, P.-T.; Liao, K.-W.; Chu, R.-M.; Lee, S.-J. *ChemBioChem* **2005**, *6*, 1899–1905.

63. Yu, M.; Yang, Y.; Han, R.; Zheng, Q.; Wang, L.; Hong, Y.; Li, Z.; Sha, Y. *Langmuir* **2010**, *26*, 8534–8539.
64. Higuchi, Y.; Oka, M.; Kawakami, S.; Hashida, M. *J. Controlled Release* **2008**, *125*, 131–136.
65. Mukhopadhyay, B.; Martins, M. B.; Karamanska, R.; Russell, D. A.; Field, R. A. *Tetrahedron Lett.* **2009**, *50*, 886–889.
66. Niikura, K.; Nishio, T.; Akita, H.; Matsuo, Y.; Kamitani, R.; Kogure, K.; Harashima, H.; Ijiro, K. *ChemBioChem* **2007**, *8*, 379–384.
67. van Kasteren, S. I.; Campbell, S. J.; Serres, S.; Anthony, D. C.; Sibson, N. R.; Davis, B. G. *Proc. Natl. Acad. Sci. U.S.A.* **2009**, *106*, 18–23.
68. El-Boubbou, K.; Zhu, D. C.; Vasileiou, C.; Borhan, B.; Prosperi, D.; Li, W.; Huang, X. *J. Am. Chem. Soc.* **2010**, *132*, 4490–4499.
69. Valero, E.; Tambalo, S.; Marzola, P.; Ortega-Munoz, M.; Lopez-Jaramillo, F. J.; Santoyo-Gonzalez, F.; de Dios Lopez, J.; Delgado, J. J.; Calvino, J. J.; Cuesta, R.; Dominguez-Vera, J. M.; Galvez, N. *J. Am. Chem. Soc.* **2011**, *133*, 4889–4895.
70. Marradi, M.; Alcantara, D.; de la Fuente, J. M.; Garcia-Martin, M. L.; Cerdan, S.; Penades, S. *Chem. Commun.* **2009**, 3922–3924.
71. Garcia, I.; Gallo, J.; Genicio, N.; Padro, D.; Penades, S. *Bioconjugate Chem.* **2011**, *22*, 264–273.
72. Stockert, R. J.; Morell, A. G.; Scheinberg, I. H. *Science* **1974**, *186*, 365–366.
73. Weigel, P. H.; Yik, J. H. N. *Biochim. Biophys. Acta, Gen. Subj.* **2002**, *1572*, 341–363.
74. Khorev, O.; Stokmaier, D.; Schwardt, O.; Cutting, B.; Ernst, B. *Bioorgan. Med. Chem.* **2008**, *16*, 5216–5231.
75. Connolly, D. T.; Townsend, R. R.; Kawaguchi, K.; Bell, W. R.; Lee, Y. C. *J. Biol. Chem.* **1982**, *257*, 939–945.
76. Cai, W.; Chen, X. *Small* **2007**, *3*, 1840–1854.
77. Nishiguchi, S.; Yamada, K.; Fuji, Y.; Shibatani, S.; Toda, A.; Nishimura, S. *Chem. Commun.* **2001**, 1944–1945.
78. Auge, C.; Malleron, A.; Tahrat, H.; Marc, A.; Goergen, J. L.; Cerutti, M.; Steelant, W. F. A.; Delannoy, P.; Lubineau, A. *Chem. Commun.* **2000**, 2017–2018.
79. Ivannikova, T.; Bintein, F.; Malleron, A.; Juliant, S.; Cerutti, M.; Harduin-Lepers, A.; Delannoy, P.; Auge, C.; Lubineau, A. *Carbohydr. Res.* **2003**, *338*, 1153–1161.
80. Chen, X.; Fang, J.; Zhang, J.; Liu, Z.; Shao, J.; Kowal, P.; Andreana, P.; Wang, P. G. *J. Am. Chem. Soc.* **2001**, *123*, 2081–2082.
81. Liu, Z.; Zhang, J.; Chen, X.; Wang, P. G. *ChemBioChem* **2002**, *3*, 348–355.
82. Naruchi, K.; Nishimura, S. *Angew. Chem., Int. Ed.* **2011**, *50*, 1328–1331.
83. Wong, L. S.; Thirlway, J.; Micklefield, J. *J. Am. Chem. Soc.* **2008**, *130*, 12456–12464.
84. Weinrich, D.; Lin, P.-C.; Jonkheijm, P.; Nguyen, U. T.; Schroder, H.; Niemeyer, C. M.; Alexandrov, K.; Goody, R.; Waldmann, H. *Angew. Chem., Int. Ed.* **2010**, *49*, 1252–1257.
85. Gauchet, C.; Labadie, G. R.; Poulter, C. D. *J. Am. Chem. Soc.* **2006**, *128*, 9274–9275.

86. Ito, T.; Sadamoto, R.; Naruchi, K.; Togame, H.; Takemoto, H.; Kondo, H.; Nishimura, S. *Biochemistry* **2010**, *49*, 2604–2614.
87. Tanaka, Y.; Tsuruda, Y.; Nishi, M.; Kamiya, N.; Goto, M. *Org. Biomol. Chem.* **2007**, *5*, 1764–70.
88. Soellner, M. B.; Dickson, K. A.; Nilsson, B. L.; Raines, R. T. *J. Am. Chem. Soc.* **2003**, *125*, 11790–11791.
89. Watzke, A.; Kohn, M.; Gutierrez-Rodriguez, M.; Wacker, R.; Schroder, H.; Breinbauer, R.; Kuhlmann, J.; Alexandrov, K.; Niemeyer, C. M.; Goody, R. S.; Waldmann, H. *Angew. Chem., Int. Ed.* **2006**, *45*, 1408–1412.
90. de Araujo, A. D.; Palomo, J. M.; Cramer, J.; Kohn, M.; Schroder, H.; Wacker, R.; Niemeyer, C.; Alexandrov, K.; Waldmann, H. *Angew. Chem., Int. Ed.* **2006**, *45*, 296–301.
91. Camarero, J. A.; Kwon, Y.; Coleman, M. A. *J. Am. Chem. Soc.* **2004**, *126*, 14730–14731.
92. Helms, B.; van Baal, I.; Merkx, M.; Meijer, E. W. *ChemBioChem* **2007**, *8*, 1790–1794.
93. Lin, P.-C.; Ueng, S.-H.; Tseng, M.-C.; Ko, J.-L.; Huang, K.-T.; Yu, S.-C.; Adak, A. K.; Chen, Y.-J.; Lin, C.-C. *Angew. Chem., Int. Ed.* **2006**, *45*, 4286–90.
94. Chen, M.-L.; Adak, A. K.; Yeh, N.-C.; Yang, W.-B.; Chuang, Y.-J.; Wong, C.-H.; Hwang, K.-C.; Hwu, J.-R.; Hsieh, S.-L.; Lin, C.-C. *Angew. Chem., Int. Ed.* **2008**, *47*, 8627–30.
95. Yu, C.-C.; Lin, P.-C.; Lin, C.-C. *Chem. Commun.* **2008**, 1308–1310.
96. Timmons, S. C.; Mosher, R. H.; Knowles, S. A.; Jakeman, D. L. *Org. Lett.* **2007**, *9*, 857–860.

Downloaded by PENNSYLVANIA STATE UNIV on June 3, 2012 | http://pubs.acs.org
Publication Date (Web): December 13, 2011 | doi: 10.1021/bk-2011-1091.ch003

Chapter 3

Chemoselectivity and Glyconanoparticles

Mikkel B. Thygesen* and Knud J. Jensen*

**IGM-Nanobioscience, Centre for Carbohydrate Recognition and Signalling,
Faculty of Life Sciences, University of Copenhagen, Thorvaldsensvej 40,
DK-1871 Frederiksberg C, Denmark
*E-mail: mbth@life.ku.dk; kjj@life.ku.dk**

This chapter provides an overview of recent research on the use of highly chemoselective reactions of carbohydrates to expedite construction of glyconanoparticles. These methodologies provide tools for chemical biology and biopolymer medicinal chemistry. The text is divided into two main sections: one describing methods based on thiol-terminated glycoconjugates, and the other describing reactions on nanoparticle surfaces. The topics covered in this focused minireview are also of importance for chemoselectivity in construction of glycoconjugates, glyco-functionalized surfaces, and functionalized nanoparticles in general.

Introduction

The progress in genomic and proteomic research over the past few decades has made a spectacular impact on pharmaceutical sciences, biomedical research, and life sciences. The success within these fields has to a large extent been fueled by chemical tools, in particular technologies that take advantage of solid supported chemistry. This includes solid supported sequencing as well as solid-phase synthesis of peptides and oligonucleotides. Additionally, microarray technology for DNA and peptides has facilitated an ingenious link between functional assessment and sequence information. In contrast to proteins, carbohydrates (also termed glycans) are not genetically template-encoded but are constructed by the concerted activity of synthesizing and modifying enzymes. This indirect linkage between genome and glycome presents a barrier to unraveling the complex biology of glycans. Many of the milestone technologies that have been so important for understanding the structures and biology of oligonucleotides and

In Petite and Sweet: Glyco-Nanotechnology as a Bridge to New Medicines; Huang, X., et al.;
ACS Symposium Series; American Chemical Society: Washington, DC, 2011.

proteins cannot be readily applied to carbohydrates. There is a pressing need to develop general methodologies that can be used to analyze the occurrence of carbohydrates and their interactions with proteins or other carbohydrates (*1*). Such chemical tools hold great promise to provide novel insights to combat disease and develop new medicines including new vaccines.

A central theme in functional analysis of carbohydrate recognition is the prevalent requirement for clustering of the ligands; the low affinities characterizing most glycan-protein and glycan-glycan interactions (typically in the millimolar to micromolar range) represent a challenge to structure-activity determinations based on traditional ligand binding assays. Nature takes advantage of this seeming problem by the multivalent presentation of glycan ligands and their receptors to achieve high observed affinities (avidity) with high specificities (*2–4*). Modern synthetic macromolecules and assemblies capable of mimicking the multivalent representation and interactions of glycan structures in nature are emerging as enabling tools for the broad study of glycan interactions. Of particular importance in this field is the use of glyco-functionalized (*5*) dendrimers, liposomes, globular proteins, arrays, and nanoparticles.

Glyconanoparticles have recently attracted attention as a platform for studying and intervening in carbohydrate–protein and carbohydrate–carbohydrate interactions. Several recent literature reviews have dealt with their synthesis and use (*1*, *6–10*). In broad terms, glyconanoparticles consist of an inorganic core of nanoscale dimensions on top of which is a flexible organic layer (linker or polymer) conjugated (covalently or non-covalently) with carbohydrates. Different materials may be utilized for the core depending on the application of the glyconanoparticles, e.g. noble metal nanoparticles, semiconductor quantum dots, or magnetic nanomaterials. The developing field of glyconanoparticle research constitutes perhaps one of the most intriguing research areas within biomolecular nanoscience due to the convergence of the inherent characteristics of nanoparticles and the aforementioned multivalency effects of carbohydrate interactions. Quantitative studies have revealed that optimized anchoring of glycans on nanoparticles may lead to binding enhancements of 1-5 orders of magnitude compared to the free glycans in solution (*11*), thus paralleling the best of synthetically tailored scaffolds (*12*). The high degree of solubility and stability in biological and buffered aqueous media makes glyconanoparticles well-suited for interactions with biological material (*13*).

In order to advance glyconanoparticle research into a broadly applicable chemical tool for life science research it is imperative that synthetic methods are devised to allow easy access to glyconanoparticles containing various oligosaccharides of interest. This implies the development of general methods that utilize easily accessible oligosaccharides with minimal chemical manipulations and efficiently anchor the carbohydrates to a nanoparticle surface via highly chemoselective reactions. Anchoring principally has two levels of implication for the glyconanoparticles. While the first level is the formation of a firm, covalent bond between the carbohydrate and an aglycon (e.g., the linker), the second level includes requirements for the covalently fabricated carbohydrate surface. The linker between the glycan and the surface should provide optimal presentation of glycans and prevent non-specific binding of, *e.g.*, proteins. Additionally,

Downloaded by PENNSYLVANIA STATE UNIV on June 3, 2012 | http://pubs.acs.org
Publication Date (Web): December 13, 2011 | doi: 10.1021/bk-2011-1091.ch003

incorporation of cleavable linkers for selective release of modified carbohydrates after screening could be imagined to in some cases aid the development of glyconanoparticles by enabling mass spectrometry of glycans.

Chemoselective Conjugation of Carbohydrates to Thiol-Terminated Linkers

Conventionally, the main methods for construction of glyconanoparticles have relied on the application of neo-glycoconjugates possessing thiol-terminated linkers (also termed thiolated carbohydrates) either via (*i*) *in situ* reduction of metal salts in the presence of thiolated carbohydrates, or (*ii*) ligand exchange of thiolated carbohydrates onto pre-formed nanoparticle cores (Figure 1). Thus, the development of efficient and simple conjugation protocols to enable thiolation of biologically relevant carbohydrate ligands is central to the advancement of glyconanoparticle synthesis. Procedures based on chemical glycosylation with fully protected glycosyl donors and thiol-terminated linkers can be efficiently applied for simple mono- and disaccharides. However, as the complexity of the carbohydrate ligand increases, this approach becomes challenging (*14*) and often requires optimization of reaction conditions for individual ligands. These procedures will not be discussed here.

Downloaded by PENNSYLVANIA STATE UNIV on June 3, 2012 | http://pubs.acs.org
Publication Date (Web): December 13, 2011 | doi: 10.1021/bk-2011-1091.ch003

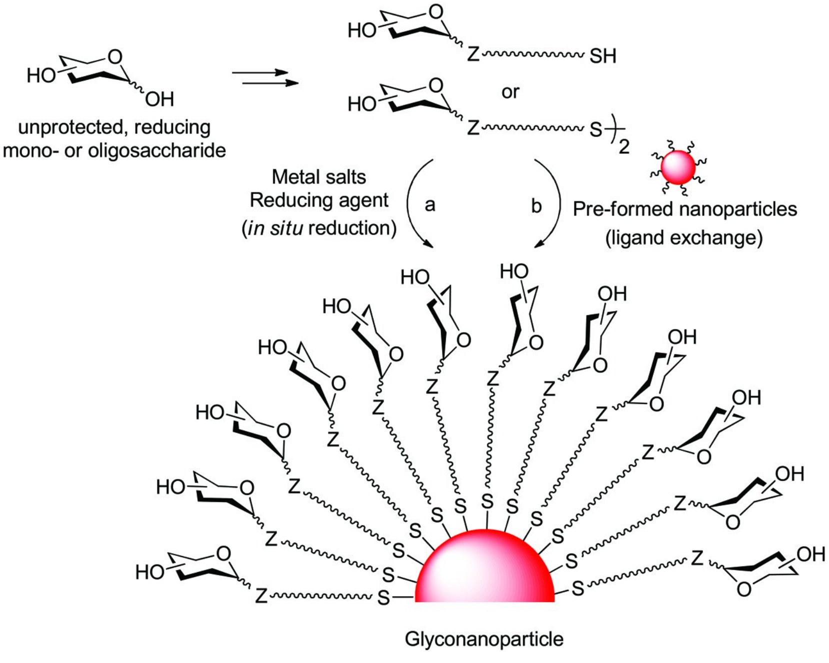

Figure 1. Synthesis of glyconanoparticles from thiol-terminated glycoconjugates by in situ reduction (a) or ligand exchange (b). Z=anomeric heteroatom.

Ideally, the chemistry used for installment of suitable thiol-terminated linkers should be simple, high yielding, and chemoselective and should only rely on protecting group-free conjugation conditions. This would allow for maximum flexibility in the selection of linker design.

Reactions of Suitably Derivatized *O*-Glycosides

A few examples in the literature describe the application of anomeric moieties that allow easy and efficient conjugation to thiol-terminated linkers for glyconanoparticle synthesis.

Kamerling and co-workers have developed a methodology based on the synthesis of allyl glycosides that are conjugated with 1,6-hexane-dithiol in a thiol-ene reaction (Figure 2a). The allyl glycoside is stable to conditions for oligosaccharide synthesis and a range of thiol-terminated mono- and disaccharides could be prepared and used for synthesis of gold nanoparticles (*15*).

More recently, in 2009, Penadés and co-workers have introduced a heterobifunctional linker based on thiourea coupling between aminoethyl glycosides and a terminal isothiocyanate group (Figure 2b). Oligosaccharide synthesis could be conducted with benzyloxycarbonyl-protection of the amino group (*14*).

Downloaded by PENNSYLVANIA STATE UNIV on June 3, 2012 | http://pubs.acs.org
Publication Date (Web): December 13, 2011 | doi: 10.1021/bk-2011-1091.ch003

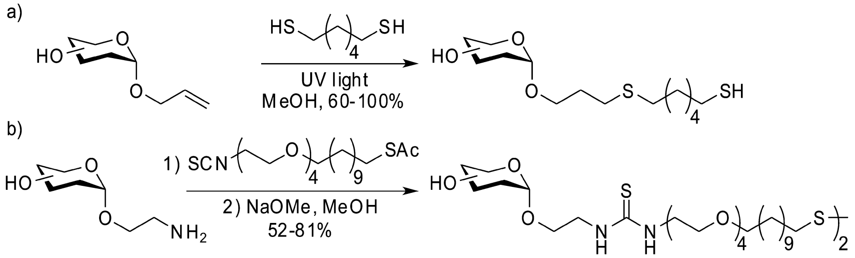

Figure 2. Chemoselective approaches to thiol-terminated neo-glycoconjugates from O-allyl glycosides via thiol-ene coupling (a), or from O-aminoethyl glycosides via thiourea coupling (b).

Reactions of Unprotected Reducing Carbohydrates

Reducing carbohydrates in general include a structural feature that can aid significantly in the immobilization of carbohydrates. This is the presence of an aldehyde or ketone moiety at the ‘reducing end’ which presents a single uniquely reactive functional group in carbohydrates and a group normally not present in other biopolymers. The reducing end aldehyde moiety, in the open chain form, is in equilibrium with the corresponding hemi-acetal in the ring-closed form of the carbohydrate. However, the electrophilic aldehyde moiety can still react with nucleophiles. The nucleophiles most commonly used for the reaction with the reducing end are aminooxy or hydrazide compounds, providing relatively stable

Downloaded by PENNSYLVANIA STATE UNIV on June 3, 2012 | http://pubs.acs.org
Publication Date (Web): December 13, 2011 | doi: 10.1021/bk-2011-1091.ch003

oximes or hydrazides. Other nucleophiles, e.g. amines, can also react. However, the initially formed product is less stable and needs to be transformed, e.g. by reductive amination, or by the use of 1,2-amino thiols which can form stable thiazolidines (*16*).

Reductive amination chemistry has been described by Kamerling and co-workers for the preparation of mercaptoethylamine-terminated oligosaccharides from unprotected, reducing mono- to hexasaccharides containing various degrees of branching (*17*). In this procedure, the reducing end monosaccharide unit is converted into an open-chain secondary amine (Figure 3). These glycoconjugates were used in the preparation of gold glyconanoparticles via a modified Brust-Schiffrin protocol (*18*). The drawback of reductive amination protocols, however, is the potential lack of specific binding between proteins and short oligosaccharides, imposed by the reductively opened monosaccharide units (*19*).

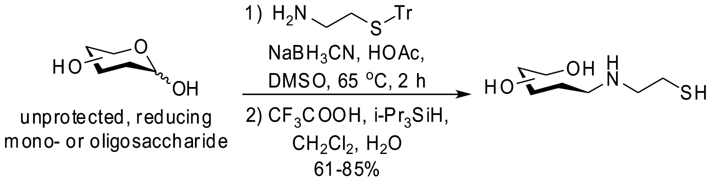
1) H2N S Tr
NaBH3CN, HOAc,
DMSO, 65 °C, 2 h
2) CF3COOH, i-Pr3SiH,
CH2Cl2, H2O
61-85%
HO
O
OH
unprotected, reducing
mono- or oligosaccharide
HO
OH
H
N
SH

Figure 3. Chemoselective synthesis of mercaptoethylamine-terminated carbohydrates from reducing carbohydrates.

The highly chemoselective reaction of glycans through their reducing ends with aminooxy groups, via oxime formation, has become an important method in glycoconjugate synthesis. However, it is sometimes speculated that this leaves the monosaccharide at the reducing end solely in a non-native open-chain form, as in the case of reductive amination. In contrast, carbohydrate oximes and oxime ethers exist as a dynamic mixture of several tautomeric forms involving both ring and open-chain forms, the distribution being dependent on the monosaccharide unit. The open-chain *E*- and *Z*-forms generally predominate over the α- and β-pyranosyl forms, while α- and β-furanosyl forms may constitute only minor tautomers (Figure 4).

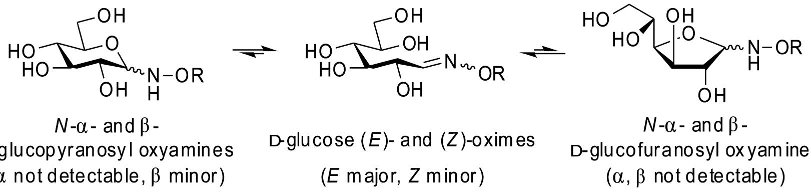
OH
HO
HO
O
N−OR
OH H
N-α- and β-
D-glucopyranosyl oxyamines
(α not detectable, β minor)
OH
HO
HO
OH
N
OR
OH
D-glucose (*E*)- and (*Z*)-oximes
(*E* major, *Z* minor)
HO
HO
OH
O
N−OR
H
OH
N-α- and β-
D-glucofuranosyl oxyamines
(α, β not detectable)

Figure 4. Ring-chain tautomeric equilibria for D-glucose oximes.

Downloaded by PENNSYLVANIA STATE UNIV on June 3, 2012 | http://pubs.acs.org
Publication Date (Web): December 13, 2011 | doi: 10.1021/bk-2011-1091.ch003

Hydrolysis of oximes, i.e., the reverse reaction of their formation, is known to occur, especially at pH values below 5-6. However, our group has recently shown (*20*) that some aminooxy reagents provide carbohydrate oximes with a remarkable and very useful stability.

The rate of formation of carbohydrate oximes can in certain cases be too low to be of practical use. It had previously been demonstrated that anilines catalyze the formation of oximes (*21*, *22*). We recently demonstrated that aniline catalysis indeed also can occur in the more complex formation of carbohydrate oximes (*23*). For carbohydrates, aniline catalysis is more complicated as the aldehyde moiety is in equilibrium with the cyclic hemi-acetal and because of the possibility of formation of unstable, cyclic glycosyl amines (Figure 5). Aniline plays a dual role, as it provides an enhanced electrophile for the aminooxy nucleophile, in the form of a protonated iminium ion, and additionally it shifts the equilibrium away from the hemi-acetal. Aniline catalyzed the formation of carbohydrate oximes with up to 20-fold rate increases (at 100 mM aniline) and was especially useful for the formation of oximes of carbohydrates with a GlcNAc at the reducing end. This very useful methodology enabled the formation of complex glycoconjugates (*23*).

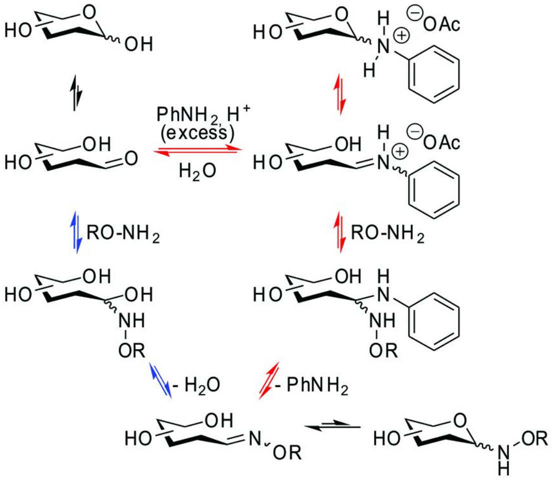

Figure 5. Nucleophilic catalysis of carbohydrate oxime formation by aniline in acetate buffer pH 4.6. Oxime formation in the absence (blue arrows, left) or presence of aniline (red arrows, right). Redrawn after reference (23).

In 2009, we introduced the application of chemoselective carbohydrate oxime formation for the anchoring of reducing glycans to gold nanoparticles (*24*). The strategy is based on a heterobifunctional linker comprising an aminooxy group in one end, and a trityl-protected thiol in the other end of a tetra(ethylene glycol) spacer, which provides flexibility for the carbohydrate ligands and prevents unspecific binding with proteins (Figure 6). Carbohydrate oxime formation with this linker has been conducted with a range of reducing mono- and oligosaccharides, in some cases under aniline catalysis to increase the reaction rate (*23*, *24*). The trityl group functions as a liphophilic and UV active tag that facilitated easy analysis of reagent conversion, and isolation of the oxime products. After removal of the trityl group, the thiol-terminated glycoconjugates were anchored on citrate-stabilized gold nanoparticles via ligand exchange. The obtained glyconanoparticles were soluble under a wide range of aqueous conditions. This approach provides very simple handling and high efficiency for the generation of functionalized glyconanoparticles for bioanalytical assays.

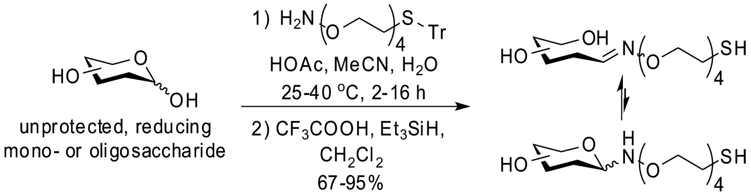
unprotected, reducing mono- or oligosaccharide
1) $H_2N(O\frown)_4S-Tr$
HOAc, MeCN, H_2O
25-40 °C, 2-16 h
2) CF_3COOH, Et_3SiH, CH_2Cl_2
67-95%
HO
OH
SH
4

Figure 6. Chemoselective oxime formation with heterobifunctional linker.

We studied the ability of proteins to interact via specific molecular recognition with carbohydrate oxime conjugates by comparing the functional binding of oxime ring-chain tautomers with analogs trapped in an open-chain configuration by reduction of the oximes to the corresponding hydroxylamines (*24*). The results with the enzyme glucoamylase from *A. niger* showed that the equilibration of tautomers mediated productive enzyme binding at a stoichiometric level. With the lectin concanavalin A from *C. ensiformis*, the results showed that specific recognition of monosaccharide oximes could be obtained while these were attached to gold nanoparticle surfaces. Thus, carbohydrate oximes may provide efficient anchoring of glycans through the reducing end while maintaining a biologically relevant presentation of the glycan. These findings have very general significance for construction of glycoconjugates.

Chemoselective Reactions of Carbohydrates on Nanoparticle Surfaces

The previous part of this chapter has described methods that rely on chemoselective formation of thiol-terminated glycoconjugate intermediates for glyconanoparticle synthesis. An alternative strategy that obviates this need is the application of chemoselective reactions between carbohydrates and reactive functional groups on linker or polymer coated nanoparticles (Figure 7). A key requirement for these reactions is that they should be chemoselective and high yielding, i.e., essentially byprodct-free, due to the fact that glyconanoparticles carrying side-products cannot be removed. Ideally, the reaction conditions involving nanoparticles should be mild and not contain an excessive number of transformations in order to avoid degeneration or aggregation, and to maintain a homogenous population of nanoparticles.

Downloaded by PENNSYLVANIA STATE UNIV on June 3, 2012 | http://pubs.acs.org
Publication Date (Web): December 13, 2011 | doi: 10.1021/bk-2011-1091.ch003

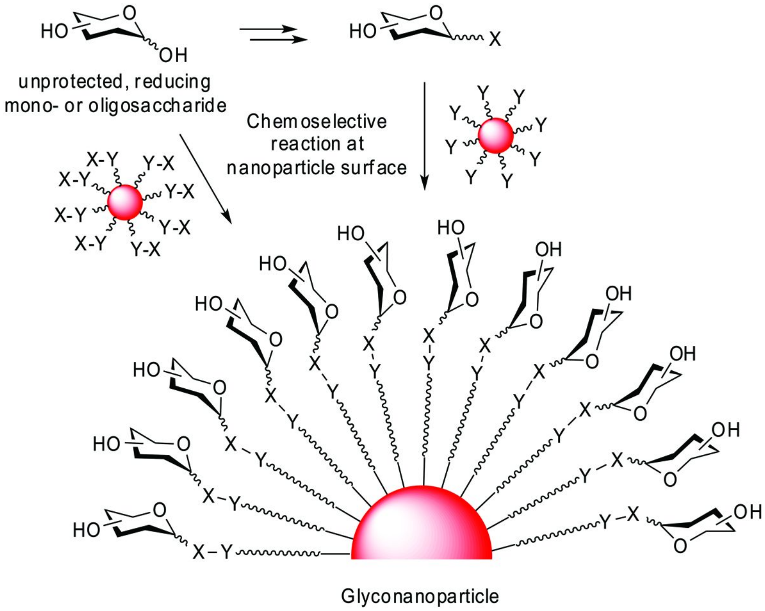
HO
O
OH
unprotected, reducing mono- or oligosaccharide
HO
O
X
Chemoselective reaction at nanoparticle surface
Y
X-Y
Y-X
Glyconanoparticle

Figure 7. Synthesis of glyconanoparticles by chemoselective reaction at nanoparticle surface. X, Y= mutually reactive groups.

Methods Utilizing Pre-Modified Glycosides

In 2001, Kataoka and co-workers published the first example of the strategy, whereby gold nanoparticles were synthesized in the presence of a heterobifunctional PEG polymer, carrying a thiol and an acetal-protected aldehyde moiety (*25*). After liberation of the aldehyde groups on the nanoparticle surface under mildly acidic conditions, these particles were reductively aminated with unprotected 4-aminophenyl glycosides in the presence of borane-dimethylamine in aqueous phosphate buffer pH 7 (Figure 8a).

More recently, Davis and co-workers have published methodology for chemoselective reaction between unprotected 2-imido-2-methoxyethyl β-thioglycosides and amino-functionalized, dextran-stabilized iron oxide nanoparticles (*26*). Oligosaccharide synthesis was conducted with a terminal cyanomethyl 2-acetamido-2-deoxy-β-thioglucoside which subsequently could be converted into the imidate with methoxide. Anchoring to the nanoparticles via formation of an amidine linkage was effected in aqueous borate buffer pH 8 (Figure 8b).

Downloaded by PENNSYLVANIA STATE UNIV on June 3, 2012 | http://pubs.acs.org
Publication Date (Web): December 13, 2011 | doi: 10.1021/bk-2011-1091.ch003

Downloaded by PENNSYLVANIA STATE UNIV on June 3, 2012 | http://pubs.acs.org
Publication Date (Web): December 13, 2011 | doi: 10.1021/bk-2011-1091.ch003

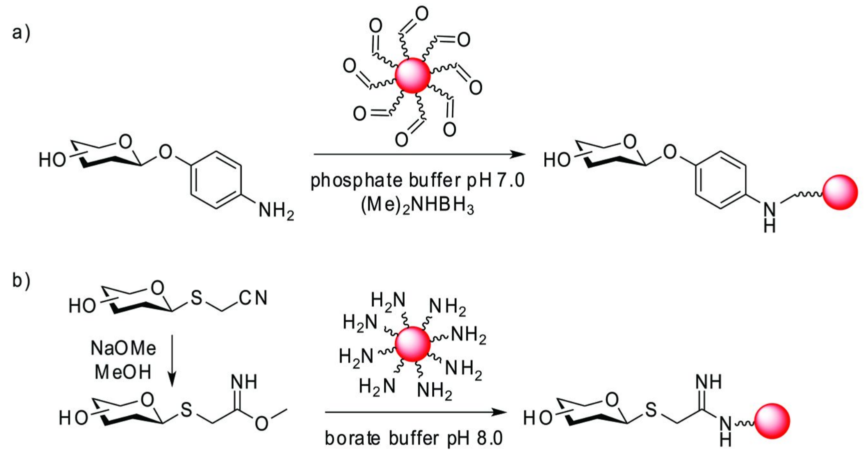
a)
HO
O
O
NH2
phosphate buffer pH 7.0
(Me)2NHBH3
N
H
b)
S
CN
NaOMe
MeOH
NH
H2N
NH2
borate buffer pH 8.0

Figure 8. Chemoselective reactions on nanoparticle surfaces via reductive amination (a) or amidine formation (b).

Reaction with Reducing Carbohydrates

Our group has developed methodology for synthesis of gold glyconanoparticles where unmodified, i.e. unprotected, reducing glycans are anchored directly via a single chemoselective reaction on surface-bound aminooxy groups (Figure 9). We have shown, in addition, that oxime coupling on terminal aminooxy groups allows anchoring of various other aldehyde-containing biomolecules, e.g., glycopeptide aldehydes. Anchoring is conducted under mild conditions in neutral aqueous solutions (*27*).

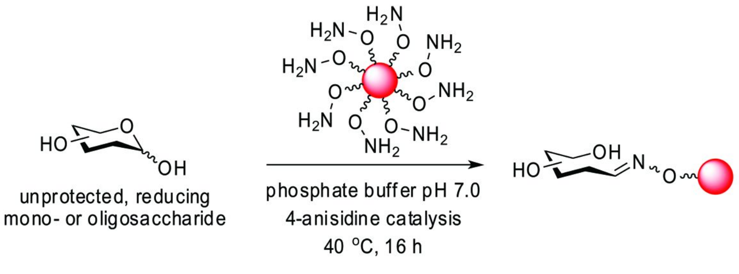
HO
O
OH
unprotected, reducing
mono- or oligosaccharide
H2N
O
NH2
phosphate buffer pH 7.0
4-anisidine catalysis
40 °C, 16 h
OH
N

Figure 9. Chemoselective oxime formation with reducing carbohydrates on aminooxy-functionalized nanoparticles.

Our methodology (*27*) is based on the anchoring of a heterobifunctional tetra(ethylene glycol) spacer, carrying a protected aminooxy group and a thiol group to water-soluble, citrate-stabilized gold nanoparticles. We applied a 4-carboxy-phthaloyl protecting group for the aminooxy moiety; the carboxylate group served to provide a high degree of aqueous solubility of the nanoparticles under neutral conditions. The protecting group could be removed by dilute (1 mM) aqueous hydrazine, and in addition it allowed quantification of release of aminooxy groups on the nanoparticles. The mild conditions ensured that the nanoparticles were not compromised by aggregation. The aminooxy-terminated gold nanoparticles (termed reactive core-shell nanoparticles) were reacted with unprotected, reducing disaccharides. Carbohydrate oxime formation could be promoted by nucleophilic catalysis with 4-anisidine at 40 °C.

Zhou and co-workers (*28*) have published a related strategy, however without aniline catalysis, based on hydrazide-coated gold nanoparticles that may react chemoselectively with unprotected, reducing glycans under microwave heating conditions at pH 5.4 to obtain high reaction rates (Figure 10).

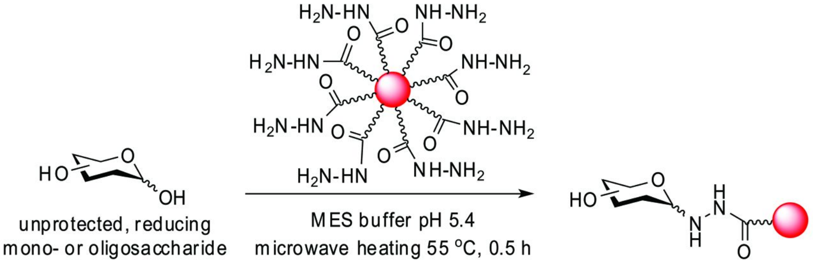

Figure 10. Chemoselective hydrazide formation on the surface of gold nanoparticles.

Non-Selective Methods

Ramström, Yan and co-workers have recently developed a methodology based on photochemical coupling between unprotected carbohydrates and perfluorophenylazide groups on nanoparticle surfaces (*29*). The azide moiety was activated by UV light, via conversion into a reactive nitrene intermediate that underwent insertion reactions into C-H bonds of the carbohydrate. The technique allows easy access to glyconanoparticles, however, the orientation of the anchored glycans cannot be controlled, and part of the structures may be presented in denatured forms in which they may not be able to interact specifically. For more details regarding this method, please see Chapter # in this book.

Conclusion

Chemical methodologies are emerging which profoundly facilitate the generation of glyconanoparticles from simple starting materials. We believe that highly chemoselective reactions, especially sequential chemoselective reactions that minimize the use of protecting groups, will further aid the widespread use of glyconanoparticles as tools in chemical biology and medicinal chemistry. The potential benefits from using the inherent properties of the nanoparticles, including metal and semiconductor nanoparticles, have not yet been fully utilized.

In Petite and Sweet: Glyco-Nanotechnology as a Bridge to New Medicines; Huang, X., et al.; ACS Symposium Series; American Chemical Society: Washington, DC, 2011.
Downloaded by PENNSYLVANIA STATE UNIV on June 3, 2012 | http://pubs.acs.org
Publication Date (Web): December 13, 2011 | doi: 10.1021/bk-2011-1091.ch003

Downloaded by PENNSYLVANIA STATE UNIV on June 3, 2012 | http://pubs.acs.org
Publication Date (Web): December 13, 2011 | doi: 10.1021/bk-2011-1091.ch003

References

1. Larsen, K.; Thygesen, M. B.; Guillaumie, F.; Willats, W. G. T.; Jensen, K. J. *Carbohydr. Res.* **2006**, *341*, 1209–1234.
2. Lee, Y. C.; Lee, R. T. *Acc. Chem. Res.* **1995**, *28*, 321–327.
3. Mammen, M.; Choi, S. K.; Whitesides, G. M. *Angew. Chem., Int. Ed.* **1998**, *37*, 2755–2794.
4. Kitov, P. I.; Bundle, D. R. *J. Am. Chem. Soc.* **2003**, *125*, 16271–16284.
5. Bertozzi, C. R.; Kiessling, L. L. *Science* **2001**, *291*, 2357–2364.
6. de la Fuente, J. M.; Penadés, S. *Biochim. Biophys. Acta, Gen. Subj.* **2006**, *1760*, 636–651.
7. Sihelníková, L.; Tvaroska, I. *Chem. Pap.* **2007**, *61*, 237–255.
8. García, I.; Marradi, M.; Penadés, S. *Nanomedicine* **2010**, *5*, 777–792.
9. Wang, X.; Ramström, O.; Yan, M. D. *Adv. Mater.* **2010**, *22*, 1946–1953.
10. Marradi, M.; Martín-Lomas, M.; Penadés, S. In *Advances in Carbohydrate Chemistry and Biochemistry*; Horton, D., Ed.; Elsevier Academic Press, Inc: San Diego, CA, 2010; Vol. 64, pp 211−290.
11. Chien, Y. Y.; Jan, M. D.; Adak, A. K.; Tzeng, H. C.; Lin, Y. P.; Chen, Y. J.; Wang, K. T.; Chen, C. T.; Chen, C. C.; Lin, C. C. *ChemBioChem* **2008**, *9*, 1100–1109.
12. Kitov, P. I.; Sadowska, J. M.; Mulvey, G.; Armstrong, G. D.; Ling, H.; Pannu, N. S.; Read, R. J.; Bundle, D. R. *Nature* **2000**, *403*, 669–672.
13. Barrientos, A. G.; de la Fuente, J. M.; Jiménez, M.; Solis, D.; Cañada, F. J.; Martín-Lomas, M.; Penadés, S. *Carbohydr. Res.* **2009**, *344*, 1474–1478.
14. Martínez-Ávila, O.; Hijazi, K.; Marradi, M.; Clavel, C.; Campion, C.; Kelly, C.; Penadés, S. *Chem. Eur. J.* **2009**, *15*, 9874–9888.
15. Carvalho de Souza, A.; Halkes, K. M.; Meeldijk, J. D.; Verkleij, A. J.; Vliegenthart, J. F. G.; Kamerling, J. P. *Eur. J. Org. Chem.* **2004**, 4323–4339.
16. Guillaumie, F.; Thomas, O. R. T.; Jensen, K. J. *Bioconjugate Chem.* **2002**, *13*, 285–294.
17. Halkes, K. M.; Carvalho de Souza, A.; Maljaars, C. E. P.; Gerwig, G. J.; Kamerling, J. P. *Eur. J. Org. Chem.* **2005**, 3650–3659.
18. Brust, M.; Walker, M.; Bethell, D.; Schiffrin, D. J.; Whyman, R. *J. Chem. Soc., Chem. Commun.* **1994**, 801–802.
19. Liu, Y.; Feizi, T.; Carnpanero-Rhodes, M. A.; Childs, R. A.; Zhang, Y. N.; Muiioy, B.; Evans, P. G.; Osborn, H. M. I.; Otto, D.; Crocker, P. R.; Chai, W. C. *Chem. Biol.* **2007**, *14*, 847–859.
20. Cló, E.; Blixt, O.; Jensen, K. J. *Eur. J. Org. Chem.* **2010**, 540–554.
21. Cordes, E. H.; Jencks, W. P. *J. Am. Chem. Soc.* **1962**, *84*, 826–831.
22. Dirksen, A.; Hackeng, T. M.; Dawson, P. E. *Angew. Chem., Int. Ed.* **2006**, *45*, 7581–7584.
23. Thygesen, M. B.; Munch, H.; Sauer, J.; Cló, E.; Jørgensen, M. R.; Hindsgaul, O.; Jensen, K. J. *J. Org. Chem.* **2010**, *75*, 1752–1755.
24. Thygesen, M. B.; Sauer, J.; Jensen, K. J. *Chem. Eur. J.* **2009**, *15*, 1649–1660.
25. Otsuka, H.; Akiyama, Y.; Nagasaki, Y.; Kataoka, K. *J. Am. Chem. Soc.* **2001**, *123*, 8226–8230.

26. van Kasteren, S. I.; Campbell, S. J.; Serres, S.; Anthony, D. C.; Sibson, N. R.; Davis, B. G. *Proc. Natl. Acad. Sci. U. S. A.* **2009**, *106*, 18–23.
27. Thygesen, M. B.; Sørensen, K. K.; Cló, E.; Jensen, K. J. *Chem. Commun.* **2009**, 6367–6369.
28. Chuang, Y. J.; Zhou, X. C.; Pan, Z. W.; Turchi, C. *Biochem. Biophys. Res. Commun.* **2009**, *389*, 22–27.
29. Wang, X.; Ramström, O.; Yan, M. D. *J. Mater. Chem.* **2009**, *19*, 8944–8949.

Downloaded by PENNSYLVANIA STATE UNIV on June 3, 2012 | http://pubs.acs.org
Publication Date (Web): December 13, 2011 | doi: 10.1021/bk-2011-1091.ch003

Downloaded by STANFORD UNIV GREEN LIBR on June 3, 2012 | http://pubs.acs.org
Publication Date (Web): December 13, 2011 | doi: 10.1021/bk-2011-1091.ch004

Chapter 4

Synthesis of Glyconanomaterials via Photo-Initiated Coupling Chemistry

Xin Wang,[1] Oscar Norberg,[2] Lingquan Deng,[2] Olof Ramström,*[,2] and Mingdi Yan*[,1,2]

**[1]Department of Chemistry, Portland State University,
P.O. Box 751, Portland, Oregon, 97207-0751 USA
[2]Department of Chemistry, KTH - Royal Institute of Technology,
Teknikringen 30, S-10044 Stockholm, Sweden
*E-mails: ramstrom@kth.se; Mingdi_Yan@uml.edu**

Glyconanomaterials, broadly defined as carbohydrate-presenting structures below 100 nm in size, exhibit remarkable chemical and physical properties with high potential for modern biomedical applications. In this chapter, current synthetic approaches for fabricating glyconanomaterials are summarized, with special emphasis on a novel photocoupling strategy to conjugate carbohydrates onto a wide variety of nanomaterials. Based on the photochemically induced reaction of perfluorophenylazide, different glyconanomaterials were efficiently synthesized, and the resulting structures used in a range of applications. The results demonstrate that this approach to carbohydrate presentation at nanomaterial surfaces leads to efficient and selective binding to cognate proteins, enabling new applications in carbohydrate-lectin recognition, profiling, biosensing, screening, cell imaging, and bacteria detection.

Introduction

Over the past decades, research on nanoscience and nanotechnology has increased dramatically, and the scope for nanomaterials in new applications is continuously being extended (*1*). Recent investigations of functionalized nanomaterials have for example advanced the life science area, providing versatile

In Petite and Sweet: Glyco-Nanotechnology as a Bridge to New Medicines; Huang, X., et al.;
ACS Symposium Series; American Chemical Society: Washington, DC, 2011.

platforms in biology, biomedicine and biotechnology. For these applications, nanomaterials research is highly interdisciplinary, and merges the fields of materials science, chemistry, physics, biology, medicine and engineering, yielding core frameworks possessing multiple, biocompatible, and selective functionalities (*2*). These remarkable materials exhibit important physico-chemical properties, and constitute powerful tools in numerous applications to study biological processes, such as cell communication, enzymatic activity, protein interaction, and DNA hybridization (*3–7*). Taking advantage of pioneering synthetic work and physical properties investigated over the past decades, the research focus of the field is now progressing into developing diverse and versatile nanomaterials-based applications, and adopting nanomaterials into biomedicine (*8–13*). Rapid development of device fabrication has thus led to a number of commercially available clinical applications, including nano-based medicines, imaging and drug-delivery systems.

Carbohydrates, one of the most important classes of compounds in living systems, are involved in a wide variety of biological recognition events through their interactions with proteins and other biomolecules (*14–20*). The study of these processes and mechanisms is a significant challenge in glycoscience. This is primarily due to 1) the complexity of cellular glycans and hence the difficulty to obtain pure compounds in sufficient quantities, and 2) the inherent weak binding of monovalent carbohydrates to proteins. Thus, there is an urgent need to facilitate the development of new methodologies. In this respect, multivalent materials have shown especially high potential to address these challenges. Scaffolds coupled with high density glycans have been produced to mimic the glycan clustering effect presented on cell surfaces, enhancing the affinity to carbohydrate-binding entities (*21–23*), including carbohydrate-conjugated peptides, lipids, and proteins (*24*, *25*). Glyconanomaterials exert in this context particular potential, since they combine the unique characteristics of nanosized objects, with the synthetic efficiency and presentation versatility of surface-tethered carbohydrate ligands, allowing for the comprehensive probing and analysis of biological processes associated with glycans (*26*).

One of the essential steps in glyconanomaterial fabrication is to develop efficient, and highly controlled surface coupling chemistry (*27*). In this chapter, common approaches to synthesizing glyconanomaterials are briefly summarized, ranging from simple adsorption to different covalent coupling reactions (see also other chapters in this volume for more examples). These methods generally rely on physisorption or derivatized glycan structures carrying for example, thiol, silane or phosphate functionalities. All of these are associated with specific advantages and drawbacks, and new methods are required to advance the field further. Of special interest is to develop efficient chemistry to conjugate underivatized carbohydrates onto nanomaterials, in order to avoid glycan derivatization schemes.

We have focused our efforts on photoconjugation techniques using photochemically initiated perfluorophenylazide (PFPA) chemistry, resulting in high control, efficiency and versatility of the functionalization process. We have also developed a very straightforward method to synthesize glyconanomaterials by coupling underivatized carbohydrates using this photochemistry. In this

Downloaded by STANFORD UNIV GREEN LIBR on June 3, 2012 | http://pubs.acs.org
Publication Date (Web): December 13, 2011 | doi: 10.1021/bk-2011-1091.ch004

chapter, various photoconjugation approaches will be discussed and summarized. Examples will be given where the synthesized glyconanomaterials are applied to study glycan-lectin interactions, to detect and image bacteria, and to screen glycan-binding lectins on glycan microarrays.

Synthetic Methods to Glyconanomaterials

Non-Covalent Conjugation

One of the general strategies for conjugating biomolecules including carbohydrates/glycans onto nanomaterials is through adsorption. This strategy relies on weak, non-covalent interactions between the carbohydrate structures and the surface, such as hydrogen bonding, electrostatic interactions, van der Waals' forces and hydrophobic effects. For example, Coulon and coworkers incubated thioglycolic acid-stabilized CdTe quantum dots (QDs) with mannose (Man), glucose (Glc) or galactose (Gal), and used the resulting glyconanoparticles for labeling and detecting yeast cells (*28*). A synthetic protocol to dextran-coated CdS-ZnS QDs was described by Chen *et al.* in 2003, where negatively-charged carboxymethyldextran was adsorbed onto QDs coated with positively-charged polylysine via electrostatic interactions (*29*). Another versatile method was reported by Huang *et al.* where metallic glyconanoparticles were prepared (*30*). Au, Ag, Pt and Pd nanoparticles were synthesized by reducing metal salts in the presence of chitosan where ligand adsorption occurred during nanoparticle formation (Figure 1). The non-covalent approach was also adapted in the preparation of QDs and magnetic beads by Sun *et al.* in 2004 (*31*). The authors developed a strategy of grafting high-density biotin-terminated carbohydrate polymers onto streptavidin-derivatized QDs and magnetic beads, which were used to recognize lectins (Figure 2). Ahmed *et al.* described a one-pot method of synthesizing cationic glycopolymer-stabilized gold nanoparticles (*32*). The resulting glyconanoparticles served as effective gene delivery scaffolds, which exhibited a unique property of forming complexes with DNA (Figure 3). Assali and coworkers functionalized carbon nanotubes (CNTs) using pyrene-modified neoglycolipids (*33*). The resulting carbohydrate-CNT bundles were used to selectively recognize lectins.

Downloaded by STANFORD UNIV GREEN LIBR on June 3, 2012 | http://pubs.acs.org
Publication Date (Web): December 13, 2011 | doi: 10.1021/bk-2011-1091.ch004

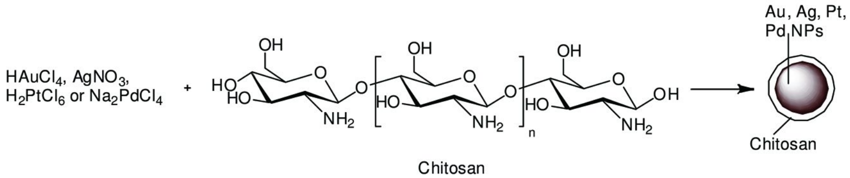

Figure 1. Non-covalent attachment of chitosan onto Au, Ag, Pt and Pd nanoparticles (30).

In Petite and Sweet: Glyco-Nanotechnology as a Bridge to New Medicines; Huang, X., et al.;
ACS Symposium Series; American Chemical Society: Washington, DC, 2011.

Downloaded by STANFORD UNIV GREEN LIBR on June 3, 2012 | http://pubs.acs.org
Publication Date (Web): December 13, 2011 | doi: 10.1021/bk-2011-1091.ch004

As noticed from these examples, a general advantage of the adsorption strategy is that the reaction conditions can be relatively mild. However, without covalent bonding to the carbohydrate structures, this methodology is generally limited to (charged) polysaccharides, where efficient adsorption can be obtained. In addition, due to the nature of most non-covalent interaction types, the resulting bonds are relatively random and disordered. The inherently weak bond strength may also lead to potential desorption of the carbohydrate ligands during the subsequent biomolecular interactions, which can be a significant drawback impacting the outcome of the analyses.

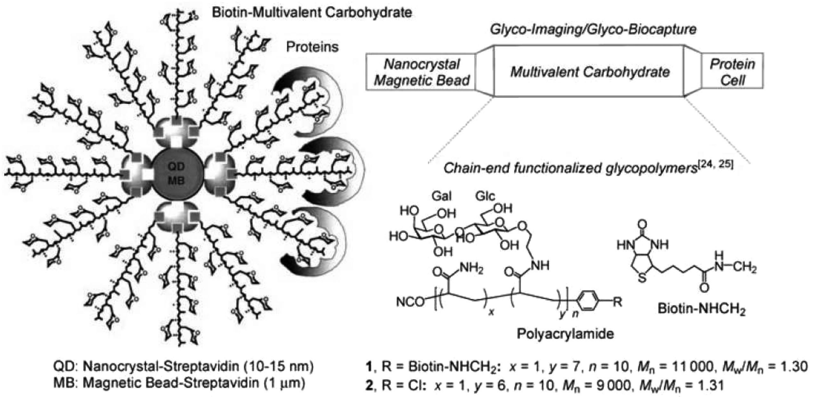
Biotin-Multivalent Carbohydrate
Proteins
QD
MB
Glyco-Imaging/Glyco-Biocapture
Nanocrystal Magnetic Bead
Multivalent Carbohydrate
Protein Cell
Chain-end functionalized glycopolymers[24, 25]
Gal
Glc
Polyacrylamide
Biotin-NHCH2
QD: Nanocrystal-Streptavidin (10-15 nm)
MB: Magnetic Bead-Streptavidin (1 μm)
1, R = Biotin-NHCH2: x = 1, y = 7, n = 10, Mn = 11 000, Mw/Mn = 1.30
2, R = Cl: x = 1, y = 6, n = 10, Mn = 9 000, Mw/Mn = 1.31

Figure 2. Preparation of glyco-QDs and magnetic nanoparticles via biotin-streptavidin interactions. (Reprinted with permission from reference (31). Copyright 2004 Wiley-VCH and Sons.)

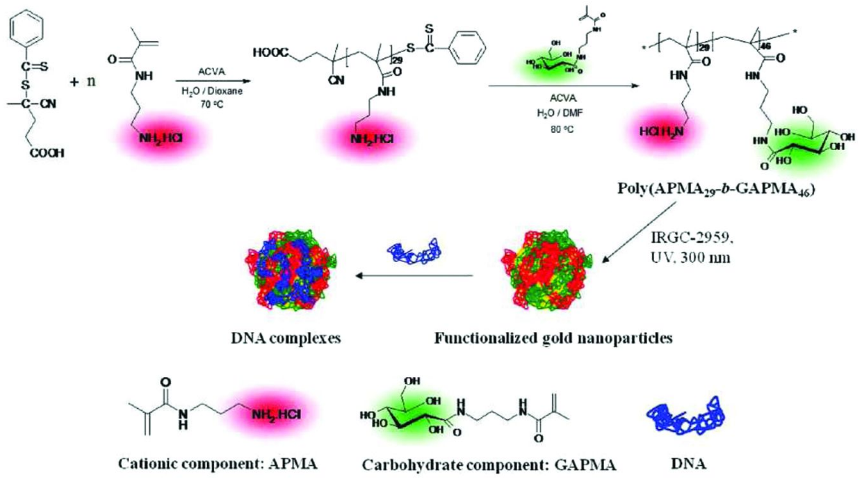
ACVA
H2O / Dioxane
70 °C
ACVA
H2O / DMF
80 °C
Poly(APMA29-b-GAPMA46)
IRGC-2959,
UV, 300 nm
DNA complexes
Functionalized gold nanoparticles
Cationic component: APMA
Carbohydrate component: GAPMA
DNA

Figure 3. Conjugation of glycopolymers to gold glyconanoparticles and subsequent formation of DNA complexes. Reprinted with permission from reference (32). Copyright 2009 American Chemical Society.

Downloaded by STANFORD UNIV GREEN LIBR on June 3, 2012 | http://pubs.acs.org
Publication Date (Web): December 13, 2011 | doi: 10.1021/bk-2011-1091.ch004

Covalent Conjugation

The drawbacks encountered using non-covalent protocols are circumvented using covalent conjugation protocols, where robust and well-controlled glyconanomaterials can be synthesized. This approach is more commonly used for conjugating carbohydrates to nanomaterials, and is becoming established for various applications. Among different types of biofunctional nanomaterials, gold nanoparticles (Au NPs) maintain a privileged position. Au NPs of different sizes are relatively easy to synthesize, and can be adapted for use in aqueous solutions, thus providing a nano-sized platform to study biological interactions (*34*). The most popular protocol makes use of the self-assembly behavior of thiols or disulfides on Au surfaces via the Au-S bond, and the first methodology of preparing alkanethiol-protected Au NPs in a two-phase system was reported by Brust *et al.* in 1994 (*35*). The thiol-protected Au NPs provide a robust, reproducible and well-characterized system for general applications in nanoscience and nanotechnology, and numerous examples of Au NPs terminated with different functional groups have been presented. Biomolecules such as nucleic acids, peptides, proteins, and carbohydrates, have also been successfully applied to the Au NP system (*3*, *24*, *36*).

Seminal studies regarding specific carbohydrate-functionalized Au NPs, so-called Au glyconanoparticles, were presented by de la Fuente *et al.* and Otsuka *et al.* in 2001 (*37*, *38*). In the first of these, the authors used derivatives of lactose (Lac, Galβ1-4Glc) and the Lewis^x trisaccharide (Le^x, CD15, Galβ1-4[Fucα1-3]GlcNAc), carrying thiol-terminated alkane/polyethylene glycol-linkers, and adopted thiol-gold chemistry to obtain carbohydrate-functionalized Au NPs while reducing $HAuCl_4$ with $NaBH_4$. The glyconanoparticles were subsequently used as probes in carbohydrate-carbohydrate self-interaction studies. Based on this successful strategy, other glyconanoparticles based on monosaccharides (Glc), disaccharides (maltose, Glcα1-4Glc) and a tetrasaccharide (Lewis^y tetrasaccharide, Le^y, CD174, Fucα1-2Galβ1-4[Fucα1-3]GlcNAc) were prepared, with which various biological interactions were investigated (Figure 4) (*37*, *39*, *40*). Otsuka *et al.* instead developed a stepwise strategy, where a thiolated derivative of poly(ethylene glycol) (PEG) was first used to fabricate PEG-coated Au NPs, and a lactose derivative was subsequently conjugated in three steps to the PEG-chains. The resulting glyconanoparticles were in this case evaluated for lectin (*Ricinus communis* agglutinin, RCA-I) interaction studies (*38*). Similar strategies have subsequently been adopted to produce Au glyconanoparticles with a variety of thiolated carbohydrates (*41–46*). Furthermore, thiol chemistry was also applied in the preparation of glyco-QDs (*47*, *48*), yielding a range of functional glyconanomaterials for use in biological imaging, targeting and sensing (*49–51*). For example, Robinson *et al.* described CdSe/ZnS core-shell QDs treated with *N*-acetylglucosamine (GlcNAc) and Man disulfide derivatives, resulting in GlcNAc- and Man-encapsulated QDs that were subsequently evaluated for binding to wheat germ agglutinin (WGA) and sperm from mice, pigs and sea-urchins (*52*).

Downloaded by STANFORD UNIV GREEN LIBR on June 3, 2012 | http://pubs.acs.org
Publication Date (Web): December 13, 2011 | doi: 10.1021/bk-2011-1091.ch004

Parallel to gold-based nanomaterials, silver nanoparticles (Ag NPs) have also been evaluated for carbohydrate functionalization. In an example taking advantage of reversible covalent bonds, Zhang *et al.*, for example, reported a ligand-exchange synthesis of thiolated boronic acid-capped Ag NPs, which were then used to attach a monosaccharide (Glc) and a polysaccharide (dextran) (*53*). In a more recent study, Veerapandian *et al.* reported the preparation of glucosamine-functionalized Ag NPs using a stepwise approach where surfactant adsorption was first combined with thiol-Ag bond formation, and the carbohydrate coupled to carboxyl-terminated chains (*54*). The materials were subsequently evaluated for bacterial growth inhibition.

Magnetite (Fe_3O_4) constitutes another type of core structure, in this case adding magnetic properties to the nanomaterials. In a recent example, El-Boubbou *et al.* prepared Fe_3O_4-based glyconanoparticles functionalized with a panel of monosaccharides (Man, Gal, Fuc, *N*-acetylneuraminic acid (Neu5Ac), GlcNAc) via amide coupling and copper-catalyzed azide-alkyne cycloaddition (CuAAC or "click" reaction), and application of the resulting nanoparticles in magnetic resonance imaging facilitated the detection of cancer cells (Figure 5) (*55*).

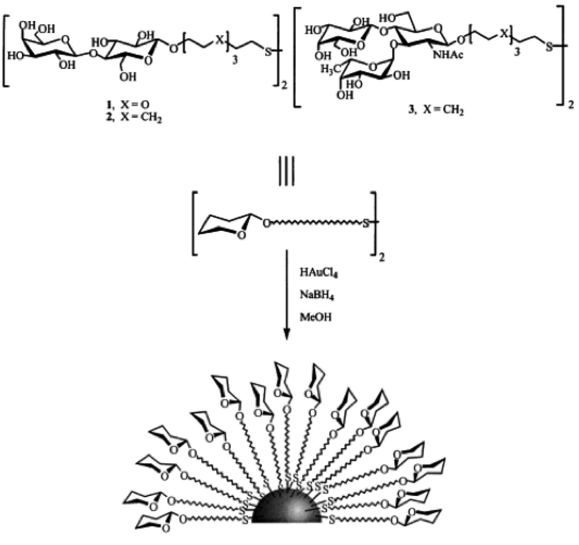

Figure 4. Conjugation of thiolated carbohydrates onto gold nanoparticles. Reprinted with permission from reference (37). Copyright 2001 Wiley-VCH and Sons.

Downloaded by STANFORD UNIV GREEN LIBR on June 3, 2012 | http://pubs.acs.org
Publication Date (Web): December 13, 2011 | doi: 10.1021/bk-2011-1091.ch004

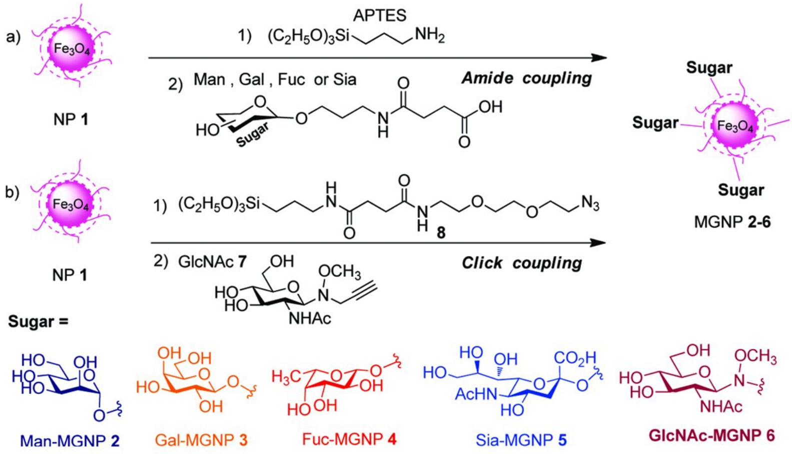

Figure 5. Synthesis of carbohydrate-functionalized magnetic nanoparticles via amide and click coupling. Reprinted with permission from reference (55). Copyright 2010 American Chemical Society.

Photo-Initiated Coupling Methods and Applications

In addition to the aforementioned conjugation methods, based on adsorption or chemical conjugation to primarily metal-based surfaces, photochemistry can be used to efficiently synthesize glyconanomaterials in a controlled way. An attractive approach is in this context to utilize the reactive perfluorophenylazides (PFPAs). This group of structures possesses the ability to form covalent bonds to a wide range of organic materials, and has proven especially useful for carbohydrate functionalization. Under photochemical (or thermal) activation conditions, the PFPA moiety decomposes to an electron deficient perfluorophenylnitrene, which has sufficient life time in the singlet state, leading to efficient insertion and addition reactions (Figure 6) (*56*). Perfluorophenylnitrenes from PFPAs thus efficiently insert into C-H and N-H bonds, or adds to C=C bonds, creating covalent linkages to the acceptor structures (*57*). PFPAs carrying carbonyl functionalities can be readily converted to *e.g.* esters, carboxylic acids and amides, allowing for efficient and versatile functionalization of the core structure (*56*).

PFPA-based chemistry has proven especially useful for conjugation to structures that lack reactive functional groups, such as polyolefins (*58–63*), carbon materials (*64*), and nanoparticles (*65–70*), providing highly robust and stable linkages. PFPAs have also been used to functionalize polymeric material *per se*, creating functional nanolayers (*59*, *67*, *71*). To conjugate carbohydrates, two general approaches can be envisioned. The first approach involves PFPA-functionalized carbohydrates whereby the PFPA-carbohydrate conjugates are synthesized and subsequently immobilized on polymeric or carbon substrates by photoactivation (Figure 7a). In the second approach, nanomaterials are functionalized with PFPA, and carbohydrates are subsequently immobilized by photoactivation (Figure 7b).

Downloaded by STANFORD UNIV GREEN LIBR on June 3, 2012 | http://pubs.acs.org
Publication Date (Web): December 13, 2011 | doi: 10.1021/bk-2011-1091.ch004

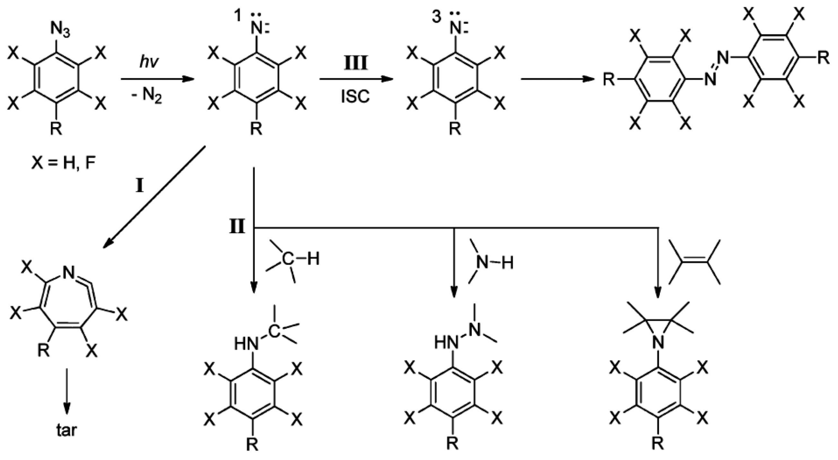

Figure 6. Simplified description of phenylazide photochemistry. Reprinted with permission from reference (56). Copyright 2010 American Chemical Society.

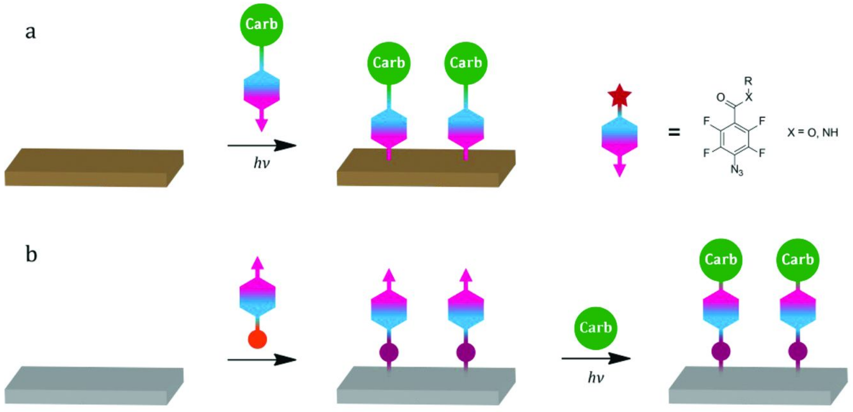

Figure 7. Two general approaches to photocoupling of carbohydrates using PFPA; a) Coupling of carbohydrate-conjugated PFPA photoprobes onto material such as polymers or CNTs; b) Functionalization of substrates (e.g., gold, iron oxides, silica) with activated PFPA-conjugates, and subsequent coupling of underivatized carbohydrates.

Downloaded by STANFORD UNIV GREEN LIBR on June 3, 2012 | http://pubs.acs.org
Publication Date (Web): December 13, 2011 | doi: 10.1021/bk-2011-1091.ch004

Approach I. Carbohydrate-PFPA Conjugates

In order to apply this chemistry to glyconanomaterials, Pei *et al.* reported in 2007 the fabrication of polymer thin films via PFPA formed by treating amine-coated glass with *N*-hydroxysuccinimide (NHS)-activated PFPA (*60*). The resulting polymeric layers were then functionalized with a panel of PFPA-functionalized carbohydrate structures (Man, Glc, Gal, Fuc, GlcNAc, cellobiose (Glcβ1-4Glc), lactose (Lac), arabinose (Ara), xylose (Xyl)) and subsequently interrogated with fluorescently-labeled lectins (*Bandeiraea simplicifolia* lectin II (BS-II), peanut agglutinin (PNA), Concanavalin A (Con A), soybean agglutinin (SBA), Figure 8). The resulting surfaces showed selective binding to the respective cognate lectins, validating the approach. In another example employing a similar strategy, polymer-coated quartz crystals were functionalized with PFPA-conjugated carbohydrates (Man, Gal, Fuc) and evaluated for interaction with lectins (Con A, *Pisum sativum* agglutinin (PSA), *Ulex europaeus* lectin I (UEA-I), *Viscum album* agglutinin (VAA)) in a quartz crystal microbalance (QCM) flow-through system (*59*). It was thus shown that PFPAs can be used both to efficiently coat various surfaces with low molecular weight, hydrophilic polymers and to functionalize polymers with carbohydrate species (Figure 9). The method was subsequently further developed in addressing the effects of surface glycan presentation, of high importance for efficient protein-carbohydrate recognition. The glycosidic structures and linker lengths were thus evaluated in lectin interaction studies (Figure 10) (*72*). PFPA-conjugated carbohydrate derivatives with different linker lengths were synthesized, and subsequently immobilized on polymer-coated surface plasmon resonance- (SPR)-surfaces. The results underscored the importance of the linker length, and the necessity of optimizing the corresponding structure. In a complementary study, Madwar *et al.* reported the implementation of similar structures for single molecule force spectroscopy of the Con A-Man interaction. Atomic force microscopy (AFM) tips functionalized with Con A were thus subjected to mannose-presenting surfaces prepared using PFPA-conjugation, and the rupture force and kinetics of the Con A-Man interaction were evaluated (*58*).

The PFPA chemistry can also be combined with other conjugation methods, and Norberg *et al.* recently reported a method in which a range of polymeric surfaces were conjugated with alkyne-functionalized PFPA (*73*). Carbohydrate presenting surfaces were produced in a stepwise methodology, where the alkyne layers were functionalized with a range of carbohydrate azides (Man, Gal, GlcNAc) by CuAAC chemistry, and the resulting materials analyzed with QCM (Figure 11). The materials were evaluated for interaction with several unlabeled lectins (Con A, WGA, PSA, RCA-I, BS-II), and results showed high binding and good selectivity to the respective cognate lectins, demonstrating the potential of the method (*74*). More recently, the concept was further extended towards photochemical conjugation using photoinitiated radical thiol-ene/-yne chemistry (*75*). In this case, alkene or alkyne-functionalized materials were prepared using the PFPA chemistry, and subsequently conjugated with carbohydrate thiol derivatives. The resulting surfaces were analyzed by QCM, validating the approach for a series of carbohydrate-lectin interaction systems.

Downloaded by STANFORD UNIV GREEN LIBR on June 3, 2012 | http://pubs.acs.org
Publication Date (Web): December 13, 2011 | doi: 10.1021/bk-2011-1091.ch004

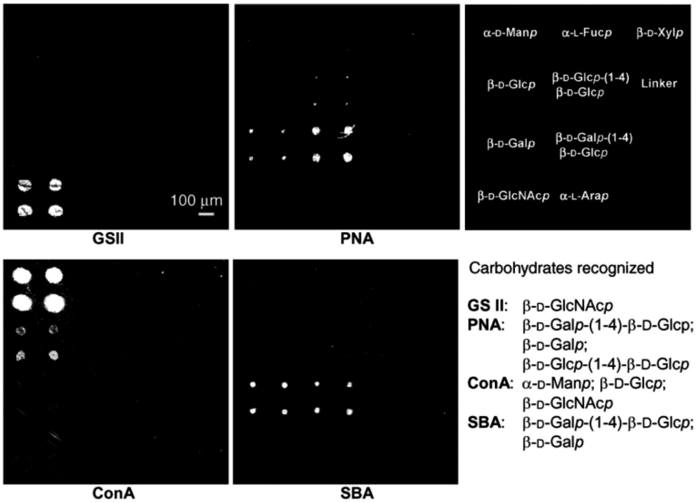
α-D-Manp
α-L-Fucp
β-D-Xylp
β-D-Glcp
β-D-Glcp-(1-4) β-D-Glcp
Linker
β-D-Galp
β-D-Galp-(1-4) β-D-Glcp
β-D-GlcNAcp
α-L-Arap
100 μm
GSII
PNA
ConA
SBA
Carbohydrates recognized
GS II: β-D-GlcNAcp
PNA: β-D-Galp-(1-4)-β-D-Glcp; β-D-Galp; β-D-Glcp-(1-4)-β-D-Glcp
ConA: α-D-Manp; β-D-Glcp; β-D-GlcNAcp
SBA: β-D-Galp-(1-4)-β-D-Glcp; β-D-Galp

Figure 8. Illustration of carbohydrate microarrays produced with PFPA-coupled carbohydrate structures. Modified from reference (60), copyright Wiley-VCH Verlag GmbH & Co. KGaA. Reproduced with permission.

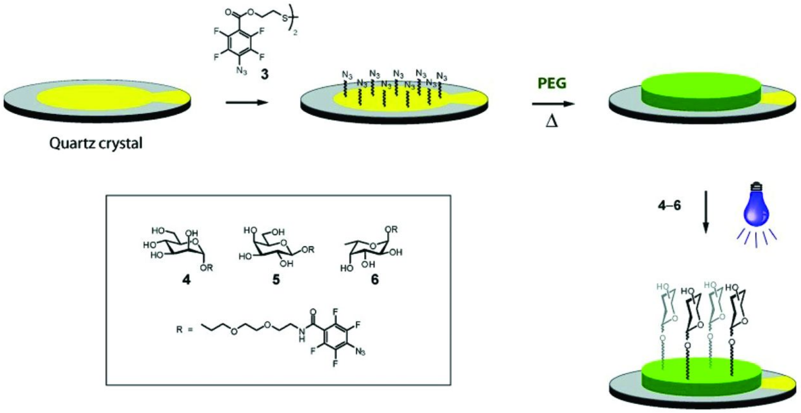
3
Quartz crystal
PEG
Δ
4–6
4
5
6
R =

Figure 9. Illustration of double surface functionalization method. Gold-plated quartz crystals were covalently functionalized with a polymer thin film using PFPA-disulfides. The polymer layer was then conjugated using a range of PFPA-coupled carbohydrate structures. Reprinted with permission from reference (59). Copyright 2007 American Chemical Society.

Downloaded by STANFORD UNIV GREEN LIBR on June 3, 2012 | http://pubs.acs.org
Publication Date (Web): December 13, 2011 | doi: 10.1021/bk-2011-1091.ch004

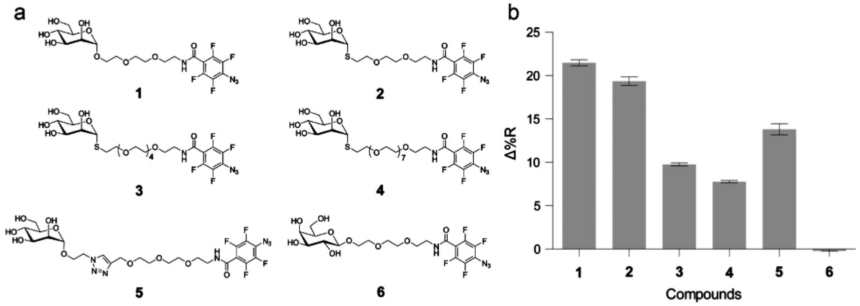

Figure 10. Evaluation of linker length effect on protein binding; a) Carbohydrate structures with different linker lengths utilized in the study; b) Lectin binding response in subsequent SPR binding experiments. Reproduced by permission of reference (72). The Royal Society of Chemistry (RSC).

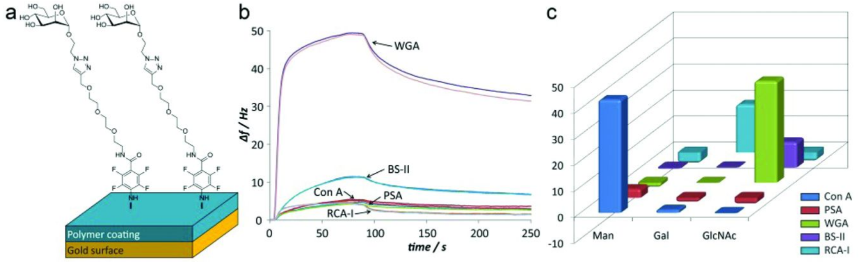

Figure 11. Carbohydrate-presenting surfaces based on PFPA-coupling and CuAAC chemistry; a) Schematic illustration of Man-presenting surfaces; b) Lectin binding pattern to GlcNAc-functionalized polystyrene showing selective binding of GlcNAc-binding lectins WGA and BS-II; c) Lectin binding pattern to poly(ethylene glycol)-functionalized carbohydrate surfaces. Reprinted with permission from reference (74). Copyright 2011 American Chemical Society.

Approach II: Direct Conjugation of Underivatized Carbohydrates

As highlighted in the aforementioned examples, current preparation approaches to carbohydrate-conjugated nanomaterials are generally based on derivatized carbohydrate structures, most often taking advantage of sulfur-metal bonds. The direct conjugation of underivatized carbohydrates to surfaces is however still very challenging, generally targeting the reducing end of the glycan chains. These methods are however often associated with ring opening of the terminal monosaccharide unit, which could affect the binding properties of shorter structures, or may otherwise require relatively harsh conditions. Efficient conjugation methods of underivatized entities would thus greatly facilitate the use of native glycan structures that are difficult to isolate in larger quantities. To address this challenge, PFPA photochemistry has been developed to conjugate underivatized carbohydrate structures to gold (*69*), magnetic (*68*), and silica nanoparticles using the strategy outline in Figure 7b (*70*). A similar strategy was also reported by Joester *et al.*, where hyaluronan structures were grafted to polystyrene beads via PFPA (*76*). A key step of this strategy is to introduce PFPA moieties to the nanomaterial core structures. Towards this end, PFPA-structures derivatized with different terminal groups, including thiols/disulfides, phosphates, or silanes were designed and synthesized (Figure 12). These structures were subsequently used to functionalize different nanomaterials, such as gold-, iron oxide- and silica nanoparticles. Photo-initiated conjugation of underivatized carbohydrate structures was then performed under a fast UV irradiation condition, conveniently applying a solution of the underivatized carbohydrates to the PFPA-modified nanomaterials (Figure 12). This protocol proved very reliable, general, and applicable to a wide range of carbohydrate structures. Most importantly, the immobilized carbohydrates retained their recognition abilities and selectivities. This was demonstrated for a range of nanomaterials in various applications, validating the approach. For instance, Wang and coworkers successfully conjugated 21 different carbohydrate structures including mono-, oligo- and poly-saccharides, as well as non-reducing sugars on a poly(L-lysine)-based PFPA surface with high coupling efficiencies (*77*). The resulting surfaces were characterized with X-ray photoelectron spectroscopy (XPS), and affinity to lectins interrogated with fluorescence and surface plasmon resonance imaging (SPRi). Tyagi *et al.* produced surfaces with increasing PFPA densities, to which underivatized mono- (Man, Glc, Gal), di- (Manα1-2Man) and trisaccharides (Manα1-3[Manα1-6]Man) were covalently conjugated. Interaction studies with different lectins (Con A, SBA, BS-II) using SPRi showed that the affinity was highly dependent on the ligand density (*78*).

In 2009, Wang *et al.* described the fabrication of carbohydrate-presenting Au NPs following this approach. Ligand exchange of citrate-stabilized Au NPs using a disulfide-containing PFPA derivative first produced PFPA-functionalized Au NPs, which were subsequently conjugated with a range of underivatized carbohydrate structures (Man, Glc, Gal, Manα1-4Man, maltose, Glcα1-3Glc, Galα1-3Gal) (*69*). Applying these glyconanoparticles to various lectins (Con A, SBA, BS-II, PNA) led to selective interactions. For example, aggregation of Man-conjugated Au NPs occurred when Con A was applied, and a red-shift of the SPR absorption peak was observed, associated with a rapid color change of Au NPs solution (Figure 13a). In addition, the binding strength measured by the SPR red-shift was consistent with the binding affinity of the free carbohydrate with the corresponding lectin (*69*). A similar protocol to glyconanoparticles was also adopted to generate Au NPs targeting the cyanobacterial lectin cyanovirin-N (CV-N) (*79*). In this case, oligo-mannose structures (Manα1-2Man, Manα1-2Manα1-2Man) were conjugated to the Au NPs using PFPA photochemistry, and the resulting glyconanoparticles used to evaluate the binding to different CV-N mutants. Using a fluorescence competition assay, the apparent binding constants of the two different binding sites of CV-N were determined.

Downloaded by STANFORD UNIV GREEN LIBR on June 3, 2012 | http://pubs.acs.org
Publication Date (Web): December 13, 2011 | doi: 10.1021/bk-2011-1091.ch004

Downloaded by STANFORD UNIV GREEN LIBR on June 3, 2012 | http://pubs.acs.org
Publication Date (Web): December 13, 2011 | doi: 10.1021/bk-2011-1091.ch004

Liu *et al.* used a phosphate-linked PFPA structure to functionalize iron oxide NPs of hematite and magnetite, which were then photo-conjugated with Man (Figure 14) (*68*). The resulting glyconanoparticles showed selective binding to the lectin Con A, and *E. coli* strain ORN178 which possesses a Man-binding FimH domain on type 1 pili (Figure 13b).

Recently, Wang *et al.* developed dye-doped fluorescent silica NPs (FSNPs) as highly efficient labels for glycans using a similar approach (Figure 15) (*70*). The FSNPs were functionalized with a PFPA-silane structure, to which mono- (Man, Glc, Gal) and oligosaccharides (Manα1-2Man, Manα1-3[Manα1-6]Man, maltopentaose) were conjugated using the PFPA-based photocoupling reaction. The FSNP-labeled glycans retained their specific binding activities with lectins, and the FSNPs could also be applied in the imaging and detection of *E. coli* strain ORN178, targeting the FimH lectin (Figure 13c). The utility of the method was further demonstrated in the study of carbohydrate-lectin interactions on a lectin microarray (Figure 13d). From these results, a new application of FSNPs was recently developed, resulting in a high-throughput screening protocol for glycans on a so-called lectin "super-microarray" (unpublished data).

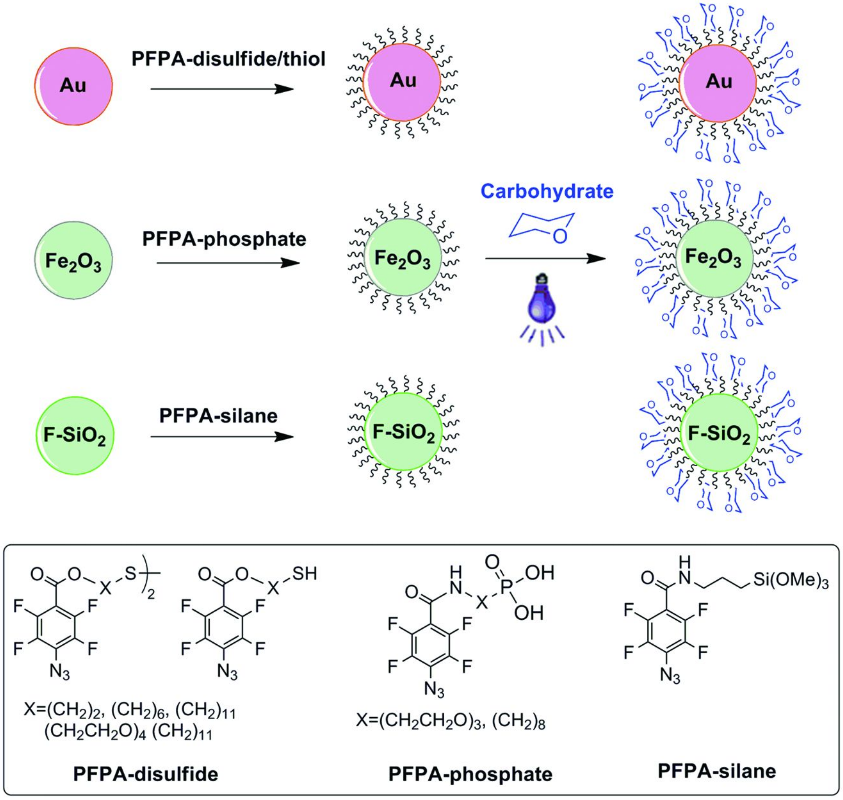
Au
PFPA-disulfide/thiol
Au
Au
Carbohydrate
Fe2O3
PFPA-phosphate
Fe2O3
Fe2O3
F-SiO2
PFPA-silane
F-SiO2
F-SiO2
X=(CH2)2, (CH2)6, (CH2)11
(CH2CH2O)4 (CH2)11
X=(CH2CH2O)3, (CH2)8
Si(OMe)3
PFPA-disulfide
PFPA-phosphate
PFPA-silane

Figure 12. Synthesis of glyconanoparticles by direct conjugation of underivatized carbohydrates on PFPA-functionalized nanoparticles.

Downloaded by STANFORD UNIV GREEN LIBR on June 3, 2012 | http://pubs.acs.org
Publication Date (Web): December 13, 2011 | doi: 10.1021/bk-2011-1091.ch004

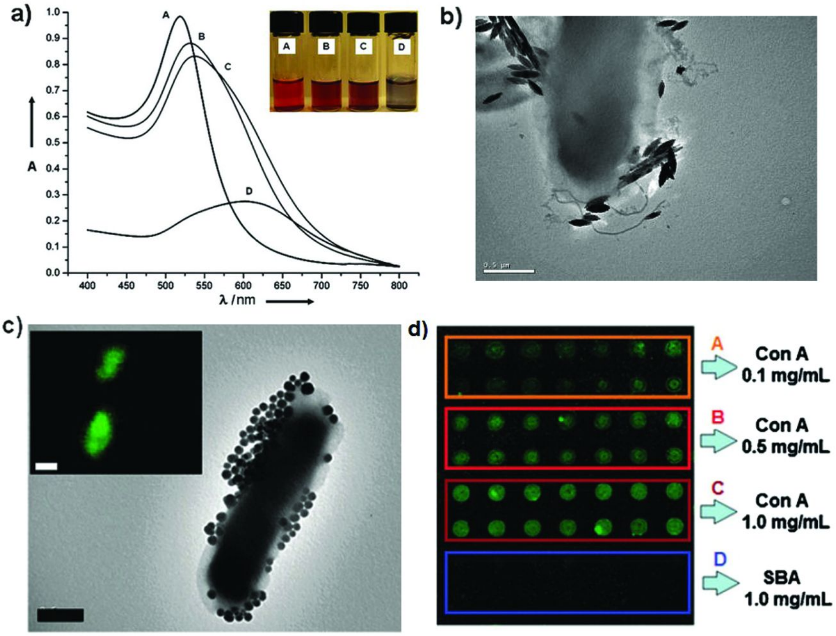

Figure 13. (a) UV-vis spectra (insert: Au nanoparticle solutions) of Au NPs (A), PFPA-disulfide-functionalized Au NPs (B), Au NPs with surface-coupled α-1,4-mannobiose (C), and subsequent treatment with Con A (D) Reproduced by permission of reference (69). The Royal Society of Chemistry (RSC); (b) TEM images of mannose-modified hematite nanoparticles after treatment with E. coli strain ORN178 (Reprinted with permission from Reference (68). Copyright 2009 American Chemical Society); (c) TEM and fluorescent image of mannose-modified fluorescent silica nanoparticles (FSNP-Man) after treatment with E. coli strain ORN178. Reproduced by permission of reference (70). The Royal Society of Chemistry (RSC); (d) Fluorescence image of the lectin microarray after treating with FSNP-Man. Reproduced by permission of reference (70). The Royal Society of Chemistry (RSC).

Downloaded by STANFORD UNIV GREEN LIBR on June 3, 2012 | http://pubs.acs.org
Publication Date (Web): December 13, 2011 | doi: 10.1021/bk-2011-1091.ch004

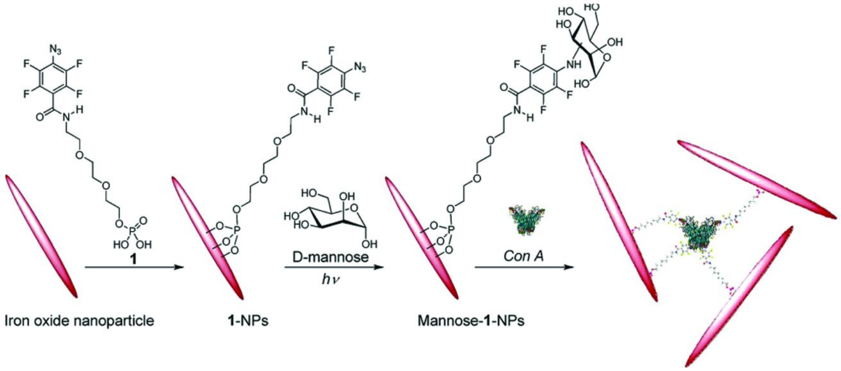
Iron oxide nanoparticle
1
1-NPs
D-mannose
hν
Mannose-1-NPs
Con A

Figure 14. Preparation of magnetic glyconanoparticle via PFPA coupling chemistry. Reprinted with permission from reference (68). Copyright 2009 American Chemical Society.

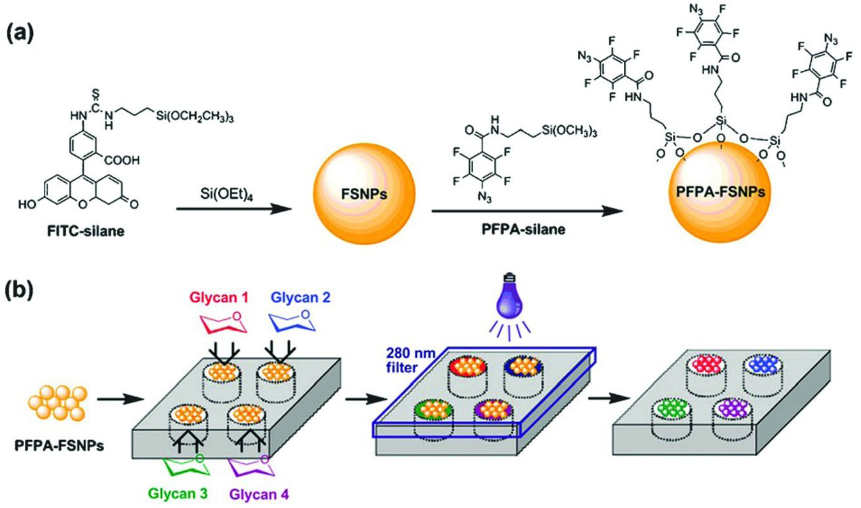
(a)
FITC-silane
Si(OEt)4
FSNPs
PFPA-silane
PFPA-FSNPs
(b)
Glycan 1
Glycan 2
280 nm filter
PFPA-FSNPs
Glycan 3
Glycan 4

Figure 15. Synthesis of PFPA-functionalized dye-doped silica nanoparticles and photochemically-initialed carbohydrate conjugation. Reproduced by permission of reference (70). The Royal Society of Chemistry (RSC).

Downloaded by STANFORD UNIV GREEN LIBR on June 3, 2012 | http://pubs.acs.org
Publication Date (Web): December 13, 2011 | doi: 10.1021/bk-2011-1091.ch004

Conclusion

In a relatively short time, the glycoscience field has experienced rapid progress, in part owing to recent advancements of new carbohydrate-presenting nanomaterials. The development of new surface coupling chemistry is however essential for further improvements of glyconanomaterials, currently relying on traditional protocols primarily based on derivatized carbohydrates. In this respect, PFPA-based photochemistry has evolved as a highly versatile and efficient conjugation method. This method can be used for immobilizing carbohydrate structures to a variety of nanomaterials, including polymers, silicon wafers, gold, iron oxide and silica nanoparticles. A wide range of carbohydrate structures have been efficiently immobilized on surfaces and nanoparticles by fast and efficient light activation, resulting in high coupling yields as well as high ligand surface coverage. Most importantly, a series of validation studies have confirmed that the surface-bound carbohydrates retained their affinities and selectivities towards the corresponding binding lectins. The results have also shown that the design and fabrication of glyconanomaterials, as well as the in-depth understanding of the associated ligand presentation and multivalency effects, can greatly enhance the fundamental understanding of carbohydrate-lectin interactions. These comprehensive studies will furthermore facilitate the development of glyconanomaterials-based tools and devices for applications such as diagnosis and nanomedicine.

References

1. Koch, C. C. *Nanostructured Materials: Processing Properties, and Potential Applications*; Noyes Publications: Norwich, NY, 2002.
2. *Biomedical Nanostructures* Gonsalves, K., Halberstadt, C., Laurencin, C. T., Nair, L., Eds.; John Wiley & Sons, Inc.: Hoboken, NJ, 2007.
3. Elghanian, R.; Storhoff, J. J.; Mucic, R. C.; Letsinger, R. L.; Mirkin, C. A. *Science* **1997**, *277*, 1078–1081.
4. Liu, R.; Liew, R.; Zhou, J.; Xing, B. *Angew. Chem., Int. Ed.* **2007**, *46*, 8799–8803.
5. Oh, E.; Lee, D.; Kim, Y.-P.; Cha, S. Y.; Oh, D.-B.; Kang, H. A.; Kim, J.; Kim, H.-S. *Angew. Chem., Int. Ed.* **2006**, *45*, 7959–7963.
6. Storhoff, J. J.; Lucas, A. D.; Garimella, V.; Bao, Y. P.; Müller, U. R. *Nat. Biotechnol.* **2004**, *22*, 883–887.
7. Tsai, C. S.; Yu, T. B.; Chen, C. T. *Chem. Commun.* **2005**, *34*, 4273–4275.
8. Cipolla, L.; Peri, F.; Airoldi, C. *Anti-Cancer Agents Med. Chem.* **2008**, *8*, 92–121.
9. De, M.; Ghosh, P. S.; Rotello, V. M. *Adv. Mater.* **2008**, *20*, 4225–4241.
10. Jaiswal, J. K.; Mattoussi, H.; Mauro, J. M.; Simon, S. M. *Nat. Biotechnol.* **2003**, *21*, 47–51.
11. Rojo, J.; Díaz, V.; de la Fuente, J. M.; Segura, I.; Barrientos, A. G.; Riese, H. H.; Bernade, A.; Penadés, S. *ChemBioChem* **2004**, *5*, 291–297.
12. Sihelníková, L.; Tvaroška, I. *Chem. Pap.* **2007**, *61*, 237–255.

In Petite and Sweet: Glyco-Nanotechnology as a Bridge to New Medicines; Huang, X., et al.;
ACS Symposium Series; American Chemical Society: Washington, DC, 2011.

13. Sperling, R.; Rivera, G. P.; Zhang, F.; Zanella, M.; Parak, W. *Chem. Soc. Rev.* **2008**, *37*, 1896–1908.
14. Crocker, P. R.; Paulson, J. C.; Varki, A. *Nat. Rev. Immunol.* **2007**, *7*, 255–266.
15. Dube, D. H.; Bertozzi, C. R. *Nat. Rev. Drug Discovery* **2005**, *4*, 477–488.
16. Fuster, M. M.; Esko, J. D. *Nat. Rev. Cancer* **2005**, *5*, 526–542.
17. Liu, F.-T.; Rabinovich, G. A. *Nat. Rev. Cancer* **2005**, *5*, 29–41.
18. Ohtsubo, K.; Marth, J. D. *Cell* **2006**, *126*, 855–867.
19. Sharon, N. *Biochim. Biophys. Acta, Gen. Subj.* **2006**, *1760*, 527–537.
20. Szymanski, C. M.; Wren, B. W. *Nat. Rev. Microbiol.* **2005**, *3*, 225–237.
21. Huskens, J. *Curr. Opin. Chem. Biol.* **2006**, *10*, 537–543.
22. Lee, Y. C.; Lee, R. T. *Acc. Chem. Res.* **1995**, *28*, 321–327.
23. Mammen, M.; Choi, S. K.; Whitesides, G. M. *Angew. Chem., Int. Ed.* **1998**, *37*, 2755–2794.
24. Drechsler, U.; Erdogan, B.; Rotello, V. M. *Chem. Eur. J.* **2004**, *10*, 5570–5579.
25. Jayaraman, N. *Chem. Soc. Rev.* **2009**, *38*, 3463–3483.
26. Wang, X.; Ramström, O.; Yan, M. *Adv. Mater.* **2010**, *22*, 1946–1953.
27. Wang, X.; Liu, L.-H.; Ramström, O.; Yan, M. *Exp. Biol. Med.* **2009**, *234*, 1128–1139.
28. Coulon, J.; Thouvenin, I.; Aldeek, F.; Balan, L.; Schneider, R. *J. Fluoresc.* **2010**, *20*, 591–597.
29. Chen, Y.; Ji, T.; Rosenzweig, Z. *Nano Lett.* **2003**, *3*, 581–584.
30. Huang, H.; Yuan, Q.; Yang, X. *Colloids Surf., B.* **2004**, *39*, 31–37.
31. Sun, X. L.; Cui, W. X.; Haller, C.; Chaikof, E. L. *ChemBioChem* **2004**, *5*, 1593–1596.
32. Ahmed, M.; Deng, Z.; Liu, S.; Lafrenie, R.; Kumar, A.; Narain, R. *Bioconjugate Chem.* **2009**, *20*, 2169–2176.
33. Assali, M.; Leal, M. P.; Fernandez, I.; Baati, R.; Mioskowski, C.; Khiar, N. *Soft Matter* **2009**, *5*, 948–950.
34. El-Kouedi, M.; Keating, C. D. In *Nanobiotechnology*; Niemeyer, C. M., Mirkin, C. A., Eds.; Wiley-VCH: Weinheim, 2004.
35. Brust, M.; Walker, M.; Bethell, D.; Schiffrin, D. J.; Whyman, R. *J. Chem. Soc., Chem. Commun.* **1994**, 801–802.
36. Daniel, M.-C.; Astruc, D. *Chem. Rev.* **2003**, *104*, 293–346.
37. de La Fuente, J. M.; Barrientos, A. G.; Rojas, T. C.; Rojo, J.; Cañada, J.; Fernández, A.; Penadés, S. *Angew. Chem., Int. Ed.* **2001**, *40*, 2257–2261.
38. Otsuka, H.; Akiyama, Y.; Nagasaki, Y.; Kataoka, K. *J. Am. Chem. Soc.* **2001**, *123*, 8226–8230.
39. de Paz, J. L.; Ojeda, R.; Barrientos, A. G.; Penadés, S.; Martín-Lomas, M. *Tetrahedron: Asymmetry* **2005**, *16*, 149–158.
40. Hernáiz, M. J.; de la Fuente, J. M.; Barrientos, A. G.; Penadés, S. *Angew. Chem., Int. Ed.* **2002**, *41*, 1554–1557.
41. Earhart, C.; Jana, N. R.; Erathodiyil, N.; Ying, J. Y. *Langmuir* **2008**, *24*, 6215–6219.
42. Halkes, K. M.; Carvalho de Souza, A.; Maljaars, C. E. P.; Gerwig, G. J.; Kamerling, J. P. *Eur. J. Org. Chem.* **2005**, *2005*, 3650–3659.

Downloaded by STANFORD UNIV GREEN LIBR on June 3, 2012 | http://pubs.acs.org
Publication Date (Web): December 13, 2011 | doi: 10.1021/bk-2011-1091.ch004

43. Huang, C.-C.; Chen, C.-T.; Shiang, Y.-C.; Lin, Z.-H.; Chang, H.-T. *Anal. Chem.* **2009**, *81*, 875–882.
44. Marradi, M.; Alcántara, D.; de la Fuente, J. M.; García-Martín, M. L.; Cerdán, S.; Penadés, S. *Chem. Commun.* **2009**, 3922–3924.
45. Rojas, T. C.; de la Fuente, J. M.; Barrientos, A. G.; Penadés, S.; Ponsonnet, L.; Fernández, A. *Adv. Mater.* **2002**, *14*, 585–588.
46. Schofield, C. L.; Field, R. A.; Russell, D. A. *Anal. Chem.* **2007**, *79*, 1356–1361.
47. Babu, P.; Sinha, S.; Surolia, A. *Bioconjugate Chem.* **2007**, *18*, 146–151.
48. Svarovsky, S. A.; Barchi, J. J., Jr. In *Frontiers in Modern Carbohydrate Chemistry*; Demchenko, A. V., Ed.; ACS Symposium Series 960; American Chemical Society: Washington, DC, 2007; pp 375−392.
49. Chan, W. C.; Nie, S. *Science* **1998**, *281*, 2016–2018.
50. Goldman, E. R.; Clapp, A. R.; Anderson, G. P.; Uyeda, H. T.; Mauro, J. M.; Medintz, I. L.; Mattoussi, H. *Anal. Chem.* **2004**, *76*, 684–688.
51. Medintz, I. L.; Uyeda, H. T.; Goldman, E. R.; Mattoussi, H. *Nat. Mater.* **2005**, *4*, 435–446.
52. Robinson, A.; Fang, J. M.; Chou, P. T.; Liao, K. W.; Chu, R. M.; Lee, S. J. *ChemBioChem* **2005**, *6*, 1899–1905.
53. Zhang, J.; Geddes, C. D.; Lakowicz, J. R. *Anal. Biochem.* **2004**, *332*, 253–260.
54. Veerapandian, M.; Lim, S.; Nam, H.; Kuppannan, G.; Yun, K. *Anal. Bioanal. Chem.* **2010**, *398*, 867–876.
55. El-Boubbou, K.; Zhu, D. C.; Vasileiou, C.; Borhan, B.; Prosperi, D.; Li, W.; Huang, X. *J. Am. Chem. Soc.* **2010**, *132*, 4490–4499.
56. Liu, L.-H.; Yan, M. *Acc. Chem. Res.* **2010**, *43*, 1434–1443.
57. Yan, M. *Chem. Eur. J.* **2007**, *13*, 4138–4144.
58. Madwar, C.; Chu Kwan, W.; Deng, L.; Ramström, O.; Schmidt, R.; Zou, S.; Cuccia, L. A. *Langmuir* **2010**, *26*, 16677–16680.
59. Pei, Y.; Yu, H.; Pei, Z.; Theurer, M.; Ammer, C.; André, S.; Gabius, H.-J.; Yan, M.; Ramström, O. *Anal. Chem.* **2007**, *79*, 6897–6902.
60. Pei, Z.; Yu, H.; Theurer, M.; Waldén, A.; Nilsson, P.; Yan, M.; Ramström, O. *ChemBioChem* **2007**, *8*, 166–168.
61. Yan, M.; Harnish, B. *Adv. Mater.* **2003**, *15*, 244–248.
62. Yan, M.; Ren, J. *Chem. Mater.* **2004**, *16*, 1627–1632.
63. Yan, M.; Ren, J. *J. Mater. Chem.* **2005**, *15*, 523–527.
64. Liu, L.-H.; Lerner, M. M.; Yan, M. *Nano Lett.* **2010**, *10*, 3754–3756.
65. Gann, J. P.; Yan, M. *Langmuir* **2008**, *24*, 5319–5323.
66. Liu, L.; Engelhard, M. H.; Yan, M. *J. Am. Chem. Soc.* **2006**, *128*, 14067–14072.
67. Liu, L.; Yan, M. *Angew. Chem., Int. Ed.* **2006**, *45*, 6207–6210.
68. Liu, L.-H.; Dietsch, H.; Schurtenberger, P.; Yan, M. *Bioconjugate Chem.* **2009**, *20*, 1349–1355.
69. Wang, X.; Ramström, O.; Yan, M. *J. Mater. Chem.* **2009**, *19*, 8944–8949.
70. Wang, X.; Ramström, O.; Yan, M. *Chem. Commun.* **2011**, *47*, 4261–4263.
71. Yan, M.; Bartlett, M. A. *Nano Lett.* **2002**, *2*, 275–278.

Downloaded by STANFORD UNIV GREEN LIBR on June 3, 2012 | http://pubs.acs.org
Publication Date (Web): December 13, 2011 | doi: 10.1021/bk-2011-1091.ch004

72. Deng, L.; Norberg, O.; Uppalapati, S.; Yan, M.; Ramström, O. *Org. Biomol. Chem.* **2011**, *9*, 3188–3198.
73. Norberg, O.; Deng, L.; Yan, M.; Ramström, O. *Bioconjugate Chem.* **2009**, *20*, 2364–2370.
74. Norberg, O.; Deng, L.; Aastrup, T.; Yan, M.; Ramström, O. *Anal. Chem.* **2011**, *83*, 1000–1007.
75. Norberg, O.; Lee, I. H.; Aastrup, T.; Yan, M.; Ramström, O. **2011**, submitted.
76. Joester, D.; Klein, E.; Geiger, B.; Addadi, L. *J. Am. Chem. Soc.* **2006**, *128*, 1119–1124.
77. Wang, H.; Zhang, Y.; Yuan, X.; Chen, Y.; Yan, M. *Bioconjugate Chem.* **2011**, *22*, 26–32.
78. Tyagi, A.; Wang, X.; Deng, L.; Ramström, O.; Yan, M. *Biosens. Bioelectron.* **2010**, *26*, 344–350.
79. Wang, X.; Matei, E.; Deng, L.; Ramström, O.; Gronenborn, A. M.; Yan, M. *Chem. Commun.* **2011**, *47*, 8620–8622.

Downloaded by STANFORD UNIV GREEN LIBR on June 3, 2012 | http://pubs.acs.org
Publication Date (Web): December 13, 2011 | doi: 10.1021/bk-2011-1091.ch004

Downloaded by UNIV OF DELAWARE MORRIS LIB on June 3, 2012 | http://pubs.acs.org
Publication Date (Web): December 13, 2011 | doi: 10.1021/bk-2011-1091.ch005

Chapter 5

Strategies for the Characterization of the Saccharidic Moiety in Composite Nanoparticles

**Carlo Morasso,*[,1] Paolo Verderio,[2] Miriam Colombo,[2]
and Davide Prosperi*[,1,2]**

**[1]Biophysics and Nanomedicine Laboratory,
Fondazione Don Carlo Gnocchi Onlus, via Capecelatro 66,
20148 Milano, Italy
[2]NanoBioLab, Dipartimento di Biotecnologie e Bioscienze,
Università di Milano-Bicocca, Piazza della Scienza 2,
20126 Milano, Italy
*E-mails: cmorasso@dongnocchi.it; davide.prosperi@unimib.it**

The exciting aptitude of sugars to form high-affinity interactions with various biological entities exploiting multivalency has led to the assessment of the potential of conjugating mono- and oligosaccharides to nanoparticles to investigate the biorecognition events and interfere with biological processes involving carbohydrates. Since a critical step in these studies is the fine control on the presentation of the saccharide molecules, reliable methods to check their presence and, possibly, their arrangement on the surface of nanoparticles are urgently required. In this chapter, we provide an overview of the most common analytical techniques useful to characterize the saccharidic portion of glycoconjugate nanomaterials. Among them, HRMAS NMR looks particularly promising, as it can resolve the structures of the immobilized ligands and may provide information on their orientation on the nanoparticle surface.

In Petite and Sweet: Glyco-Nanotechnology as a Bridge to New Medicines; Huang, X., et al.;
ACS Symposium Series; American Chemical Society: Washington, DC, 2011.

Downloaded by UNIV OF DELAWARE MORRIS LIB on June 3, 2012 | http://pubs.acs.org
Publication Date (Web): December 13, 2011 | doi: 10.1021/bk-2011-1091.ch005

Introduction

Carbohydrates are a widespread class of biomolecules involved in several fundamental biological processes. It is well known that they represent an essential source of energy for chemical and biological transformations and are involved in structural scaffoldings in living organisms. However, their function is not limited to these tasks. It is now well documented that carbohydrates play a crucial role in the mediation of biological recognition events involving interactions with other carbohydrate-based systems, proteins, entire cells, bacteria and viruses, by exploiting the huge diversity which can be achieved by combining the naturally available monosaccharide units.

Nevertheless, the study of the properties of biologically interesting oligosaccharides is associated with many challenges, as they frequently present extremely complex structures, which are often not easily accessible by chemical synthesis. A further complication resides in the fact that the affinities of the interactions that sugars establish with other species are singularly weak, but they can become remarkably stronger by exploiting multivalency. This point is particularly important as it is assumed that the way, in which carbohydrates are spatially organized, is a fundamental parameter of their biological activities (*1*).

Nanomaterials have recently emerged as an important scaffold for the investigation of carbohydrate properties and for their application in biomedicine. Indeed, nanoparticles can be used to present the saccharidic systems in a multivalent fashion, *e.g.*, with the aim of mimicking cell surface.

Some physical characteristics of nanoparticles, including size, shape, state of crystallinity, etc., can be accurately modulated and there is now a well developed surface chemistry that allows their functionalization with sugars and with other kinds of biomolecules. Concomitantly, nanomaterials possess unique optical, electronic, magnetic, and mechanical properties that can be exploited for biomedical imaging, diagnostics, and therapeutics. Thus, nanoparticles for biomedical application can tremendously benefit from the advantages provided by the chemical properties of mono-/oligosaccharides in terms of solubility, compatibility with the physiological environment and selectivity of action towards specific biological targets that a carbohydrate can provide. For this reason, in the last 10 years, several research groups have produced an abundant amount of literature on glyconanoparticles (*2*, *3*).

Unfortunately, the possibility to chemically modify the rigid surface of nanomaterials is hardly ever adequately matched by a comparable capability to characterize the organic species at a molecular level once they are immobilized on that surface. The lack of information at this level is thence usually unconsidered, erroneously assuming that the surface of nanoparticles is completely and uniformly coated by a perfect monolayer of the sugar used for the conjugation. However, such approximation, although widely employed, does not consider the defects in coating and the absence of control on the molecular localization/orientation deriving from the inherent limitations of the synthetic route chosen for the preparation. This is, at least, not realistic.

Hence, several analytical techniques have been applied to study the organic layer conjugated to nanomaterials. Due to the significantly high specific surface area of nanomaterials, conventional analytical methods can be readily used for the characterization of hybrid nanoparticles. However, in most cases, such conventional tools limit their potential to the identification of the presence or absence of particular portions of the organic components, but fail in providing an exhaustive description of the structural features of anchored molecules. For this reason, only recently, novel methods have been proposed to try to improve the amount of information that can be made available on those elements, which enable identifying the structure and/or conformation of the saccharide conjugates. The aim of the present chapter is to provide a general view of the analytical techniques currently used to confirm the occurred immobilization of carbohydrates in hybrid nanoparticles, including these recent more sophisticated approaches enabling fine structure elucidation.

Downloaded by UNIV OF DELAWARE MORRIS LIB on June 3, 2012 | http://pubs.acs.org
Publication Date (Web): December 13, 2011 | doi: 10.1021/bk-2011-1091.ch005

UV-Vis Spectroscopy

UV-Vis spectroscopy is the most common tool used to confirm the conjugation of organic molecules (SAM, polymers or biomolecules as DNA or Protein) on the surface of gold and silver nanoparticles. Gold nanoparticles interact strongly with light and have a deep red colour because of the Surface Plasmon Band absorption of the light in the region around 520nm (*4*). This phenomenon has been explained in 1908 by Mie (*5*) and is given by oscillation of the electrons on the surface of the particles. The position of the absorption peak is related with the environment that surrounds the particles, and in particular with the dielectric constant of the medium. A variation of the capping agents on the surface gives rise to a variation of the position of the peak of absorption and can be quickly monitored by a spectrophotometer.

Usually the spectra of absorption are measured before and after the conjugation of the organic layer; the two spectra are normalized, in order to take count of the loss of material occurred during the purification of the capped nanoparticles, and a red shift of the peak is considered as an indication of the conjugation (Figure 1).

UV-Vis absorption is a very simple and quick measure that can be used as a first indicator of the conjugation, however the amount of information that can be extracted is limited. Spectrophotometers do not provide any information on the nature of the adsorbed material or on the amount conjugated; moreover, several factors can affect this analysis, giving misleading results.

The shift of the peak due to the adsorption of an organic molecule is limited and must be of 2-3 nm; if a major shift is observed, it could indicate other phenomena like a partial aggregation of the nanoparticles (*6*). When gold nanoparticles start to aggregate the cluster acquires a new peak, red-shifted significantly from the original position of the isolated nanoparticles. This phenomena cannot be distinguished from the variation of the surface layer except for completely aggregated systems where the peak is shifted at 600 nm.

In many cases the aggregation is itself the final purpose of the preparation of glyconanoparticles. The red/blue transition of the solution is in fact used as an indication of the presence of a particular analyte if it causes a selective aggregation just of the particles coated by the sugars (*7*) or it has been employed to study the head-to-head interaction between complex polysaccharides in presence of divalent ions (e.g., Ca^{2+}).

UV-Vis spectroscopy is used even in some colorimetric assays for the quantification of the adsorbed organic layer or to test the presence or the absence of some reactive groups on the surface of nanoparticles. These kinds of assays are usually based on the conversion of the sugar to furfuraldehyde derivates by dehydration (e. g. using sulphuric acid) and then on the reaction of these intermediates with aromatic compounds as phenol, resorcinol, orcinol or anthrone to give highly conjugated and coloured products that can be quantified spectroscopically.

Downloaded by UNIV OF DELAWARE MORRIS LIB on June 3, 2012 | http://pubs.acs.org
Publication Date (Web): December 13, 2011 | doi: 10.1021/bk-2011-1091.ch005

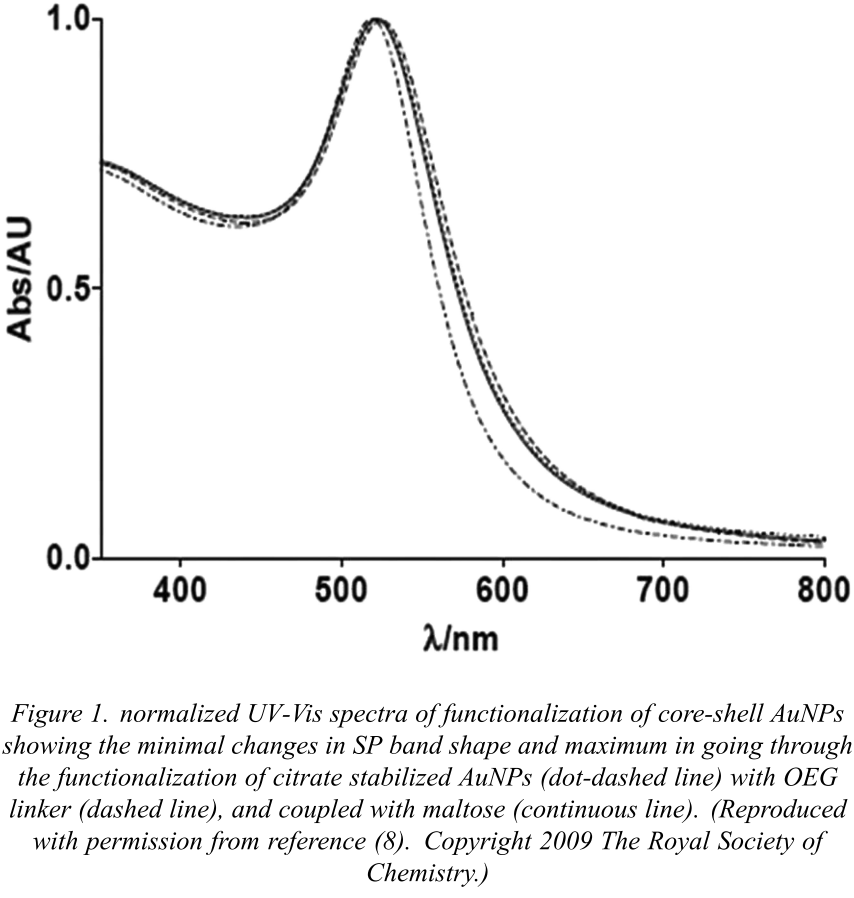

Figure 1. normalized UV-Vis spectra of functionalization of core-shell AuNPs showing the minimal changes in SP band shape and maximum in going through the functionalization of citrate stabilized AuNPs (dot-dashed line) with OEG linker (dashed line), and coupled with maltose (continuous line). (Reproduced with permission from reference (8). Copyright 2009 The Royal Society of Chemistry.)

Recently Chien and coworkers used anthrone for the quantification of sugars conjugated on nanoparticles (*9*). This method can be used to determine both reducing and non-reducing sugars because it is performed in the strongly oxidizing sulfuric acid; however, some differences in the test appears between pentoses and hexoses. It must be noticed that as all these methods are non-stoichiometric. It is always necessary to prepare a calibration curve using a series of standards of known carbohydrate concentration (*10*). Another approach to evaluate the amount of sugars conjugated on gold nanoparticles is based on their acetylation and evaluation through gas-liquid chromatography as demonstrated by Kamerling and co-workers (*11*).

Vibrational Spectroscopies (IR and Raman)

In Fourier transform infrared spectroscopy (FTIR) when the incident light energy matches the energy of a specific molecular vibration it is possible to observe an absorption indicative of the presence of specific chemical functional groups in the sample analyzed.

Most of the value of this technique resides in the fact that, despite it does not allow a complete characterization of the organic layer, it can be used on virtually any kind of particle. FTIR instrumentation is quite cheap and available in most Chemistry and Biochemistry Departments. Moreover, the rules for the interpretation of the spectra are relatively simple and well-documented.

The presence of the glycans on the surface of nanoparticles can be usually determined looking at the band around 3500-3600 cm^{-1} where lies the O-H stretching. Another important band lies at 2900 cm^{-1}, which corresponds to the C-H stretching. Even if this band is weaker for the isolated sugar, it is commonly contained in the linker used for the conjugation of the functional sugar or can be used to monitor the exchange of a capping agent with the compound of interest.

Gallo et al. prepared mixed superparamagnetic gold nanoparticles with an hydrophobic coating in hexane (*12*). By a two-phase ligand exchange reaction they were able to strip the original hydrophobic coating and replace it with glycoconjugated capping molecules. FTIR spectra clearly showed an enhancement of the hydroxyl peak around 3500 cm^{-1} given by the presence of the carbohydrates and a reduction of the band relative to the aliphatic chains at 3000 cm^{-1} (Figure 2).

The presence or the absence of the bands in the spectra must be evaluated carefully. The broad band attributable to OH groups can be found independently from the sugars. This is particularly true with iron oxide particles and when silane chemistry is used. Moreover the use of this technique is limited by some issues relative to the preparation of the sample that must be completely desiccated as water strongly adsorbs IR light and does not allow any kind of analysis. Due to the low specificity of diagnostic signals in IR spectra of deprotected sugars, in some circumstances the effectiveness of monosaccharide conjugation onto the surface of metal oxide nanoparticles has been assessed by using protected (e.g., acetylated) sugars, thus determining the presence of diagnostic stretching bands associated with the protecting groups (*13*).

Downloaded by UNIV OF DELAWARE MORRIS LIB on June 3, 2012 | http://pubs.acs.org
Publication Date (Web): December 13, 2011 | doi: 10.1021/bk-2011-1091.ch005

Downloaded by UNIV OF DELAWARE MORRIS LIB on June 3, 2012 | http://pubs.acs.org
Publication Date (Web): December 13, 2011 | doi: 10.1021/bk-2011-1091.ch005

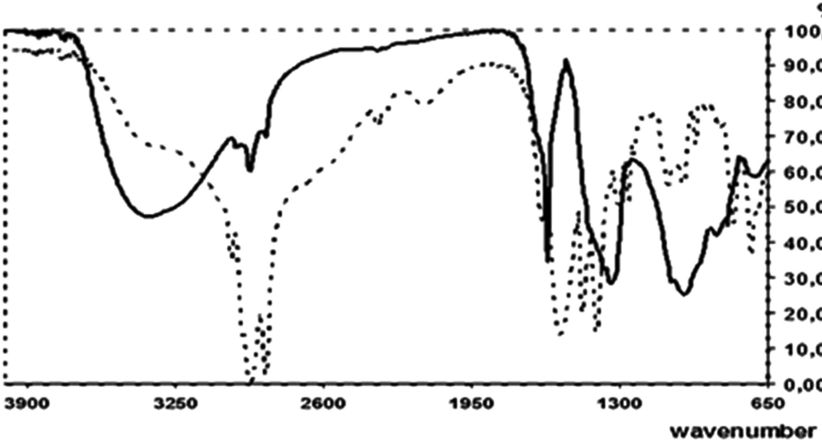

Figure 2. FT IR spectra of iron oxide@gold nanoparticles coated by an hydrophobic self-assembled monolayer (dot line) and by a glycol-conjugated self assembled monolayer (continuous line). (Adapted with permission from reference (12). Copyright 2010 The Royal Society of Chemistry.)

A valid alternative to IR is Raman spectroscopy. Raman spectroscopy does not require any particular preparation of the sample and can be performed directly in water or in the buffer where glyconanoparticles presumably need to be used. During the last five years, a huge amount of literature has been produced on the use of plasmonic (gold and silver) nanoparticles and Raman spectroscopy in order to exploit the surface enhanced Raman scattering (SERS) effect for biosensing purposes (*14*). Despite these studies, the use of Raman spectroscopy has been seldom exploited for the characterization of ligands on nanoparticles as the use of this technique is still confined in specialized laboratories.

Raman spectroscopy can give information similar to the one obtained with FTIR. However, the bands are sharper and a more precise description of the glycoconjugate can be accomplished. Another important feature is the fact that the selection rules of Raman are different from those of IR. The O-H stretching is barely observable and the sugars are described more properly by the peaks corresponding to C-H bond. Verapandian et al. prepared glucosamine functionalized silver glyconanoparticles and used Raman spectroscopy for the characterization (*15*). The spectra clearly showed the presence of some of the chemical bonds of glucosamine conjugated on the surface: C(1)-H at 876 cm^{-1}; C(6)-H at 2282 cm^{-1}; C(2)-H at 2932 cm^{-1}; C-O at 1042 and 1081 cm^{-1}; O-H at 3221 and 3329 cm^{-1} (Figure 3) with a strongly improved resolution as compared with FTIR spectroscopy.

Downloaded by UNIV OF DELAWARE MORRIS LIB on June 3, 2012 | http://pubs.acs.org
Publication Date (Web): December 13, 2011 | doi: 10.1021/bk-2011-1091.ch005

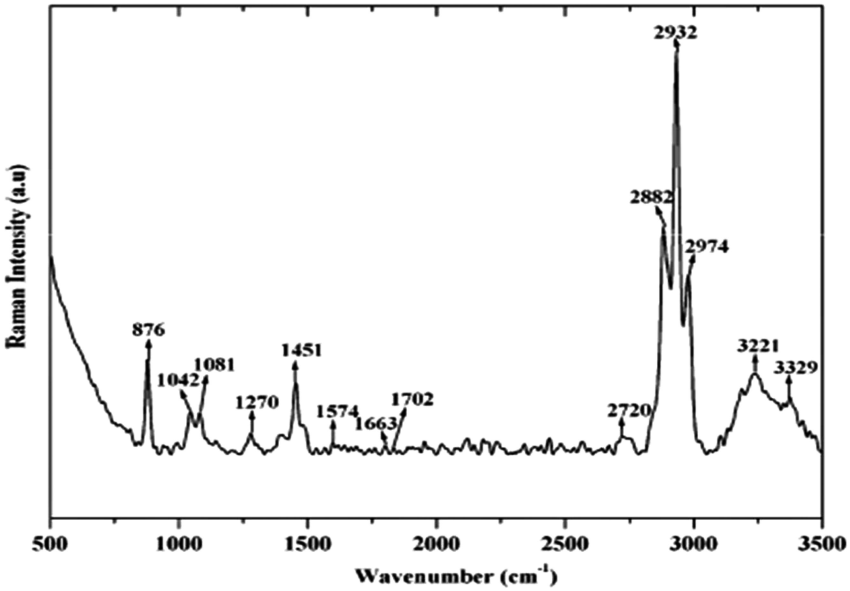

Figure 3. Raman spectra of glucosamine conjugated on the surface of silver nanoparticles. (Reproduced with permission from reference (15). Copyright 2010 Springer-Verlag.)

Thermogravimetry

Thermogravimetry (TGA) is one of the few available techniques that allows a semi-quantitative characterization of the organic materials adsorbed or immobilized on nanoparticles. In a thermogravimetric analysis, the sample is progressively heated on top of a microbalance. The instrument is thence able to relate differences in the weight of the sample with the temperature at which such variations occur.

Glyconanoparticles are thus decomposed upon heating and the reduction of the weight of the sample can provide information on the amount of molecules conjugated and on the chemical bonds that are exploited for the immobilization. The amount of sugars immobilized can be deduced looking at the percent loss of weight of the sample at a certain temperature that represents the corresponding fraction of sugar. As size and chemical composition of the core can be measured with other techniques, it is possible to calculate the molecular weight of each particle and thus obtain the average number of saccharide molecules conjugated on each nanoparticle.

Liu et al. synthesized mannose coated hematite (Fe_2O_3) and magnetite (Fe_3O_4) nanoparticles by covalent coupling the carbohydrate on photochemically activated perfluorophenylazides (PFPA). By TGA, the authors were able to determine a ligand density of 128 D-mannose molecules per Fe_3O_4 nanoparticle of 5 nm in average diameter. The TGA results also showed that there were roughly the same numbers of PFPA and coupled D-mannose molecules on the nanoparticles, indicating that the coupling reaction was fairly efficient (Figure 4) (*16*). Other information can be obtained from the temperature at which the loss of weight occurs. For example thiolated molecules tend to be desorbed quite sharply around 200°C, while silanes or phosphates are associated with a broader loss of weight at higher temperature (*17*).

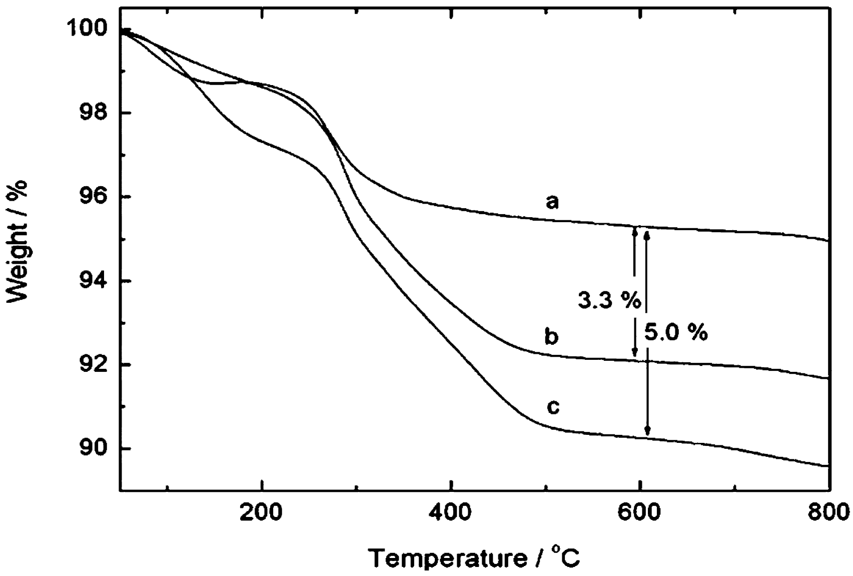

Figure 4. TGA curves of a) Fe_3O_4 nanoparticles; b) polymer-coated-Fe_3O_4-NPs; c) mannose-polymer coated-Fe_3O_4-NPs. (Reproduced from reference (16). Copyright 2009 American Chemical Society.)

X-ray Photoelectron Spectroscopy

X-ray Photoelectron Spectroscopy (XPS) determines the kinetic energy of the electrons emitted by the core level of atoms irradiated with X ray photons. As photons can move in the sample just for few nanometers, XPS has been traditionally employed for the study of surfaces but is a powerful tool even for the characterization of nanoparticles especially because of the large amount of data that it can provide.

Because each element has a characteristic binding energy, XPS can be used to analyze the elemental composition of particles in a quantitative way providing information both on the inorganic core and on the glycosylated-shell. One of the advantages of XPS over other techniques for the determination of elemental composition is the fact that it can distinguish different oxidation state of atoms. Electrons emitted by carbons not bounded to an oxygen lie at 285 eV while the ones emitted by oxygen conjugated carbon atoms have higher energy (C-O: 287

Downloaded by UNIV OF DELAWARE MORRIS LIB on June 3, 2012 | http://pubs.acs.org
Publication Date (Web): December 13, 2011 | doi: 10.1021/bk-2011-1091.ch005

eV, C=O: 288 eV; esters: 289 eV) (*18*). Several other lines are important for the characterization of glyconanoparticles and can be analyzed as the ones relative to oxygen (532 eV) and nitrogen (400 eV) depending from the molecular structure of the organic layer.

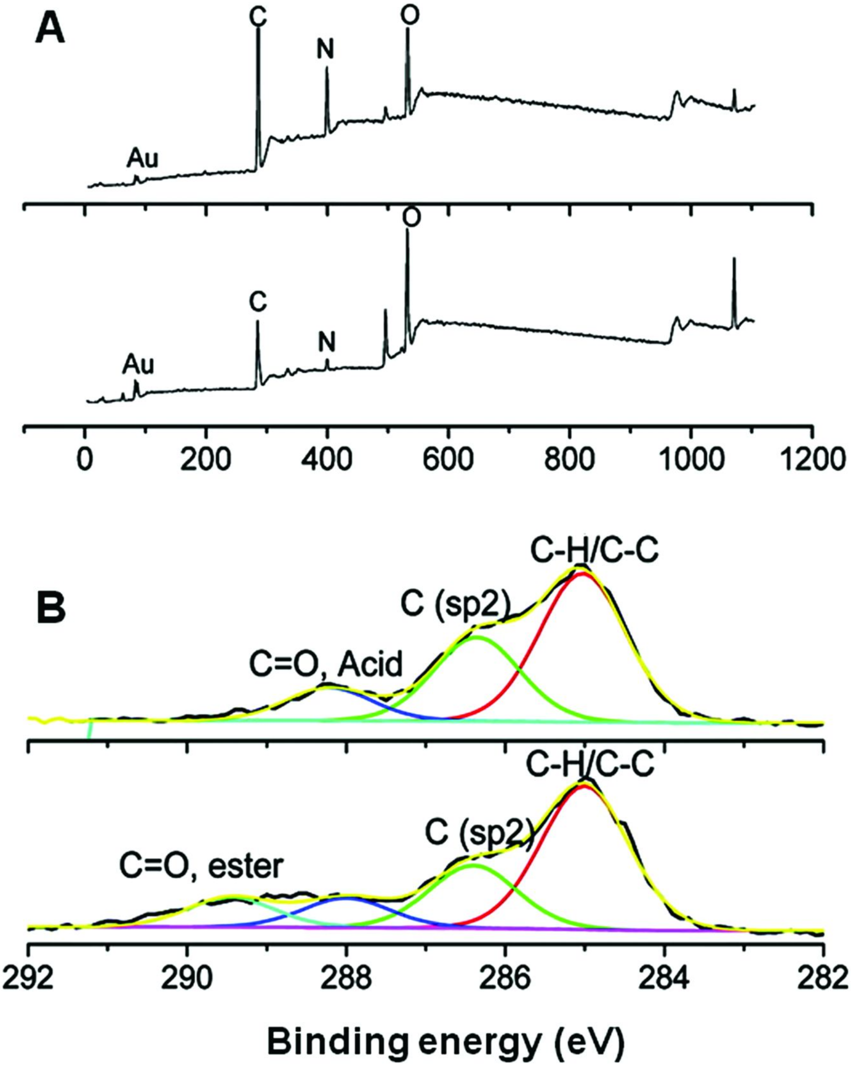

Figure 5. Wide XPS spectra of polymer coated gold nanoparticles before (up) and after (down) sugar conjugation (panel A). C1s region of the spectra before (up) and after (down) sugar conjugation where is possible to observe the presence of esters on the particles (panel B). (Reproduced from reference (19). Copyright 2010 American Chemical Society.)

Downloaded by UNIV OF DELAWARE MORRIS LIB on June 3, 2012 | http://pubs.acs.org
Publication Date (Web): December 13, 2011 | doi: 10.1021/bk-2011-1091.ch005

Boyer et al., prepared gold glyconanoparticles modifying the inorganic core with charged polymers using a layer by layer approach and then used a nucleophilic substitution for the conjugation of galactose. Using XPS, they were able to monitor the deposition of the different polymeric layers and the conjugation of galactose looking at the relative content of carbon and oxygen and at the different composition of the electronic state of carbon before and after the sugar conjugation (Figure 5) (*19*).

Despite the fact that XPS is an extremely powerful technology that is able to provide qualitative and quantitative information both on the core and on the shell of glyconanoparticles, it must be noticed that the instrumentation is very expensive and requires a high level of training to be used. For this reason it is unlikely that this approach will become a standard technique for the characterization of glyconanoparticles.

MALDI Mass Spectroscopy

MALDI mass spectroscopy is a powerful technique used for the determination of the exact molecular weight of molecules. In a typical experiment the analyte is prepared in a solution with an UV adsorbing molecule (matrix) able to transfer the energy coming from an UV laser (typically a 337 nm Nitrogen laser) to the sample and at the same time allows the vaporization of the sample that is thence directed towards the mass detector.

Many groups interested in analytical chemistry have been interested in the idea of using metallic nanoparticles, in particular gold nanoparticles, as inorganic matrix for laser assisted mass spectroscopy as they adsorb the UV region of the light spectra (*20*). Gold nanoparticles have several advantages over traditional matrices. In particular when traditionally organic matrices are used it is not possible to work with low molecular mass molecules because the matrix itself is also ionized and produces a high background signal in the region below 500-1000 Daltons (*21*). Moreover, gold nanoparticles are able to ionize specifically the molecules adsorbed on the surface even in the presence of complex organic mixtures (*22*).

For the characterization of nanoparticles it is thence possible to use MALDI mass spectroscopy in order to confirm the presence of the glycomolecules conjugated on gold nanoparticles. The main problem related with mass spectroscopy is that just charged molecules can be detected by the instrument. Despite the fact that many carbohydrates are charged, most of the glyconanoparticles have been coated with simple uncharged sugars as mannose or lactose. The ionization of these kinds of molecules can be obtained using a PEG spacer as this polymer is well known to have an affinity for Na^+ ions and the adducts produced by the molecules and sodium is usually recorded (*23*).

As the biological properties of carbohydrates depend drastically on the spatial orientation of the hydroxyl functional groups, laser desorption/ionization mass spectroscopy cannot provide a complete characterization of sugars, however the sensitivity and robustness of mass spectroscopy has been successfully employed

Downloaded by UNIV OF DELAWARE MORRIS LIB on June 3, 2012 | http://pubs.acs.org
Publication Date (Web): December 13, 2011 | doi: 10.1021/bk-2011-1091.ch005

to monitor enzymatic and chemical glycosylation occurred directly on the surface of nanoparticles (Figure 6) (*24*, *25*).

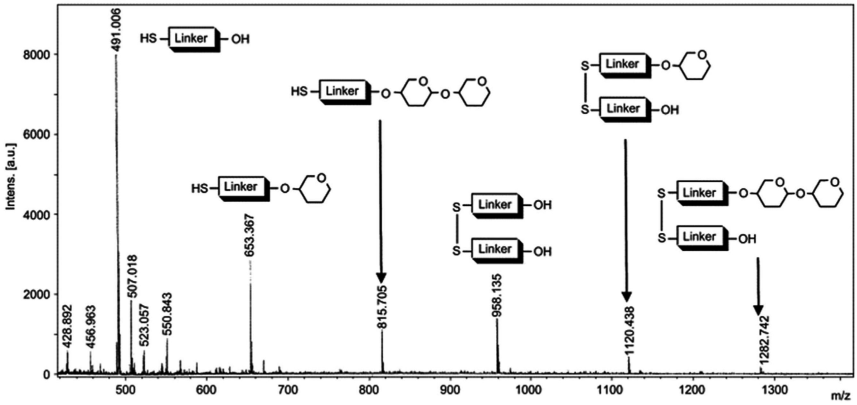

Figure 6. MALDI-TOF MS of a chemical glycosylation onto the surface of gold nanoparticles. The spectra clearly show the monosulfides and disulfides of the ethylene glycol (starting product) monosaccharides (intermediate) and disaccharide (obtained product). (Reproduced with permission from reference (25). Copyright 2007 Elsevier Ltd.)

Nuclear Magnetic Resonance

Nuclear Magnetic Resonance (NMR) spectroscopy is currently the gold standard for the characterization of compounds in organic chemistry. In comparison to other spectroscopies NMR provides an incomparable amount of information on the chemical structure of organic molecules assessing not only the presence or the absence of a chemical functional group but also the relative position of each atoms.

Unfortunately the detailed resolution of NMR spectroscopy is difficult to be achieved on nanomaterials, as the mobility of molecules in homogeneous media (liquid-like samples) is fundamental to obtain resolved spectra. Moreover many kind of nanoparticles (eg. Fe_XO_Y or Co) have strong magnetic properties that can generate inhomogeneities in the magnetic field basically preventing the use of NMR for the characterization of adsorbed organic layers.

In theory, non magnetic, small and fast rotating particles may reorient rapidly enough to yield an almost complete averaging during NMR timescale giving good signals, however bigger particles and aggregates appear as static objects leading to unresolved spectra (Figure 8) (*26*). From a practical point of view, NMR signals give by molecules conjugated on inorganic nanoparticles appear broad and unresolved.

The solubility of the particles in the solvent used is thence fundamental. Glyconanoparticles are usually analyzed in D_2O as the sugars are supposed to provide both solubility in water and specificity of action to the particles. Gold

Downloaded by UNIV OF DELAWARE MORRIS LIB on June 3, 2012 | http://pubs.acs.org
Publication Date (Web): December 13, 2011 | doi: 10.1021/bk-2011-1091.ch005

core however is not soluble itself in water and the nature of the spacer seems thence to be very important for the solubility. NMR spectra performed on sugars conjugated through a PEG spacer are better resolved than the ones where an alkane chain is used (*27*).

Another approach consists in changing the solvent. In one of the pioneering works on glyconanoparticles, Penades and coworkers synthetized very small gold particles coated with mannose through an hydrophobic linker (*28*). In this work, they compared the NMR spectra acquired in D_2O and in [D_6]DMSO by obtaining much resolved lines in the second solvent (Figure 7).

It must be noticed that even when a complete characterization of the organic layer is not possible, a lot of information can be obtained from NMR just observing the presence (or at the absence) of some characteristic peaks (as in IR spectroscopy). At last, for thiol coupled nanoparticles it is possible to analyze the small molecules cleaved from the surface by oxidation with iodine (*29*).

Downloaded by UNIV OF DELAWARE MORRIS LIB on June 3, 2012 | http://pubs.acs.org
Publication Date (Web): December 13, 2011 | doi: 10.1021/bk-2011-1091.ch005

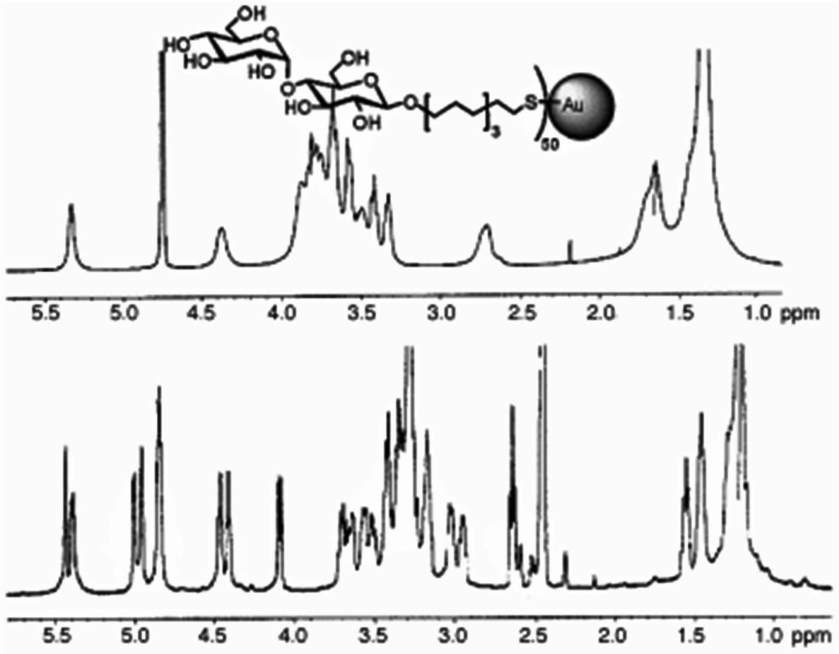

Figure 7. ^{1}H NMR spectra of maltose coated gold nanoparticles dissolved in D_2O (up) and [D6] DMSO (bottom). (Reproduced with permission from reference (28). Copyright 2003 Wiley-VCH Verlagh GmbH & Co. KgaA, Weinheim.)

Downloaded by UNIV OF DELAWARE MORRIS LIB on June 3, 2012 | http://pubs.acs.org
Publication Date (Web): December 13, 2011 | doi: 10.1021/bk-2011-1091.ch005

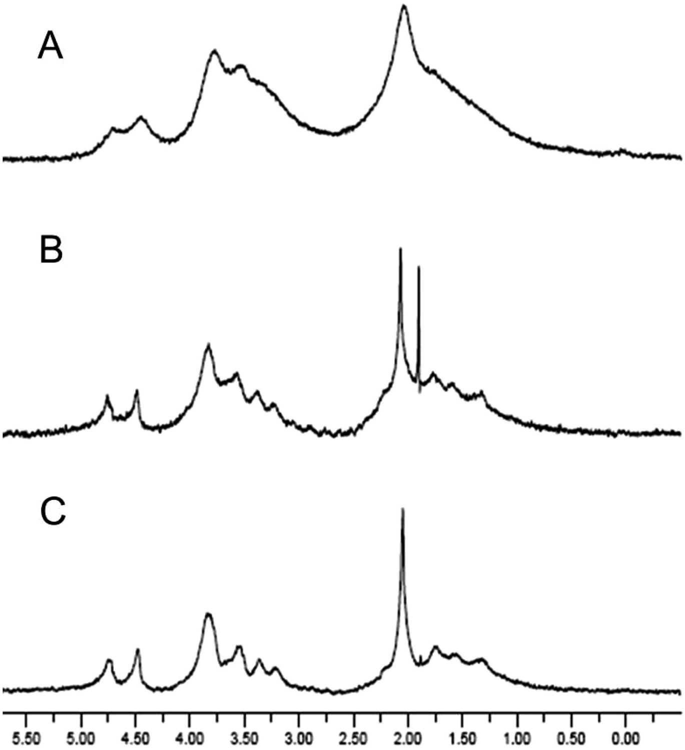

Figure 8. ^{1}H-NMR (300 MHz) spectra of sugar linked throught an hydrophobic spacer to 5.2 nm (panel A), 3.5 nm (panel B) and 1.9 nm (panel C) on gold nanoparticles dissolved in D$_2$O. Increased particles size results in increased broadening of the signals of the coating thiols. (Reproduced with permission from reference (29). Copyright 2008 Wiley-VCH Verlagh GmbH & Co. KgaA, Weinheim.)

High-Resolution Magic Angle Spinning (HRMAS) NMR Spectroscopy

Traditional solution NMR spectroscopy generally fails with magnetic nanoparticles (MNPs). This is of particular significance with broadly utilized superparamagnetic iron oxide nanocrystals. In general, performing NMR experiments with ligands immobilized on MNPs is complicated by large broadening effects deriving from the absence of ligand mobility on the crystal surface combined with field interferences caused by the nanomaterial intrinsic paramagnetism. This also affects the nuclear magnetic relaxation of solvent protons at distances up to 50 μm, resulting in the loss of peak splitting (*30*). For these reasons, only rare attempts have been reported, making use of extremely dilute dispersions of MNPs bearing unsophisticated ligands, which provided low spectral resolution lacking a well-defined first-order splitting pattern (*31*, *32*).

Downloaded by UNIV OF DELAWARE MORRIS LIB on June 3, 2012 | http://pubs.acs.org
Publication Date (Web): December 13, 2011 | doi: 10.1021/bk-2011-1091.ch005

It has been observed that the various sources of NMR interferences, including the anisotropy of magnetic susceptibilities and dipolar interactions, can be averaged to their isotropic contributions by means of high resolution magic angle spinning (HRMAS) and, in several circumstances, completely removed to produce spectra with enhanced sharp resonances (*33*). In the last years, HRMAS has become an extremely versatile analytical technique to study heterogeneous and nanostructured systems. This method is based on the spinning of the sample at the magic angle (54.7°), which has the unique property of averaging out to zero most of the differences in magnetic susceptibility in the sample, thus obtaining high resolution resonance linewidths similar to those of liquid state NMR (*34*).

If the differences in magnetic susceptibilities are small and isotropic, the additional magnetic field created by a volume element of magnetization $\boldsymbol{M_j}$ of coordinates $\boldsymbol{r_J} = (r_j, \theta_j, \varphi_j)$ at a point $\boldsymbol{r_i} = (r_i, \theta_i, \varphi_i)$ can be treated as a dipolar interaction. For static samples, this dipolar field is given by the equation (*35*, *36*):

$$B(r_i, \theta_i, \phi_i) = \sum_j \frac{M_j}{r_{ij}^3} \frac{1}{2}\left(3\cos^2\theta_{ij} - 1\right) \qquad 1$$

where $\boldsymbol{r_{ij}}$ is the distance between the points r_i and r_j, θ_{ij} is the angle between the magnetic field applied $\boldsymbol{B_0}$ and the vector from r_i to r_j; the summation expresses that point r_i experiences the sum of all the different magnetic dipoles $\boldsymbol{Mj}$ in its vicinity. When the sample is rotated at an angle β respect to the main field $\boldsymbol{B_0}$ at a speed ω_R, equation 1 can be rewritten as the following (*37*):

$$\begin{aligned} B(r_i, \theta_i, \phi_i, t) = \sum_j \frac{M_j}{r_{ij}^3} \Big[& \frac{1}{4}\left(3\cos^2\beta - 1\right)\left(3\cos^2\beta_{ij} - 1\right) \\ & + \frac{3}{4}\sin 2\beta \sin 2\beta'_{ij} \cos\left(\omega_R t + \phi_{ij}\right) \\ & + \frac{3}{4}\sin^2\beta \sin^2\beta'_{ij} \cos\left(2\omega_R t + 2\phi_{ij}\right) \Big] \end{aligned} \qquad 2$$

where φ_{ij} is a phase factor describing the angular position of $\boldsymbol{r_i}$. If the angle is set at 54.7°, the term ($3\cos^2\beta$ -1) is removed and there remains only two terms leading to spinning side-bands modulated by $\boldsymbol{\omega}_R$ and $2\boldsymbol{\omega}_R$ frequencies. In this way, the contribution to the width of the NMR resonance is cancelled and only spinning side-bands remain in the spectrum. In order to have highly resolved NMR spectra, spinning sidebands produced by slow-rate spinning need to be suppressed.

In HRMAS technique, the sample is routinely rotated at a frequency between 2 and 18 kHz (max 50 kHz). The spectra are extremely easy to interpret when the spinning frequency exceeds the overall width of the anisotropic powder spectrum that is obtained by measuring a static sample. Fast spinning of a sample demands a precise and mechanical design and a robust construction of the rotor system. Hence, a suitable rotor is a fundamental component required to run HRMAS experiments properly. Strong centrifugal forces on the walls of the rotor at high spinning speeds are present; in this way, it has to be extremely resistant and, for that reason, the material used is generally ZrO_2. Furthermore, the rotor can be

Downloaded by UNIV OF DELAWARE MORRIS LIB on June 3, 2012 | http://pubs.acs.org
Publication Date (Web): December 13, 2011 | doi: 10.1021/bk-2011-1091.ch005

designed in order to optimize the sensitivity of the probe, with an inner volume that matches exactly the detection volume of the solenoidal coil.

In this way, under appropriate conditions, HRMAS technique yields NMR spectra of semisolid samples and MNP dispersions, that look similar to those obtained in solution (Figure 9) (*38*). This method is not restricted to one dimensional (1D) NMR experiments. In fact, it is also possible to perform 2D experiments such as homonuclear ^{1}H-^{1}H correlation spectroscopy (COSY) and heteronuclear single-quantum coherence ^{1}H-^{13}C (HSQC), in order to obtain a complete structural profile of the sample fingerprint.

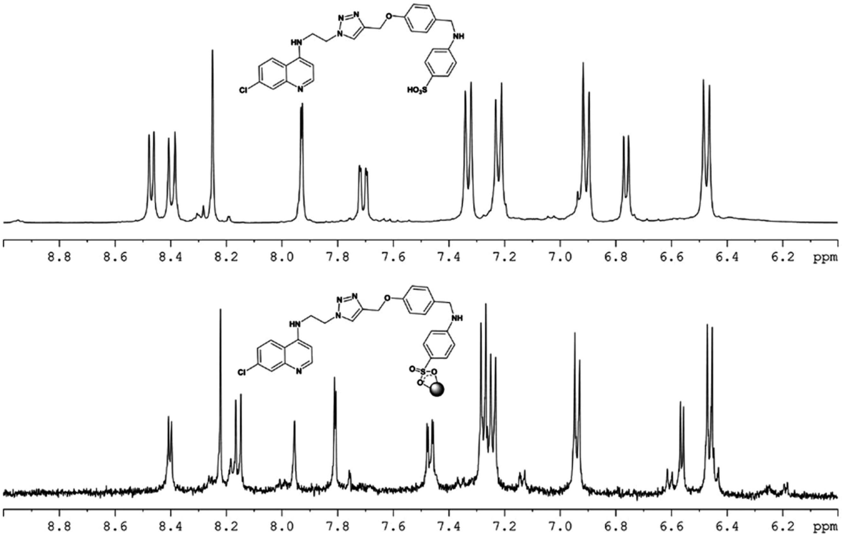

Figure 9. Comparison between a ^{1}H NMR solution spectra of an organic compound (upper) and the ^{1}H-HRMAS (lower) of the same ligand supported on magnetic iron oxide nanoparticles. (Reproduced from reference (38). Copyright 2008 American Chemical Society.)

As a proof of concept, Prosperi and coworkers have demonstrated that HRMAS NMR technology has the potential to provide a robust device for the direct structure-resolved characterization of various organic molecules immobilized on the surface of magnetic nanoparticles, avoiding ligand removal or particle decomposition. With this method all signals were sharp and well-resolved, even with complex organic substrates (*38*).

HRMAS NMR technology was used for the first time by Polito et al. to characterize various carbohydrates, including lactosides and mannosides, immobilized via "click" chemistry on the surface of magnetic nanoparticles (MNP3 and MNP5, respectively) (*39*). Signals were very well resolved and the presence of a peak around 8.0 ppm in the spectrum of MNP3 due to the triazole proton confirmed the successful occurrence of the 1,3 dipolar cycloaddition

Downloaded by UNIV OF DELAWARE MORRIS LIB on June 3, 2012 | http://pubs.acs.org
Publication Date (Web): December 13, 2011 | doi: 10.1021/bk-2011-1091.ch005

reaction between the azido terminal group exposed on the surface of nanoparticles and a propargyl group, introduced through a tetraethylene glycol chain, of the carbohydrates (Figure 10).

The comparison between ^{1}H NMR in solution of free organic compounds and ^{1}H NMR made by HRMAS confirmed the presence of the sugars on nanoparticles and also allowed the authors to attribute the complete carbohydrate structure. Noteworthy, anomeric protons for lactose in MNP3 are located at 4.41 ppm and 4.48 ppm, respectively, and the multiplicity for those proton signals is clearly detectable (*d*, J = 10 Hz, for β-galacto, and *d*, J = 10 Hz, for β-gluco).

In another example by El-Boubbou et al. (*40*), a magnetic glyconanoparticle (MGNP) based nanosensor system, bearing carbohydrate ligands, was used to detect and differentiate cancer cells and also to quantitatively determine the glycoconjugate binding abilities by magnetic resonance imaging (MRI). Drastic line broadening was observed in ^{1}H NMR spectra recorded with a conventional NMR technique in solution, which led to undistinguishable peaks (Figure 11, panel B). In contrast, HRMAS NMR proved to be a powerful tool to overcome this problem. These MGNPs gave completely resolved, solution-like spectra with splitting pattern, including correct signal multiplicities and peak integrations (Figure 11, panel C). For example, the anomeric proton of the galactoside ligand on Gal-MGNPs was well resolved as a doublet (J = 8.0 Hz) at 4.3 ppm, giving information also on the configuration of the carbohydrate, which was unaltered after immobilization. Therefore, the fact that only one set of peaks from carbohydrates was observed, suggested that the carbohydrate loading was homogeneous overall the nanoparticle surface.

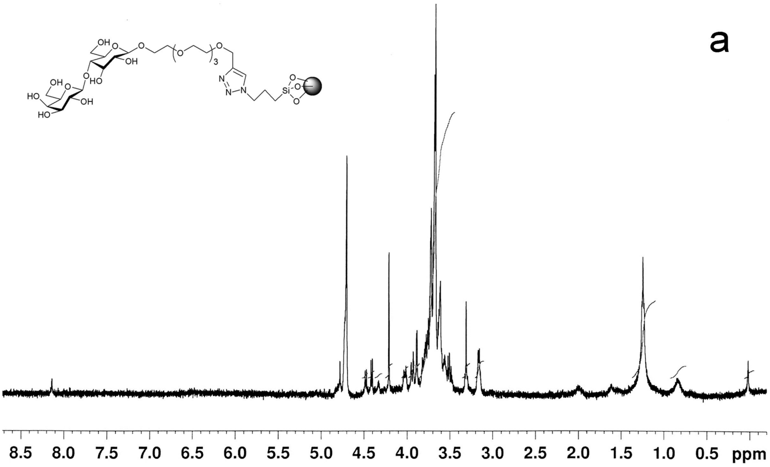

Figure 10. ^{1}H NMR spectra of MNP3 in D_2O obtained by HRMAS. Triazole proton is clearly distinguishable at 8.14 ppm. (Adapted with permission from reference (39). Copyright 2008 The Royal Society of Chemistry.)

Downloaded by UNIV OF DELAWARE MORRIS LIB on June 3, 2012 | http://pubs.acs.org
Publication Date (Web): December 13, 2011 | doi: 10.1021/bk-2011-1091.ch005

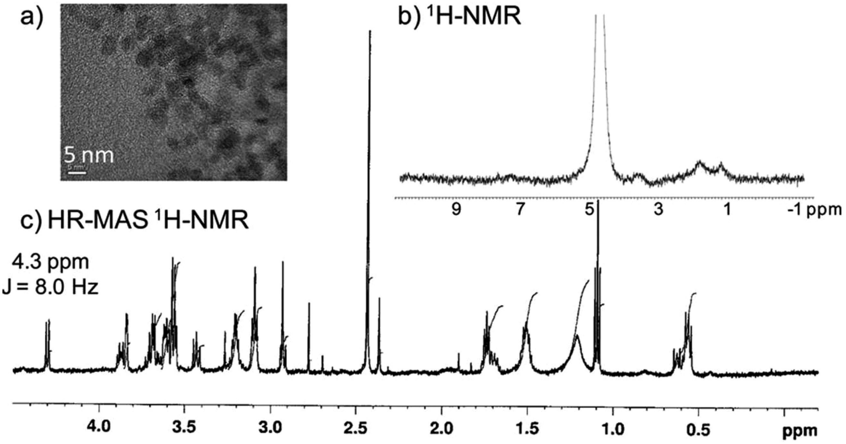

Figure 11. TEM image of Gal-MGNP (panel a). A ^1H spectrum in solution of a Gal-MGNP acquired with a conventional 5 mm probe (panel b). The HRMAS ^1H-NMR spectrum of Gal-MGNP (panel c). (Reproduced from reference (40). Copyright 2010 American Chemical Society.)

Gu and colleagues presented a series of dendritic α-D-galactopyranosides and β-D-mannopyranosides with a terminal amino group that were used for the functionalization of single walled nanotubes (SWNTs) by targeting the defect-derived carboxylic acid moieties on the nanotube surface (*41*). Sugar dendron-functionalized carbon nanotube samples were characterized by NMR, both in solution and in the gel phase. For example, the ^1H NMR spectra of Gal_2-SWNT and Gal_2-N_3 in solutions are compared in Figure 12a. The signals of the nanotube sample were significantly broader than those of the corresponding free dendron, which may be attributed to the high molecular weight and low mobility of carbon nanotubes.

The gel-phase NMR spectrum of the same Gal_2-SWNT sample in a HRMAS probe showed better resolved bands, with the signal patterns in the sugar region comparable with those of the free dendron. The aromatic proton signals were slightly downfield shifted to 6.82 ppm and 6.70 ppm for the nanotube-bound dendron, from 6.72 ppm and 6.66 ppm for the free dendron, which could be attributable to the formation of amide bonds in the proximity of aromatic rings of the nanotube. The absence of the benzyl proton signal in the spectrum of Gal_2-SWNT was caused by the same effect due to the nanotube structure. Indeed, in the spectrum of Gal_2-N_3 in solution, this proton had a chemical shift of 4.36 ppm.

Concluding this paragraph, we wish to highlight that, although only pioneering studies have been performed so far, HRMAS method looks promising as a versatile and valuable technique enabling a structure-resolved ^1H NMR of carbohydrates exposed on the surface of various nanomaterials. The first attempts suggest that this kind of NMR technique could be a powerful tool for the ultra-fine qualitative and quantitative structure characterization of organic moieties, including sugars, in hybrid nanosystems.

Downloaded by UNIV OF DELAWARE MORRIS LIB on June 3, 2012 | http://pubs.acs.org
Publication Date (Web): December 13, 2011 | doi: 10.1021/bk-2011-1091.ch005

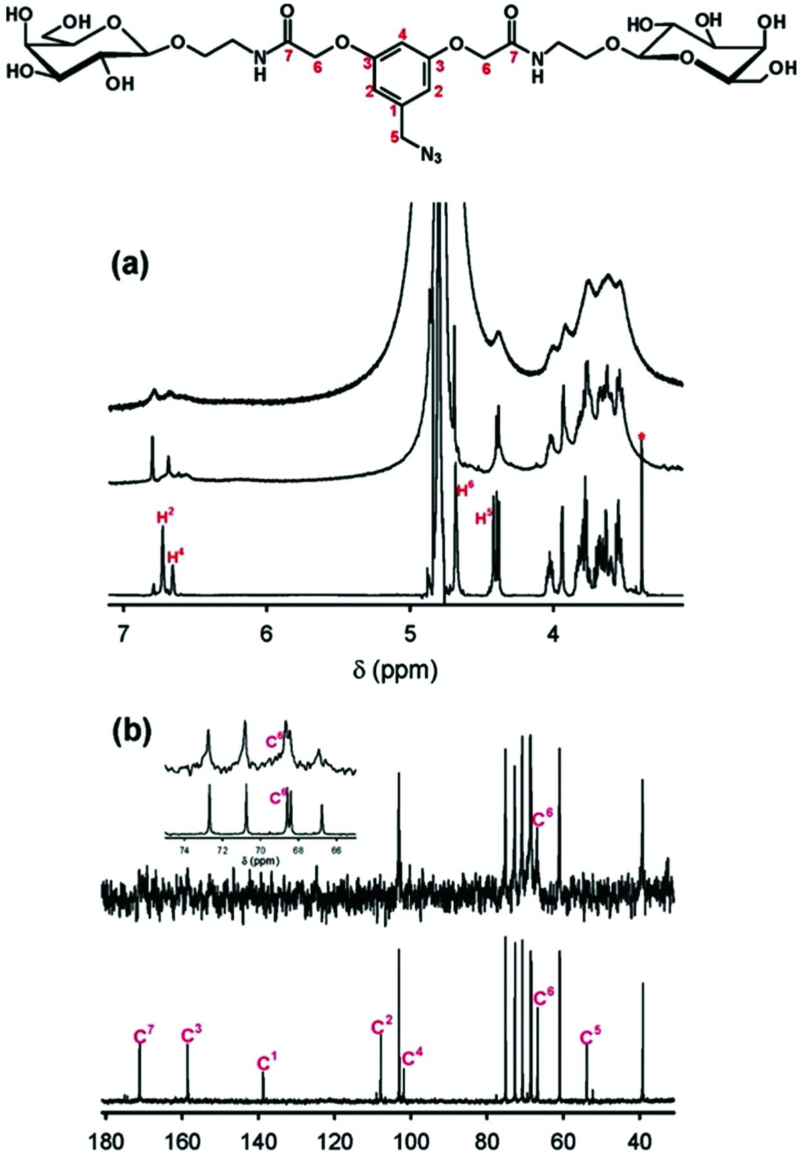

Figure 12. Structure of Gal$_2$-N$_3$ (top). ^{1}H NMR spectra of Gal$_2$-SWNT (top, solution phase; middle, gel phase) and Gal$_2$-N$_3$ (bottom) (panel a). ^{13}C NMR spectra of Gal$_2$-SWNT (top, with inset) and Gal$_2$-N$_3$ (bottom), acquired in D$_2$O (panel b). (Reproduced from reference (41). Copyright 2008 American Chemical Society.)

Downloaded by UNIV OF DELAWARE MORRIS LIB on June 3, 2012 | http://pubs.acs.org
Publication Date (Web): December 13, 2011 | doi: 10.1021/bk-2011-1091.ch005

Outlook

Despite the huge amount of work done by the scientific community on the preparation of glycoconjugated, and, more in general, of bioconjugated nanomaterials, the accurate characterization of organic molecules immobilized on the surface of nanoparticles is still a bottleneck (*42*, *43*). Since the large surface area is one of the most distinctive properties of nanoparticles, rigor in surface analysis is critical. Nonetheless, only a small number of reliable techniques are available for this purpose so far. Optical spectroscopies are able to provide some useful information, and often they can be used to monitor step-by-step the chemical reactions on the surface of nanoparticles. Mass spectroscopy can be utilized, at least on gold particles, with good results. We have evidenced that a particularly promising approach is HRMAS nuclear magnetic resonance spectroscopy, which allows for a unique description of the structures and conformations of organic molecules, including carbohydrates, conjugated on the surface of any kind of particles with a precision very close to the one that is usually obtained with uniform organic solutions.

However, this is just part of the problem. The quantification of the amount of different molecules immobilized on individual nanoparticles is still far from being optimal, as the data, which can be actually obtained by thermogravimetry and by XPS, are just indicative. Finally, in most cases, the spatial distribution of the molecules on the nanoparticle surface after conjugation is almost completely ignored, and the dream to reach a full control on the number and geometric orientation of immobilized carbohydrate ligands is far from being approached.

More work is still necessary to gain a satisfactory understanding of the principles, which rule the assembly of the organic layer when chemical conjugation is performed on the surface of nanoparticles in interphase systems. However, this work is vital to enable us to predict and control the stability, toxicology (*44*) and biodistribution of glyconanomaterials and to transform them from scientifically exciting tools into real clinical solutions.

References

1. Mammen, M.; Choi, S.-K.; Whitesides, G. M. *Angew. Chem., Int. Ed.* **1998**, *37*, 2754–2794.
2. Wang, X.; Ramström, O.; Yan, M. *Adv. Mater.* **2010**, *22*, 1946–1953.
3. de la Fuente, J. M.; Penadés, S. *Biochim. Biophys. Acta.* **2006**, *1760*, 636–651.
4. Daniel, M. C.; Astruc, D. *Chem. Rev.* **2004**, *104*, 293–346.
5. Mie, G. *Ann. Phys. (Berlin, Germany)* **1908**, *330*, 377–445.
6. Kumar, S.; Aaron, J.; Sokolov, K. *Nat. Protoc.* **2008**, *3*, 314–320.
7. Hone, D. C.; Haines, A. H.; Russell, D. A. *Langmuir* **2003**, *19*, 7141–7144.
8. Thygesen, M. B.; Sørensen, K. K.; Cló, E.; Jensen, K. J. *Chem. Commun.* **2009**, *42*, 6367–6369.
9. Chien, Y.-Y.; Jan, M.-D.; Adak, A. K.; Tzeng, H.-C.; Lin, Y.-P.; Chen, Y.-J.; Wang, K.-T.; Chen, C.-T.; Chen, C.-C.; Lin, C.-C. *ChemBioChem* **2008**, *9*, 1100–1109.

10. Yemm, E. W.; Willis, A. J. *Biochem. J.* **1954**, *57*, 508–514.
11. de Souza, A. C.; Kamerling, J. P. *Methods Enzymol.* **2006**, *417*, 221–243.
12. Gallo, J.; García, I.; Padro, D.; Arnráiz, B.; Penadés, S. *J. Mater. Chem.* **2010**, *20*, 10010–10020.
13. Lartigue, L.; Innocenti, C.; Kalaivani, T.; Awwad, A.; del Mar Sanchez Duque, M.; Guari, Y.; Larionova, J.; Guérin, C.; Montero, J.-L. G.; Barragan-Montero, V.; Arosio, P.; Lascialfari, A.; Gatteschi, D.; Sangregorio, C. *J. Am. Chem. Soc.* **2011**, *133*, 10459–10472.
14. Porter, M. D.; Lipert, R. J.; Siperko, L. M.; Wang, G.; Narayanan, R. *Chem. Soc. Rev.* **2008**, *37*, 1001–1011.
15. Veerapandian, M.; Lim, S. K.; Nam, H. M.; Kuppannan, G.; Yun, K. S. *Anal. Bioanal. Chem.* **2010**, *398*, 867–876.
16. Liu, L.-H.; Dietsch, H.; Schurtenberger, P.; Yan, M. *Bioconjugate Chem* **2009**, *20*, 1349–1355.
17. Ristau, R.; Tiruvalam, R.; Clasen, P. L.; Gorskowski, E. P.; Harmer, M. P.; Kiely, C. J. *Gold Bull.* **2009**, *42*, 133–143.
18. Kundu, S.; Wang, Y.; Xia, W.; Muhler, M. *J. Phys. Chem. C.* **2008**, *112*, 16869–16878.
19. Boyer, C.; Bousquet, A.; Rondolo, J.; Whittaker, M. R.; Stenzel, M. H.; Davis, T. P. *Macromolecules* **2010**, *43*, 3775–3784.
20. Chiu, T. C.; Huang, L. S.; Lin, P. C.; Chen, Y. C.; Chen, Y. J.; Lin, C. C.; Chang, H. T. *Recent Pat. Nanotechnol.* **2007**, *1*, 99–111.
21. Su, C.-L.; Tseng, W.-L. *Anal. Chem.* **2007**, *79*, 1626–1633.
22. Zhu, Z.-J.; Ghosh, P. S.; Miranda, O. R.; Vachet, R. W.; Rotello, V. M. *J. Am. Chem. Soc.* **2008**, *130*, 14139–14143.
23. Yan, B.; Zhu, Z.-J.; Miranda, O. R.; Chompoosor, A.; Rotello, V. M.; Vachet, R. W. *Anal. Bioanal. Chem.* **2010**, *396*, 1025–1035.
24. Nagahori, N.; Nishimura, S.-I. *Chem.--Eur. J.* **2006**, *12*, 6478–6485.
25. Shimizu, H.; Sakamoto, M.; Nagahori, N.; Nishimura, S.-I. *Tetrahedron* **2007**, *63*, 2418–2425.
26. Mayer, C. *Prog. Nucl. Magn. Reson. Spectrosc.* **2002**, *40*, 307–366.
27. Du, F.; Zhou, H.; Chen, L; Zhang, B.; Yan, B. *TrAC, Trends Anal. Chem.* **2009**, *28*, 88–95.
28. Barrientos, Á. G.; de la Fuente, J. M.; Rojas, T. C.; Fernández, A.; Penadés, S. *Chemistry.--Eur. J.* **2003**, *9*, 1909–1921.
29. Manea, F.; Bindoli, C.; Fallarini, S.; Lombardi, G.; Polito, L.; Lay, L.; Bonomi, R.; Mancin, F.; Scrimin, P. *Adv. Mater.* **2008**, *20*, 4348–4352.
30. Sillerud, L. O.; McDowell, A. F.; Adolphi, N. L.; Serda, R. E.; Adams, D. P.; Vasile, M. J.; Alam, T. M. *J. Magn. Reson.* **2006**, *181*, 181–190.
31. White, M. A.; Johnson, J. A.; Koberstein, J. T.; Turro, N. J. *J. Am. Chem. Soc.* **2006**, *128*, 11356–11357.
32. Willis, A. L.; Turro, N. J.; O'Brien, S. *Chem. Mater.* **2005**, *17*, 5970–5975.
33. Piotto, M.; Elbayed, K.; Wieruszeski, J-M.; Lippens, G. *J. Magn. Reson.* **2005**, *173*, 84–89.
34. Elbayed, K.; Dillmann, B.; Raya, J.; Piotto, M.; Engelke, F. *J. Magn. Reson.* **2005**, *174*, 2–26.

Downloaded by UNIV OF DELAWARE MORRIS LIB on June 3, 2012 | http://pubs.acs.org
Publication Date (Web): December 13, 2011 | doi: 10.1021/bk-2011-1091.ch005

35. Lippens, G. M.; Bourdonneau, M.; Dhalluin, C.; Warrass, R.; Richert, T.; Seetharaman, C.; Boutillon, C.; Piotto, M. *Curr. Org. Chem.* **1999**, *3*, 147–169.
36. Leu, G.; Tang, X-W.; Peled, S.; Maas, W. E.; Singer, S.; Cory, D. G.; Sen, P. N. *Chem. Phys. Lett.* **2000**, *332*, 344–350.
37. Andrew, E. R. In *Magnetic Angle Spinning*; Encyclopedia of Nuclear Magnetic Resonance; Grant, D. M., Harris, R. K., Eds.; Wiley: New York, 1996; Vol. 5, pp 2891–2901.
38. Polito, L.; Colombo, M.; Monti, D.; Melato, S.; Caneva, E.; Prosperi, D. *J. Am. Chem. Soc.* **2008**, *130*, 12712–12724.
39. Polito, L.; Monti, D.; Caneva, E.; Delnevo, E.; Russo, G.; Prosperi, D. *Chem. Commun.* **2008**, *5*, 621–623.
40. El-Boubbou, K.; Zhu, D. C.; Vasileiou, C.; Borhan, B.; Prosperi, D.; Li, W.; Huang, X. *J. Am. Chem. Soc.* **2010**, *132*, 4490–4499.
41. Gu, L.; Luo, P. G.; Wang, H.; Meziani, M. J.; Lin, Y.; Veca, L. M.; Li, C.; Lu, F.; Wang, X.; Quinn, R. A.; Wang, W.; Zhang, P.; Lacher, S.; Sun, Y.-P. *Biomacromulecules* **2008**, *9*, 2408–2418.
42. Zang, B.; Yang, B. *Anal. Bioanal. Chem.* **2010**, *396*, 973–982.
43. Grainger, D. W.; Castner, D. G. *Adv. Mater.* **2008**, *20*, 867–877.
44. Krug, H. F.; Wick, P. *Angew. Chem., Int. Ed.* **2011**, *50*, 1260–1278.

Downloaded by UNIV OF DELAWARE MORRIS LIB on June 3, 2012 | http://pubs.acs.org
Publication Date (Web): December 13, 2011 | doi: 10.1021/bk-2011-1091.ch005

Downloaded by STANFORD UNIV GREEN LIBR on June 3, 2012 | http://pubs.acs.org
Publication Date (Web): December 13, 2011 | doi: 10.1021/bk-2011-1091.ch006

Chapter 6

Enhanced Inhibition of Protein Carbohydrate Interactions by Dendritic Multivalent Glycoligands

Roland J. Pieters*

**Department of Medicinal Chemistry and Chemical Biology,
Utrecht Institute for Pharmaceutical Sciences, Utrecht University,
P.O. Box 80082, 3508 TB Utrecht, The Netherlands
*E-mail: R.J.Pieters@uu.nl**

Dendritic glycoligands of numerous sizes and shapes have provided a wealth of information about multivalency effects in the binding and inhibition of carbohydrate binding proteins over the years. Considering the biological roles of many such proteins, inhibition can be a highly valuable goal. Here a number of well-studied proteins have been selected and the effectiveness of the various dendritic ligands is discussed in relation to the nature of the protein target and the relevant multivalency mechanisms.

Introduction

Protein carbohydrate interactions are involved in many essential processes in living systems. Additionally, various pathogenic processes rely on the specific recognition of carbohydrate structures. Such processes include the diseases caused by microorganism such as viruses and bacteria as well as their toxins. In many cases the carbohydrate recognition is required for the disease progression, e.g., for a bacterial pathogen to colonize or invade or for a toxin or virus to be internalized. Considering the importance of these disease processes and the problematic eradication due to antibiotic resistance or the lack of suitable antiviral agents, scientists have attempted to selectively interfere with the recognition processes. One of the limitations encountered is the relatively weak binding of carbohydrate binding proteins to their ligands. To overcome this, multivalency effects are often operative in nature, which means that multiple copies of the

In Petite and Sweet: Glyco-Nanotechnology as a Bridge to New Medicines; Huang, X., et al.;
ACS Symposium Series; American Chemical Society: Washington, DC, 2011.

Downloaded by STANFORD UNIV GREEN LIBR on June 3, 2012 | http://pubs.acs.org
Publication Date (Web): December 13, 2011 | doi: 10.1021/bk-2011-1091.ch006

carbohydrate are involved in the recognition process. This phenomenon, also termed the cluster effect, is essential and a characteristic of the carbohydrate recognition process (*1*). For this reason scientists have turned to the use of synthetic multivalent carbohydrates to inhibit natural carbohydrate recognition processes. Dendrimers are a logical choice as the backbone for the synthesis of multivalent carbohydrates (*2*, *3*). They are easily synthesized molecules that can accommodate numerous carbohydrate moieties at relatively well-defined densities and distances. Considering the enormous wealth of dendrimer structures, a large variety of glycodendrimer structures can be prepared ranging in valencies from 2 to over 200. With such a large variety of structures available, which combination of dendrimer, valency, spacers and conjugation chemistry must one choose? The answer depends to some extent on the process to be inhibited. For this it is good to go back to the origin of the multivalency or cluster effect. The origin is by no means obvious and has given rise to avid speculation. Nevertheless, some empirical rules can be linked to commonly used explanations (*4*). If the multivalent ligand is capable of simultaneous binding to two protein binding sites, the mechanism is considered to be of the chelation type. This usually requires the binding sites to be separated by relatively short distances. As such, compounds of small size and low valency can exhibit large potency increases in inhibition processes. An example of this case is the lectin wheat germ agglutinin (WGA, *vide infra*), and examples of its inhibitors are shown below. The usual explanation is that a large part of the entropic penalty of binding was already paid for by the binding of the first (sub)ligand and need not be paid by the second, resulting in an overall potency increase. If the space between binding sites is too large to be effectively bridged by a suitable spacer, or if only a single binding site is present, multivalent carbohydrates can still be capable of inhibiting or binding these proteins with significantly enhanced potency compared to a single monovalent ligand with a similar aglycon. The nature of this effect is coined the statistical rebinding effect, where the dissociation of a ligand is slowed down because a replacement ligand readily takes the place of the dissociating one. It seems that the reported cases where this mechanism can be suspected typically involve larger multivalent systems of higher valency. The inhibition of concanavalin A (ConA, *vide infra*) fits this category. However, it should be kept in mind that when a multivalent carbohydrate system becomes larger, chelation can also start to play a role, so a mixing of the mechanism is often taking place. Furthermore, in many cases of multivalent binding an aggregate of numerous copies of either or both the protein and carbohydrate may be formed. It is possible that this aggregation process is favorable and the cause of the enhanced potency of the multivalent ligand. On the other hand, it may simply be a consequence of the inherently favorable multivalent binding. In this chapter examples of multivalent carbohydrates are shown, mostly glycodendrimers, which clearly show enhanced potency in the binding or inhibition of carbohydrate binding proteins. Besides the aforementioned plant lectins WGA, and ConA, targets of medicinal interests are discussed, which include a bacterial toxin, and a few bacterial adhesins. Finally, the attachment of glycodendrimers to a microarray is shown as an example of how the identification of multivalency effects can be made more efficient.

Wheat Germ Agglutinin (WGA)

The WGA lectin has been used on numerous occasions in the past to evaluate multivalency or cluster effects of newly synthesized multivalent carbohydrates. The 36-kDa protein is a dimer and contains 4 binding sites in each subunit. The distance between the two closest binding sites is ca. 14 Å, when measuring the distance between the anomeric oxygens of two bound GlcNAc moieties. The protein can also bind *N*-acetyl neuraminic acid besides GlcNAc. Figure 1a shows a number of explored multivalent ligands. The calixarene derivative **1** was shown to inhibit WGA 312-fold more strongly per attached sugar in comparison to the free sugar GlcNAc in a hemagglutination inhibition assay (*5*). Similarly, large enhancements were found for the tetravalent ligand **2** based on a cyclic peptide scaffold (*6*). Here a potency enhancement of 360-fold was determined relative to GlcNAc in an ELISA-type assay. Even larger enhancements in the same assay were observed for the octavalent glycodendrimer **4**, with a 4700-fold potency enhancement (*42*). Recently, Wittmann and coworkers found that α-linked GlcNAc moieties are much more effective when built into multivalent ligands (*7*). This can be seen when comparing β-linked GlcNAc **2** with **3**, which contains α-linkages and showed a potency increase of 6400-fold in comparison with free GlcNAc. The simple divalent **5** is another example of this with an impressive potency enhancement of 1170-fold. The closely related **8**, is a somewhat weaker ligand, but it proved possible to crystallize this ligand while bound to the protein. As expected, but now visible for the first time, true chelation occurred as can be seen in Figure 1b (*7*). From the structure the usefulness of the α-linkages can also be understood, since a β-linkage would require a considerably longer spacer to simultaneously accommodate both bound GlcNAc units. Additional support for the chelation mechanism was recently obtained with the use of a spin label and ESR measurements in solution (*8*). Besides monosaccharides, trisaccharides have also been made multivalent as can be seen in structure **6**, which is based on a lipophilic silicon-based dendrimer system (*9*). Here a potency enhancement of 424 fold per sugar was observed in comparison with the unconjugated sugar. Overall it is clear that the inhibition of WGA follows the chelate mechanism, which now has also been confirmed by X-ray crystallography. The fact that small ligands of low valency already show sizeable potency enhancements is consistent with this notion. This does by no means indicate that larger systems of higher valency cannot be effective. They certainly can be as exemplified by the quantum dot **7**, which has shown very high potency enhancements (*10*).

Downloaded by STANFORD UNIV GREEN LIBR on June 3, 2012 | http://pubs.acs.org
Publication Date (Web): December 13, 2011 | doi: 10.1021/bk-2011-1091.ch006

Downloaded by STANFORD UNIV GREEN LIBR on June 3, 2012 | http://pubs.acs.org
Publication Date (Web): December 13, 2011 | doi: 10.1021/bk-2011-1091.ch006

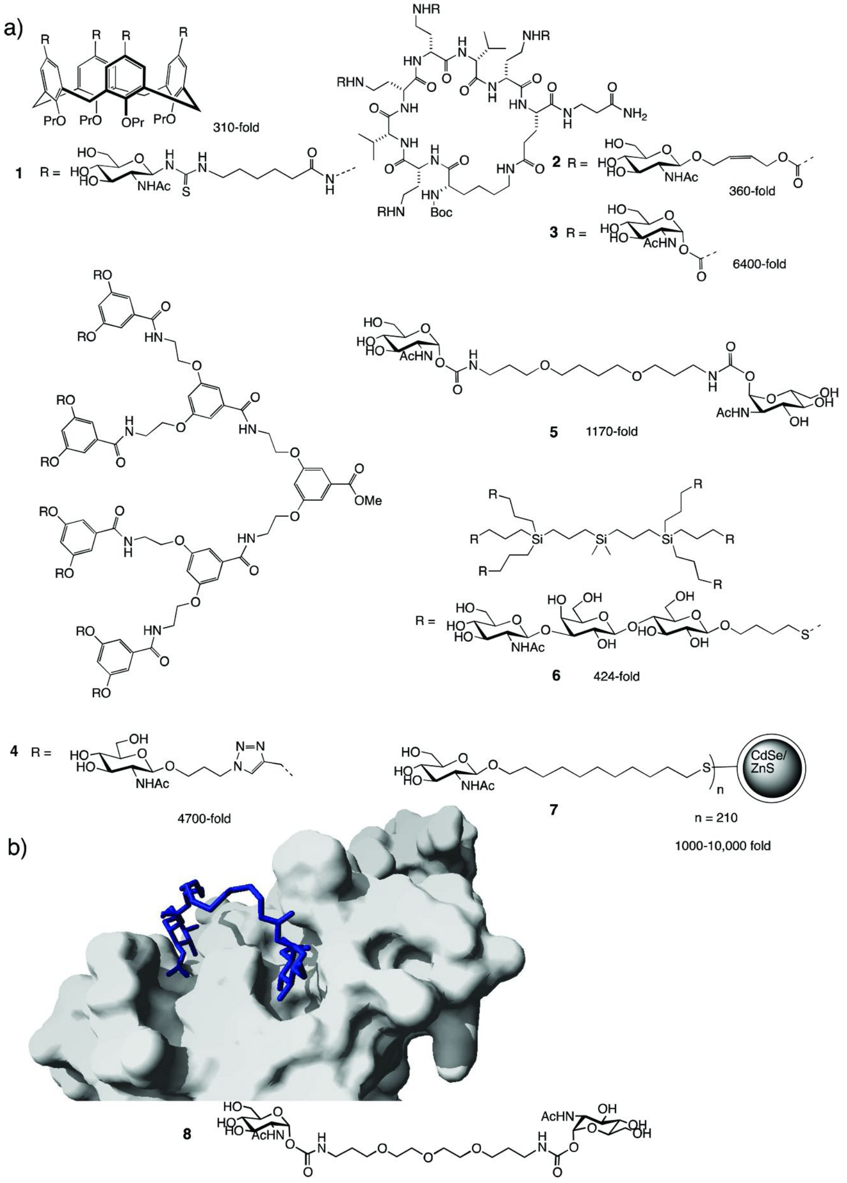
a)
310-fold
1 R =
2 R =
360-fold
3 R =
6400-fold
5
1170-fold
6
424-fold
R =
4 R =
4700-fold
7
CdSe/ZnS
n = 210
1000-10,000 fold
b)
8

Figure 1. a) Structures of ligands of WGA and their multivalent potency enhancement per sugar, compared to relevant monovalent ligands; b) X-ray structure of ConA bound to ***8****.*

Downloaded by STANFORD UNIV GREEN LIBR on June 3, 2012 | http://pubs.acs.org
Publication Date (Web): December 13, 2011 | doi: 10.1021/bk-2011-1091.ch006

Concanavalin A (ConA)

Many studies on multivalency effects have been performed with the lectin ConA from the Jack bean. This lectin binds to both α-linked glucosides and mannosides with a preference for the latter. It contains four tetrahedrally oriented subunits that are spaced ca. 72 Å, i.e., more than 5 times longer than the shortest distance in WGA. Small multivalency ligands of low valency tend to be relatively ineffective. The divalent **9** still showed a 19-fold enhancement (Figure 2) (*11*), but the small PAMAM glycodendrimer **10**, showed hardly any noticeable enhancement. In contrast, larger systems, such as the higher generation PAMAM glycodendrimer **11** showed a large multivalency enhancement per sugar of 660 fold (*12*, *13*) and similar observations were made for hyperbranched polyglycerol based glycodendrimers (*14*). These enhancements of larger systems are not limited to dendrimers since polymers, micelles, quantum dots, and linear glycopolymers were also shown to exhibit these effects (*15*, *16*). However there was a report of an exception to these trends, i.e., compound **12**, which is both relatively small and of relatively low valency, yet exhibited a very large potency enhancement of 3750-fold per sugar in a hemagglutination inhibition assay in comparison with Me-α-D-glucopyranoside (*17*). This result indicates that the mechanistic aspects are more complicated even though in general the statistical rebinding mechanism seems to be more effective for larger systems. Chelation also plays a role, but the Cloninger group performed elegant experiments (*13*) using monomeric ConA incapable of chelation. The multivalency effects with large PAMAM glycodenrimers and the monomeric ConA were still high indicating that chelation only contributed about a factor of 4. While the PAMAM glycodendrimers reportedly do not induce it, aggregation is often observed for multivalent ConA binding and certainly for compound **12**. It seems possible that **12** is preorganized in such a way that it promotes the formation of a stable aggregate, thus explaining its remarkable multivalency effect with ConA.

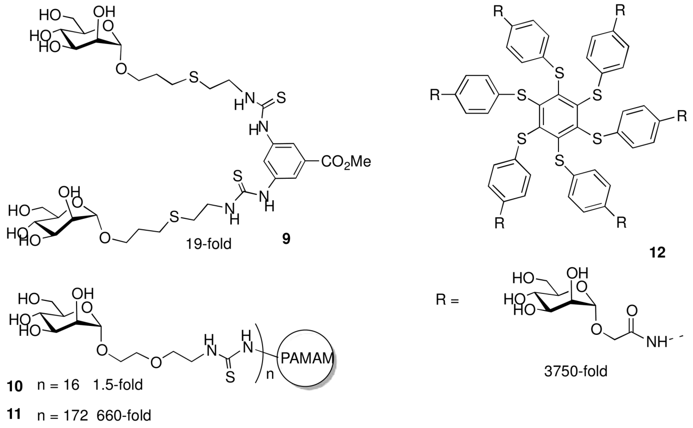

Figure 2. Multivalent inhibitors of ConA and their multivalent potency enhancement per sugar, compared to relevant monovalent ligands.

Downloaded by STANFORD UNIV GREEN LIBR on June 3, 2012 | http://pubs.acs.org
Publication Date (Web): December 13, 2011 | doi: 10.1021/bk-2011-1091.ch006

Cholera Toxin

The cholera toxin is a member of the class of bacterial AB_5 toxins and is the causative agent of the cholera disease. Its 5 B-subunits that are all present on the same side of the toxin are separated by ca. 31 Å. Therefore each can simultaneously bind to the ganglioside GM1 present on the intestinal tract surface. It binds in a multivalent manner followed by internalization and disease progression due to the A-subunit, resulting massive diarrhea. Blocking the action of the B-subunit has the potential to block the disease and its specific recognition may also aid in the development of diagnostic tools (*18*). Early on, work by Hol, Fan and coworkers was reported on a multivalent approach of inhibition by using a pentavalent core structure with 5 appendages terminating in galactoside moieties (*19*). Noteworthy of the study is that significant blocking was observed despite the use of the weakly binding sugar, and also that the spacer lengths needed to be very long to take its inherent folding into consideration. We took that lesson to heart in the design of compound **13** (Figure 3), which contained long spacer arms on the dendritic scaffold and used the optimal natural pentasaccharide ligand, the GM1 oligosaccharide (GM1os). For this compound a multivalent enhancement was observed of close to 7600 fold per sugar when compared to a monovalent GM1os derivative (*20*). Clearly very potent inhibition can be obtained for this system, and it was tempting to ascribe it to a chelation mechanism. However, the system was studied in more details and significant aggregation was observed involving both toxin and multivalent ligand (*21*). The relevance to the inhibition was not entirely certain, since these measurements were made at the higher (micromolar) concentration, due to the limitations of the instrumentation, and not at the sub-nanomolar concentrations present in the inhibition studies. It was speculated that the origin of the aggregation lies in the mismatch of valency between the toxin and the ligand, leaving binding sites open for cross-linking. Nevertheless it is still not entirely sure if the remarkable potency of inhibition is related to the aggregation forming ability of the combination of toxin and inhibitor. Considering these results multivalent galactoside **14** was also tested and found to be as effective as a monovalent GM1 derivative in the ELISA-like inhibition assay (*22*). The multivalency effect was able to overcome the many orders of magnitude lost in going from GM1os to the weakly binding galactoside monovalent ligand. Besides the multivalency approach a structure-based approach of optimizing monovalent ligands has also been ongoing (*23*). Recently such an improvement strategy was combined with the attachment of the newly built ligands to a multivalent polymeric backbone such as dextran (*24*). Very potent compounds resulted from the study as exemplified by **15**, which surprisingly contained an α-linked galactoside, in contrast to the natural ligand GM1os which contains β-linkages. The potency resulted from the combination of the optimized monovalent ligand and the effective presentation by the dextran and is illustrated by the IC_{50} for **15** in an ELISA type assay of 12 nM per ligand, while the polymer lacking the ‘clicked on’ portion showed no appreciable inhibition, presumably in the micromolar range. Indeed the ligand portion of **15** non-attached to the dextran polymer, was tested separately and found to be 100-fold more potent than galactose itself. In short the cholera toxin is a perfect target for the exploration of multivalent ligands, which has not been limited to the use of dendrimers (*15*).

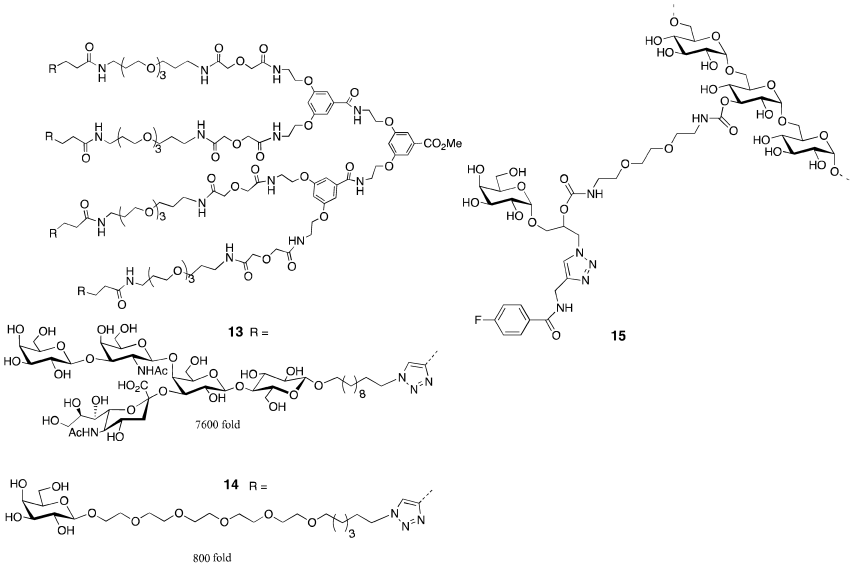

Figure 3. Inhibitors of Cholera Toxin and their multivalent potency enhancement per sugar, compared to relevant monovalent ligands.

Bacterial Adhesion

Pathogenic bacteria often need to firmly adhere to a tissue surface in order for disease progression to occur, e.g. via colonization or invasion. They often accomplish this by binding to tissue-specific carbohydrate structures. On their surface these bacteria carry so-called adhesins or adhesion proteins that are responsible for the specific recognition, which can provide the microbe with a specificity for a certain host organism and also a certain tissue type (*25*). The adhesion process is in principle an attractive and mild process for interference with bacterial infections (*26*). Furthermore, the adhesion proteins also provide a handle that should allow specific detection of virulent bacteria (*27–29*). Either process requires the use of strongly binding agents and since the recognition is based on protein carbohydrate interactions, here too multivalency seems to be needed to achieve the required potency (*30*). The best-studied case is no doubt the uropathogenic *E.coli*, i.e., a bacterium that needs to adhere strongly to the bladder cell surface in order to not be washed out. These are usually type 1 fimbriated and mannose-specific. The cases are well documented. However, since the binding sites are likely separated by long distances, glycodendrimers so far were only moderately effective (*31–33*) although a lot of progress was made on the development of enhanced monovalent ligands (*34*, *35*). An alternative target is *Streptococcus suis* a zoonotic pathogen that affects mostly newborn

Downloaded by STANFORD UNIV GREEN LIBR on June 3, 2012 | http://pubs.acs.org
Publication Date (Web): December 13, 2011 | doi: 10.1021/bk-2011-1091.ch006

Downloaded by STANFORD UNIV GREEN LIBR on June 3, 2012 | http://pubs.acs.org
Publication Date (Web): December 13, 2011 | doi: 10.1021/bk-2011-1091.ch006

piglets, thus causing serious damage in the meat industry. This Gram-positive pathogen is known to bind to the Galα1-4Gal sequence. Its adhesion inhibition responds well to multivalent versions of the sequence in two separate assays and low nanomolar inhibition was obtained as exhibited by compound **16** (Figure 4) (*36*, *37*). The same type of dendritic compounds as **16**, but now linked to the sequence GalNAcβ1,4Gal, was tested as adhesion inhibitor for the opportunistic pathogen *Pseudomonas aeruginosa*. Unfortunately multivalency enhancements were less than an order of magnitude (*38*). More recent developments on *P. aeruginosa* adhesion have focused on two soluble lectins of this pathogen, LecA and LecB (or PA-IL and PA-IIL), on the surface of the bacterium. Unlike the GalNAcβ1,4Gal adhesin that resides in the pili, the LecA and LecB proteins likely attach themselves to surface carbohydrates, utilizing their additional binding sites to adhere to the host. These lectins were shown to be virulence factors (*39*) and also of importance for biofilm formation (*40*), which makes these pathogens particularly hard to eradicate. LecA has specificity for galactosides and contains a shortest distance between binding sites of ca. 26 Å. Of a series of calix[4]arenes, compound **17** in its 1,3 alternate conformation was shown to be a particularly effective inhibitor in multiple assays especially by isothermal titration calorimetry (ITC) (*41*). It was found to have a K_d of 176 nM, 213-fold more potent per sugar in comparison to a relevant reference compound. Perhaps **17** is a particularly well preorganized divalent molecule for chelation, or alternatively its structural features allow it to chelate and simultaneously be an effective part of an aggregate. In our own studies we found that a tetravalent inhibitor of the type of compound **16**, but only outfitted with galactose moieties, was ca. 16-fold better per sugar and inhibited LecA in the low micromolar range in an ELISA type assay (*42*). In a large study involving both optimization of the mono and multivalent level, further improvements were reported (*43*). Interestingly, it was found that β-linked conjugates benefit from hydrophobic elaboration, even though α-substitution is typically more favorable. Linking the improved monovalent compound to a number of dendritic scaffolds yielded the nonavalent **18**, which was on a per sugar basis a 45-fold more potent ligand than the β-Gal-O-Me reference compound, as determined by ITC. Reymond and coworkersprepared combinatorial libraries of dendritic peptides in which each arm terminates in a carbohydrate (*44*). These were prepared and evaluated as ligands for LecB, the other tetrameric *P. aueruginosa* lectin involved in virulence and biofilm formation. This protein binds to *L*-fucosides and the screening yielded the octavalent fucoside **19** as the tightest binding ligand. In an ELISA assay it was 55-fold more potent on a per sugar basis. Experimental and computational studies with the terminal fucoside and linked amino acids clearly indicated that these amino acids did not contribute to the enhanced potency of **19**. Taken into account that the system is expected to be too small to chelate the binding sites, an explanation involving non-terminal amino acids binding favorably to the protein surface was given as the most likely possibility.

Downloaded by STANFORD UNIV GREEN LIBR on June 3, 2012 | http://pubs.acs.org
Publication Date (Web): December 13, 2011 | doi: 10.1021/bk-2011-1091.ch006

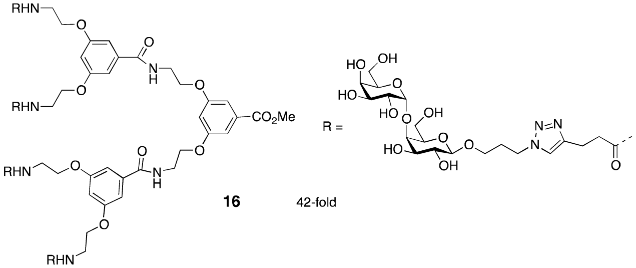
RHN
O
CO2Me
R =
HO
OH
N=N

16 42-fold

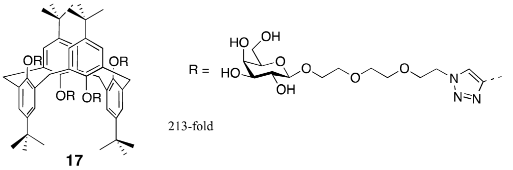

17 213-fold

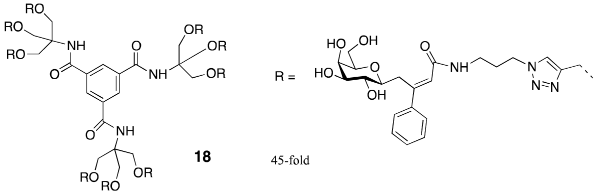
RO
NH
OR
R =
HO
OH
NH
N=N

18 45-fold

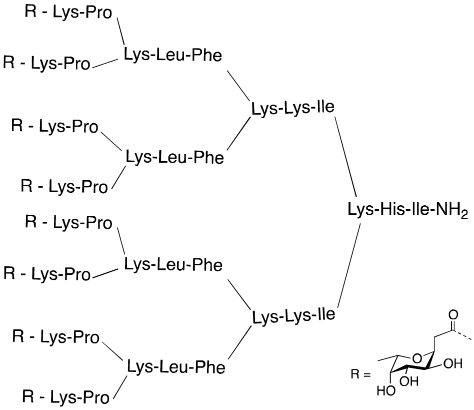
R - Lys-Pro
Lys-Leu-Phe
Lys-Lys-Ile
Lys-His-Ile-NH2
R =
OH
HO

19 55-fold

*Figure 4. Bacterial adhesion inhibitors of S. suis (**16**), P. aeruginosa lectins LecA (**17, 18**) and LecB (**19**), and their multivalent potency enhancement per sugar, compared to relevant monovalent ligands.*

Downloaded by STANFORD UNIV GREEN LIBR on June 3, 2012 | http://pubs.acs.org
Publication Date (Web): December 13, 2011 | doi: 10.1021/bk-2011-1091.ch006

Glycodendrimer Microarray

The fact that glycodendrimers can be very potent ligands should be evident from the above. A careful search for the right multivalent scaffold matched with a proper spacer and carbohydrate structures can be a labor-intensive as well as time and material consuming undertaking. In an effort to simplify the search for a good combination of protein target and multivalent ligand, we explored the use of a microarray approach. In order for this to succeed, the multivalent system needs to be amenable to specific immobilization on the chip surface. As can be seen in Figure 5, the core was simply elaborated by a PEG spacer terminating in an amino group for immobilization. While initially exploring only mannose (*45*) the subsequent incarnation of the chip featured 5 carbohydrates attached to dendrimers of valencies 8, 4, 2, and also 1 (*42*). To correct for the valency differences, the spotting concentration of the octavalent dendrimer was eight times less than that of the monovalent, while the concentration of the tetravalent was four times less etc. A porous aluminum oxide material was used for the chip, which increases the surface area by a factor of 500, coupled with technology that allowed the on-line monitoring of the binding process. Conclusions so far are that the dendrimers are spaced far enough apart that chelation type multivalency effects are identified in a single rapid experiment for all dendrimers simultaneously, using minute quantities of both dendrimers and carbohydrate binding proteins. Experiments with WGA with its closely spaced binding sites clearly show a dramatic difference in the signal for mono versus the much brighter spots of higher valency. In addition, for LecA and cholera toxin, similar effects were observed. However for ConA, where the binding sites are too far to bridge, only a moderate difference is seen between the valencies.

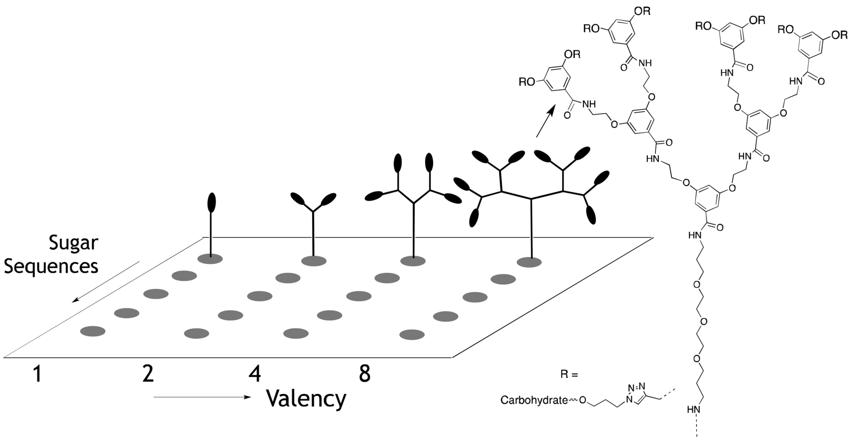

Figure 5. On the left is a cartoon depiction of the glycodendrimer array surface is shown, with ever increasing valency yet with a carbohydrate content that is the same in all cases. On the right the actual structure of a tetravalent glycodendrimer is shown.

Downloaded by STANFORD UNIV GREEN LIBR on June 3, 2012 | http://pubs.acs.org
Publication Date (Web): December 13, 2011 | doi: 10.1021/bk-2011-1091.ch006

Conclusion

In order to inhibit a carbohydrate binding protein effectively using multivalent glycoligands, it is useful to look at the organization of the binding site or sites. In case of closely spaced binding sites, dendritic glycoligands of low valency have been highly successful inhibitors and enhancements of 3 orders of magnitude or more have been observed for targets such as WGA or the cholera toxin and the *Pseudomonas aeruginosa* lectin LecA. More challenging are targets such as ConA where binding sites are further apart. For such proteins small multivalent systems are relatively ineffective while for large dendritic systems high enhancement numbers have been reported. Nevertheless for ConA a highly effective small multivalent glycoligand was reported, indicating the complexity of the mechanism. Combination of chelation, statistical rebinding and aggregation phenomena all play a role, making it hard to predict efficacy for such systems. In order to increase the efficiency of the discovery of multivalency effects, the use of a glycodendrimer array was shown to be able to identify multivalency effects for WGA and LecA in a single experiment for multiple valencies.

References

1. Lundquist, J. J.; Toone, E. J. *Chem. Rev.* **2002**, *102*, 555–578.
2. Lahmann, M. In *Glycoscience and Microbial Adhesion*; Springer-Verlag Berlin: Berlin, 2009; Vol. 288, pp 17−65.
3. Deniaud, D.; Julienne, K.; Gouin, S. G. *Org. Biomol. Chem.* **2011**, *9*, 966–979.
4. L. L. Kiessling, L. L.; Gestwicki, J. E.; Strong, L. E. *Angew. Chem., Int. Ed.* **2006**, *45*, 2348–2368.
5. Consoli, G. M. L.; Cunsolo, F.; Geraci, C.; Sgarlata, V. *Org. Lett.* **2004**, *6*, 4163–4166.
6. Maierhofer, C.; Rohmer, K.; Wittmann, V. *Bioorg. Med. Chem.* **2007**, *15*, 7661–7676.
7. Schwefel, D.; Maierhofer, C.; Beck, J. G.; Seeberger, S.; Diederichs, K.; Moller, H. M.; Welte, W.; Wittmann, V. *J. Am. Chem. Soc.* **2010**, *132*, 8704–8719.
8. Braun, P.; Nägele; Wittmann, V.; Drescher, M. *Angew. Chem., Int. Ed.* **2011**, *50*, 8428–8431.
9. Yamada, A.; Hatano, K.; Koyama, T.; Matsuoka, K.; Takahashi, N.; Hidari, K.; Suzuki, T.; Suzuki, Y.; Terunuma, D. *Biorg. Med. Chem.* **2007**, *15*, 1606–1614.
10. Robinson, A.; Fang, J.-M.; Chou, P.-T.; Liao, K.-W. *ChemBioChem* **2005**, *6*, 1899–1905.
11. Pagé, D.; R. Roy, R. *Bioorg. Med. Chem. Lett.* **1996**, *6*, 1765–1770.
12. Woller, E. K.; Walter, E. D.; Morgan, J. R.; Singel, D. J.; Cloninger, M. J. *J. Am. Chem. Soc.* **2003**, *125*, 8820–8826.
13. Mangold, S. L.; Cloninger, M. J. *Org. Biomol. Chem.* **2006**, *4*, 2458–2465.
14. Papp, I.; Dernedde, J.; Enders, S.; Riese, S. B.; Shiao, T. C.; Roy, R.; Haag, R. *ChemBioChem* **2011**, *12*, 1075–1083.

15. Pieters, R. J. *Org. Biomol. Chem.* **2009**, *7*, 2013–2025.
16. Mortell, K. H.; Weatherman, R. V.; Kiessling, L. L. *J. Am. Chem. Soc.* **1996**, *118*, 2297–2298.
17. Sleiman, M.; Varrot, A.; Raimundo, J. M.; Gingras, M.; Goekjian, P. G. *Chem. Commun.* **2008**, 6507–6509.
18. Zhang, G. T. *Expert. Opin. Drug Discovery* **2009**, *4*, 923–938.
19. Fan, E.; Zhang, Z.; Minke, W. E.; Hou, Z.; Verlinde, C. L. M. J.; Hol, W. G. J. *J. Am. Chem. Soc.* **2000**, *122*, 2663–2664.
20. Pukin, A. V.; Branderhorst, H. M.; Sisu, C.; Weijers, C.; Gilbert, M.; Liskamp, R. M. J.; Visser, G. M.; Zuilhof, H.; Pieters, R. J. *ChemBioChem* **2007**, *8*, 1500–1503.
21. Sisu, C.; Baron, A. J.; Branderhorst, H. M.; Connel, S. D.; Weijers, C.; de Vries, R.; Hayes, E. D.; Pukin, A. V.; Gilbert, M.; Pieters, R. J.; Zuilhof, H.; Visser, G. M.; Turnbull, W. B. *ChemBioChem* **2009**, *10*, 329–337.
22. Branderhorst, H. M.; Liskamp, R. M. J.; Visser, G. M.; Pieters, R. J. *Chem. Commun.* **2007**, 5043–5045.
23. Bernardi, A.; Cheshev, P. *Chem. Eur. J.* **2008**, *14*, 7434–7441.
24. Tran, H. A.; Kitov, P. I.; Paszkiewicz, E.; Sadowska, J. M.; Bundle, D. R. *Org. Biomol. Chem.* **2011**, *9*, 3658–3671.
25. Pieters, R. J. *Adv. Exp. Med. Biol.* **2011**, *715*, 227–240.
26. Imberty, A.; Chabre, Y. M.; Roy, R. *Chem. Eur. J.* **2008**, *14*, 7490–7499.
27. El-Boubbou, K.; Gruden, C.; Huang, X. *J. Am. Chem. Soc.* **2007**, *129*, 13392–13393.
28. Hatch, D. M.; Weiss, A. A.; Kale, R. R.; Iyer, S. S. *ChemBioChem* **2008**, *9*, 2433–2442.
29. Pera, N. P.; Kouki, A.; Haataja, S.; Branderhorst, H. M.; Liskamp, R. M. J.; Visser, G. M.; Finne, J.; Pieters, R. J. *Org. Biomol. Chem.* **2010**, *8*, 2425–2429.
30. Pieters, R. J. *Med. Res. Rev.* **2007**, *27*, 796–816.
31. Touaibia, M.; Wellens, A.; Shiao, T. C.; Wang, Q.; Sirois, S.; Bouckaert, J.; Roy, R. *ChemMedChem* **2007**, *2*, 1190–1201.
32. Touaibia, M.; Roy, R. *Mini-Rev. Med. Chem.* **2007**, *7*, 1270–1283.
33. Durka, M.; Buffet, K.; Iehl, J.; Holler, M.; Nierengarten, J. F.; Taganna, J.; Bouckaert, J.; Vincent, S. P. *Chem. Commun.* **2011**, *47*, 1321–1323.
34. Wellens, A.; Garofalo, C.; Nguyen, H.; Van Gerven, N.; Slattegard, R.; Hernalsteens, J. P.; Wyns, L.; Oscarson, S.; De Greve, H.; Hultgren, S.; Bouckaert, J. *PLoS One* **2008**, *3*.
35. Grabosch, C.; Hartmann, M.; Schmidt-Lassen, J.; Lindhorst, T. K. *ChemBioChem* **2011**, *12*, 1066–1074.
36. Joosten, J. A. F.; Loimaranta, V.; Appeldoorn, C. C. M.; Haataja, S.; El Maate, F. A.; Liskamp, R. M. J.; Finne, J.; Pieters, R. J. *J. Med. Chem.* **2004**, *47*, 6499–6508.
37. Branderhorst, H. M.; Kooij, R.; Salminen, A.; Jongeneel, L. H.; Arnusch, C. J.; Liskamp, R. M. J.; Finne, J.; Pieters, R. J. *Org. Biomol. Chem.* **2008**, *6*, 1425–1434.
38. Autar, R.; Khan, A. S.; Schad, M.; Hacker, J.; Liskamp, R. M. J.; Pieters, R. J. *ChemBioChem* **2003**, *4*, 1317–1325.

Downloaded by STANFORD UNIV GREEN LIBR on June 3, 2012 | http://pubs.acs.org
Publication Date (Web): December 13, 2011 | doi: 10.1021/bk-2011-1091.ch006

39. Chemani, C.; Imberty, A.; de Bentzmann, S.; Pierre, M.; Wimmerova, M.; Guery, B. P.; Faure, K. *Infect. Immun.* **2009**, *77*, 2065–2075.

40. Diggle, S. P.; Stacey, R. E.; Dodd, C.; Cámara, M.; Williams, P.; Winzer, K. *Environ. Microbiol.* **2006**, *8*, 1095–1104.

41. Cecioni, S.; Lalor, R.; Blanchard, B.; Praly, J. P.; Imberty, A.; Matthews, S. E.; Vidal, S. *Chem. Eur. J.* **2009**, *15*, 13232–13240.

42. Pera, N. P.; Branderhorst, H. M.; Kooij, R.; Maierhofer, C.; van der Kaaden, M.; Liskamp, R. M. J.; Wittmann, V.; Ruijtenbeek, R.; Pieters, R. J. *ChemBioChem* **2010**, *11*, 1896–1904.

43. Dr. Yoann M. Chabre, Y. M.; Giguère, D.; Blanchard, B.; Rodrigue, J.; Rocheleau, S.; Neault, M.; Rauthu, S.; Papadopoulos, A.; Arnold, A. A.; Imberty, A.; Roy, R. *Chem. Eur. J.* **2011**, *17*, 6545–6562.

44. Kolomiets, E.; Swiderska, M. A.; Kadam, R. U.; Johansson, E. M. V.; Jaeger, K. E.; Darbre, T.; Reymond, J. L. *ChemMedChem* **2009**, *4*, 562–569.

45. Branderhorst, H. M.; Ruijtenbeek, R.; Liskamp, R. M. J.; Pieters, R. J. *ChemBioChem* **2008**, *9*, 1836–1844.

Downloaded by STANFORD UNIV GREEN LIBR on June 3, 2012 | http://pubs.acs.org
Publication Date (Web): December 13, 2011 | doi: 10.1021/bk-2011-1091.ch006

Chapter 7

Glyco-Functionalized Quantum Dots

Jacob J. Weingart and Xue-Long Sun*

Department of Chemistry, Cleveland State University,
2121 Euclid Ave., Cleveland, Ohio 44115
***E-mail: x.sun55@csuohio.edu. Phone: 216-687-3919. Fax: 216-687-9289.**

Quantum dots (QDs), semiconductor nanoparticles with unique photo-physical properties, have become one of the dominant classes of imaging probes for monitoring or labeling biological processes. Particularly, surface bio-functionalizations have facilitated QDs in a variety of in vitro and in vivo applications. The emergence of glycobiology, glycotechnology and glycomics have opened exciting avenue of medicinal applications of carbohydrates. Among them, the biocompatibility and specific receptor recognition ability confer the ability of carbohydrates as potential targeting ligands to modify nanoparticles for site-specific bioimaging and therapeutic applications. This book chapter outlines recent glyco-functionalization of QDs related to their bioconjugation methods, characterizations, and potential applications.

Introduction

QDs: History, Properties, Synthesis, and Applications

With the recognition that materials at the intersection between single molecular to bulk fundamentally exhibit unique properties not inherent to either phase, came the advent of nanotechnology. This field, studying the control of matter on an atomic and molecular scale, has emerged with great potential in generating many new materials. These materials, usually smaller than 100 nm in at least one dimension, have been implemented in the development of a wide range of applications for various research fields, such as medicine, electronics and energy production (*1*). Of the many materials developed in various dimensions, three dimensional nanoparticles have become of great interest. Nanoparticles,

In Petite and Sweet: Glyco-Nanotechnology as a Bridge to New Medicines; Huang, X., et al.;
ACS Symposium Series; American Chemical Society: Washington, DC, 2011.

ranging from sizes mimicking that of pathogenic bacteria to even smaller viruses, come in many compositions with cores made up of either organic polymeric materials or inorganic materials and through synthetic modification have been manipulated for many studies from targeted and timed release delivery of reagents to electron transfer and imaging (*2*).

Of the various inorganic-based nanoparticle systems, quantum dot semiconductor crystals have drawn much attention due to their unique photophysical properties. These semiconductor nanocluster crystals evolved through investigations attempting to improve modern day solid state electronics. During the 1980's a variety of materials were investigated for their use in semiconductors, particularly those composed of atoms from groups II – IV or III – V elements in the periodic table (*3*). Laboratories soon began to study the three dimensional evolution of these elements, and combinations thereof, from the molecular to bulk as semiconductor nanoclusters, which came to be known as quantum dots (*4*). Of the labs involved in researching these nanoclusters, AT&T Bell Laboratories with Louis Brus pioneered such work recognizing that single electrons created by the HOMO-LUMO promotion within the molecular orbitals of the solid moved rapidly in response to electric fields, such as light (*5*, *6*). This promotion to a higher electronic state, in the absence of defects within the crystal, are typically accompanied by a relaxation of this excited state resulting in radiative decay exhibiting near unity fluorescence quantum yield. For typical fluorescent organic dye molecules, this is not the case. This, in part, is due to overlapping of vibronic interactions with the excited state when the wave function occupies just one or more bonds, which promotes fast nonradiative deactivation of electrons back to the ground state. As a result, fluorescence quantum yields for organic-based dye molecules tend to be relatively lower than that of quantum dots (*6*). Thus quantum dots, or nanocrystals with their small size ($\leq$ 10 nm), brightness, high photostability, and size-tunable spectral properties, have been recognized for their potential use as ideal chromophores for a variety applications within the fields of biology and medicine (*7*). As with other inorganic nanoparticle systems, though quantum dots exhibit great potential for a number of applications, they are limited due to the fact that synthetic optimization of such clusters and control of the surface remains very empirical with little understanding of what influences size, shape and growth limiting the ability for these materials to be produced at a manufacturing level with any consistency (*8*, *9*). This has kept quantum dots from being implemented into devices tailored for mainstream everyday use. Of the many semiconductors studied (including InP, GaAs, and Si), Cd-based quantum dots (CdSe, CdTe, CdS, CdSe-ZnS, CdSe-Si) are the most regularly synthesized, the smallest averaging to be ~ 2 nm in diameter, and implemented in research studies, represented in Figure 1 (*10*, *11*).

Though others have attempted to develop more precisely controlled synthetic procedures for producing Cd-base quantum dots, the typical synthetic route for producing quantum dots relies on the traditional high-temperature organometallic synthesis passivating the surface with either trioctylphosphine oxide (TOPO) or trioctylphosphine selenide/tellenide (TOPSe, TOPTe) groups. This involves the mixing of a solution of trioctylphoshpine and Me_2Cd with another solution of TOPX (X = Se or Te) and TOP in anaerobic conditions followed by direct injection of the whole mixture into a flask of TOPO under argon that is vigorously stirred while heating between 290 and 320 °C (*12–14*). Since alkyl groups of the TOP/TOPX cause the surface to be hydrophobic the nanoparticles are rendered insoluble in water. Thus, to enhance water solubility and biocompatibility for bio-applications, others have investigated ways of modifying the surface, typically using ligand addition methods as depicted in Scheme 1, resulting in various hybrid systems that are more amenable to water-based applications and even further surface modification (*15–18*).

As previously mentioned, quantum dots must be appropriately coated with surfaces that are water soluble and biocompatible due to toxicity concerns. Though there is little understanding of their biological fate and the exact mechanisms through which these particles induce toxicity, it is clear that if the passivated surface of the particle is compromised, exposing and allowing Cd^{2+} to leach from the core, cellular damage and even death may occur. This, however, is not the subject of this book chapter, thus for further review of quantum dots and their toxicological study the reader is referred to a more comprehensive background view (*19–23*). Due to possible toxicological implications, quantum dots have been implemented in a number of *in vitro* bio-based assay technologies, most of which heavily rely on the unique optical properties of these nanoparticles. Unlike conventional fluorophores, the discrete energy levels of quantum dots allow for longer excited state lifetimes, size and composition tunable fluorescence with the ability to use one light source to excite multiple colors, and resistance to photobleaching (*24*). These properties confer upon quantum dots the ability to be used in the imaging and tracking of multiple molecular targets simultaneously, which is difficult to accomplish using traditional organic-based fluorescent dye molecules. As a result quantum dots when functionalized with designed ligands have found themselves being used as signal amplifiers, biological markers, sensors for bioreactors, and in tissue engineering (*25*). For example, quantum dots with the attachment of targeting antibodies and proteins have been employed as biosensors in the detection of various pathogens, their associated toxins or byproducts of biosynthetic pathways, such as *E. Coli* O157:H7 (*26*), *C. parvum* (*27*), *bacillus* types of bacteria (*28*), and *Cholera* toxin (*29*). Others employing similar strategies have used functionalized quantum dots for specific cellular staining and the fluorescence imaging of cancer cell types and real-time monitoring of cellular trafficking (*30*, *31*). Whatever the use, quantum dots have become a platform for multimodality sensing for detection or monitoring in a variety of assays where the monitoring of the effective change in the fluorescence emittance is typically used to quantitate the event.

Carbohydrate as Ligands for Targeting

In the past, regardless the application, the design of ligands for targeting with quantum dots has relied heavily on the use of antibodies, proteins and even specific nucleic acids as the directing moieties until now. The recent emergences of glycobiology, glycotechnology and glycomics have been clarifying enormous roles of carbohydrates in both physiological and pathological recognition systems. It has become recognized that carbohydrates represent the third group of informational biomolecules. For example, cell surface carbohydrates existing as glycoconjugates (glycolipids, glycoproteins and proteoglycans) play crucial roles in cell-cell communication, proliferation and differentiation, tumor metastasis, inflammatory response or microbial infection. The studies of carbohydrate-protein interactions reveal promising medicinal applications of carbohydrates. Among them, the potential of carbohydrate recognition-based targeted drug or gene delivery also termed as glycotargeting has been explored since 1990s (*32*). Most of the glycotargeting strategies exploit the highly specific interactions of carbohydrates to endogenous lectins, a large number of carbohydrate-binding proteins expressed on mammalian cell surface (*33*). For example, increased expression of lectins have been confirmed on malignant cells, which are believed to be involved in cancer metastasis and thus are potential targets for delivery of drug or gene to malignant cells. Several reviews have examined early glycotargeting (*34–36*), and the reader is referred to these for a comprehensive background view.

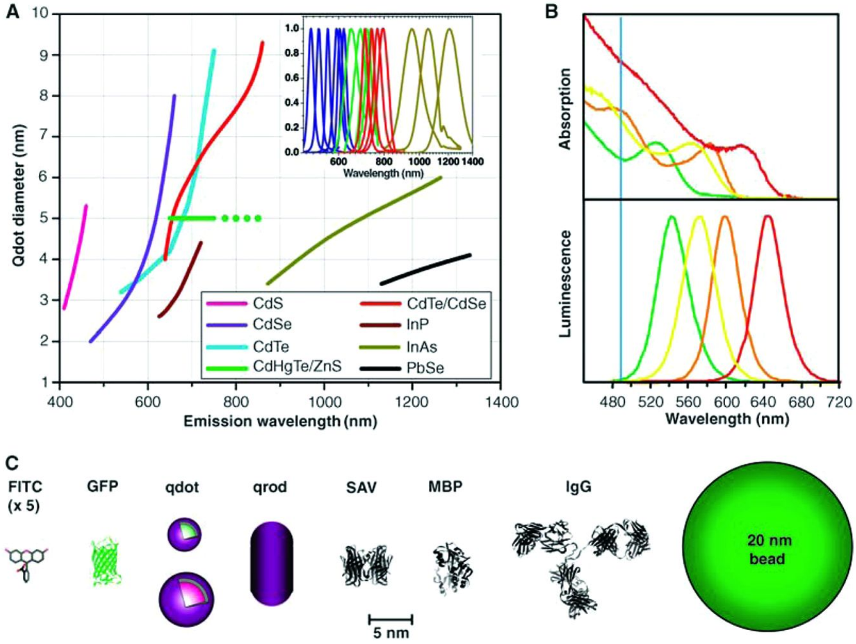

Figure 1. (A) Emission maxima and sizes of quantum dots of different composition. (B) Absorption (upper curves) and emission (lower curves) spectra of four CdSe/ZnS qdot samples. (C) Size comparison of qdots and comparable objects. (Reprinted with permission from reference 11. Copyright 2005 AAAS, all rights reserved.)

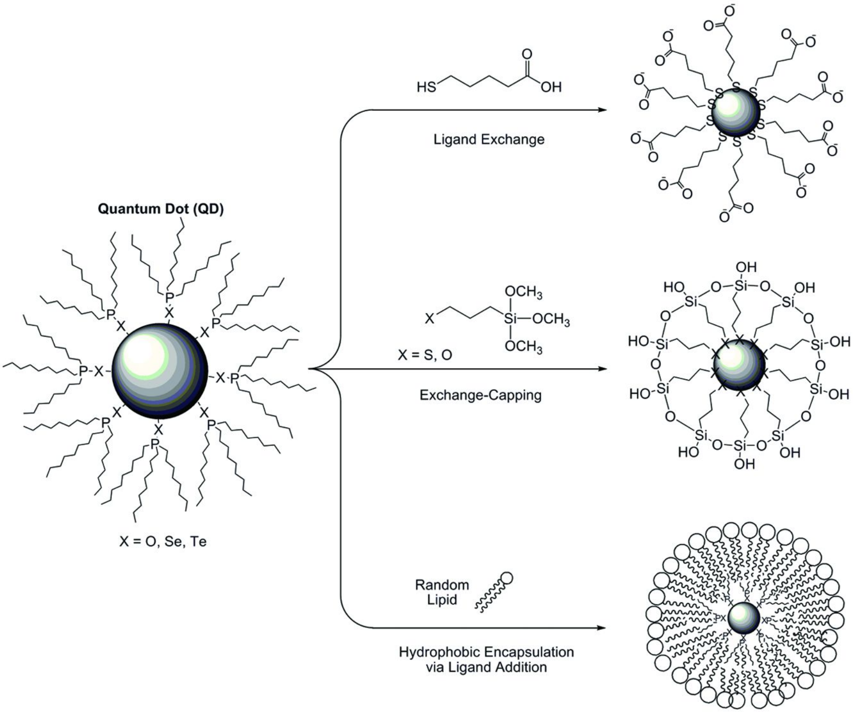

Scheme 1. A representation of types of surface modifications for quantum dots, improving water solubility.

Glyco-Functionalization

Carbohydrates Exploited on QD Surfaces

Carbohydrates as the third group of informational biomolecules represent an immense number of very complex structures important to many cellular events. The recognition of these complex carbohydrate structures within the biological system relies on several important factors. These factors include the recognition of the primary saccharide, or oligosaccharide, sequence by the target protein, several of that type of saccharide being presented and recognized along a polypeptide or on a lipid, and multiple units of that saccharide as a specific glycoconjugate, determined by the specific linkage to the glycoprotein or glycolipid, being displayed. The displaying of these saccharides as glycoconjugates, their density, distribution, relative orientations all contribute to overall binding specificity and affinity of the sequence to a particular protein target (*37*). Scheme 2 depicts the increasing complexity of this hierarchy of carbohydrate structures that contribute to cellular signaling events. This complexity only confers the idea that single saccharides, or oligosaccharides, tend to only bind weakly to their complementary proteins. A successful, enhanced binding event is achieved by the use of multiple interactions by multiple carbohydrates in a multivalent fashion (*38*).

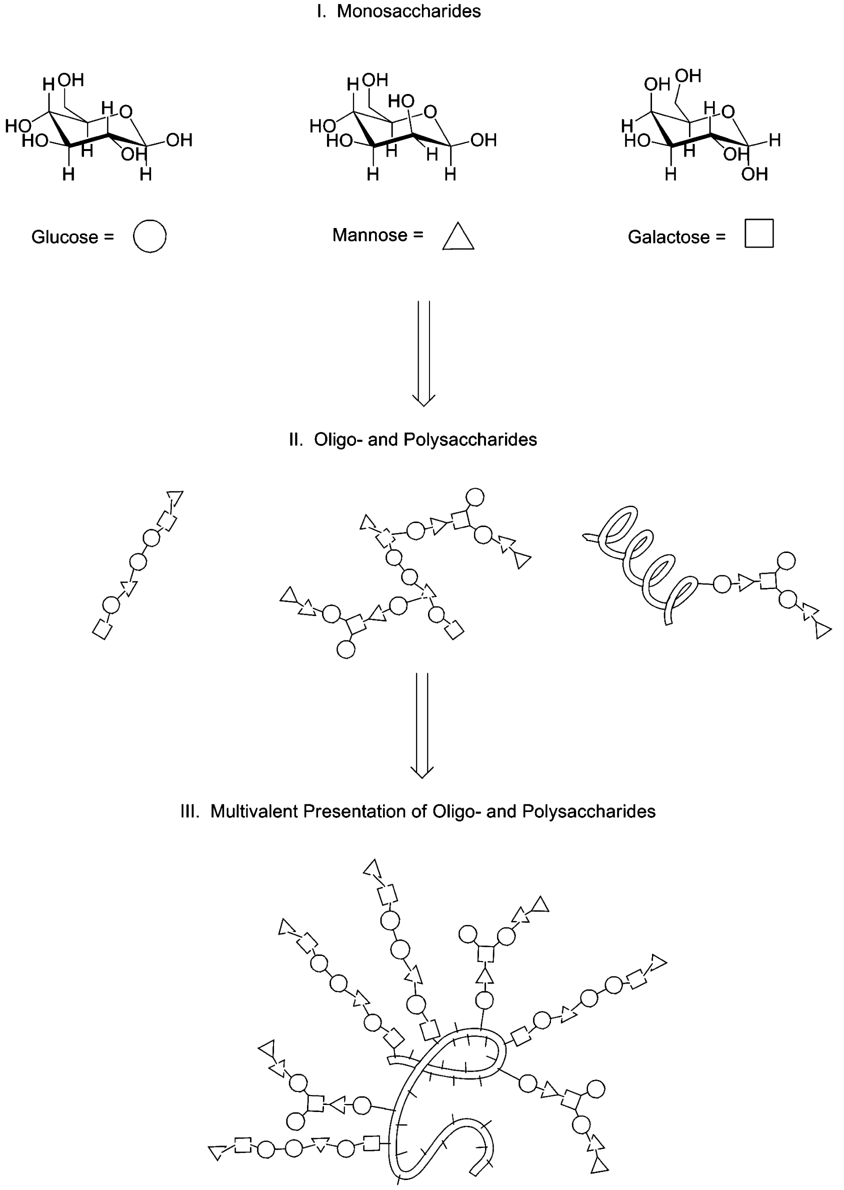
I. Monosaccharides
Glucose =
Mannose =
Galactose =
II. Oligo- and Polysaccharides
III. Multivalent Presentation of Oligo- and Polysaccharides

Scheme 2. Representation of the hierarchy carbohydrate complexity from (I) just three simple monosaccharides to (II) highly structured and branched oligo- and polysaccharides and (III) multivalent presentation of these structures on a protein for cellular signaling events.

Since the binding events of carbohydrate structures rely heavily on their multivalent display and interaction, nanoparticles as a whole have attracted much interest as scaffolds for multi-presentation of a particular ligand or set of ligands due to their high surface-to-volume ratio (*39*). Therefore, semiconductor nanoparticles, quantum dots, are just one of many systems implemented to construct glyco-clusters and study the ability of specific multivalently presented carbohydrates to bind to specific targets. Not only do these carbohydrates enable targeting but they confer water solubility and biocompatibility to the nanoparticles themselves, which is necessary for their use in bio-based applications. Thus, the synthesis of the quantum dot inorganic core to incorporate a glyco-functionalized biocompatible coating often represents a multistep process in the creation of the complete nanodevice (*38*, *39*). These devices, or nanoparticles as previously mentioned, are themselves fluorescent and act in a multimodality fashion allowing for visualization as well as quantitation of the binding events being investigated.

Glyco-Functionalization and Bioconjugation Methods

Carbohydrates, due to the large number of existing monosaccharide building blocks, are very complex. This complexity resulting from the diversity of their building blocks and their bonding linkages forming highly branching systems, has made synthesis, purification and analysis of such entities difficult. However, research has allowed for access to structurally defined monosaccharides, oligosaccharides, and polysaccharides for the profiling of structure-binding activities (*40*). These carbohydrate structures typically represent portions of larger structures their binding events translating into the ability of the entire entity to do so. Commonly used carbohydrates, or combinations thereof, are glucose (Glc), galactose (Gal), mannose (Man), lactose (Lac), N-acetylglucosamine (GlcNAc), or combinations thereof forming oligo- and polysaccharides in combination with a number of semiconductor quantum dot systems as listed in Table 1.

Glyco-functionalization of QDs happens in one of two ways, either the carbohydrate ligand is synthesized prior to functionalization of the surface or the carbohydrate is attached after the assembly of the biocompatible surface via some bioconjugation method (*37*, *38*, *41*). Regardless the method, attachment of the carbohydrate to the organic shell protecting the metal inorganic core is typically covalent in nature with the exception of wrapping the nanoparticle with charged polysaccharides (*42–45*). For all intensive purposes, most glyco-functionalization is performed by synthesizing the carbohydrate ligands before attachment via ligand addition or using a ligand exchange. One of the first to demonstrate this was Tamura and associates, synthesizing a mannose displaying trioctylphosphino-derivative and synthesizing CdSe-ZnS QDs via the ligands addition instead of TOPO (*46*). Others soon followed suite, experimenting with a number of synthesized carbohydrates containing thiol-based ligands performing ligand addition and ligand exchange. One method that has come into the spotlight for bioconjugation of a variety of molecules in robust conditions is 1,3-dipolar cycloaddition, also known as click chemistry (*41*). This typically involves the azido group reacting with an alkyne. Chen et al. demonstrated this in the glycofunctionalization of CdSe-ZnS QDs. Using an alkyne derivatized galactoside, the sugar was covalently bound to a dendrimer ligand reacting with azido groups. This thiol-containing gal-dendrimer ligand was then exchanged on the surface of the QD to form the glyco-functionalized organic shell (*47*). However, little has been done to exploit this chemistry for glycosylation of the surface of QDs post-functionalization of the metal inorganic core.

Table 1. Glyco-functionalized QDs and their applications

QDs	*Saccharides*	*Application*	*Ref.*
CdSe/ZnS	Man, Glc,Gal, GlcNAc, Maltotriose, Dextran, Pullulan	Biosensing, Labeling, Imaging, Reagent Delivery	(*24*, *37*, *42*, *43*, *46*, *47*, *50*, *51*, *56*, *57*, *59–63*, *70*)
CdSe	Glc, Gal, Maltohexose, Cyclodextrin	Biosensing, Labeling, Reagent Delivery	(*48*, *68*, *71*)
CdTe	Glc, Gal, Man, GlcNAc, TF-antigen	Biosensing, Labeling	(*58*, *64*, *69*, *72*)
CdS	Maltose, Le^x Antigen, Gal, Man	Biosensing, Labeling, Imaging	(*49*, *65*, *73*, *74*)
CdS/CdTe	Glc, Gluconic Acid, Gluconamide	Biosensing	(*22*, *75*)
ZnS	Man, Chitosan	Biosensing, Imaging	(*44*)
InGaP/ZnS	Chitosan	Imaging	(*45*)

Bioconjugation methods employed post-functionalization of the metal inorganic core with its organic shell have traditionally relied on EDC/NHS coupling (*22*, *24*, *37*, *48*, *49*). Typically, this entails the surface of the QDs being functionalized with carboxylic acid which is then coupled to an amine. Though this has proven a useful strategy, control of the reaction across the surface of the particle is limited as the concentration of the carbohydrate ligand bound increases. Carbohydrate ligands without even distributions may limit a QD's effectiveness as designed for its specific application. Others, instead of directly coupling an amino-sugar derivative and carboxylic acid, have relied on functionalizing the surface of the organic shell with maleimido groups which readily react with thiol-containing sugar derivatives (*50*). However, this type of conjugation falls prey to the same issues as EDC/NHS coupling as well as the thiol's susceptibility to oxidative damage rendering it unreactive. Though not technically covalent in nature, Sun et al. demonstrated the use of streptavidin-biotin binding as a method to glyco-functionalize QDs. Using CdSe-ZnS QDs functionalized with streptavidin, a biotin functionalized glycopolymer was bound creating a glycosphere with multiple disaccharide residues for multivalent interaction as represented in Figure 2 (*51*). The aforementioned bioconjugation methods are represented in Scheme 3.

Though proper glyco-functionalization resides as top priority in terms of glyco-QD synthesis. It is worth noting that many other factors must be accounted for, such as linker length, type and overall sugar density across the particle surface. If linker lengths are too short or too hydrophobic, it has been demonstrated using gold glyconanoparticles that effective sugar binding cannot occur due to limited accessibility of the sugar residues (*52*). Likewise, the same phenoma can be observed if sugar density across the surface is too great, reversing receptor specificity (*53*). Thus, much thought and consideration must be taken in the synthetic development of glyco-QDs for any specific application.

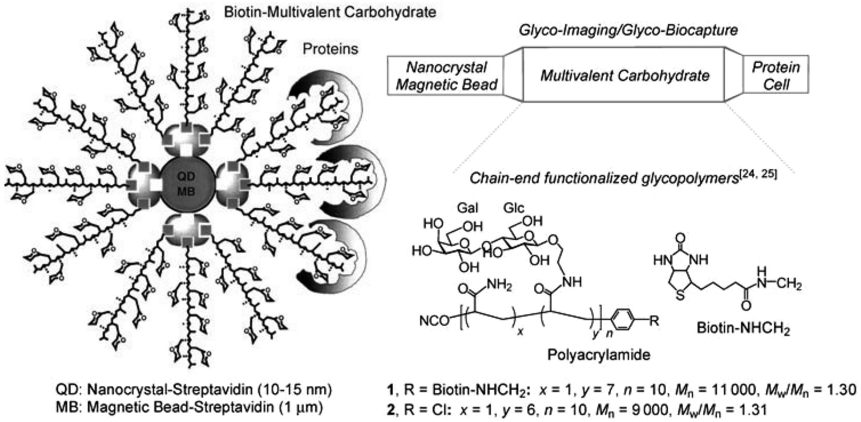
Biotin-Multivalent Carbohydrate
Proteins
QD
MB
Glyco-Imaging/Glyco-Biocapture
Nanocrystal Magnetic Bead
Multivalent Carbohydrate
Protein Cell
Chain-end functionalized glycopolymers[24, 25]
Gal
Glc
HO
OH
NH2
NH
NCO
x
y
n
R
HN
S
H
N-CH2
O
Biotin-NHCH2
Polyacrylamide
QD: Nanocrystal-Streptavidin (10-15 nm)
MB: Magnetic Bead-Streptavidin (1 μm)
1, R = Biotin-NHCH2: x = 1, y = 7, n = 10, Mn = 11 000, Mw/Mn = 1.30
2, R = Cl: x = 1, y = 6, n = 10, Mn = 9 000, Mw/Mn = 1.31

Figure 2. From publication Ref. (51) describing streptavidin QDs bound with biotin containing glycopolymer.

Glyco-QD Characterization

Glyconanomaterials are synthesized under various conditions using specific chemistry and reagents. These materials must therefore be carefully evaluated to fully characterize the structure, composition, density of surface ligands, and biological activities in order to obtain proper correlation with their performances. Synthesis and surface modification of QDs, with the exception of using UV-Vis and fluorescense emittance spectroscopies and microscopies which are typically employed in almost every QD study, are subject to characterization methods that have become standard for many nanoparticle systems (*54*, *55*). Characterization can include any combination of transmission electron microscopy (TEM), dynamic light scattering (DLS), nuclear magnetic resonance spectroscopy (NMR), X-ray diffraction (XRD), atomic force microscopy (AFM), X-ray photoelectron (XPS) and auger electron spectroscopies (AES) giving details regarding basic rheology and surface composition characteristics of the modified passivated surfaces of the synthesized metal cores.

The most basic property of a nanoparticle, besides its material, is its size, i.e. diameter. By modification of the nanoparticle surface, the size of the particle is often prone to change. The size and shape of nanoparticles are classically characterized by TEM, AFM and DLS. Aside from characterizing the size and shape of the molecules others have exploited these techniques, particularly TEM, in observing physical phenomena such as aggregation. For example, Rosenzweig and Chen demonstrated the use of TEM in identifying the aggregation of dextran-modified CdSe-ZnS QDs upon introduction of the lectin ConA, which has multiple binding sites for α-D-glucose residues (*42*). In a similar fashion, Lee's Group showed the specificity in the multivalent binding of GlcNAc-QDs with wheat germ agglutinin (WGA), a lectin, leading to aggregation versus bovine serum albumin (BSA) (*56*). Surolia and associates also investigated the ability of oligosaccharide-functionalized QDs to bind various lectins as monitored via TEM (*57*).

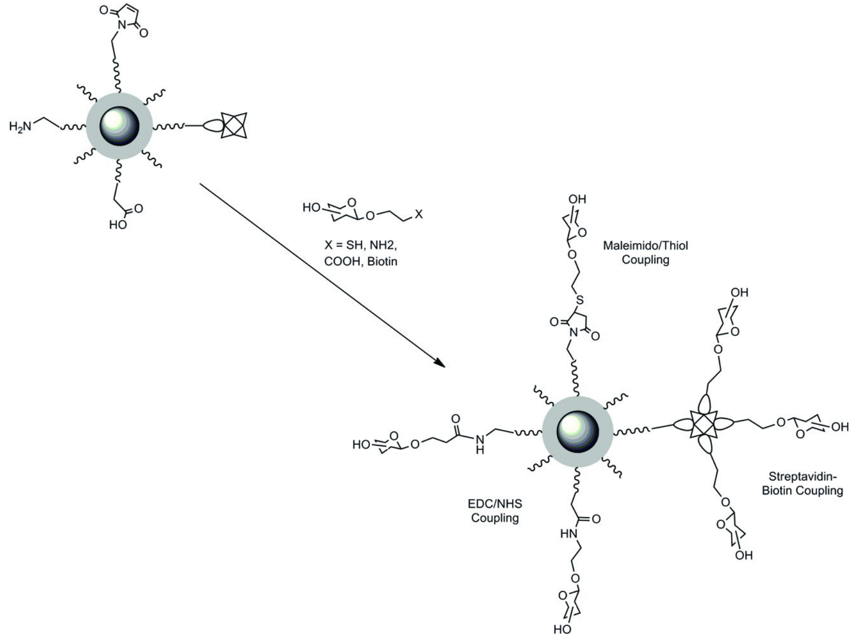

Scheme 3. Schematic representation of post glyco-functionalization of QDs with its organic shell.

Elemental analysis, XRD, AES, and XPS also provide other means of attaining similar structural information in regards to the elemental composition and chemical state of the bulk nanomaterials and the surface ligands. These methods are rarely used post-biofunctionalization due to the possible decomposition of the analytical sample rendering it unrecoverable and thus mainly remain as means for characterizing the synthesized metal inorganic core. NMR spectroscopy offers detailed structural analysis of nanomaterials and surface ligands as well as allowing for the recovery of the analytical sample for further experimental use. It represents one of the most accurate characterization techniques in regards to identifying successful functionalization via ligand exchange of thiol-based derivatives in detail beyond that of UV-Vis spectroscopy. Liu and associates used ^{1}H NMR to monitor the disappearance of the –SH signal at δ 1.30 ppm as well as broadening of other signals representing successful exchange of thiol-based Gal-dendrimer ligand across the surface of CdSe-ZnS QD (*47*). Svarovsky and Barchi performed work with the Thomsens-Friedenreich (TF) antigen attributing similar line broadening of the signals to the attachment of the glyco-functionalized thiol ligand to the QD surface resulting in increased relaxation rates as a result of increase in overall molecular weight of the particles (*58*). In multiple studies, Li used ^1H NMR monitoring of the signals corresponding to TOPO before and after functionalization the absence of these signals and the presence of the signals corresponding to the anomeric hydrogens of the glycans employed (*59–61*). In combination with thermogravimetric analysis (TGA), Li was able to further elucidate the amount of sugar displayed on the surface in terms of weight percent composition of glyco-functionalized QDs.

As previously mentioned, UV-Vis and fluorescence spectroscopies are the most widely used characterization methods for QDs, due to their inherent photooptical properties (*11*). Each QD, dependent upon the size and type, has a unique absorption maxima (λ_{max}) and emission wavelength. Thus, any change to the particles surface, such as a binding event, whether it is functionalization via ligand exchange or in application of binding a targeted entity, can result in shifts in these values. Since most applications of functionalized QDs revolve around biolabeling and imaging, most investigations measure such events looking directly at changes in intensity of the fluorescence emission wavelength. Thus, when designing a glyco-functionalized QD, the emission intensity for that desired wavelength should not be compromised, resulting in significant loss of fluorescence emission. Narain demonstrated this by comparing the emission spectra of original QDs, sugar and biotin functionalized QDs, and biotinylated glycopolymer functionalized QDs (*22*). Many others have also employed similar strategies in monitoring the fluorescence emission of their designed QDs during the functionalization process (*44*, *47*, *60*, *62–65*). Fluctuations in absorption or emission intensities are not only useful in monitoring surface functionalization, but can be used to design assays that quantitate the binding ability of a particular glycan on the surface of a modified QD to particular receptors, mainly lectins. For example, Lee's group, apart from the TEM work, was able to quantitatively access the binding ability of multivalent displaying GlcNAc-QDs towards WGA lectin calculating the association constant to be ~3–4 orders of magnitude higher than that of the corresponding monosaccharide (*56*). Similarly, measuring absorption, Surolia was able to monitor the agglutination process of various sugar-functionalized CdSe-ZnS QDs induced upon the exposure to the lectin ConA (*57*).

Employing such characterization techniques in combination with others helps to access the overall structure and composition of the glyco-functionalized QD and its binding affinities of the particular glycans employed to specific receptors. However, one challenge still remains, the exact quantification of the sugars grafted onto the QDs. Currently, reported numbers of sugars on these surfaces are only theoretical values based on calculations. Until this problem is resolved, the exact nature of the surface and the multivalent display of these ligands remains limited, hindering the exact understanding of the glyco-cluster effect. If this problem can be solved, this would enable researchers to better mimic the phenomenon that happens at the cellular level in regards to carbohydrate-receptor interactions bringing this type of nanoparticle and others to a new evolutionary stage.

Applications of Glyco-QDs

QDs have gained much attention in many areas surrounding the nanobiotechnology and biomedical fields, however, they have remained limited to mainly *in vitro* biosensing/biolabeling applications (*66*). This is mainly due to the concerns amongst clinicians about the potential toxicity of the inner metallic inorganic cores of the nanoparticles leaching out if the organic shell is compromised (*19–23*). Therefore, a majority of glyco-functionalized QDs have been implemented in research surrounding the development of fluorescent probes serving as multimodality platforms for biolabeling, imaging and biosensing. These various applications are depicted in Figure 3 (*11*).

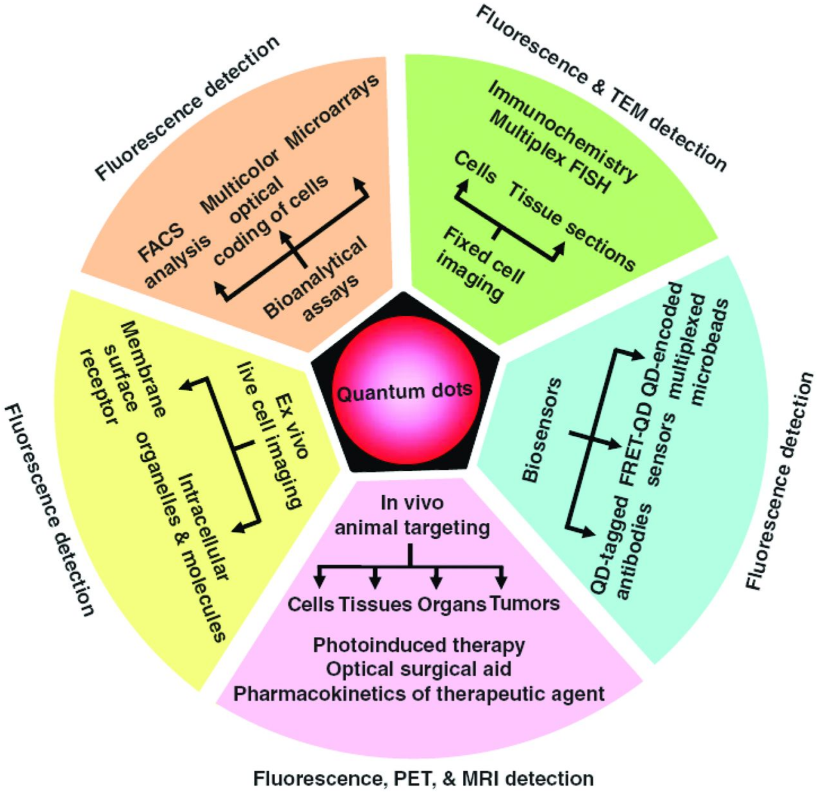
Fluorescence detection
FACS analysis
Multicolor optical coding of cells
Microarrays
Bioanalytical assays
Fluorescence & TEM detection
Immunochemistry
Multiplex FISH
Cells
Tissue sections
Fixed cell imaging
Fluorescence detection
Biosensors
FRET-QD sensors
QD-encoded multiplexed microbeads
QD-tagged antibodies
Fluorescence, PET, & MRI detection
In vivo animal targeting
Cells
Tissues
Organs
Tumors
Photoinduced therapy
Optical surgical aid
Pharmacokinetics of therapeutic agent
Fluorescence detection
Membrane surface receptor
Ex vivo live cell imaging
Intracellular organelles & molecules
Quantum dots

Figure 3. Applications of QDs as various biolabels and imaging agents. (Reprinted with permission from reference (11). Copyright 2005 AAAS, all rights reserved.)

One of the first demonstrated uses of a glyco-functionalized quantum dot platform was performed by Rosenzweig in 2003 (*42*). This experiment was not based on any specific targeting of a single carbohydrate, but instead investigated the ability of a modified polysaccharide, negatively charged carboxylmethyl dextran, to encapsulate a CdSe-ZnS QD enhancing water solubility and protein binding. The binding event of the protein, the lectin Con A, was visualized via fluorescence confocal microscopy inducing aggregation of the dextran-QDs. Recognizing that using sugars, not only as a method to induce water solubility, on the surface of QDs could be used to verify protein specificity to the particular saccharide presented. Thus, researchers have continuously used QDs in developing various assay and biosensing methods to test the binding affinities of certain sugars against specific lectins, sugar-binding proteins which reside on many types of cell surfaces responsible for cellular communication events (*40*, *48*, *49*, *57*, *67*). Due to the difficulties in synthetic accessibility to highly branched, more complex saccharides most of these studies only relied on the use of one type of saccharide as a uniform layer exposed across the surface of QDs. Therefore, it is noteworthy to mention one of the first groups of researchers to functionalize QDs with highly branched sugar displaying structures. In 2004, Sun et al. synthesized a highly branched glycopolymer, displaying Gal-Glc disaccharides, with a biotinylated end group which was bound to streptavidin-coated CdSe-ZnS QDs and effectively demonstrated the labeling of lectin-coating beads as well as the capture and detection of free lectin within nanomolar concentrations (Figure 2) (*51*).

Within the same year, Aoyama et al. investigated the uptake of QDs using a sugar bearing amphiphile intercalated across the particle surface (*68*). This study, along with the data generated from earlier work in regards to sugar specifities towards particular proteins, paved the way for the use of glyco-functionalized QDs as *in vitro* bioimaging agents. In response to the alarming rate of increasing antibiotic resistance and opportunistic infections, QDs with specific targeting groups have found themselves employed for the rapid visualization and identification of microorganisms (*26*–*28*). This has been demonstrated using glyco-functionalized dots in the selective labeling and identification of yeast, using a thioglycolic acid-conjugated QDs (*64*), and *E. coli* bacteria, using mannose-QDs (*65*). The use glyco-QDs in the identification of microorganisms and their visualization also translates to higher-level organisms. Targeting lectins of specific cell types, researchers have effectively used engineered glyco-QDs in the specific fluorescent labeling and imaging of gametes (*56*), leukocytes (*59*, *60*, *62*), and cancer cells (*44*, *47*, *61*, *63*). Even further exemplifying the specificity in which glyco-QDs can be used to label and image cells, some researchers pioneering QD nanodevices to visualize cells undergoing specific metabolic or disease states. One example of this is that of the Ijiro group which has repeatedly demonstrated the use of *N*-acetylglucosamine (GlcNAc)-CdTe QDs in the labeling and detection of chemically stressed cells targeting the heat shock protein 70 (HSP70) (*58*, *69*). To date, bioimaging *in vivo* remains a challenge, not just due to material toxicity but because most QDs that are composed of heavy elements from groups II–VI are not capable of emittance through several millimeters of absorbing tissues. The only example employing a QD for *in vivo* imaging was demonstrated using InGaP-ZnS nanoclusters (*45*). These QDs functionalized with chitosan were tested in a mouse model for *in vivo* imaging allowing for visualization ~ 6 mm below the head surface and even somewhat through the skull. However, little has been done since this study using glyco-functionalized QDs for *in vivo* bioimaging of tissues.

Conclusions

QDs show great potential as cellular nanoprobes for various biological applications due to their long-term stability and simultaneous detection of multiple signals. Although a great deal of research has been done in the past decade, only limited success has been achieved in *in vitro* and *in vivo* cell labeling with high specificity, sub-cellular targeting and single molecule trafficking. Tremendous efforts are still needed for successful transition of this technology from proof-of-concept studies towards real-life clinical applications. Particularly, knowledge of QD interactions with cells, their mechanism of cellular entry and modulation of these interactions by appropriate design of surface functionalities.

The mechanism of cellular internalization of nanoprobes remains one of the greatest challenges in the development of viable applications and should be investigated properly in order to achieve successful sub-cellular targeting. This success relies on the biofunctionalization of the inorganic QD cores, facilitating such interactions. The particle must be able to directly participate in the biological process under investigation with limited or no interference to other cellular processes, due to the possbilities of compromising the cell's metabolism and viability. Any compromise other cellular processes, may produce artifacts or inaccurate results with high deviations which in turn is often unacceptable in clinical settings. Regardless of their superior properties over common organic fluorescent dyes, due to the fact that limited work has been done, glyco-functionalized QDs have yet to enter the mainstream as alternative fluorescent probes for clinical applications, such as flow-cytometry and other commonly used biolabeling applications. Until the various interactions and phenomena associated with these nanoparticles are understood, QDs will remain unsuitable for a wide range of clinical applications. Thus, it is important that researchers across the fields of materials science, biotechnology, glycobiology and glycochemistry work together in an interdiscilplinary fashion to overcome these challenges making glyco-QDs more readily available for a wider range of applications.

This article summarized the various glyco-functionalized QD systems that have emerged and demonstrated increasing potential in biomedical imaging and diagnostics. Critical to the performance of glyco-QDs is the proper display of carbohydrate ligands, which must be taken into great consideration when choosing the type of coupling chemistry, structure and length of the spacer linkage, and the overall ligand density. Everyday, new developments for functional carbohydrate epitopes are becoming available from both synthesis and isolation. With these new discoveries, hopefully new methods and perhaps more precisely controlled cellular and subcellular labeling will be accomplished towards the goal of producing efficient and clinical applicable bioimaging probes and assays.

References

1. Buzea, C.; Blandino, I. I. P.; Robbie, K. *Biointerphases* **2007**, *2*, 17–71.
2. Husemann, M.; Mecerreyes, D.; Hawker, C. J.; Hedrick, J. L.; Shah, R.; Abbott, N. L. *Angew. Chem., Int. Ed.* **1999**, *38*, 647.
3. Edmund, A. R.; Kambalapally, S.; Wilson, T. A.; Nicolosi, R. J. *Toxicol. in Vitro* **2011**, *25*, 18–190.
4. Rossetti, R.; Nakahara, S.; Brus, L. E. *J. Chem. Phys.* **1983**, *79*, 1986.
5. Steigerwald, M. L.; Brus, L. E. *Acc. Chem. Res.* **1990**, *23*, 183–188.
6. Nirmal, M.; Brus, L. *Acc. Chem. Res.* **1999**, *32*, 407–414.
7. Willard, D. M.; Carillo, L. L.; Jung, J.; Van Orden, A. *Nano Lett.* **2001**, *1*, 469–474.
8. Sharma, C. V. K. *Cryst. Growth Des.* **2002**, *2*, 467.
9. Kikkeri, R.; Laurino, P.; Odedra, A.; Seeberger, P. H. *Angew. Chem., Int. Ed.* **2010**, *49*, 2054.
10. Peralta-Videa, J. R.; Zhao, L.; Lopez-Moreno, M. L.; de la Rosa, G.; Hong, J.; Gardea-Torresdey, J. L. *J. Hazard. Mater.* **2011**, *186*, 1–15.
11. Michalet, X.; Pinaud, F. F.; Bentolila, L. A.; Tsay, J. M.; Doose, S.; Li, J. J.; Sundaresan, G.; Wu, A. M.; Gambhir, S. S.; Weiss, S. *Science* **2005**, *307*, 538–544.
12. Wang, Y.; Herron, N. *J. Phys. Chem.* **1988**, 4988–4994.
13. Murray, C. B.; Norris, D. J.; Bawendi, M. G. *J. Am. Chem. Soc.* **1993**, *115*, 8706–8715.
14. Bowen Katari, J. E.; Colvin, V. L.; Alivisatos, A. P. *J. Phys. Chem.* **1994**, *98*, 4109–4117.
15. Rogach, A. L.; Kornowski, A.; Gao, M. Y.; Eychmuller, A.; Weller, H. *J. Phys. Chem. B* **1999**, *103*, 3065–3069.
16. Gerion, D.; Pinaud, F.; Williams, S. C.; Parak, W. J.; Zanchet, D.; Weiss, S.; Alivisatos, A. P. *J. Phys. Chem. B* **2001**, *105*, 8861–8871.
17. Yang, X. T.; Zhang, Y. *Langmuir* **2004**, *20*, 6071–6073.
18. Thanh, N. T. K.; Green, L. A. W. *Nano Today* **2010**, *5*, 213–230.
19. Derfus, A. M.; Chan, W. C. W.; Bhatia, S. N. *Nano Lett.* **2004**, *4*, 11–18.
20. Mancini, M. C.; Kairdolf, B. A.; Smith, A. M.; Nie, S. *J. Am. Chem. Soc.* **2008**, *130*, 10836–10837.
21. Lin, C. H.; Chang, L. W.; Chang, H.; Yang, M. H.; Yang, C. S.; Lai, W. H.; Chang, W. H.; Lin, P. *Nanotechnology* **2009**, *20*, 215101.
22. Jiang, X.; Ahmed, M.; Deng, Z.; Narain, R. *Bioconjugate Chem.* **2009**, *20*, 994–1001.
23. Hardman, R. *Environ. Health Perspect.* **2006**, *114*, 165–172.
24. Mazumder, S.; Dey, R.; Mitra, M. K.; Mukherjee, S.; Das, G. C. *J. Nanomater.* **2009**, 815734.
25. Engel, E.; Michiardi, A.; Navarro, M.; Lacroix, D.; Planell, J. A. *Trends Biotechnol.* **2007**, *26*, 39–47.

26. Hahn, M. A.; Tabb, J. S.; Krauss, T. D. *Anal. Chem.* **2005**, *77*, 4861–4869.
27. Lee, L. Y.; Ong, S. L.; Hu, J. Y.; Ng, W. J.; Feng, Y.; Tan, X.; Wong, S. W. *Appl. Environ. Microbiol.* **2004**, *70*, 5732–5736.
28. Kroll, A.; Pillukat, M. H.; Hahn, D.; Nealson, K. H.; Schnekenburger, J. *Eur. J. Pharm. Biopharm.* **2009**, *72*, 370–377.
29. Nie, Q.; Tan, W. B.; Zhang, Y. *Nanotechnology* **2006**, *17*, 140–144.
30. Ho, Y. P.; Leong, K. W. *Nanoscale* **2010**, *2*, 60–68.
31. Yong, K. T.; Roy, I.; Swihart, M. T.; Prasad, P. N. *J. Mater. Chem.* **2009**, *19*, 4655–4672.
32. Wadhwa, M. S.; Rice, K. G. *J. Drug Target* **1995**, *3*, 111–127.
33. Yamazakia, N; Kojimab, S; Bovinc, N. V.; André, S.; Gabiuse, S.; Gabiusd, H. J. *Adv. Drug Delivery Rev.* **2000**, *43*, 225–244.
34. Davis, B. G.; Robinson, M. A. *Curr. Opin. Drug Discovery Dev.* **2002**, *5*, 279–288.
35. Gabius, H. J. *Adv. Drug. Delivery Rev.* **2004**, *56*, 421–424.
36. Zhang, H.; Ma, Y.; Sun, X-. L. *Med. Res. Rev.* **2010**, *30*, 270–289.
37. Pieters, R. J. *Org. Biomol. Chem.* **2009**, *7*, 2013–2025.
38. Zrazhevskiy, P.; Sena, M.; Gao, X. *Chem. Soc. Rev.* **2010**, *39*, 4326–4354.
39. Martin-Lomas, M.; Penades, S. *Adv. Carbohydr. Chem. Biochem.* **2010**, *64*, 211–290.
40. Coullerez, G.; Seeberger, P. H.; Textor, M. *Macromol. Biosci.* **2006**, *6*, 634–647.
41. Larsen, K.; Thygesen, M. B.; Guillaumie, F.; Willats, W. G. T.; Jensen, K. J. *Carbohydr. Res.* **2006**, *341*, 1209–1234.
42. Chen, Y.; Ji, T.; Rosenzweig, Z. *Nano Lett.* **2003**, *3*, 581–584.
43. Hasegawa, U.; Nomura, S. M.; Kaul, S. C.; Hirano, J.; Akiyoshi, K. *Biochem. Biophys. Res. Commun.* **2005**, *331*, 917–921.
44. Jayasree, A.; Sasidharan, S.; Koyakutty, M.; Nair, S.; Menon, D. *Carbohydr. Polym.* **2011**, *85*, 37–43.
45. Sandros, M. G.; Behrendt, M.; Maysinger, D.; Tabriziar, M. *Adv. Funct. Mater.* **2007**, *17*, 3724–3730.
46. Tamura, J.; Fukuda, M.; Tanaka, J.; Kawa, M. *J. Carbohydr. Chem.* **2002**, *21*, 445–449.
47. Chen, C. T.; Munot, Y. S.; Salunke, S. B.; Wang, Y. C.; Lin, R. K.; Lin, C. C.; Chen, C. C.; Liu, Y. H. *Adv. Funct. Mater.* **2008**, *18*, 527–540.
48. Han, E.; Ding, L.; Lian, H.; Ju, H. *Chem. Commun.* **2010**, 5446–5448.
49. Dai, Z.; Kawde, A. N.; Xiang, Y.; La Belle, J. T.; Gerlach, J.; Bhavanandan, V. P.; Joshi, L.; Wang, J. *J. Am. Chem. Soc.* **2006**, *128*, 10018–10019.
50. Kikkeri, R.; Lepenies, B.; Adibekian, A.; Laurino, P.; Seeberger, P. H. *J. Am. Chem. Soc.* **2009**, *131*, 2110–2112.
51. Sun, X. L.; Cui, W.; Haller, C.; Chaikof, E. L. *ChemBioChem* **2004**, *5*, 1593–1596.
52. Reynolds, A. J.; Haines, A. H.; Russell, D. A. *Langmuir* **2006**, *22*, 1156–1163.
53. Horan, N.; Yan, H.; Isobe, H.; Whitesides, G. M.; Kahne, D. *Proc. Natl. Acad. Sci. U.S.A.* **1999**, *96*, 11782–11786.

54. Johnson, R. L.; Johnson, G. O.; Nurmi, J. T.; Tratnyek, P. G. *Environ. Sci. Technol.* **2009**, *43*, 5455–5460.
55. Jablonski, A.; Powell, C. J. *J. Vac. Sci. Technol., A* **2003**, *21*, 274–283.
56. Robinson, A.; Fang, J. M.; Chou, P. T.; Liao, K. W.; Chu, R. M.; Lee, S. J. *ChemBioChem* **2005**, *6*, 1899–1905.
57. Babu, P.; Sinha, S.; Surolia, A. *Bioconjugate Chem.* **2007**, *18*, 146–151.
58. Svarovsky, S. A.; Barchi, J. J., Jr. In *Frontiers in Modern Carbohydrate Chemistry*; Demchenko, A. V., Ed.; ACS Symposium Series 960; American Chemical Society: Washington, DC, 2007, pp 375–392.
59. Yang, Y.; Yu, M.; Yan, T. T.; Zhao, Z. H.; Sha, Y. L.; Li, Z. J. *Bioorg. Med. Chem.* **2010**, *18*, 5234–5240.
60. Yu, M.; Yang, Y.; Han, R.; Zheng, Q.; Wang, L.; Hong, Y.; Li, Z.; Sha, Y. *Langmuir* **2010**, *26*, 8534–8539.
61. Yang, Y.; Zhao, Y. T.; Yan, T. T.; Yu, M.; Sha, Y. L.; Zhao, Z. H.; Li, Z. J. *Tetrahedron Lett.* **2010**, *51*, 4182–4185.
62. Higuchi, Y.; Oka, M.; Kawakami, S.; Hashida, M. *J. Controlled Release* **2008**, *125*, 131–136.
63. Wilson, R.; Spiller, D. G.; Beckett, A.; Prior, I. A.; See, V. *Chem. Mater.* **2010**, *22*, 6361–6369.
64. Coulon, J.; Thouvenin, I.; Aldeek, F.; Balan, L.; Schneider, R. *J. Fluoresc.* **2010**, *20*, 591–597.
65. Mukhopadhyay, B.; Martins, M. B.; Karamanska, R.; Russell, D. A.; Field, R. A. *Tetrahedron Lett.* **2009**, *50*, 886–889.
66. Biju, V.; Itoh, T.; Ishikawa, M. *Chem. Soc. Rev.* **2010**, *39*, 3031–3056.
67. de la Fuente, J. M.; Penades, S. *Biochim. Biophys. Acta* **2006**, *1760*, 636–651.
68. Osaki, F.; Kanamori, T.; Sando, S.; Sera, T.; Aoyama, Y. *J. Am. Chem. Soc.* **2004**, *126*, 6520–6521.
69. Nishio, T.; Niikura, K.; Matsuo, Y.; Ijiro, K. *Int. J. Nanosci.* **2009**, *8*, 219–222.
70. Xie, M.; Liu, H. H.; Chen, P.; Zhang, Z. L.; Wang, X. H.; Xie, Z. X.; Du, Y. M.; Pan, B. Q.; Pang, D. W. *Chem. Commun.* **2005**, 5518–5520.
71. Palaniappan, K.; Xue, C.; Arumugam, G.; Hackney, S. A.; Liu, J. *J. Chem. Mater.* **2006**, *18*, 1275–1280.
72. Niikura, K.; Nishio, T.; Akita, H.; Matsuo, Y.; Kamitani, R.; Kogure, K.; Harashima, H.; Ijiro, K. *ChemBioChem* **2007**, *8*, 379–384.
73. de la Fuente, J. M.; Penades, S. *Tetrahedron: Assymetry* **2005**, *16*, 387–391.
74. Han, E.; Ding, L.; Jin, S.; Ju, H. *Biosens. Bioelectron.* **2011**, *26*, 2500–2505.
75. De Farias, P. M. A.; Santos, B. S.; Menezes, F. D.; Brasil, A. G., Jr.; Ferreira, R.; Motta, M. A.; Castro-Neto, A. G.; Vieira, A. A. S.; Silva, D. C. N.; Fontes, A.; Cesar, C. L. *Appl. Phys. A* **2007**, *89*, 957–961.

Downloaded by PENNSYLVANIA STATE UNIV on June 3, 2012 | http://pubs.acs.org
Publication Date (Web): December 13, 2011 | doi: 10.1021/bk-2011-1091.ch008

Chapter 8

Sugar-Functionalized Carbon Nanotubes: Unique Properties and Interactions with Biological Species

**Parambath Anilkumar,[†] Kenneth N. Tackett II,[†] Fushen Lu,[*,‡]
Pengju G. Luo,[*,†] Lingrong Gu,[†] Ankoma Anderson,[†]
and Ya-Ping Sun[*,†]**

**[†]Department of Chemistry and
Laboratory for Emerging Materials and Technology,
Clemson University, Clemson, South Carolina 29634-0973, U.S.A.
[‡]Department of Chemistry, Shantou University, Guangdong 515063, China
[*]E-mails: fslu@stu.edu.cn; pluo@clemson.edu; syaping@clemson.edu**

Single-walled (SWNT) and multiple-walled (MWNT) carbon nanotubes have attracted much attention for their many potential applications, including those in biology and medicine. These pseudo-one-dimensional nanostructures are capable of carrying/displaying a large number of bioactive molecules and species in aqueous solution. In this article we highlight some representative configurations of sugar-functionalized SWNTs and MWNTs, where the sugars include mannose and galactose, and also some interesting examples for illustrating their unique properties and unexpected problems in cell recognition and adhesion and also their relevance to other potential bioapplications.

In Petite and Sweet: Glyco-Nanotechnology as a Bridge to New Medicines; Huang, X., et al.;
ACS Symposium Series; American Chemical Society: Washington, DC, 2011.

Downloaded by PENNSYLVANIA STATE UNIV on June 3, 2012 | http://pubs.acs.org
Publication Date (Web): December 13, 2011 | doi: 10.1021/bk-2011-1091.ch008

Introduction

Single-walled (SWNTs) and multiple-walled carbon nanotubes (MWNTs) have attracted much attention in a number of scientific fields for their exceptional physicochemical properties. As pseudo-one-dimensional nanomaterials, carbon nanotubes offer a wide range of opportunities and application potentials in biology and medicine (*1–4*). For example, the rich electronic properties of carbon nanotubes have been explored for the development of highly sensitive and specific nanoscale biosensors (*5*, *6*). Promising results have been produced on the use of carbon nanotubes in various electroanalytical nanotube devices (*7*), and as electromechanical actuators for artificial muscles (*8*, *9*). The optical absorption of carbon nanotubes in the near-infrared has been used for the laser-induced hyperthermia cancer therapy (*10*). In recent years, the rapid development toward maturation of methodologies for the chemical modification and functionalization of carbon nanotubes has helped to address many biocompatibility-related issues, opening up an even wider range of bioapplication opportunities in areas such as drug delivery (*11–13*), bioconjugation and specific recognition (*14*), including the use of sugar-functionalized carbon nanotubes to bind and aggregate anthrax spores (*15*). The biological fate and consequences of carbon nanotubes *in vitro* and *in vivo* have also been investigated for an understanding of the important issues on environmental impact and toxicity (*16*, *17*).

Carbon nanotubes are generally aqueous insoluble, which makes their compatibility with biological systems a challenge. A widely pursued approach to address the biocompatibility issue has been the functionalization of carbon nanotubes with aqueous soluble molecules or even biological species, for which much success has been achieved (*18–25*). Among biologically significant functionalities for the aqueous solubilization of carbon nanotubes, sugars in various configurations have proven to be particularly valuable, with the resulting sugar-functionalized carbon nanotubes exhibiting unusual features in their interactions with biological species (such as above mentioned binding and aggregation of anthrax spores, for example) (*26–28*). Carbon nanotubes apparently serve as unique scaffolds for multivalent displays of mono- and poly-saccharides and their various combinations. The distinctive properties of these newly developed nanomaterials, especially with respect to their interactions with biological species and systems and related potentially significant bioapplications, have been investigated, but are still far from being understood.

In this article we highlight a few representative configurations of sugar-functionalized SWNTs and MWNTs developed and/or established mostly in our laboratories, and also some interesting examples for illustrating their potentials and unexpected problems in cell recognition and adhesion or other relevant bioapplications.

Downloaded by PENNSYLVANIA STATE UNIV on June 3, 2012 | http://pubs.acs.org
Publication Date (Web): December 13, 2011 | doi: 10.1021/bk-2011-1091.ch008

Sugar-Functionalized Carbon Nanotubes

Carbon nanotubes are intractable due to generally poor solubility in most solvents, so chemical functionalization is often used to introduce them into solution for further processing and uses. It is known that the purification of nanotubes by oxidative acid treatment produces carboxylic acids, which is derived from the oxidation of nanotube surface defect sites. These nanotube surface-bound carboxylic acid groups may be targeted in functionalization reactions. In fact, the functionalization chemistry targeting the defect sites has been explored for the functionalization of carbon nanotubes with various bioactive species such as carbohydrates, DNAs, peptides and proteins. The pseudo-one-dimensional nature and high surface area to weight ratio of carbon nanotubes make them particularly attractive scaffolds for multivalent displays of carbohydrates.

Originally, as an extension to the effort on developing sugar-tethered polymeric nanoparticles as adhesion-specific agents for agglutinating food-borne pathogens (*29–32*), Sun and coworkers functionalized SWNTs with derivatized galactoses (Gal-SWNT) to render the nanotubes readily aqueous soluble (*27*), where the functionalization chemistry was based on the classical carbodiimide-activated amidation reactions between the nanotube-bound carboxylic acids and the galactose-tethered amino groups. It was demonstrated that the nanotube-bound galactoses as polyvalent ligands could interact strongly with receptors on pathogenic *E. coli* to result in significant agglutination of the bacterial cells (*27*, *35*).

Similar to SWNTs, MWNTs could also be used to display multiple copies of sugars in physiological solution for biological applications. In addition, MWNTs are more abundant due to more efficient bulk production and thus much less expensive, with generally better sample purity. Their distinctive properties not available to SWNTs include larger inner tubular cavities, which may allow easier access and encapsulation of various species (*33*). Among the disadvantages is their less effective solubilization post functionalization. For the attachment of tethered sugar molecules more specifically, the same amidation reaction conditions used in the synthesis of Gal-SWNT resulted in Gal-MWNT that were found to be not so effective (an unstable aqueous suspension) (*34*). The difference of Gal-MWNT from Gal-SWNT might be associated with the fact that MWNTs are larger and heavier, thus requiring larger and/or more extended functional groups for the solubilization. This was demonstrated in the functionalization of MWNTs with dendritic molecules tethered with sugar moieties, such as the molecule *β*-aminophthaloyl-*N,N'*-bis[11-*O*-(*β*-D-galactopyranosyl)-ethyl]-diamide containing a galactose pair (Gal_2-MWNT, Scheme 1), where the same amidation chemistry targeting nanotube surface-bound carboxylic acids was used for the functionalization. Shown in Figure 1 is a visual comparison between Gal-MWNT and Gal_2-MWNT for their different aqueous solubilities. Experimentally, the two samples were dispersed in water, and then centrifuged under the same conditions. The resulting aqueous dispersion for Gal-MWNT was essentially colorless (Figure 1), indicating poor solubility of the sample, while colored solution of Gal_2-MWNT suggesting much better aqueous solubility of the sample (about 0.3 mg/mL according to more quantitative determination) (*34*).

Downloaded by PENNSYLVANIA STATE UNIV on June 3, 2012 | http://pubs.acs.org
Publication Date (Web): December 13, 2011 | doi: 10.1021/bk-2011-1091.ch008

The results highlighted above suggest that the sugar ligands play a major role in the solubility characteristics of the resulting functionalized carbon nanotubes. The type and number of sugars and their configurations in the molecular structures also affect significantly the bioactivity of the functionalized nanotubes. Since there are only a limited number of defect sites on the nanotube surface, the use of sugar dendrons, in addition to their benefits in the solubilization of MWNTs discussed above, may enable the display of multivalent ligands in larger numbers. The improved solubility characteristics of the sugar-dendron-functionalized carbon nanotubes is also beneficial to a more quantitative characterization in solution, thus to achieve a better understanding of the structural details on the nanotubes displaying multivalent carbohydrate ligands. Shown in Scheme 1 are a series of dendrons bearing β-D-galactopyranosides (Gal_2-NH_2 and Gal_4-NH_2) or α-D-mannopyranosides (Man_2-NH_2 and Man_4-NH_2), which have been successfully used for the functionalization of SWNTs (*35*). The design and synthesis of the dendrons took advantage of the well-established use of tri-substituted benzenes in dendrimer chemistry, where the synthetic strategy was such that the dendritic framework was constructed first before being coupled with the amine-tethered monosaccharides. An important advantage of the strategy is that the sugar molecules were involved only in the final steps, so that difficulties associated with the sugar de-protection and stereo hindrance in the chemical coupling were mostly avoided. The functionalization of carbon nanotubes with the sugar dendrons was the same carbodiimide-activated amidation reaction. Because the reaction was under mostly heterogeneous condition, an excess amount of the dendrons was preferred in the functionalization. As a more specific example, in the functionalization with Man- (Scheme 1), the molar ratio of Man- to the nanotube-bound carboxylic acids (estimated at 5% mole fraction of the nanotube carbons) was varied, with a higher ratio found to be more effective. Similarly between Man- and different dendrons in the functionalization reactions under the experimental conditions, the percentage of the starting purified SWNTs solubilized by Man- was about 25%, increased to 35% for Man_2- and further to 50% for Man_4- (*35*). The results confirmed the expectation that higher-order sugar dendrons should be more effective in the functionalization and solubilization of carbon nanotubes.

For carbon nanotubes functionalized with many molecules or polymers, an effective way to remove the functional groups or “defunctionalization” is thermal treatment under inert atmosphere (as carbon nanotubes are very stable under such conditions that selectively decompose and evaporate the functional groups). However, it is important to note that the thermal defunctionalization behavior of the sugar-SWNT samples is very different. For example, the sugars or sugar dendrons could not be removed from the nanotube surface in thermogravimetric analysis (TGA) under inert atmosphere up to 800 °C. Instead, they were carbonized under the thermal defunctionalization conditions. Therefore, the removal of functional groups in the sugar-functionalized carbon nanotubes may have to rely on chemical decomposition, such as base-catalyzed hydrolysis reactions.

Downloaded by PENNSYLVANIA STATE UNIV on June 3, 2012 | http://pubs.acs.org
Publication Date (Web): December 13, 2011 | doi: 10.1021/bk-2011-1091.ch008

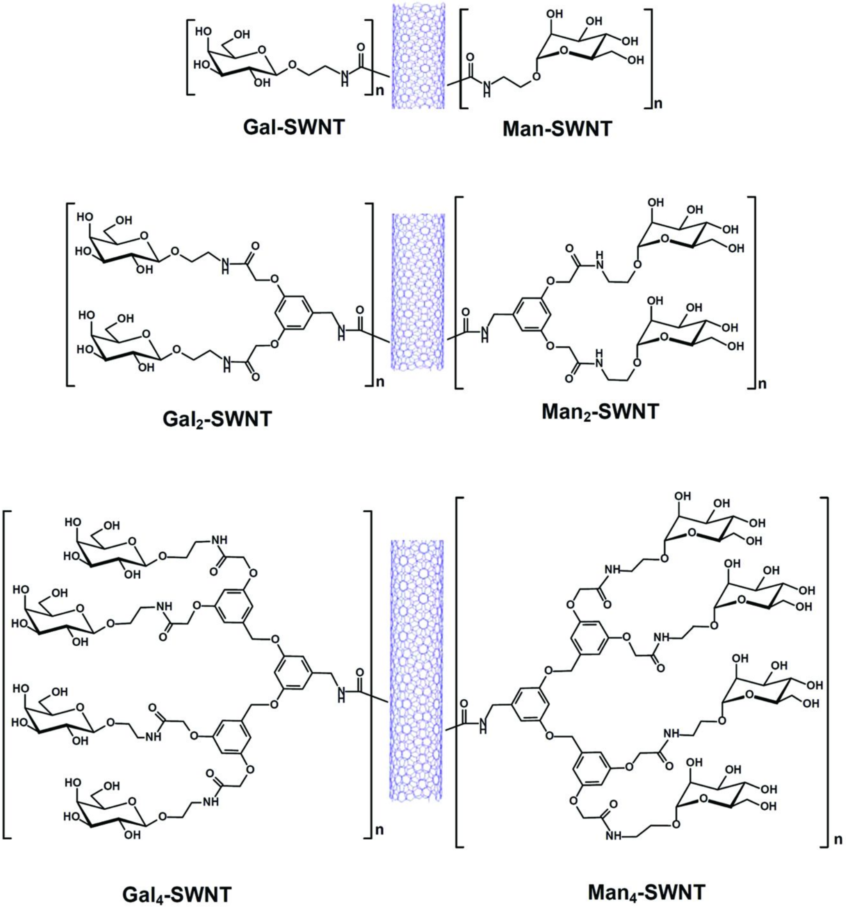
Gal-SWNT
Man-SWNT
Gal$_2$-SWNT
Man$_2$-SWNT
Gal$_4$-SWNT
Man$_4$-SWNT

Scheme 1. Carbon nanotubes functionalized with Gal, Man, or their dendrons. (Adapted from ref. (35).)

Downloaded by PENNSYLVANIA STATE UNIV on June 3, 2012 | http://pubs.acs.org
Publication Date (Web): December 13, 2011 | doi: 10.1021/bk-2011-1091.ch008

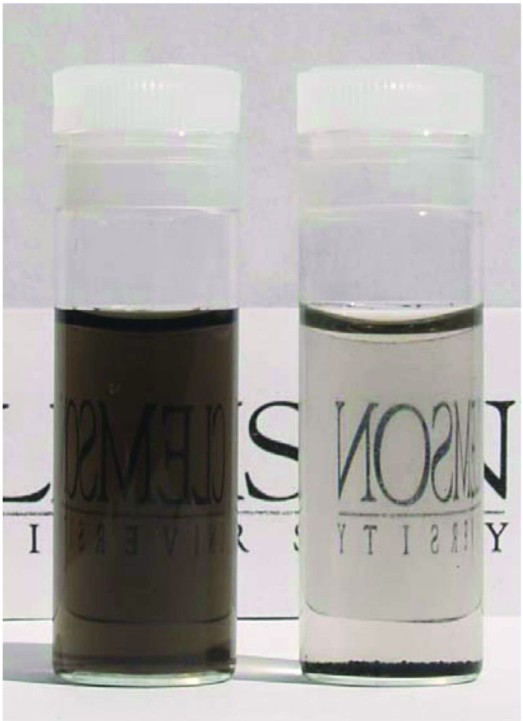

Figure 1. Visual comparison on the aqueous dispersions of Gal_2 MWNT (left) and Gal-MWNT (right). (Adapted from ref. (34).)

Characterization and Properties

Carbon nanotubes upon functionalization and solubilization are still inhomogeneous systems in terms of chemical compositions and structures due to distributions of different nanotube lengths and diameters (MWNTs in particular) and numbers and locations of surface defect sites, which present challenges to the characterization and understanding of the functionalized carbon nanotubes in general. However, the solubility in the sugar-functionalized carbon nanotubes and the fact that with the sugar dendrons covering the nanotube surface the structural differences in the nanotubes became less important enabled the characterization of the samples by using conventional organic spectroscopy techniques, especially solution-phase (and related gel-phase) NMR methods (*36*, *37*).

Again, the sugar dendron-functionalized carbon nanotube samples (Gal_2-SWNT, Man_2-SWNT, Gal_4-SWNT, and Man_4-SWNT) were all readily soluble in water, so that NMR characterization could be used to extract more structural information. As shown in Figure 2 for a comparison between the ^1H NMR spectra of Gal_2-SWNT and Gal_2-N_3 (precursor to Gal_2-NH_2) in solutions, the former exhibits significantly broader signals, consistent with decreased mobility of the dendrons upon their attachment to carbon nanotubes. These large species of a solid-like core and floppy surface tethers are ideal for the gel-phase NMR technique (*38*). For Gal_2-SWNT, as an example, the gel-phase ^1H NMR spectrum obtained with a high resolution-magic angle spinning (HR-MAS) probe is obviously better resolved, with the signals in the sugar region comparable (in terms of the peak resolution) with those for the corresponding free dendrons (Figure 2). The formation of amide linkages in Gal_2-SWNT shifted the relevant proton signals downfield, 6.82 ppm and 6.70 ppm for the nanotube-bound dendron vs 6.72 ppm and 6.66 ppm for the free dendron, respectively (*35*). The attachment of dendrons to carbon nanotubes might also be responsible for the absence of benzyl proton signals in the Gal_2-SWNT spectrum, as it is known in the literature that protons in close proximity to large aromatic ring currents may be affected in such a way to make their detection difficult (*39*, *40*).

The comparisons and results were similar between ^1H NMR spectra of Gal_4-SWNT and Gal_4-N_3 (precursor to Gal_4-NH_2) and those of Man_4-SWNT and Man_4-N_3 (precursor to Man_4-NH_2) (*35*).The much improved solubilities of these higher-order dendron-functionalized carbon nanotubes also enabled their ^{13}C NMR characterization. Similar to the ^1H NMR results, the ^{13}C signals also exhibited broadening effect upon the dendrons attached to nanotubes. Interestingly, however, the ^{13}C spectrum of Gal_4-SWNT (Figure 3) also exhibits some of the tether carbon signals, likely due to the higher solution concentration and the fact that these carbons are farther away from the nanotubes and therefore less affected by the large ring currents (*39*, *40*).

As discussed earlier, the determination of compositions in sugar-functionalized carbon nanotubes is more challenging. This is due to the fact that the relatively simple yet generally effective (for many other functionalized carbon nanotube samples) TGA method is not applicable because of the carbonization of sugars under thermal defunctionalization conditions (*35*). On the other hand, sugars are readily quantified in term of classical sugar analysis, such as the use of anthrone reagent (*41*). Results from the sugar tests indicated no meaningful differences in sample compositions (sugar-nanotube weight ratio) between Gal-SWNT and Man-SWNT, between Gal_2-SWNT and Man_2-SWNT, and between Gal_4-SWNT and Man_4-SWNTs, despite the fact that the Gal-based functionalization agents were consistently less effective (a lower percentage of the starting purified SWNTs solubilized) than their Man-based counterparts in the nanotube functionalization and solubilization (Table 1). For Gal_4-SWNT and Man_4-SWNT, their improved aqueous solubility and the specific configuration in which the tethered galactoses or mannoses are displayed in quartet, resulted in interesting properties not available to other configurations. For example, the Gal- and Man-functionalized SWNT samples could self-aggregate in the presence of a divalent cation due to the cation-mediated monosaccharide-monosaccharide interactions (*28*, *35*), but the sugar dendron-functionalized nanotube samples, including Man_2-SWNT, Gal_2-SWNT, Man_4-SWNT, and Gal_4-SWNT, were found to be only weakly responsive toward divalent cations (*28*).

Downloaded by PENNSYLVANIA STATE UNIV on June 3, 2012 | http://pubs.acs.org
Publication Date (Web): December 13, 2011 | doi: 10.1021/bk-2011-1091.ch008

Downloaded by PENNSYLVANIA STATE UNIV on June 3, 2012 | http://pubs.acs.org
Publication Date (Web): December 13, 2011 | doi: 10.1021/bk-2011-1091.ch008

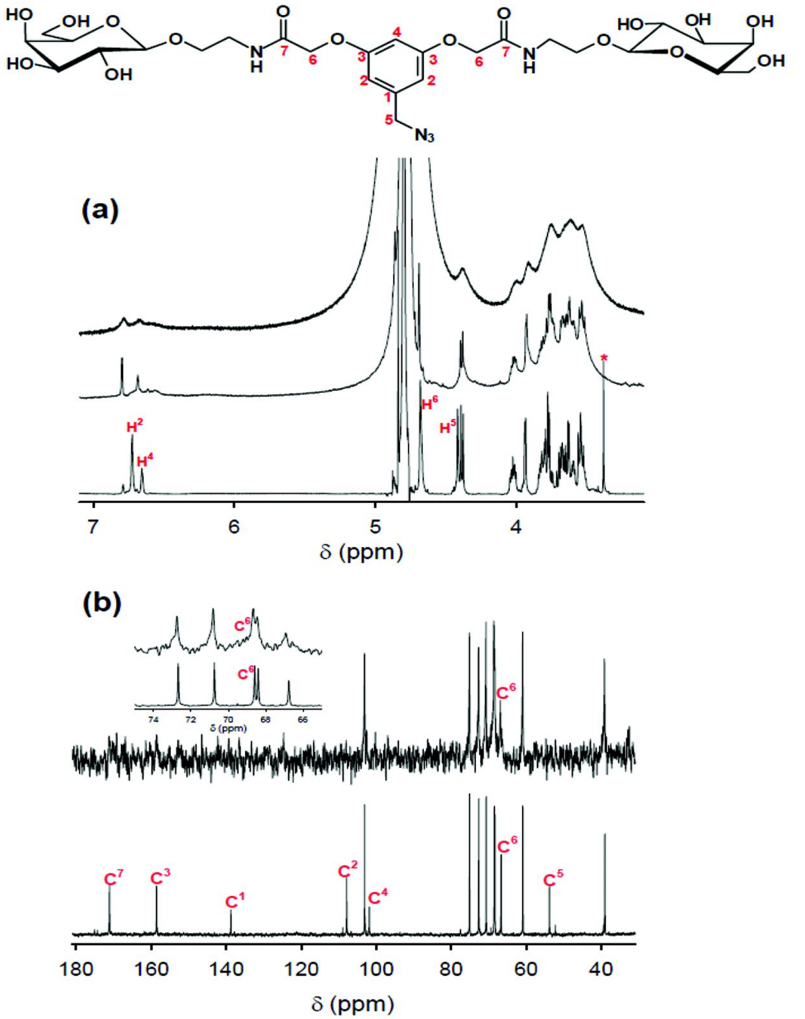

*Figure 2. (a) ^{1}H NMR spectra of Gal$_2$-SWNT (top: solution phase; middle: gel phase) and Gal$_2$-N$_3$ (bottom); and (b) ^{13}C NMR spectra of Gal$_2$-SWNT (top with inset) and Gal$_2$-N$_3$ (bottom) all in D$_2$O. * denotes residual methanol peaks. (Adapted from ref. (35).)*

Downloaded by PENNSYLVANIA STATE UNIV on June 3, 2012 | http://pubs.acs.org
Publication Date (Web): December 13, 2011 | doi: 10.1021/bk-2011-1091.ch008

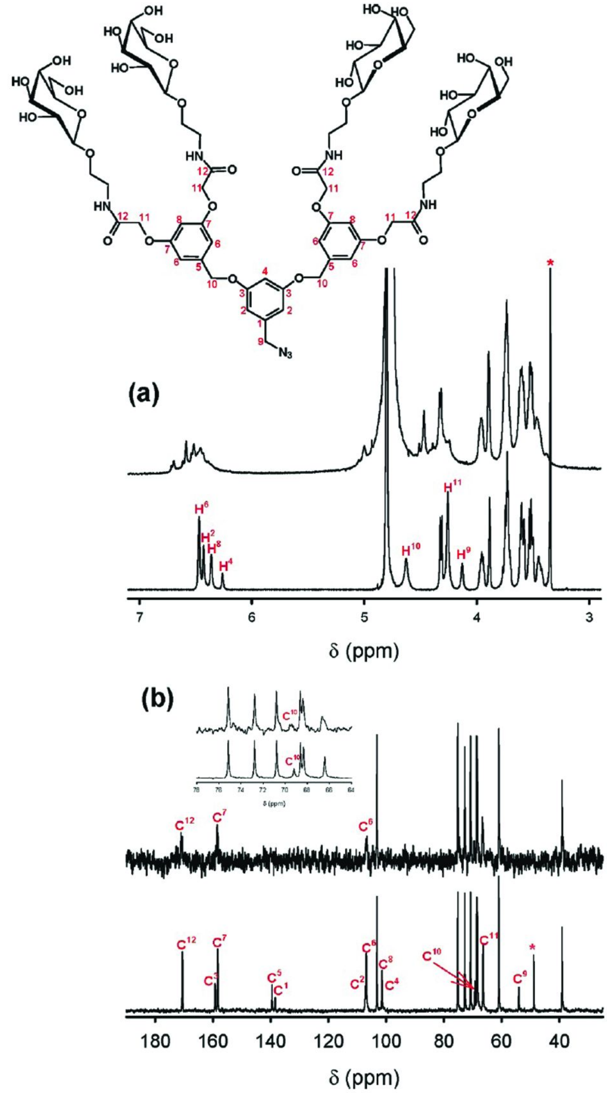

*Figure 3. (a) ^{1}H NMR spectra of Gal$_4$-SWNT (top) and Gal$_4$-N$_3$ (bottom); and (b) ^{13}C NMR spectra of Gal$_4$-SWNT (top with inset) and Gal$_4$-N$_3$ (bottom) all in D$_2$O. * denotes residual methanol peaks. (Adapted from ref. (35)).*

Downloaded by PENNSYLVANIA STATE UNIV on June 3, 2012 | http://pubs.acs.org
Publication Date (Web): December 13, 2011 | doi: 10.1021/bk-2011-1091.ch008

Table 1. Compositions in the Functionalized Nanotube Samples and Related Parameters

Nanotube type	*Sugar content[a] (%)*	*SWNT content[a] (%)*	*Avg No. of nanotube carbon per sugar unit[b]*	*Aqueous solubility (SWNT equivalant mg/mL)*	*Starting SWNT solubilized (%)*
Gal-SWNT	45	43	14	0.83	11
Man-SWNT	47	42	13	0.84	22
Gal_2-SWNT	44	19	6	1.7	20
Man_2-SWNT	45	18	6	1.6	35
Gal_4-SWNT	37	23	9	3.1	27
Man_4-SWNT	35	29	11	4.3	50

[a] The remaining (100% - sugar content - SWNT content) is the content of linkers/tethers. [b] The degree of functionalization exceeding that for the estimated COOH population might be due to preferable solubilization of those nanotubes with more than average COOH contents and also some noncovalent but strong adsorption of the amines.

The functionalization of carbon nanotubes with the sugars or related dendrons was apparently capable of exfoliating and dispersing the nanotubes, as made evident by the electron microscopy results. For example, scanning electron microscopy (SEM) images for the Gal_2-SWNT specimen (mechanically fractured) showed that abundant nanotubes randomly oriented at the edge of the specimen but more ordered in the fractured portion of the same specimen (Figure 4). The images for the Gal_4-SWNT specimen from a very dilute aqueous solution showed generally dispersed nanotubes (Figure 4).

The optical spectroscopy characterization yielded results generally suggesting that the optical transitions intrinsic of carbon nanotubes are mostly preserved in the sugar-functionalized samples. In optical absorption spectra measured in both D_2O solution and the solid-state film, the S_{11} (~ 1,880 nm) and S_{22} (~ 1,050 nm) bands due to electronic transitions between the van Hove singularity pairs in semiconducting SWNTs and the weak M_{11} transition (~ 740 nm) in metallic SWNTs were all present for the sugar dendron-functionalized nanotube samples (Figure 5) (*35*, *42*). The preservation of the electronic properties of the nanotubes is a feature for the functionalization targeting nanotube surface defects-derived carboxylic acid moieties, as also observed in the same functionalization with many non-sugar molecules.

Downloaded by PENNSYLVANIA STATE UNIV on June 3, 2012 | http://pubs.acs.org
Publication Date (Web): December 13, 2011 | doi: 10.1021/bk-2011-1091.ch008

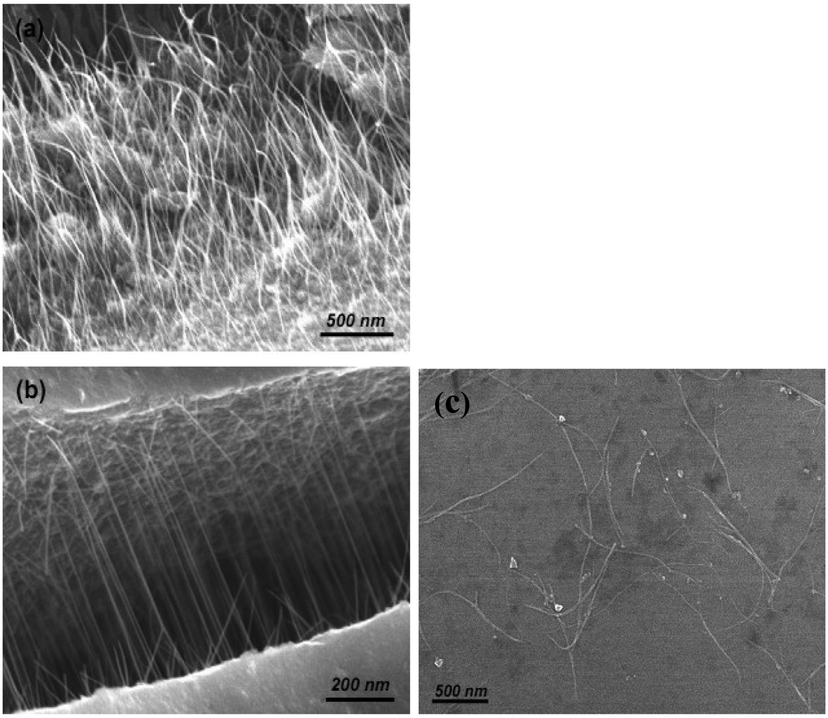

Figure 4. SEM images for a Gal_2-SWNT specimen (ultra-thin film) at the edge of the specimen (a) and in the fractured portion of the specimen (b), and for a Gal_4-SWNT specimen prepared from a very dilute sample solution (c). (Adapted from ref. (35).)

The Raman spectra of the various sugar-functionalized SWNTs are generally similar to that of the purified SWNTs pre-functionalization (Figure 6), including the typical radial breathing mode peaks at 140 cm^{-1} and 160 cm^{-1} for SWNTs produced by the arc-discharge method. Therefore, the optical spectroscopy techniques including Raman serve as relatively convenient tools for the characterization and quantification of carbon nanotubes in the functionalized samples.

Downloaded by PENNSYLVANIA STATE UNIV on June 3, 2012 | http://pubs.acs.org
Publication Date (Web): December 13, 2011 | doi: 10.1021/bk-2011-1091.ch008

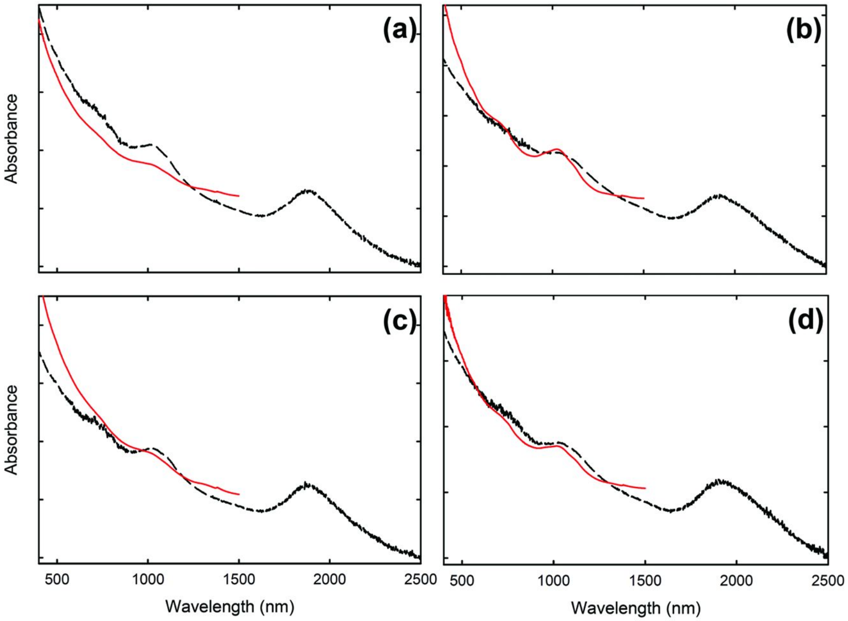

Figure 5. Optical absorption spectra of (a) Gal_2-SWNT, (b) Gal_4-SWNT, (c) Man_2-SWNT, and (d) Man_4-SWNT (solid line: in D_2O solution; dashed line: in the solid-state on glass substrate). (Adapted from ref. (35).)

Bioapplications

The sugar-functionalized carbon nanotubes with their relatively successful characterization and their desired properties, especially the excellent aqueous compatibility, have been explored for potential bioapplications, particularly for their selective interactions with cells and other biological species (*15*, *27*, *28*, *43–48*).

An earlier example was for the use of Gal-SWNT to bind to the pathogenic *E. coli* O157:H7 (a deadly food-borne pathogen and often referred to in the general public as “burger bug”). There are apparently strong interactions between Gal-SWNT and the *E. coli* cells, with multiple nanotubes binding to one cell and also some nanotubes “bridging” adjacent cells to result in significant agglutination (*27*). The binding has been attributed to carbohydrate-protein interaction between Gal-SWNT and *E. coli* O157:H7. The latter is known to express periplasmic galactose-binding proteins on the bacterial cell surface. The observed binding was apparently specific to Gal-SWNT because there was no such binding in the controls with SWNTs covalently functionalized with either α-D-mannose (Man-SWNT) or bovine serum albumin (BSA) protein under the same experimental conditions, suggesting that the nanotube-bound galactoses in Gal-SWNT were responsible for the binding and cell agglutination (*27*).

Downloaded by PENNSYLVANIA STATE UNIV on June 3, 2012 | http://pubs.acs.org
Publication Date (Web): December 13, 2011 | doi: 10.1021/bk-2011-1091.ch008

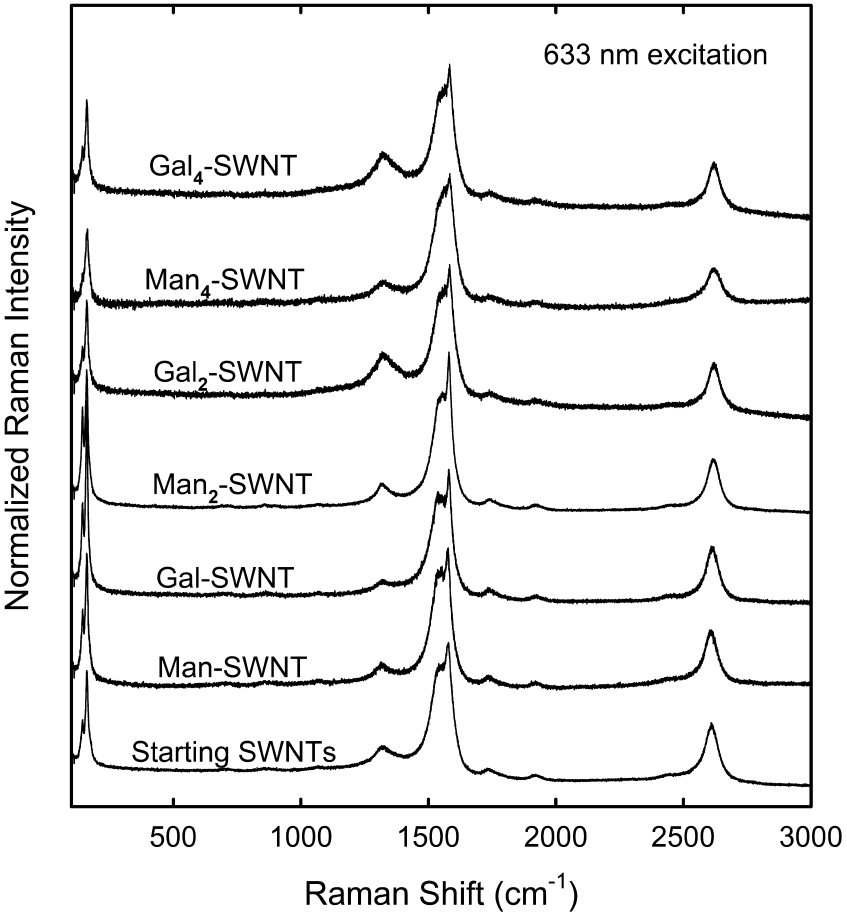

Figure 6. Comparison for Raman spectra (633 nm excitation) of the functionalized SWNTs and the starting purified nanotube sample. (Adapted from ref. (35).)

For sugar-functionalized carbon nanotubes to potentially serve as agents to counter the threat of anthrax was an interesting topic, generating much attention (*13*). Scientifically, there has been significant interest in the surface structure and characteristics of anthrax (*Bacillus anthracis*) spores as related to their binding by molecular species (*15*, *49*). Practically, the investigation of such binding and subsequent spore aggregation may potentially lead to the development of countermeasure technologies for the detection and decontamination of anthrax spores, as it is known that aggregated spores would pose significantly less or diminished threat in terms of the most lethal inhalation anthrax infection.

The interaction of monosaccharide-functionalized nanotube samples (Man-SWNT or Gal-SWNT) with *B. anthracis* spores was studied in aqueous suspension. The addition of a solution of Man-SWNT or Gal- SWNT to the suspension of *B. anthracis* spores (Sterne 34F2) apparently resulted in a homogeneous mixture. However, upon the addition of divalent cation Ca^{2+} to the mixture, there was immediate formation of spore aggregates, large enough to be visible to naked eyes. An examination of the aggregates under microscopes revealed that the *B. anthracis* spores in the aggregates were "wrapped" by the sugar-functionalized SWNTs (Figure 7). According to a quantitative CFU reduction assay on the *B. anthracis* spore aggregation by Man-SWNT in the presence of Ca^{2+}, close to 98% CFU reduction for the spores could be achieved with Man-SWNT at a mannose-equivalent concentration 0.12 mg/mL (*15*).

Downloaded by PENNSYLVANIA STATE UNIV on June 3, 2012 | http://pubs.acs.org
Publication Date (Web): December 13, 2011 | doi: 10.1021/bk-2011-1091.ch008

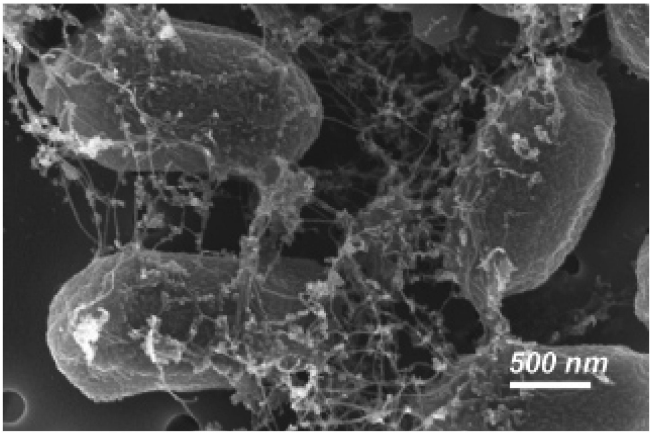

Figure 7. A high-resolution SEM image showing the interactions of Man-SWNT with B. anthracis spores. (Adapted from ref. (15).)

Interestingly and somewhat surprisingly, the binding that aggregated *B. anthracis* spores was only observed for the nanotube-displayed monosaccharide molecules, not available to other displaying platforms such as polymeric nanoparticles (Scheme 2) (*15*). These nanoparticles with a polystyrene core and surface-tethered mannoses or galactoses, while known for their adhesion to various *E. coli* strains to result in substantial cell agglutination (*29–31*), exhibited no interactions with the spores in the presence or absence of Ca^{2+}. It seems that specific arrangements of the carbohydrate ligands are probably required for multivalent interactions with the spore surface, for which the pseudo-one-dimensional structure of SWNTs is apparently a viable scaffold (*15*).

In a more systematic study to compare the aggregation of different spores, both *B. anthracis* and the genetically closely related *B. subtilis* were studied (*28*). SWNTs functionalized with various sugars in different configurations, including monosaccharide molecules (Man-SWNT and Gal-SWNT) and the sugar dendrons

(Man_2-SWNT, Gal_2-SWNT, Man_4-SWNT, and Gal_4-SWNT) (Scheme 1) in aqueous solution were added to the suspended *B. anthracis* or *B. subtilis* spores for binding interactions with or without the presence of a divalent cation. Major differences or significant variations in the interactions were observed for the different sugars and their configurations and between the two *Bacillus* spores (Table 2) (*28*).

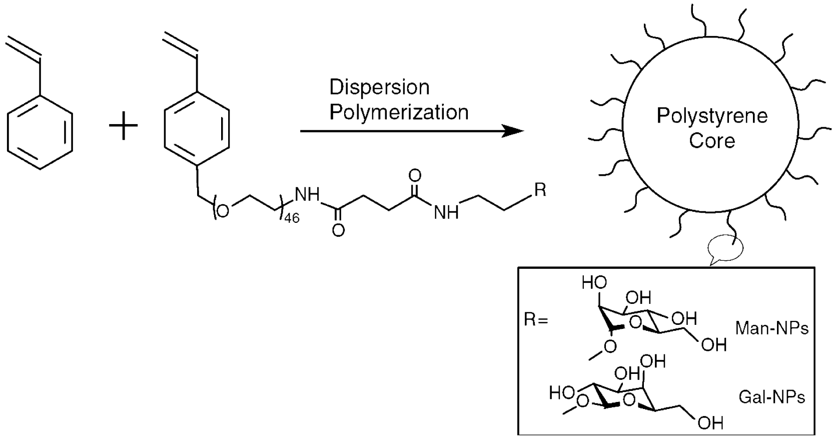

Scheme 2. Synthesis via emulsion (dispersion) polymerization for polymeric nanoparticles tethered with the sugar molecules. (Adapted from ref. (31).)

The results presented in Table 2 suggest that both *B. anthracis* (Sterne) and *B. subtilis* spores could be aggregated effectively by the monosaccharide-functionalized SWNTs (Man-SWNT and Gal-SWNT) in the presence of a divalent cation, without any pronounced selectivity. However, the high selectivity became evident in the absence of any divalent cations, with the binding and aggregation observed only for Man-SWNT with *B. subtilis* spores.

Although the current knowledge is still limited on the spore surface characteristics of these two species of *Bacillus* genus, it has been suggested that the spore surface is mainly composed of glycoproteins and carbohydrates. Thus mechanistically the binding between the sugar-functionalized SWNTs and the spores (Table 2) has been explained in terms of carbohydrate-carbohydrate interactions and carbohydrate-protein interactions (*28*). In the presence of Ca^{2+}, the observed aggregation and CFU reduction for the *Bacillus* spores (*B. anthracis* and *B. subtilis*) were attributed to divalent cation-mediated multivalent carbohydrate-carbohydrate interactions, or more specifically, the carbohydrates tethered to SWNTs with those expressed on the spore surface. Experimentally, the interactions were apparently not disrupted by the presence of the corresponding free sugars as competition. The role of Ca^{2+} mediation was confirmed by the experiment in which the aggregation of *Bacillus* spores was reversed with the addition of EDTA, a strong chelating agent for Ca^{2+} and other divalent cations.

Downloaded by PENNSYLVANIA STATE UNIV on June 3, 2012 | http://pubs.acs.org
Publication Date (Web): December 13, 2011 | doi: 10.1021/bk-2011-1091.ch008

Such reversibility with the use of EDTA to take the divalent cation out of the mediation could be explained in terms of a "zipper" model (*28*).

In the absence of Ca^{2+}, the selective binding of Man-SWNT with *B. subtilis* spores was attributed to carbohydrate-protein interactions of the nanotube-tethered mannoses with the specific protein receptors on the *B. subtilis* spore surface. The observed high specificity, not available for Gal-SWNT on the carbohydrate side or *B. anthracis* on the spore side, seems consistent with carbohydrate-protein binding, which is known to be more specific (*28*).

Table 2. SWNTs Functionalized with Various Configurations of Sugars (Mannose or Galactose) and Their Interactions with B. anthracis or B. subtilis spores with or without the presence of Ca^{2+}

Sugar configurations		*Divalent cation†*		*Without divalent cation*	
		B. anthracis	*B. subtilis*	*B. anthracis*	*B. subtilis*
Monomer	Man-SWNT	+++	+++	-	++
	Gal-SWNT	+++	+++	-	-
Dimer	Man_2-SWNT	-*	++	-	+
	Gal_2-SWNT	-*	+	-	-
Tetramer	Man_4-SWNT	-	-	-	-*
	Gal_4-SWNT	-	NA	-	-

† : Different divalent cations were tested and CFU reduction was in the order of $Mg^{2+} < Ca^{2+} < Ba^{2+}$; all percentage denoted in this table shows data obtained from Ca^{2+}. +++: significant binding and aggregation; more than 67% of CFU reduction. ++: substantial binding and aggregation; more than 50% of CFU reduction. +: some binding and aggregation; less than 10% of CFU reduction. -*: little binding or aggregation, CFU reduction within experimental uncertainty margin. -: no meaningful effect of binding or aggregation.

Obviously, the carbohydrate configuration in the functionalized SWNTs is expected to play a significant role in terms of binding and aggregation. The sugar dendrons were prepared for the purpose of displaying the sugars in pairs or quartets, thus intuitively for significantly improved multivalency. Surprisingly the sugar dendron-functionalized SWNTs, especially Man_4-SWNT and Gal_4-SWNT, were generally ineffective in the binding and aggregation of the *Bacillus* spores either with or without the divalent cation mediation, indicating that much remains to be explored and understood on the interactions of the sugars displayed on

Downloaded by PENNSYLVANIA STATE UNIV on June 3, 2012 | http://pubs.acs.org
Publication Date (Web): December 13, 2011 | doi: 10.1021/bk-2011-1091.ch008

carbon nanotubes with the spores or similar biological species and also on the related mechanistic origins.

In summary, sugar-functionalized carbon nanotubes are unique nanostructures and offer great opportunities for the exploration of their potential uses in biology and medicine. As illustrated in this article, the functionalization chemistry targeting the defect-derived carboxylic acid moieties on the nanotube surface is versatile, enabling relatively convenient synthesis of a variety of carbon nanotubes with tethered β-D-galactopyranosides and α-D-mannopyranosides or their dendritic structures, which with the ready aqueous solubility could be characterized structurally or property-wise by techniques including those in the solution phase. Carbon nanotubes apparently serve as unique pseudo-one-dimensional scaffolds for multivalent display of the sugar molecules, resulting in significant biological interactions, with some of which not available to other sugar-functionalized nanomaterials or species. Therefore, this may represent a new platform in the study of multivalent carbohydrate configurations and their biological functions.

Downloaded by PENNSYLVANIA STATE UNIV on June 3, 2012 | http://pubs.acs.org
Publication Date (Web): December 13, 2011 | doi: 10.1021/bk-2011-1091.ch008

Acknowledgments

Financial support from NSF and in part from NIH is gratefully acknowledged. A.A. was the recipient of a graduate research fellowship awarded by South Carolina Space Grant Consortium.

References

1. Wong, S. S.; Joselevich, E.; Woolley, A. T.; Cheung, C. C.; Lieber, C. M. *Nature* **1998**, *394*, 52.
2. Mattson, M. P.; Haddon, R. C.; Rao, A. M. *J. Mol. Neurosci.* **2000**, *14*, 175.
3. Lin, Y.; Taylor, S.; Li, H.; Fernando, K. A. S.; Qu, L.; Wang, W.; Gu, L.; Zhou, B.; Sun, Y.-P. *J. Mater. Chem.* **2004**, *14*, 527.
4. Lu, F.; Gu, L.; Meziani, M. J.; Wang, X.; Luo, P. G.; Veca, L. M.; Cao, L.; Sun, Y.-P. *Adv. Mater.* **2009**, *21*, 139–152.
5. Wang, J. *Electroanalysis* **2005**, *17*, 7.
6. Yun, Y.; Dong, Z.; Shanov, V.; Heineman, W. R.; Halsall, H. B.; Bhattacharya, A.; Conforti, L.; Narayan, R. K.; Ball, W. S.; Schulz, M. J. *Nano Today* **2007**, *2*, 30.
7. Rivas, G. A.; Rubianes, M. D.; Rodríguez, M. C.; Ferreyra, N. F.; Luque, G. L.; Pedano, M. L.; Miscoria, S. A.; Parrado, C. *Talanta* **2007**, *74*, 291.
8. Baughman, R. H.; Cui, C.; Zakhidov, A. A.; Iqbal, Z.; Barisci, J. N.; Spinks, G. M.; Wallace, G. G.; Mazzoldi, A.; De Rossi, D.; Rinzler, A. G.; Jaschinski, O.; Roth, S.; Kertesz, M. *Science* **1999**, *284*, 1340.
9. Fennimore, A. M.; Yuzvinsky, T. D.; Han, W. -Q.; Fuhrer, M. S.; Cumings, J.; Zettl, A. *Nature* **2003**, *424*, 408.
10. Kam, N. W. S.; O'Connell, M.; Wisdom, J. A.; Dai, H. *Proc. Natl. Acad. Sci. USA* **2005**, *102*, 11600.
11. Kam, N. W. S.; Dai, H. *Phys. Status Solidi B* **2006**, *243*, 3561.

Downloaded by PENNSYLVANIA STATE UNIV on June 3, 2012 | http://pubs.acs.org
Publication Date (Web): December 13, 2011 | doi: 10.1021/bk-2011-1091.ch008

12. Lacerda, L.; Raffa, S.; Prato, M.; Bianco, A.; Kostarelos, K. *Nano Today* **2007**, *2*, 38.
13. Prato, M.; Kostarelos, K.; Bianco, A. *Acc. Chem. Res.* **2008**, *41*, 60.
14. Akasaka, T.; Watari, F. *Fullerenes, Nanotubes, Carbon Nanostruct.* **2008**, *16*, 114.
15. Wang, H.; Gu, L.; Lin, Y.; Lu, F.; Meziani, M. J.; Luo, P. G.; Wang, W.; Cao, L.; Sun, Y.-P. *J. Am. Chem. Soc.* **2006**, *128*, 13364.
16. Lam, C. W.; James, J. T.; McCluskey, R.; Arepalli, S.; Hunter, R. L. *Crit. Rev. Toxicol.* **2006**, *36*, 189.
17. Kolosnjaj, J.; Szwarc, H.; Moussa, F. In *Bio-Applications of Nanoparticles*; Chan, W. C. W., Ed.; Springer: Germany, 2007; Vol. 620, p 181.
18. Bianco, A.; Prato, M. *Adv. Mater.* **2003**, *15*, 1765.
19. Chen, R. J.; Bangsaruntip, S.; Drouvalakis, K. A.; Dim, N. W. S.; Shim, M.; Li, Y.; Kim, W.; Utz, P. J.; Dai, H. *Proc. Natl. Acad. Sci. U.S.A.* **2003**, *100*, 4984.
20. Li, J.; Ng, H. T.; Cassell, A.; Fan, W.; Chen, H.; Ye, Q.; Koehne, J.; Han, J.; Meyyappan, M. *Nano Lett.* **2003**, *3*, 597.
21. Pompeo, F.; Resasco, D. E. *Nano Lett.* **2002**, *2*, 369.
22. Matsuura, K.; Hayashi, K.; Kimizuka, N. *Chem. Lett.* **2003**, *32*, 212.
23. Baker, S. E.; Cai, W.; Lasseter, T. L.; Weidkamp, K. P.; Hamers, R. J. *Nano Lett.* **2002**, *2*, 1413.
24. Huang, W.; Taylor, S.; Fu, K.; Lin, Y.; Zhang, D.; Hanks, T. W.; Rao, A. M.; Sun, Y.-P. *Nano Lett.* **2002**, *2*, 311.
25. Pantarotto, D.; Singh, R.; McCarthy, D.; Erhardt, M.; Briand, J.-P.; Prato, M.; Kostarelos, K.; Bianco, A. *Angew. Chem., Int. Ed.* **2004**, *43*, 5242.
26. Gorityala, B. K.; Ma, J.; Wang, X.; Chenb, P.; Liu, X.-W. *Chem. Soc. Rev.* **2010**, *39*, 2925.
27. Gu, L.; Elkin, T.; Jiang, X.; Li, H.; Lin, Y.; Qu, L.; Tzeng, T.-R. J.; Joseph, R.; Sun, Y.-P. *Chem. Commun.* **2005**, 874.
28. Luo, P. G.; Wang, H.; Gu, L.; Lu, F.; Lin, Y.; Christensen, K. A.; Yang, S.-T.; Sun, Y.-P. *ACS Nano* **2009**, *3*, 3909.
29. Qu, L.; Luo, P. G.; Taylor, S.; Lin, Y.; Huang, W.; Anyadike, N.; Tzeng, T.-R.; Stutzenberger, F.; Latour, R. A.; Sun, Y.-P. *J. Nanosci. Nanotechnol.* **2005**, *5*, 320.
30. Qu, L.; Gu, L.; Li, H.; Taylor, S.; Elkin, T.; Luo, P. G.; Tzeng, T.-R. J.; Jiang, X.; Latour, R. A.; Stutzenberger, F.; Williams, A.; Sun, Y.-P. *J. Biomed. Nanotechnol.* **2005**, *1*, 61.
31. Luo, P. G.; Tzeng, T.-R.; Qu, L.; Lin, Y.; Caldwell, E.; Latour, R. A.; Stutzenberger, F.; Sun, Y.-P. *J. Biomed. Nanotechnol.* **2005**, *1*, 291.
32. Molugu, S.; Qu, L.; Lin, Y.; Sun, Y.-P.; Tzeng, T.-R.; Stutzenberger, F. J.; Latour, R. A. *J. Biomed. Nanotechnol.* **2006**, *2*, 1.
33. Ye, Y.; Ju, H. *Biosens. Bioelectron.* **2005**, *21*, 735.
34. Gu, L.; Lin, Y.; Qu, L.; Sun, Y.-P. *Biomacromolecules* **2006**, *7*, 400.
35. Gu, L.; Luo, P. G.; Wang, H.; Meziani, M. J.; Lin, Y.; Veca, L. M.; Cao, L.; Lu, F.; Wang, X.; Quinn, R. A.; Wang, W.; Zhang, P.; Lacher, S.; Sun, Y.-P. *Biomacromolecules* **2008**, *9*, 2408.
36. Sun, Y.-P.; Fu, K.; Lin, Y.; Huang, W. *Acc. Chem. Res.* **2002**, *35*, 1096.

37. Chen, J.; Liu, H.; Weimer, W. A.; Halls, M. D.; Waldeck, D. H.; Walker, G. C. *J. Am. Chem. Soc.* **2002**, *124*, 9034.
38. Qu, L.; Lin, Y.; Hill, D. E.; Zhou, B.; Wang, W.; Sun, X.; Kitaygorodskiy, A.; Suarez, M.; Connell, J. W.; Allard, L. F.; Sun, Y.-P. *Macromolecules* **2004**, *37*, 6055.
39. Qu, L.; Veca, L. M.; Lin, Y.; Kitaygorodskiy, A.; Chen, B.; McCall, A. M.; Connell, J. W.; Sun, Y.-P. *Macromolecules* **2005**, *38*, 10328.
40. Holzinger, M.; Abraha, J.; Whelan, P.; Graupner, R.; Ley, L.; Hennrich, F.; Kappes, M.; Hirsch, A. *J. Am. Chem. Soc.* **2003**, *125*, 8566.
41. Jermyn, M. A. *Anal. Biochem.* **1975**, *68*, 332.
42. Zhou, B.; Lin, Y.; Li, H.; Huang, W.; Connell, J. W.; Allard, L. F.; Sun, Y.-P. *J. Phys. Chem. B* **2003**, *107*, 13588.
43. Elkin, T.; Jiang, X.; Taylor, S.; Lin, Y.; Gu, L.; Yang, H.; Brown, J.; Collins, S.; Sun, Y.-P. *ChemBioChem.* **2005**, *6*, 640.
44. Hasegawa, T.; Fujisawa, T.; Numata, M.; Umeda, M.; Matsumoto, T.; Kimura, T.; Okumura, S.; Sakurai, K.; Shinkai, S. *Chem. Commun.* **2004**, 2150.
45. Wu, P.; Chen, X.; Hu, N.; Tam, U. C.; Blixt, O.; Zettl, A.; Bertozzi, C. R. *Angew. Chem., Int. Ed.* **2008**, *47*, 5022.
46. Kang, S.; Pinault, M.; Pfefferle, L. D.; Elimelech, M. *Langmuir* **2007**, *23*, 8670.
47. Nimmagadda, A.; Thurston, K.; Nollert, M. U.; McFetridge, P. S. *J. Biomed. Mater. Res., Part A* **2006**, *76a*, 614.
48. Ahmed, M.; Jiang, X.; Deng, Z.; Narain, R. *Bioconjugate Chem.* **2009**, *20*, 2017.
49. Knurr, J.; Benedek, O.; Heslop, J.; Vinson, R. B.; Boydston, J. A.; McAndrew, J.; Kearney, J. F.; Turnbough, C. L. *Appl. Environ. Microbiol.* **2003**, *69*, 6841.

Downloaded by PENNSYLVANIA STATE UNIV on June 3, 2012 | http://pubs.acs.org
Publication Date (Web): December 13, 2011 | doi: 10.1021/bk-2011-1091.ch008

Chapter 9

Synthetic Glycans, Glycoarrays, and Glyconanoparticles To Investigate Host Infection by *Trypanosoma cruzi*

Robert A. Field,[*,1,2] Peterson Andrade,[3] Vanessa L. Campo,[3]
Ivone Carvalho,[3] Beatrice Y. M. Collet,[2] Paul R. Crocker,[4]
Margherita Fais,[1,2] Rositsa Karamanska,[1,2]
Balaram Mukhopadhayay,[2] Sergey A. Nepogodiev,[1,2]
Abdul Rashid,[1] Martin Rejzek,[1] David A. Russell,[2]
Claire L. Schofield,[2] and Renate M. van Well[2]

[1]Department of Biological Chemistry, John Innes Centre,
Norwich Research Park, Norwich NR4 7UH, U.K.
[2]School of Chemistry, University of East Anglia, Norwich NR4 7TJ, U.K.
[3]Faculdade de Ciências Farmacêuticas de Ribeirão Preto, USP,
Av. Café S/N, CEP 14040-903, Ribeirão Preto, SP, Brazil
[4]Division of Cell Biology and Immunology, Wellcome Trust Biocentre,
College of Life Sciences, University of Dundee, Dundee DD1 5EH, U.K.
[*]E-mail: Rob.Field@bbsrc.ac.uk

Downloaded by CORNELL UNIV on June 3, 2012 | http://pubs.acs.org
Publication Date (Web): December 13, 2011 | doi: 10.1021/bk-2011-1091.ch009

Carbohydrate libraries, synthetic glycans and glycopeptides are contributing to understanding of the role of sialic acid recognition in host infection by the parasite *Trypanosoma cruzi*. Further, glycoarray approaches are allowing us to explore similarities and differences in the carbohydrate-binding specificity of host lectins while glyconanoparticles enable us to ask questions about the structure, sialylation and recognition of parasite mucins.

In Petite and Sweet: Glyco-Nanotechnology as a Bridge to New Medicines; Huang, X., et al.;
ACS Symposium Series; American Chemical Society: Washington, DC, 2011.

Downloaded by CORNELL UNIV on June 3, 2012 | http://pubs.acs.org
Publication Date (Web): December 13, 2011 | doi: 10.1021/bk-2011-1091.ch009

Introduction

Trypanosoma cruzi, the etiologic agent of Chagas' disease, is a blood-borne protozoan parasite that is prevalent in South and Central America. The Pan American Health Organization (PAHO) estimates that in the 21 endemic countries, which range from the southern and southwestern United States to central Argentina and Chile, currently 7.7 million people have *T. cruzi* infection. A further 100 million are at risk of infection. At any one time around 2-3 million individuals show clinical symptoms of the chronic phase of the disease and 45000 people die each year (*1–3*). The only drugs approved for the treatment of Chagas' disease, nifurtimox and benznidazole, were introduced for therapeutic use over thirty years ago. However, limited efficacy in the chronic stage of the disease and toxic side effects highlight the need for new drugs. While some progress is being made in the discovery and development of new therapeutics (*4*, *5*), there is scope to evaluate new parasite-specific targets. Given that *T. cruzi* is an obligate intracellular parasite, needing to invade host cells in order to replicate, parasite adhesion to host cells offers the possibility for the development of chemotherapeutic agents (*6*, *7*). Likewise, as *T. cruzi* is blood-borne, agents capable of interfering with the cell surface biochemistry of the parasite might render it sensitive to the host immune response (*6*, *7*).

In keeping with many other parasitic protozoa (*8*), *T. cruzi* makes extensive use of cell surface carbohydrate structures (*9*) to sustain itself in hostile environments (i.e. the gut of the insect vector, the host blood stream). This parasite displays marked host-dependent surface coat diversity, dominated by mucin *O*-linked glycoproteins (*10*). Mucins contribute to protection of the parasite against host agents (protease action; immune response) and facilitate the establishment and development of infection through enabling parasite adhesion to host tissues as a prelude to cell invasion. The key role that mucins play in the life of the parasite is evident from the fact that the *T. cruzi* genome contains roughly 850 mucin-encoding genes, corresponding to approximately 6% of all predicted genes (*10*). A representative glycopeptide fragment of the mucin found in the human form of *T. cruzi* Y strain is illustrated in Figure 1.

The *T. cruzi* mucin *O*-glycans resemble those of mammalian mucins, although the oligosaccharides are linked to the threonine or serine of the parasite protein *via* an α-linked *N*-acetyl-glucosamine (GlcNAc) rather than an α-linked *N*-acetylgalactosamine (GalNAc), as in vertebrate mucins (*11*, *12*). The α-GlcNAc is substituted by galactose (Gal) on *O*-4 and *O*-6, with further galactosylation leading to complex branched structures (*13–15*). In the human blood-stream form of the parasite, the mucin glycans also contain sialic acid (NeuAc). However, *T. cruzi* is unable to synthesize sialic acid *de novo* and so uses a cell surface *trans*- sialidase enzyme (*16*, *17*) to scavenge this monosaccharide from host glycoconjugates in order to generate α-2,3-linked sialylated β-galactopyranose units on the parasite mucins. The similarity of the parasite *trans*-sialidase to the numerous microbial/viral sialidases (neuraminidases) that have been investigated (*18*) suggests the potential for this enzyme as a therapeutic target. However, despite its similarity to the microbial and viral enzymes, *T. cruzi trans*-sialidase is essentially insensitive to the classical glycal-based inhibitors used as anti-flu drugs and there are currently no known potent reversible inhibitors of this enzyme (*19*). With this in mind, we set out to explore substrate and inhibitor binding to *T. cruzi trans*-sialidase and to evaluate the role of mucin glycans in parasite recognition by the host. In turn, this encouraged us to explore a range of new tools, techniques and approaches that are finding use in glycosciences research (*20–22*).

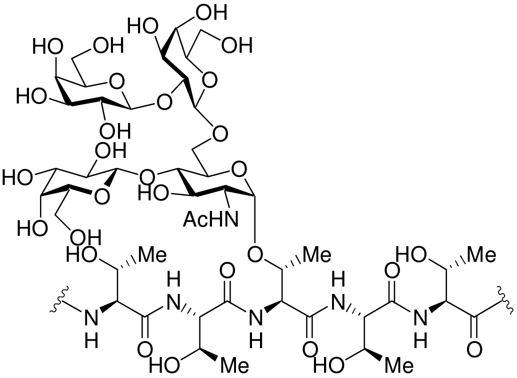

Figure 1. Trypanosoma cruzi Y strain mucin glycopeptide fragment.

Questions, Challenges, and Solutions

The nature of *T. cruzi* mucin glycopeptides presents a number of questions about structure, synthesis and recognition:

- Does the glycan-peptide α-GlcNAc linkage have an impact of the presentation and recognition of mucin glycans? How can the α-GlcNAc linkage be installed efficiently by chemical synthesis?
- How do the branched structures of mucin glycans contribute to biological recognition? How may enzymatic or chemical approaches contribute to the regiocontrolled installation of β-galactopyranose units?
- The *trans*-sialidase-catalysed incorporation of one molecule of sialic acid into *T. cruzi* mucin glycans hinders the introduction of a second sialic acid even when further potential acceptor sites are available (*23*). Why is this the case and does it inform us about the function of elements of mucin structure?
- Which host lectins are involved in parasite recognition? Do we currently have the tools to assess the nature of parasite glycan-host lectin interactions?

Downloaded by CORNELL UNIV on June 3, 2012 | http://pubs.acs.org
Publication Date (Web): December 13, 2011 | doi: 10.1021/bk-2011-1091.ch009

Stereoselective α-GlcNAc-ylation

Originally we reported the α-selective iodine-promoted glycosylation of partially protected serine and threonine with 2-azido-2-deoxyglycosyl iodides (*24*), but sought a shorter route to α-linked GlcNAc aminoacids and galactosylated versions thereof. Although the use of a glycosyl donor possessing a C-2 participating group when attempting to synthesize a 1,2-*cis*-linked glycoside is counter intuitive, 3,4,6-tri-*O*-acetyl-2-acetamido-2-deoxy-α-D-glucopyranosyl chloride is a readily accessible, cheap and shelf-stable material. With this donor we demonstrated that mercury salt-mediated β-glycosylation of *N*-Fmoc-protected serine or threonine proceeded in reasonable yield (typically *ca* 60-65 %) (*25*). On closer inspection, however, the reaction mixture was found to contain low levels of the corresponding α-linked glycoside, which on optimization of reaction conditions with the aminoacid benzyl ester could be improved to a modest but reliable 20 % yield (Scheme 1) (*26*). While lacking elegance, this direct approach saves several synthesis and chromatography steps over more conventional approaches.

Downloaded by CORNELL UNIV on June 3, 2012 | http://pubs.acs.org
Publication Date (Web): December 13, 2011 | doi: 10.1021/bk-2011-1091.ch009

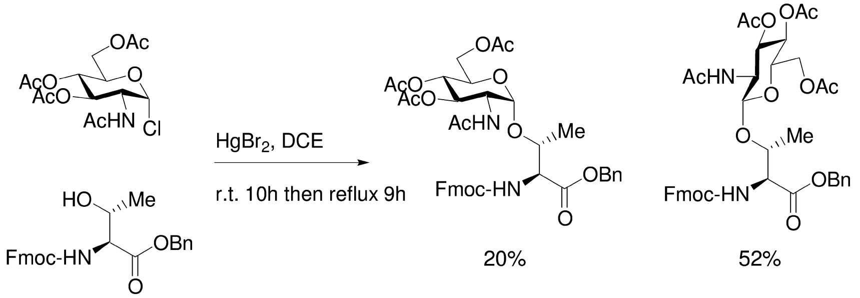

Scheme 1. Direct synthesis of α-GlcNAc-threonine

Regioselective β-Galactosylation

In order to generate simpler mucin glycan or glycoaminoacid fragments, we resorted to enzymatic β-galactosylation procedures. While bovine milk β-1,4-galactosyltransferase has a clear-cut preference for β-linked acceptor substrates, both β- and α-linked GlcNAc-threonine proved to be substrates (*26*). While the β-linked acceptor turned over readily to give the LacNAc product in 85% yield, the α-linked LacNAc product was isolated in 57% yield only when longer incubation times and elevated levels of enzyme were employed (Scheme 2).

Downloaded by CORNELL UNIV on June 3, 2012 | http://pubs.acs.org
Publication Date (Web): December 13, 2011 | doi: 10.1021/bk-2011-1091.ch009

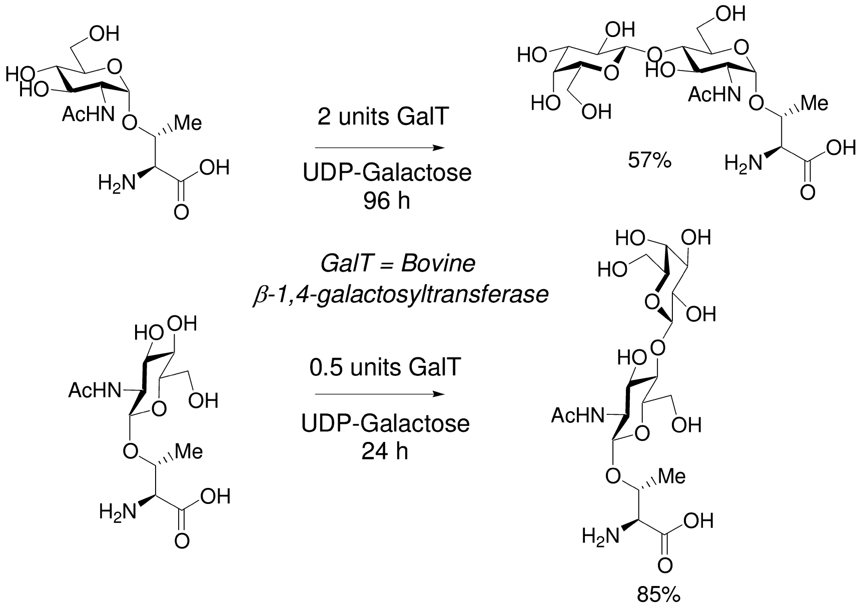

Scheme 2. Enzymatic β-galactosylation of glycoaminoacids

1,2-*cis*-Glycosylation

Moving towards more elaborate mucin glycan structures, the chemical synthesis of a tetrasaccharide (Figure 2) was also explored (*27*). This target presents a number of potential disconnections from a retrosynthesis perspective. In initial efforts, we explored both a 2 + 1 + 1 and a (2 x 1) + 2 approach. The former route was unsuccessful due to problems with selective deacetylation in the presence of benzoate protecting groups elsewhere in a trisaccharide intermediate. Double glycosylation of a 1,6-linked diol acceptor in a 2 + (2 x 1) approach yielded only low yields of a trisaccharide. Finally, a blockwise 2 + 2 approach, relying on the participating solvent MeCN to control anomeric stereochemistry, gave a protected tetrasaccharide intermediate in 79 % yield as an inseparable mixture of diastereoisomers (>10:1, β:α). Reductive acetylation of the azide group and de-*O*-acetylation gave the target tetrasaccharide, which was assessed as a substrate for *trans*-sialidase-catalysed sialylation.

Downloaded by CORNELL UNIV on June 3, 2012 | http://pubs.acs.org
Publication Date (Web): December 13, 2011 | doi: 10.1021/bk-2011-1091.ch009

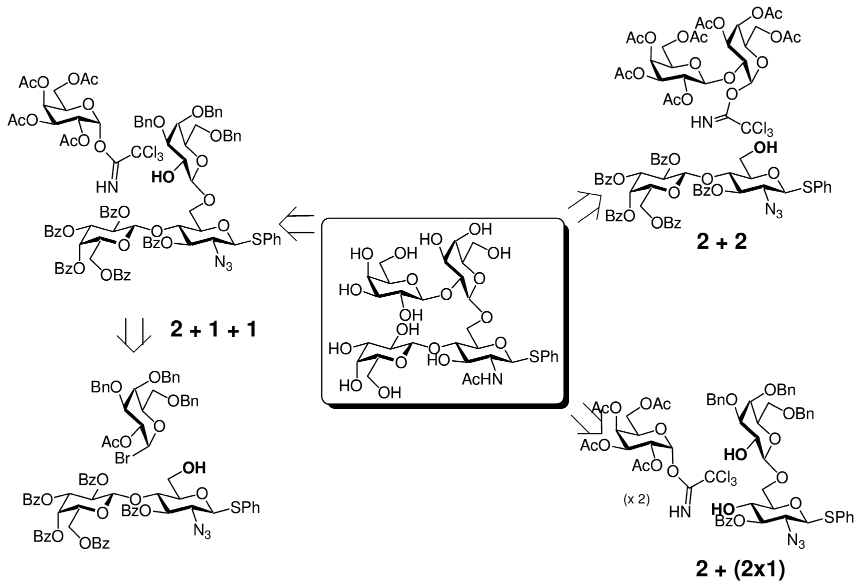

Figure 2. Disconnections for mucin tetrasaccharide synthesis.

Enzymatic Sialylation with *trans*-Sialidase

In these studies we employed a recombinant form of *trans*-sialidase containing just the 70 kDa catalytic domain (*28*). We had previously shown this form of the enzyme to be an excellent catalyst for the chemoenzymatic synthesis of ^{13}C-enriched α-2,3-sialylated glycans (*29*) for use in stable-isotope-assisted NMR studies to probe the conformation of sialyl Lewis x tetrasaccharide bound to E-selectin (*30*, *31*). Mass spectrometry analysis of the product from *trans*-sialidase action on the mucin tetrasaccharide fragment confirmed the successful addition of two sialic acid residues (Scheme 3). The sites of sialylation remained to be established, but were subsequently inferred from work with systematically modified substrates (next section). The double addition of sialic acid raised the question why not three sialic acid additions, given that there are three galactose 3-OH groups free for sialylation by the α-2,3-specific *trans*-sialidase. On the other hand, it also raises the question why two sialic acids and not one, in keeping with the observations of Previato and colleagues (*23*). In order to address these points, we explored both galactose-based compound libraries and synthetic fragments of *T. cruzi* mucin glycopeptides.

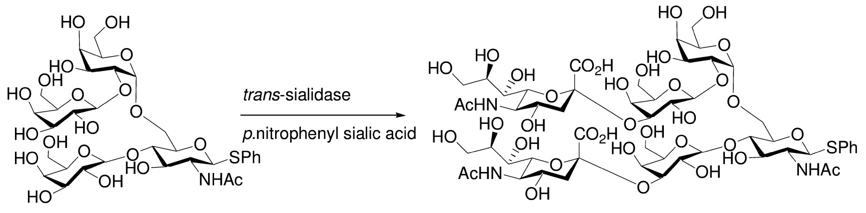
trans-sialidase
p.nitrophenyl sialic acid

Scheme 3. Enzymatic sialylation of mucin tetrasaccharide fragment

Carbohydrate Libraries

In order to assess which part of the galactose molecule may be important for *trans*-sialidase recognition, we set about probing the acceptor substrate binding site of the enzyme with systematically modified substrates and glycoside libraries (*32*). These compounds were based on modified octyl galactosides (*33*), a range of compounds derived from *N*-acetyllactosamine *O*-cyanomethyl ethers (*34*, *35*), and a >100 component library of thiogalactoside-derived compounds (*36*, *37*). These studies highlighted a marked tolerance of *trans*-sialidase for substituent variation at the aglycone site and the 6-position of galactose, with very limited or no tolerance of substitution at galactose position 2 or 4 (Figure 3).

The intolerance to substitution at position 2 is significant in that it accounts for why only two of the three galactose residues in the mucin tetrasaccharide (Scheme 4) are able to serve as acceptor sites for *trans*-sialidase action.

Extending these studies, we have also exploited Cu(I)-catalyzed azide-alkyne cycloaddition ‘click’ chemistry (*38*, *39*) for the development of *trans*-sialidase substrates and inhibitors (*40*, *41*), some of which display potent anti-trypanosomal activity (*42*).

Downloaded by CORNELL UNIV on June 3, 2012 | http://pubs.acs.org
Publication Date (Web): December 13, 2011 | doi: 10.1021/bk-2011-1091.ch009

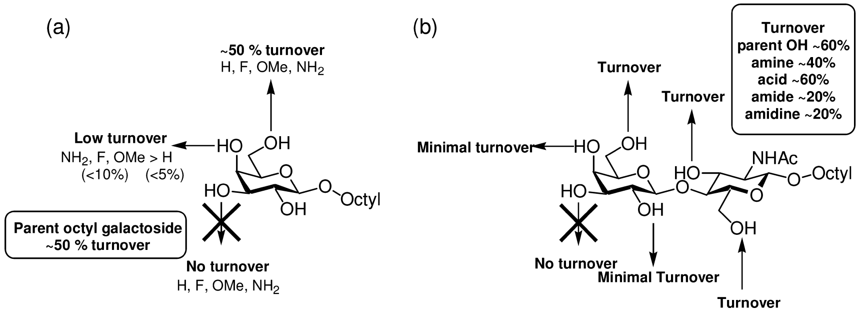
(a)
~50 % turnover
H, F, OMe, NH2
Low turnover
NH2, F, OMe > H
(<10%) (<5%)
Parent octyl galactoside
~50 % turnover
No turnover
H, F, OMe, NH2
Octyl
(b)
Turnover
parent OH ~60%
amine ~40%
acid ~60%
amide ~20%
amidine ~20%
Turnover
Turnover
Minimal turnover
No turnover
Minimal Turnover
Turnover
NHAc
Octyl

Figure 3. Acceptor analogues and their potential to serve as trans-sialidase substrates: (a) systematically modified octyl galactosides, (b) series of amines, acids, amides and amidines derived from octyl LacNAc O-cyanomethyl ethers.

Downloaded by CORNELL UNIV on June 3, 2012 | http://pubs.acs.org
Publication Date (Web): December 13, 2011 | doi: 10.1021/bk-2011-1091.ch009

Synthetic Mucin Glycopeptides

The results presented above account for why a tri-galactose-based mucin glycan can only provide two sites for *trans*-sialidase action, but perhaps one needs to consider both glycan and peptide to account for the apparent preference for only single sialylation. With this in mind, we embarked on the synthesis of mucin glycopeptides fragments, capitalizing on the building blocks developed above and standard solid-phase/Fmoc protection chemistry (Scheme 4) (*26*).

In contrast to the α-linked LacNAc-peptide, the overall yield for the synthesis of the isomeric β-linked material was much higher (80% compared to 22%), largely as a result of low yields in peptide coupling subsequent to introduction of the α-linked glycoaminoacid unit. The change of anomeric stereochemistry appears to have a profound impact on the accessibility of the *N*-terminus of the glycopeptide chain, suggesting that the α-linked sugar is in close proximity to the peptide whereas the sugar in the β-isomer is not. This point is also reflected in the enzymatic sialylation of the α-linked glycopeptide with *trans*-sialidase, which was achievable (*25*), but sluggish. Again, this is consistent with the α-linked LacNAc structure lying down against the peptide chain and limiting its accessibility.

If the α-linkage in mucin glycopeptides results in the glycan lying close to the peptide surface, can we mimic this effect with a glyconanotechnology approach?

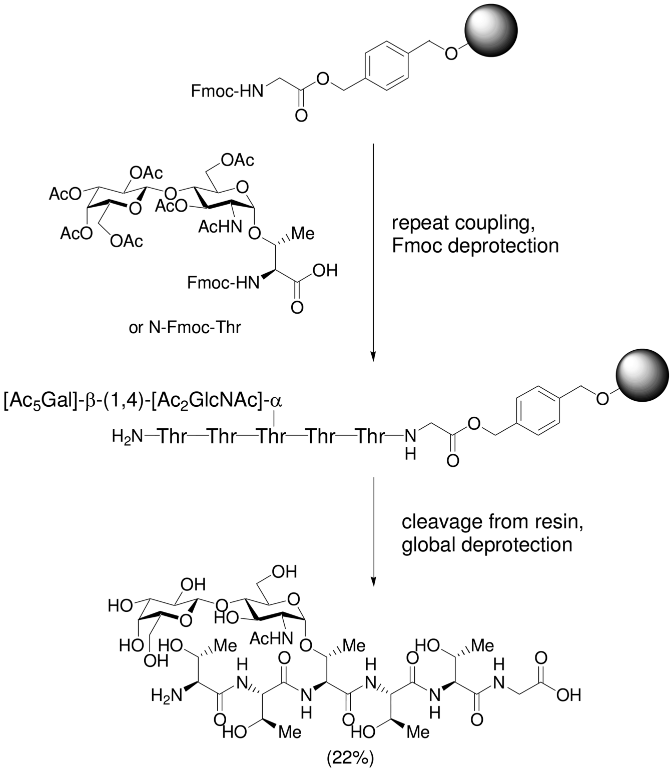
Fmoc-HN
O
O
O
OAc
OAc
AcO
AcO
O
O
AcO
O
AcO
OAc
AcHN
O
Me
Fmoc-HN
OH
O
or N-Fmoc-Thr
repeat coupling,
Fmoc deprotection
[Ac$_5$Gal]-β-(1,4)-[Ac$_2$GlcNAc]-α
H$_2$N—Thr—Thr—Thr—Thr—Thr—N
H
O
O
cleavage from resin,
global deprotection
OH
OH
HO
O
O
HO
O
HO
HO
OH
AcHN
O
Me
Me
HO
Me
H$_2$N
N
H
N
H
N
H
N
H
N
H
OH
O
O
O
O
O
O
O
HO
Me
HO
Me
(22%)

Scheme 4. Solid-phase synthesis of mucin glycopeptides fragment

Downloaded by CORNELL UNIV on June 3, 2012 | http://pubs.acs.org
Publication Date (Web): December 13, 2011 | doi: 10.1021/bk-2011-1091.ch009

Glyconanoparticle-Based Mucin Mimetics

The immobilization of carbohydrates on surfaces, whether conventional sensors 'chips' or on nanoparticles, is finding widespread use in the glycosciences (*20–22*, *43–45*). In the course of our work, we have relied upon 15 nm diameter gold particles due to their optical properties: a 3 nM suspension generates a bright read color. Suspensions of such particles undergo an aggregation-induced colorimetric change (red to blue/black), which in the case of appropriately derivatized particles can be induced by a cognate binding partner (Figure 4).

An early example of this approach comes from the work of Mirkin (*46*), who demonstrated selective colorimetric detection of polynucleotides, based on their hybridization, due to distance-dependent optical properties of gold nanoparticles. We have adapted this approach, using thiol- or disulfide-derivatized sugars (*48*) immobilized on gold or silver nanoparticles (*49*), generating glyconanoparticles, for the detection of lectins, such as concanavalin A (*47*), for the analysis of carbohydrate-carbohydrate interactions (*50*), and for the development of sensors for cholera toxin (*51*), and *Ricinus communis* agglutinin 120 (*52*), a surrogate for ricin (see reference (*53*) for ligand optimization using the glycoarray approaches described later in this chapter).

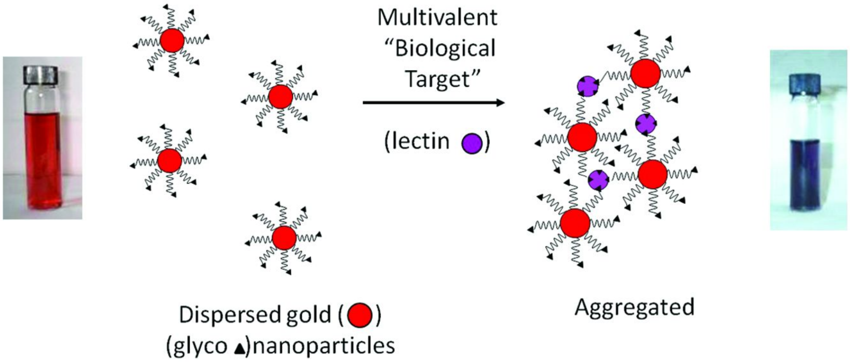

Figure 4. Analyte-induced colorimetric change of functionalized gold nanoparticles resulting from particle aggregation.

In connection with *T. cruzi* mucin work, we explored the use of glyconanoparticles to ask questions about the significance of the branched nature of the mucin glycans (Collet and Field, unpublished observations). Specifically, linear disaccharide and branched trisaccharide mimetics (Figure 5) of mucin glycans were synthesized, on this occasion α-mannoside linkages were used for synthetic convenience in place of α-GlcNAc. The glycans, coupled to short PEG-thiols, were conjugated to gold nanoparticles and the accessibility of the terminal galactose residues was assessed. This was achieved using the β-galactoside-recognizing lectin RCA_{120}, with the mannose-specific lectin concanavalin A as a negative control. Unexpectedly, nanoparticles presenting the α-linked disaccharide did not respond to either lectin, whilst those presenting the trisaccharide responded strongly and selectively to RCA_{120} only. In keeping with observations on glycopeptide sialylation referred to above, these data suggest that the 1,4-linked arm of the trisaccharide lies parallel to the gold surface and it is inaccessible to the RCA_{120} lectin, while the 1,6-linked arm is presented up and away from the surface and is lectin-accessible (Figure 5).

One might therefore infer from these data that the branched nature of the mucin glycans satisfies more than one function: the 1,4-linked arm contributes to protection of the mucin protein from host responses and also spaces out the 1,6-arms for optimal presentation of sites for *trans*-sialidase action and/or adhesion to host cells. But which type(s) of cells does *T. cruzi* bind to?

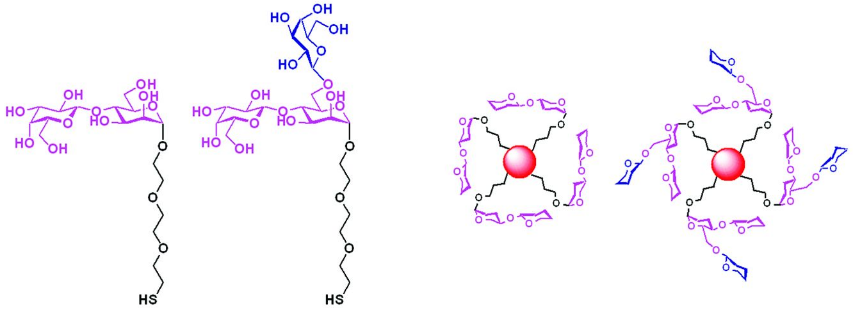

Figure 5. (a) T. cruzi mucin glycan mimetics used to generate glyconanoparticles, and (b) model representation of glyconanoparticles to explain the differences in lectin responsiveness of linear di- and branched tri-saccharides.

Host Lectins and Sialic Acid Recognition

When *T. cruzi* is transmitted to man, it invades the bloodstream and lymphatic system. It lodges in muscle and heart tissue, the digestive system and phagocytic cells. This marked tissue/cell tropism may be associated with specific recognition of these tissues/cells by the parasite mucin glycans. It has previously been reported that binding of *T. cruzi* bloodstream forms to human laminin (*54*) is enhanced by galectin-3 and also that galectin-3 expression is required for *T. cruzi* adhesion to human cells, contributing to parasite internalization (*55*). The sialylation of non-reducing terminal galactose residues of *T. cruzi* mucins may contribute to evasion of the immune response, and could mask galectin-3 binding sites. Mucin sialylation may therefore bring into play the repertoire of human siglecs (*56*, *57*). With a range of mucin glycans and many human siglecs to investigate, we engaged in the development of carbohydrate microarray (glycoarray) methods for the medium through-put analysis of carbohydrate-lectin interactions (*53*, *58*, *59*).

Surface plasmon resonance imaging (SPRi) provides a convenient method for the real-time, label-free analysis of protein interactions with carbohydrate microarrays. In a typical experiment with a 40-membered glycan library, Table 1 of which 22 compounds have non-reducing terminal sialic acid, human siglec 7 and its ortholog murine siglec E display pronounced differences in their glycan binding potential (Figure 6).

Downloaded by CORNELL UNIV on June 3, 2012 | http://pubs.acs.org
Publication Date (Web): December 13, 2011 | doi: 10.1021/bk-2011-1091.ch009

Table 1. Glycan library used in SPR imaging studies with siglecs

CFG No	*Name*	*Common name*
B80	Lacβ-SpNH-LC-LC-Bt	Lac
B81	LacNAcβ-SpNH-LC-LC-Bt	LN
B82	Galβ1-3GlcNAcβ-SpNH-LC-LC-Bt	LeC
B83	Neu5Acα2-3Galβ1-4Glcβ-SpNH-LC-LC-Bt	3′SLac
B84	Neu5Acα2-3Galβ1-4GlcNAcβ-SpNH-LC-LC-Bt	3′SLN
B85	Neu5Acα2-3Galβ1-3GlcNAcβ-SpNH-LC-LC-Bt	3′SLeC
B86	Neu5Acα2-6Galβ1-4Glcβ-SpNH-LC-LC-Bt	6′SLac
B87	Neu5Acα2-6Galβ1-4GlcNAcβ-SpNH-LC-LC-Bt	6′SLN
B89	Neu5Gcα2-3Galβ1-4Glcβ-SpNH-LC-LC-Bt	3′S(Gc)Lac
B90	Neu5Gcα2-3Galβ1-4GlcNAcβ-SpNH-LC-LC-Bt	3′S(Gc)LN
B93	Neu5Gcα2-6Galβ1-4GlcNAcβ-SpNH-LC-LC-Bt	6′S(Gc)LN
B107	Neu5Acα2-8Neu5Acα2-3Galβ1-4Glcβ-SpNH-LC-LC-Bt	GD3
B108	Neu5Acα2-8Neu5Acα2-8Neu5Acα2-3Galβ1-4Glcβ-SpNH-LC-LC-Bt	GT3
B111	(Galβ1-4GlcNAcβ)2-SpNH-LC-LC-Bt	Di-LN
B114	GlcNAcβ1-3Galβ1-4Glcβ-SpNH-LC-LC-Bt	LNT2
B115	Galβ1-4GlcNAcβ1-3Galβ1-4Glcβ-SpNH-LC-LC-Bt	LNnT
B121	GlcNAcβ-SpNH-LC-LC-Bt	GN
B156	Galβ1-3[Fucα1-4]GlcNAcβ-SpNH-LC-LC-Bt	LeA
B157	Neu5Acα2-3Galβ1-4[Fucα1-3]GlcNAcβ-SpNH-LC-LC-Bt	SLeX
B174	Neu5Acα2-3Galβ1-3[Fucα1-3]GlcNAcβ-SpNH-LC-LC-Bt	SLeA
B177	Neu5Acα2-3[GalNAcβ1-4]Galβ1-4Glcβ-SpNH-LC-LC-Bt	GM2
B178	Neu5Acα2-3[Galβ1-4GlcNAcβ]2-SpNH-LC-LC-Bt	3′-SLN-LN
B179	Neu5Acα2-6[Galβ1-4GlcNAcβ]2-SpNH-LC-LC-Bt	6′-SLN-LN
B180	GalNAcβ1-4GlcNAcβ-SpNH-LC-LC-Bt	LDN
B181	GlcNAcβ1-3Galβ1-4GlcNAcβ-SpNH-LC-LC-Bt	GN-LN
B184	Neu5Acα2-8Neu5Acα2-3[GalNAcβ1-4]Galβ1-4Glcβ-SpNH-LC-LC-Bt	GD2
B185	(6OSO3)Galβ1-4Glcβ-SpNH-LC-LC-Bt	6′SuLac
B186	Galβ1-4(6OSO3)Glcβ-SpNH-LC-LC-Bt	6SuLac
B187	[3OSO3]Galβ1-4(6OSO3)Glcβ-SpNH-LC-LC-Bt	6, 3′-di-SuLac

Continued on next page.

Downloaded by CORNELL UNIV on June 3, 2012 | http://pubs.acs.org
Publication Date (Web): December 13, 2011 | doi: 10.1021/bk-2011-1091.ch009

Table 1. (Continued). Glycan library used in SPR imaging studies with siglecs

CFG No	*Name*	*Common name*
B194	Neu5Acα2-3[Galβ1-4GlcNAcβ1-3]3-SpNH-LC-LC-Bt	3′SLN-LN-LN
B197	[3OSO3]Galβ1-4Glcβ-SpNH-LC-LC-Bt	3′SuLac
B202	Neu5Acα2-3[Galβ1-3GlcNAcβ1-4]Galβ1-4Glcβ-SpNH-LC-LC-Bt	GM1
B204	Neu5Acα2-3[Galβ1-3GalNAcβ1-4]Galβ1-4GlcNAcβ-SpNH-LC-LC-Bt	GM2(NAc)
B266	Galβ1-4[Fucα1-3]GlcNAcβ-SpNH-LC-LC-Bt	LeX
B273	Neu5Acα2-3LacDiNAcβ-SpNH-LC-LC-Bt	3′SLDN
B274	Neu5Acα2-6LacDiNAcβ-SpNH-LC-LC-Bt	6′SLDN
B277	Galβ1-3GlcNAcβ1-3Galβ1-4GlcNAcβ-SpNH-LC-LC-Bt	LeC-LN
B298	Neu5Acα2-3[Neu5Acα2-3Galβ1-3GalNAcβ1-4]Galβ1-4Glcβ-SpNH-LC-LC-Bt	GD4
B299	GlcNAcβ1-3Galβ1-3GlcNAcβ-SpNH-LC-LC-Bt	GN-LeC
B301	Galβ1-4GlcNAcβ1-3Galβ1-3GlcNAcβ-SpNH-LC-LC-Bt	LN-LeC

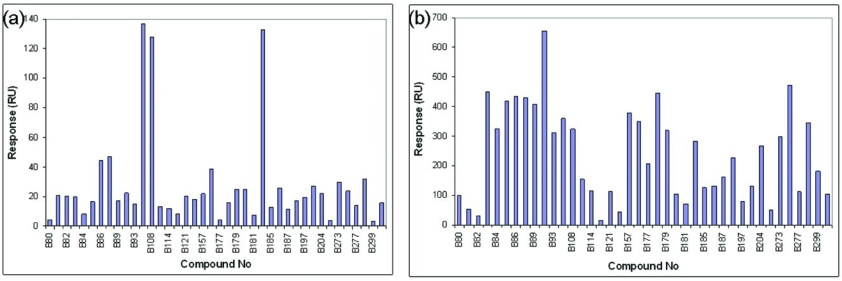

Figure 6. SPR imaging binding responses of (a) human siglec 7 and (b) murine siglec E (for full experimental details see ref. (59)).

While the human protein shows a high specificity for α-2,8-linked sialic acid (only 3 of the 40 compounds), the mouse protein shows a clear preference for terminal sialic acid (22 of the 40 compounds) and it shows no preference for the residue to which sialic acid is attached (Figure 6) (see reference (*53*) for ligand optimization approaches using SPR imaging and glycoarray).

Downloaded by CORNELL UNIV on June 3, 2012 | http://pubs.acs.org
Publication Date (Web): December 13, 2011 | doi: 10.1021/bk-2011-1091.ch009

Downloaded by CORNELL UNIV on June 3, 2012 | http://pubs.acs.org
Publication Date (Web): December 13, 2011 | doi: 10.1021/bk-2011-1091.ch009

Glyconanoparticles To Explore Cell-Based Expression of Lectins

In the context of method development, the poorly selective murine Siglec E presents opportunities. While experiments with soluble recombinant proteins provide useful information about ligand specificity, ultimately the siglecs are cell surface proteins. A convenient way to assess siglec ligand specificity when presented on cell surfaces would be useful; similarly, a convenient set of tools to assess the potential of siglecs in human tissue isolates for their ability to recognise parasite mucin glycans would be invaluable. Sialic acid tethered to gold nanoparticles satisfies these goals. Such materials (Figure 7) change color in the presence of soluble murine siglec E (but not in the presence of human siglec 7, as expected), providing quality control of the batch of glyconanoparticles (Field, Russell and co-workers, unpublished). These particles can also be used, in conjunction with electron microscopy, to image transformed Chinese Hamster Ovary (CHO) cells presenting heterologously expressed murine siglec E on their surface (*60*). That is, transformed cell lines incubated with sialic acid-presenting glyconanoparticles give rise to EM-detectable glyconanoparticle-CHO cell complexes when a cognate sialic acid-binding lectin, such as murine siglec E, is expressed on the cell surface but not when human siglec 7 is presented in the same manner. Ongoing studies to extend these experiments aim to identify parasite glycan-host lectin pairs that may be of direct relevance to the infection process.

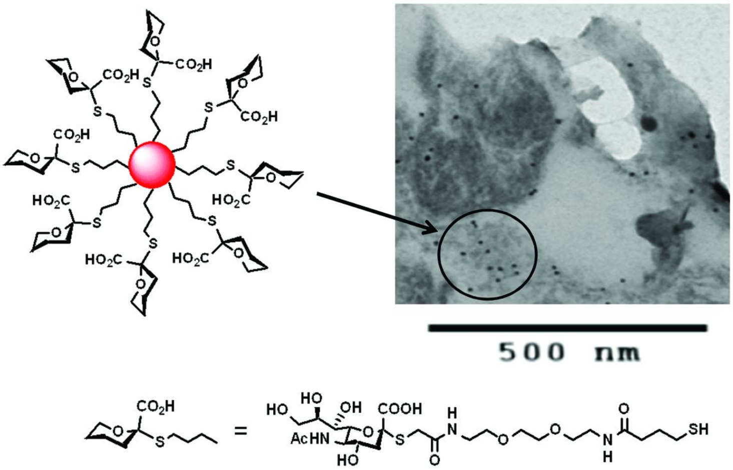

Figure 7. Glyconanoparticles prepared from a sialic acid-derived thiol and their use in imaging cell surface expression of murine siglec E on Chinese Hamster Ovary cells by electron microscopy.

Downloaded by CORNELL UNIV on June 3, 2012 | http://pubs.acs.org
Publication Date (Web): December 13, 2011 | doi: 10.1021/bk-2011-1091.ch009

Conclusion

Coupled with high through-put expression systems for screening proteins for glycan and protein interactions (*60*), and the potential to look directly at lectins in tissue samples, glyconanoparticle approaches of the type described above offer new ways to investigate the molecular basis of parasite-host interactions. In addition, SPR imaging presents novel opportunities to identify natural sugar ligands for lectins and to optimize non-natural ligands with therapeutic potential (*53*).

In summary, chemical and enzymatic synthesis deployed in conjunction with glycoarrays and nanoparticles technologies provides new opportunities to dissect the molecular basis of infection by the protozoan *Trypanosoma cruzi*. Such studies will provide information that may contribute to the identification of new drug targets for the prevention or treatment of Chagas' disease.

Acknowledgments

These studies were supported by Research Councils UK Basic Technology Grant GR/S79268/02 (http://www.glycoarrays.org.uk/) and by the UK Engineering and Physical Sciences Research Council Grant EP/G037604/1. Biotinylated carbohydrate derivatives used in this study were kindly provided by the Carbohydrate Synthesis Core of the Consortium for Functional Glycomics (http://www.functionalglycomics.org/fg/), which is funded by US National Institute of General Medical Sciences grant GM62116. We gratefully acknowledge the support and camaraderie of the UK Glycoarrays Consortium.

References

1. Coura, J. R.; Borges-Pereira, J. *Acta Trop.* **2010**, *115*, 5–13.
2. Chagas Disease. World Health Organization. http://www.who.int/topics/chagas_disease/en/.
3. Sanchez-Sancho, F.; Campillo, N. E.; Paez, J. A. *Curr. Med. Chem.* **2010**, *17*, 423–452.
4. Buckner, F. S.; Navabi, N. *Curr. Opin. Infect. Dis.* **2010**, *23*, 609–616.
5. Castillo, E.; Dea-Ayuela, M. A.; Bolas-Fernandez, F.; Rangel, M.; Gonzalez-Rosende, M. E. *Curr. Med. Chem.* **2010**, *17*, 4027–4051.
6. Epting, C. L.; Coates, B. M.; Engman, D. M. *Exp. Parasitol.* **2010**, *126*, 283–291.
7. Villalta, F; Madison, M. N.; Kleshchenko, Y. Y.; Nde, P. N.; Lima, M. F. *Front. Biosci.* **2008**, *13*, 3714–3734.
8. Mendonca-Previato, L.; Todeschini, A. R.; Heise, N.; Agrellos, O. A.; Dias, W. B.; Previato, J. O. *Curr. Org. Chem.* **2008**, *12*, 926–939.
9. de Lederkremer, R. M.; Agusti, R. *Adv. Carbohydr. Chem. Biochem.* **2009**, *62*, 311–366.
10. Buscaglia, C. A.; Campo, V. A.; Frasch, A. C. C.; Di Noia, J. M. *Nature Rev. Microbiol.* **2006**, *4*, 229–236.

Downloaded by CORNELL UNIV on June 3, 2012 | http://pubs.acs.org
Publication Date (Web): December 13, 2011 | doi: 10.1021/bk-2011-1091.ch009

11. Acosta-Serrano, A.; Almeida, I. C.; Freitas, L. H.; Yoshida, N.; Schenkman, S. *Mol. Biochem. Parasitol.* **2001**, *114*, 143–150.
12. Agrellos, O. A.; Jones, C.; Todeschini, A. R.; Previato, J. O.; Previato, L. M. *Mol. Biochem. Parasitol.* **2003**, *126*, 93–96.
13. Salto, M. L.; Gallo-Rodriguez, C.; Lima, C.; de Lederkremer, R. M. *Anal. Biochem.* **2000**, *279*, 79–84.
14. Pollevick, G. D.; Di Noia, J. M.; Salto, M. L.; Lima, C.; Leguizamon, M. S.; de Lederkremer, R. M.; Frasch, A. C. C. *J. Biol. Chem.* **2000**, *275*, 27671–27680.
15. Todeschini, A. R.; da Silveira, E. X.; Jones, C.; Wait, R.; Previato, J. O.; Mendonca-Previato, L. *Glycobiology* **2001**, *11*, 47–55.
16. Schenkman, S.; Jiang, M.-S.; Hart, G. W.; Nussenzweig, V. *Cell* **1991**, *65*, 1117–1125.
17. Cross, G. A. M.; Takle, G. B. *Annu. Rev. Microbiol.* **1993**, *47*, 385–411.
18. Amaya, M. F.; Watts, A. G.; Damager, I.; Wehenkel, A.; Nguyen, T.; Buschiazzo, A.; Paris, G.; Frasch, A. C. C.; Withers, S. G.; Alzari, P. M. *Structure* 2004, *12*, 775-784 and citations therein.
19. Neres, J.; Bryce, R. A.; Douglas, K. T. *Drug Discovery Today* **2008**, *13*, 110–117.
20. Turnbull, J. E.; Field, R. A. *Nature Chem. Biol.* **2007**, *3*, 74–77.
21. Fais, M.; Karamanska, R.; Russell, D. A.; Field, R. A. *J. Cereal Sci.* **2009**, *50*, 306–311.
22. Kiessling, L. L.; Splain, R. A. *Annu. Rev. Biochem.* **2010**, *79*, 619–653.
23. Previato, J. P.; Jones, C.; Xavier, M. T.; Wait, R.; Travassos, L. R.; Parodi, A. J.; Mendonca-Previato, L. *J. Biol. Chem.* **1995**, *270*, 7241–7250.
24. van Well, R. M.; Kartha, K. P. R.; Field, R. A. *J. Carbohydr. Chem.* **2005**, *24*, 463–474.
25. Carvalho, I.; Scheuerl, S. L.; Kartha, K. P. R.; Field, R. A. *Carbohydr. Res.* **2003**, *338*, 1039–1043.
26. Campo, V. L.; Carvalho, I.; Allman, S.; Davis, B. G.; Field, R. A. *Org. Biomol. Chem.* **2007**, *5*, 2645–2657.
27. van Well, R. M.; Collet, B. Y. M.; Field, R. A. *Synlett* **2008**, *2175*, 2177.
28. Schenkman, S.; Chaves, L. B.; de Carvalho, L. C. P.; Eichinger, D. *J. Biol. Chem.* **1994**, *269*, 7960–7975.
29. Probert, M. A.; Milton, M. J.; Harris, R.; Schenkman, S.; Brown, J. M.; Homans, S. W.; Field, R. A. *Tetrahedron Lett.* **1997**, *38*, 5861–5864.
30. Milton, M. J.; Harris, R.; Probert, M. A.; Field, R. A.; Homans, S. W. *Glycobiology* **1998**, *8*, 147–153.
31. Harris, R.; Kiddle, G. R.; Field, R. A.; Milton, M. J.; Ernst, B.; Magnani, J. L.; Homans, S. W. *J. Am. Chem. Soc.* **1999**, *121*, 2546–2551.
32. Harrison, J. A.; Kartha, K. P. R.; Fournier, E. J. L.; Lowary, T. L.; Malet, C.; Nilsson, U. J.; Hindsgaul, O.; Schenkman, S.; Naismith, J. H; Field, R. A. *Org. Biomol. Chem.* **2011**, *9*, 1653–1660.
33. Lowary, T. L.; Hindsgaul, O. *Carbohydr. Res.* **1994**, *251*, 33–67.
34. Malet, C.; Hindsgaul, O. *J. Org. Chem.* **1996**, *61*, 4649–4654.
35. Malet, C.; Hindsgaul, O. *Carbohydr. Res.* **1997**, *303*, 51–65.

36. Nilsson, U. J.; Fournier, E. J. L.; Hindsgaul, O. *Bioorg. Med. Chem.* **1998**, *6*, 1563–1575.

37. Nilsson, U. J.; Fournier, E. J. L.; Fryz, E. J.; Hindsgaul, O. *Comb. Chem. High Throughput Screening* **1999**, *2*, 335–352.

38. Reviewed in Meldal, M.; Tornoe, C. W. *Chem. Rev.* **2008**, *108*, 2952−3015.

39. For examples of the use of CuAAC click chemistry with carbohydrates see: (a) Aragao-Leoneti, V.; Campo, V. L.; Gomes, A. S.; Field, R. A.; Carvalho, I. *Tetrahedron* **2010**, *66*, 9475−9492. (b) Dedola, S.; Nepogodiev, S. A.; Field, R. A. *Org. Biomol. Chem.* **2007**, *5*, 1006−1017.

40. Carvalho, I.; Andrade, P.; Campo, V. L.; Guedes, P. M. M.; Sesti-Costa, R.; Silva, J. S.; Schenkman, S.; Dedola, S.; Hill, L.; Rejzek, M.; Nepogodiev, S. A.; Field, R. A. *Bioorg. Med. Chem.* **2010**, *18*, 2412–2427.

41. Campo, V. L.; Carvalho, I.; Da Silva, C. H. T. P.; Schenkman, S.; Hill, L.; Nepogodiev, S. A.; Field, R. A. *Chem. Sci.* **2010**, *1*, 507–524.

42. Galante, E.; Geraci, C.; Campo, V. L.; Sesti-Costa, R.; Guedes, P. M. M.; Silva, J. S.; Hill, L.; Nepogodiev, S. A.; Field, R. A. *Tetrahedron* **2011**, *67*, 2901–2912.

43. Larsen, K.; Thygesen, M. B.; Guillaumie, F.; Willats, W. G. T.; Jensen, K. J. *Carbohydr. Res.* **2006**, *341*, 1209–1234.

44. Garcia, I.; Marradi, M.; Penades, S. *Nanomedicine* **2010**, *5*, 777–792.

45. El-Boubbou, K.; Huang, X. *Curr. Med. Chem.* **2011**, *18*, 2060–2078.

46. Elghanian, R.; Storhoff, J. J.; Mucic, R. C.; Letsinger, R. L.; Mirkin, C. A. *Science* **1997**, *277*, 1078–1081.

47. Hone, D. C.; Haines, A. H.; Russell, D. A. *Langmuir* **2003**, *19*, 7141–7144.

48. Karamanska, R.; Mukhopadhyay, B.; Russell, D. A.; Field, R. A. *Chem. Commun.* **2005**, 3334–3336.

49. Schofield, C. L.; Haines, A. H.; Field, R. A.; Russell, D. A. *Langmuir* **2006**, *22*, 6707–6711.

50. Reynolds, A. J.; Haines, A. H.; Russell, D. A. *Langmuir* **2006**, *22*, 1156–1163.

51. Schofield, C. L.; Field, R. A.; Russell, D. A. *Anal. Chem.* **2007**, *79*, 1356–1361.

52. Schofield, C. L.; Mukhopadhyay, B.; Hardy, S. M.; McDonnell, M. B.; Field, R. A.; Russell, D. A. *Analyst* **2008**, *133*, 626–634.

53. Fais, M.; Karamanska, R.; Allman, S.; Fairhurst, S. A.; Innocenti, P.; Fairbanks, A. J.; Donohoe, T. J.; Davis, B. G.; Russell, D. A.; Field, R. A. *Chem. Sci.* **2011**, *2*, 1952–1959.

54. Moody, T. N.; Ochieng, J.; Villalta, F. *FEBS Lett.* **2000**, *470*, 305–308.

55. Kleshchenko, Y. Y.; Moody, T. N.; Furtak, V. A.; Ochieng, J.; Lima, M. F.; Villalta, F. *Infect. Immun.* **2004**, *72*, 6717–6721.

56. Crocker, P. R. *Curr. Opin. Pharmacol.* **2005**, *5*, 431–437.

57. Crocker, P. R.; Paulson, J. C.; Varki, A. *Nature Rev. Immunol.* **2007**, *7*, 255–266.

58. Zhi, Z. L.; Laurent, N.; Powell, A. K.; Karamanska, R.; Fais, M.; Voglmeir, J.; Wright, A.; Blackburn, J. M.; Crocker, P. R.; Russell, D. A.; Flitsch, S.; Field, R. A.; Turnbull, J. E. *ChemBioChem* **2008**, *9*, 1568–1575.

Downloaded by CORNELL UNIV on June 3, 2012 | http://pubs.acs.org
Publication Date (Web): December 13, 2011 | doi: 10.1021/bk-2011-1091.ch009

59. Karamanska, R.; Clarke, J.; Blixt, O.; MacRae, J. I.; Zhang, J. Q.; Crocker, P. R.; Laurent, N.; Wright, A.; Flitsch, S. L.; Russell, D. A.; Field, R. A. *Glycoconj. J.* **2008**, *25*, 69–74.
60. Otto, D. M. E.; Campanero-Rhodes, M. A.; Karamanska, R.; Powell, A. K.; Bovin, N.; Turnbull, J. E.; Field, R. A.; Blackburn, J.; Feizi, T.; Crocker, P. R. *Anal. Biochem.* **2011**, *411*, 261–270.

Downloaded by CORNELL UNIV on June 3, 2012 | http://pubs.acs.org
Publication Date (Web): December 13, 2011 | doi: 10.1021/bk-2011-1091.ch009

Chapter 10

Glyco-Nanoparticles as Platforms for Antitumor Therapeutic Strategies

Joseph J. Barchi, Jr.*

Chemical Biology Laboratory, Molecular Discovery Program,
Center for Cancer Research, National Cancer Institute at Frederick,
Frederick, Maryland 21702
***barchi@helix.nih.gov**

There has been an explosion of progress in the development of novel nanotechnology-based platforms for a variety of applications. One reason for this development is that the properties of nanomaterials (optical, scattering, physical) can be dramatically different than those of macro-based technologies. Many of these unique properties can be exploited to develop novel imaging agents and delivery systems. A host of biologically relevant molecules can be conjugated to nanoparticles to functionalize these platforms. Cellular glycans are one family of biomolecules that have been coated on different nanoparticle platforms and some of these tools are being successfully employed for specific biomedical applications. To date however, the application of these so-called glyconanoparticles for antitumor therapeutics has been sparse. Fortunately, some initial results with glyconanoparticles have been very encouraging for possible translation to clinically relevant anti-tumor therapies. This chapter will examine the most recent work reported on the synthesis, development and application of the most promising platforms.

Not subject to U.S. Copyright. Published 2011 by American Chemical Society
In Petite and Sweet: Glyco-Nanotechnology as a Bridge to New Medicines; Huang, X., et al.;
ACS Symposium Series; American Chemical Society: Washington, DC, 2011.

Introduction

Eradication of primary tumors through the standard regimen of surgery/chemotherapy/radiation does not always affect long-time survival rates. Better initial evaluation of cell-surface markers associated with certain cancers, more selective therapies, better follow-up analysis post-surgery/therapy and better detection and destruction of residual circulating tumor cells would dramatically improve prognostic outcomes and survival. Research directed toward meeting these stringent demands focuses on several goals, not limited to: 1) better identification and imaging of specific tumor markers to stratify patients into groups where specific therapies may be beneficial, 2) increasing the efficacy of new therapeutic strategies (increasing potency and selectivity while reducing toxicity) and, 3) improved utilization of the immune system to eliminate tumors at various stages through the development of novel antitumor vaccines and immuonotherapies. Highly successful advances in many areas such as biomarker discovery (*1*), novel imaging agents (*2*) and the approval of the first anticancer vaccine by the FDA (*3*) last year has contributed to the progress in these and other areas of anticancer research. The "traditional" approach of lead discovery followed by optimization with medicinal chemistry is being reshaped by the expansive knowledge databases that have been amassed to guide focused library design and "druggable" target identification with improved translational predictions and outcomes.

With all these advances, there remains a shortage of new approved tumor therapies, be they small molecules, biologicals or immunotherapies. Reasons for this may be related to more stringent requirements for approval, but the majority of drugs fail due to lack of efficacy and the closing phases of clinical trials. Besides the need for preclinical models that are better predictors of efficacy in human subjects, there is a distinct call for the design of "smarter" and more selective therapies where toxicity can be kept at a minimum to widen therapeutic indices. In very recent years, the use of nanotechnology particles and platforms has been providing new ways of designing novel therapies. A variety of constructions on the order of 1-100 nm can be prepared from either organic or inorganic materials, and in this size regime properties can be very different than those on the macro scale. Nanoparticles (NP) commonly possess surfaces that can be chemically modified to conjugate various biologically relevant molecules and impart many layers of functionality to the particle by tailoring the surface with appropriate drugs and/or probes. The advantages and improvements that nanotechnology can bring to the design process have been outlined in a variety of reviews (*4*, *5*) but will be paraphrased briefly here: 1) NP may alter the solubility of various families of molecules and hence "deliver" otherwise insoluble agents; 2) most NP have "built in" multivalency by presenting multiple copies of species on their surface thereby enhancing macromolecular binding events; 3) The pharmacokinetic/pharmacodynamic properties of molecules are altered with respect to the free molecule; and 4) Presenting drug-like molecules on NP often reduces the systemic toxicity of a specific agent with concomitant enhancement of potency and/or efficacy. About 10 years ago, the National Cancer Institute put in motion an initiative called the NCI Alliance for Nanotechnology

In Petite and Sweet: Glyco-Nanotechnology as a Bridge to New Medicines; Huang, X., et al.;
ACS Symposium Series; American Chemical Society: Washington, DC, 2011.

in Cancer (http://nano.cancer.gov) to study novel nanotechnology platforms and fund excellence in nanoscience. Part of this program is to accurately characterize NPs that are slated to translate into a clinical setting. The Nanotechnology Characterization Laboratory (NCL) housed at the NCI in Frederick, Maryland, has amassed over the past several years a database of "biocompatibility" data for various nanoplatforms (*6*). Figure 1 outlines the trends observed in the course of their work showing the importance of various NP features for eventual translation to the clinic.

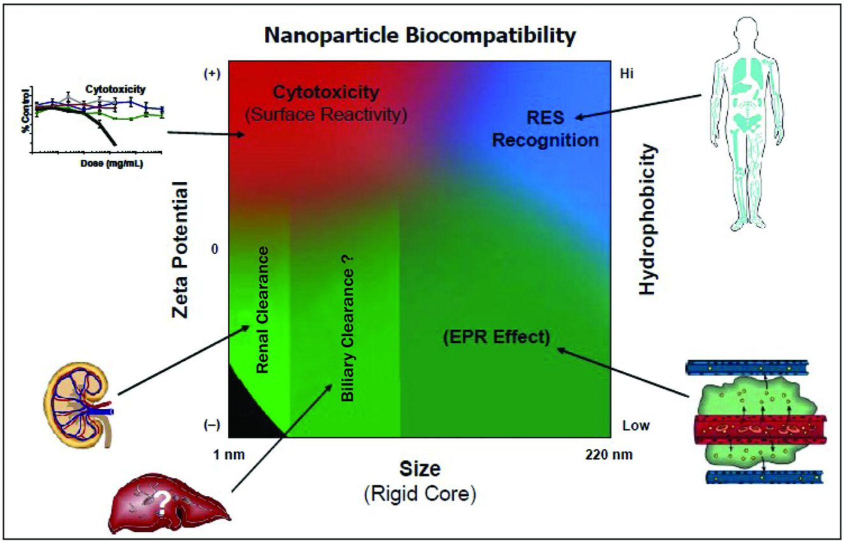

Figure 1. Trends in nanoparticle biocompatibility based on data obtained at the Nanotechnology Characterization Laboratory at the National Cancer Institute. The chart relates physical characteristics (size, zeta potential and hydrophobicity) with compatibility parameters (cytotoxicity, RES, uptake and clearance). Reprinted with permission from McNeil, WIRES Nanomedicine and Nanobiotechnology, 2009.

Specific macromolecular interactions are integral to the division, growth and proper functioning of all cells. These events are mediated primarily by proteins and nucleic acids; binding between these molecular families is critical for proper gene expression and protein function. However, binding with carbohydrates structures, in all their various guises, is also critically important in a host of cellular processes ranging from tissue formation to immune cell function and tumor metastasis (*7*). This review will concentrate on the combining of NP platforms with biologically relevant carbohydrate structures for the purpose of discovering new therapeutic agents, in particular those that can inhibit tumor growth/progression or enhance immune responses to cancer antigens. Since there have been several recent reviews on the synthesis and applications of glyconanoparticles (*8–13*), this treatise will be highly focused on cancer and cover research conducted in the last decade, with references to earlier work where appropriate.

Nanotechnology and Cancer Cell Biology

When designing any novel antitumor agents, there are many considerations that one needs to be aware of due to the complex cellular architecture and biology of solid tumors. Moving from free drug agents in solution to association with specific nano-platforms may offer distinct advantages when treating cancer (Table 1). Cancers develop their own set of blood vessels that supply nutrients to keep themselves flourishing; however, the vessel network is “leaky” and fenestrated allowing specific size particles to penetrate, the so-called Enhanced Permeability and Retention (EPR) effect. Add poor lymphatic drainage in tumor masses and you have a scenario where drug loaded NPs may sneak into tumor tissue but have a difficult time exiting, an ideal situation for multifunctional nanoparticle design. In addition, tumors harbor some unique abilities to resist or evade chemotherapy. Overexpression of drug degrading/metabolizing enzymes, the production of efflux pumps and therapy-inhibiting mutations in drug targets are but a few ways that tumors develop resistance. Tumors can also enhance local immunosuppressive mechanisms that allow cancers to evade immune-surveillance. Fortunately, using nanotechnology helps to overcome many of these resistive mechanisms through a variety of physical and bio-physical properties. Two excellent recent reviews have been published regarding the role of nanotechnology in overcoming chemotherapy resistance (*14*, *15*). Basically, encapsulation into liposomal preparations or conjugation to self-assembled surfaces drives the uptake of agents into tumor cells via mechanisms other than those seen with small molecule (e.g., passive or facilitated diffusion), thus allowing these constructs to bypass interactions with efflux pumps and enter the cell through endocytotic mechanisms. Interestingly, the inherent properties of tumor biology offer many opportunities for modified intervention through nanotechnology.

Sugars, Tumors, and Nanotechnology

It is now firmly established that one of the many hallmarks of tumorigenesis and progression is the aberrant expression of glycan chains (both N- and O-linked) on cell surface proteins (*16–18*). Modified tumor N-linked glycans can be directly linked to metastatic potential (aggressiveness) (*19*). Aberrant O-linked glycans on tumor mucins are considered tumor-associated carbohydrate antigens (TACAs) and are targets of the host immune system (*20*); a variety of tumor vaccines have been designed and developed based on their cell presentation and properties. Some TACAs also bind to specific lectins involved in cell adhesion and with pro-metastatic function (*21*), and hence are viable targets for antitumor/antimetastatic intervention. These properties have prompted many researchers to target these unusual glycans and their biosynthetic machinery in the development of cancer therapeutics.

Table 1. Features of cancer cells that can be exploited for nano-therapeutic intervention

Tumor Feature	*Nanoparticle Design*	*Advantages Over Free Drug*
Leaky Vasculature, Poor Lymphatic Drainage	Control size, surface chemistry to optimum for tumor entry	Longer Circulation Times; Tailored size allows enhanced passage through tumor vasculature
Overexpressed Cell Surface Markers	Coat with high affinity targeting agent, antibody	Less need for complex conjugation chemistry, drug can be encapsulated and non-covalently "attached" to the nanoparticle
Low Extracellular pH	pH-dependent agent coated on particle surface for endosomal release	Multifunctional nature of the particle, non covalent drug-pH-sensitive linker
Glutathione Concentration Gradient	Thiol-linked particles that take advantage of place-exchange kinetics	Novel mechanism for drug release from stable, non-immunogenic platforms
(Multi)Drug Resistance	Several designs, primarily encapsulated drugs	Activate endocytotic pathways and avoid MDR efflux pumps; higher concentration of drug available at tumor cell

Leading the charge in recent years has been the design and synthesis of different glycans on a host of nano-platforms. Sugars have been coated on several different flavors of NPs, including various polymers, dendrimers, gold, silver and ferric oxide NPs, quantum dots, and carbon nanotubes. All of these platforms offer both advantages and drawbacks and the choice obviously varies with the specific application. Most all of these platforms have some use in defining carbohydrate binding and interactions with other molecular families (primarily proteins (*22–24*), and other carbohydrates (*25–27*)). Many of these studies have provided tremendous insight into multivalency (*23*), a concept by which multiple copies of a glycan may interact with clusters of protein receptors to enhance avidity (molecular "Velcro®"). These types of carbohydrate-macromolecular interactions can be critical for propagation of signals from the surface of cells (*28*), for re-polarizing the cell surface through the aforementioned clustering (*29*) or for inhibition of multivalent protein-carbohydrate interactions that mediate cell adhesion (*30*). All of these functions can be extremely useful in the design of agents for tumor imaging and/or therapy.

In the following sections, a survey of the many glyconanotechnology designs will be given with relation to the following areas of antitumor research: imaging and radio-sensitization, drug delivery and immunology/vaccine design.

Imaging and Radio-Sensitization

Specific NPs have inherent optical properties that allow functionalization with various molecular families while maintaining nascent fluorescent or luminescent behavior. For example gold nanoparticles (AuNPs) have both high light scattering and light absorbing properties. The plasmon absorption band, which arises from the movement of free conductive electrons in the presence of an electromagnetic field, is in the visible spectrum at ~520 nm for spherical AuNPs; this wavelength is tunable by both the size and shape of the particle (*31*). The absorptive and scattering properties also make AuNPs excellent X-ray contrast agents, where they have the unique property of attenuating X-rays (*32–38*). Hence, AuNPs are extremely useful as computed tomography (CT) contrast agents, and they have been shown to rival commercial iodine-based agents in CT values (*39*). Some work has postulated that AuNPs may be able to replace iodine as a CT contrast agent since AuNPs can be targeted to specific tissue based on facile surface functionalization (*37*). More importantly, AuNPs have the unique property of sensitizing specific tissue to radiotherapy (*40*). Gold is a high-Z atom where Auger electron dissociation upon irradiation produces reactive oxygen species causing DNA damage (*34*) (see Figure 2). The unique properties of AuNPs (size-dependent cellular uptake, ease of preparation and surface targeting chemistry and, for the most part, low toxicity (*41*, *42*)) allow tailoring of the radiosensitizer to accumulate in targeted tissue (tumors) and thus selectively kill those cells. This has been a goal of radiobiologists for decades: selectively increase tumor cell killing at lower incident energies while reducing damage to healthy cells. AuNPs may be an ideal platform to achieve these goals.

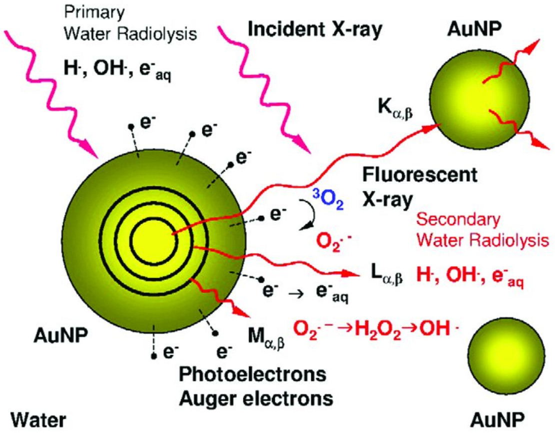
Primary
Water Radiolysis
H·, OH·, e^-_{aq}
Incident X-ray
AuNP
$K_{\alpha,\beta}$
e^-
Fluorescent
X-ray
$^3O_2$
$O_2^{\cdot -}$
Secondary
Water Radiolysis
$L_{\alpha,\beta}$
H·, OH·, e^-_{aq}
$e^- \rightarrow e^-_{aq}$
AuNP
$M_{\alpha,\beta}$
$O_2^{\cdot -} \rightarrow H_2O_2 \rightarrow OH\cdot$
Photoelectrons
Auger electrons
Water
AuNP

Figure 2. Interactions of incident X-rays with AuNPs. Reprinted with permission from Misawa and Takahashi, Nanomedicine: Nanotechnology, Biology, and Medicine, 2011.

An example of a sugar-coated AuNP for radiosensitization comes from the Xing lab. Hainfeld had shown in 1995 that AuNPs can enhance radiotherapy of tumor cells and that targeting with tumor specific antibodies would greatly improve selectivity for cancer cells (*43*). More recently, work based on the uptake of glucose in many tissues for cellular energy metabolism (as exploited by the use of ^{18}F deoxyglucose for positron emission tomography, PET) employed thioglucose-coated AuNPs for enhanced uptake into MCF-7 breast tumors to enhance radiation killing of those cells (*44*). Similar results were obtained by the same group with the ovarian cancer line SK-OV-3 where enhanced inhibition of cell proliferation was observed with production of reactive oxygen species (*45*). The use of AuNPs for radiotherapy, possibly tagged with specific sugars designed to bind to tumor-associated lectins may prove clinically useful in the future.

Despite many desirable properties, imaging cancer cells or solid tumors with gold glyconanoparticles has not been widely utilized. This may be due to the fact that targeting groups used on the particles are typically not carbohydrate in nature (antibodies, growth factors, folate). The Penades group synthesized a AuNPs-based MRI contrast agent where a gadolinium chelate (tetraazacyclododecane triacetic acid) was added to a hybrid AuNPs bearing various sugar entities (*46*). The sugar molecules served to adjust the relaxivity of the Gd(III) contrast agent. Interestingly, relaxivity enhancement was dependent on the stereochemistry of the sugar (Gal > Glc) and the distance of the sugar relative to the metal contrast agent (adjusted by varying the carbon chain length in the AuNPS thiol-linkers). The best AuNPs outperformed a clinically used contrast agent. Another very interesting example to highlight is the work of Lee, et al., who coated AuNPs with low-molecular weight hyaluronic acid (HA) capped with a near infrared dye. It has long been known that 3D-self-assembled monolayers of gold can quench nearby fluorescence via nonradiative energy transfer from the dye to the metal (*47*). The study be Lee showed that diseases such as rheumatoid arthritis and cancer, where there is an overabundance of reactive oxygen species and hyaluronidase, respectively, could be detected at high sensitivity by cleavage of the gold-coated HA fragments and reactivation of the quenched fluorophore, both *in vitro* and *in vivo*. Thus, the majority of the work on imaging with glyco-AuNPs is via “indirect” pathways of released fluorescence or conjugation with imaging contrast agents.

The two other families of NP’s used more extensively in tumor imaging are magnetic nanoparticles (MNP) and quantum dots (QDs). Several reviews in this series have excellent summaries of the use of glyco-QDs and magnetic glyconanoparticles, respectively, in imaging and therapy. An exhaustive survey of imaging with QDs has also very recently appeared (*48*). QDs are highly powerful imaging agents due to their intriguing photo-physical properties. QD fluorescence emission wavelengths can be tuned by the size of the particle, and their core-shell nature prevents them from photobleaching unlike organic dyes. Add to this the versatile surface chemistry that can be amended to specific applications and you have an extremely useful imaging platform. An array of cell imaging experiments have been reported for QDs, however, relatively few with regard to glycan-coated QDs (see Review by Weingart and Sun, this series).

Magnetic glyconanoparticles are gaining steady momentum with the work of the Penades, Davis and Huang groups as robust nanoconjugates for cell imaging and MRI contrast agents that can target cells that bind specific glycans. The Penades group, being one of the first to prepare and apply gold glyconanoparticles, later branched into other platforms including MNP, and even synthesizing AuNP-MNP hybrids for attachment of sugars on an outer gold shell of an iron oxide nanoparticle (*49*). This group's latest foray into this field is the production of carbohydrate decorated glyco-ferrites, where a gold shell surrounds an iron oxide core. The carbohydrate is now present for "biocompatibility", in contrast to their original work that used the sugar for specific bio-recognition (*27*, *50*, *51*). The carbohydrates impart water solubility, they reduce non-specific protein binding much like polyethylene glycol and they tune the relaxivity properties of the particles (*52*) (*vide supra)*. The work demonstrated that these particles can selectively immunolabel and stain cells derived from lymphoma and cervical carcinoma lines. The versatility of the platform allows for future functionalization with other molecules for highly sensitive cell labeling and detection.

The beautiful work of Huang (*53*) showed that preparation and evaluation of a series of glyco-MNP allows the differentiation of various tumor cell lines based on their carbohydrate binding properties, as shown by an array of techniques that comprehensively defined their system. T_2 weighted MRI images were quantitated with their series of different carbohydrate coated MNP, allowing a statistical analysis of the various properties of nine separate tumor cell lines. The particles can also behave as anti-adhesive agents that may prevent metastasis, similar to some of the results obtained for glyco-AuNPs (*50*). The usefulness of these glyco-NPs for a variety of applications is clear and many other sugars can be conjugated and evaluated in a similar fashion.

Drug Delivery and Therapy

Drug delivery applications of nano-systems, in particular those based on liposomes, nanoemulsions and similar organic constructions have been a hallmark of pharmaceutical research for many years (*54*). There are several lipid "nanoparticle"-based formulations that have been FDA approved (for a comprehensive treatise on these agents, see Puri, et al (*55*)), two notable examples being Abraxane, an albumin formulation of paclitaxel (http://www.abraxane.com/), and Doxil, a formulation of doxorubicin in a specialized STEALTH liposomes (http://www.doxil.com/). Aurimune, an AuNP coated with the antitumor cytokine TNF-α and PEG in specific proportions, is in phase 2 clinical trials for treatment of several types of cancers (see http://www.cytimmune.com). From the above discussion, it seems clear that there is also an enormous potential for various types of inorganic and hybrid NPs to be used for drug delivery. Since virtually any molecular subtype including therapeutic antibodies or drug molecules can be conjugated in some form to AuNPs and other metallic platforms, hundreds of studies have been published where these particles can inhibit tumor cell growth, or can be delivered to tumors for therapeutic applications. However, as was described above for imaging, very few examples of the synthesis and evaluation of antitumor glyconanoparticles have been described.

The Penades group first described a therapeutic effect from lactose-coated GNP's in vivo where B16-F10 melanoma metastasis to the lungs was potently inhibited by these particles (*50*). In the same year, our group observed a similar effect with Thomsen-Friedenreich (TF) coated GNP's in separate animal model of breast cancer (4T1) (*56*) Since both particles contained disaccharides terminated in galactose, a reasonable conclusion would be that inhibition of engagement of galactose-binding lectins (possibly galectins) with tumor cell surface carbohydrates was partially responsible for the antimetastatic effect. This was further capitulated in the work by Huang and co-workers with their results regarding carbohydrate coated MNP's (*53*). Interestingly, we were not able to reproduce our original findings after several other *in vivo* experiments with different batches of TF-coated GNP's. There also have not been any reports by the Penades group following up on their original results. The lapse in additional data on *in vivo* efficacy of this model suggests that working *in vivo* with tumor models can be difficult and the proper design of the particle is critical to consistent success for translational progress.

Several drug delivery and therapeutic studies have been performed with NPs derived from chitosan or cyclodextrin (Figure 3). These platforms are comprised of carbohydrates and can be "indirectly" considered glyconanparticles; however, the sugar is technically not the targeting or therapeutic agent. Chitosan is a 1,4-glucosamine polymer with both free and acetylated 2′-amino groups. It is produced from deacetylation of chitin, present in the shells of many crustaceans.

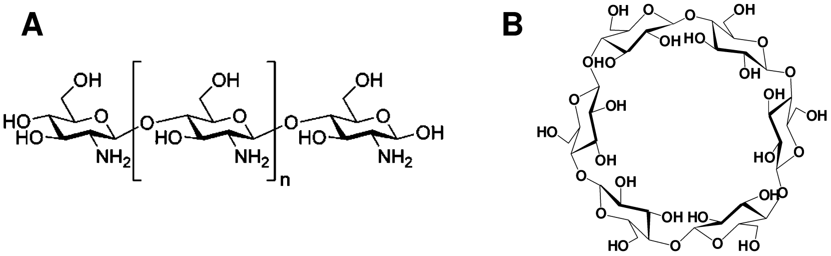

Figure 3. General structures of A) chitosan and B) cyclodextrin.

The physical properties of chitosan can be modulated by different degrees of deacetylation (DD). The free amino groups in chitosan are positively charged at acidic pH where the polymer is soluble. It is insoluble at neutral and basic pH, and hence its unique properties as a pH-dependent drug delivery system. The chitosan matrix is non-toxic, non-immunogenic and biodegradable, making it an ideal system for drug incorporation and delivery. Chitosan nano- and microparticles have a rich history as drug delivery systems (*57–61*) including several instances for tumor-selective delivery and therapy (*62*). Now several modified chitosans, such as glycol chitosan, are commercially available as water soluble, biocompatible and degradable polymers of choice for drug delivery of hydrophobic antitumor drugs such as paclitaxel (*63–68*) and doxorubicin (*69–74*).

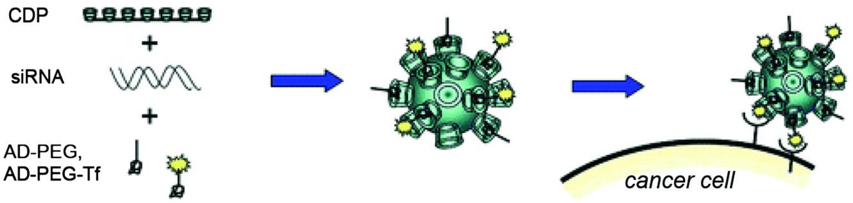

Figure 4. Schematic diagram of CALA-01 (adapted from ref. (75)). A β-cyclodextrin linear polymer (CDP) when mixed with siRNA (or other oligonulceotides) forms self-assembled NPs due to the ionic interaction between the anionic RNA and cationic character of the linkers (which contain amidine and histidine moieties) connecting the cyclodextrin units. Adamantane units are connected to 5000 MW PEG chains as a form of "steric stabilization" (AD-PEG); the AD groups serve as high affinity guests for the cyclodextrin hosts. A similar design strategy adds an adamantine conjugate of human transferrin (AD-PEG-Tf) to assemble with CD units and engage transferring receptors that are overexpressed on tumor cells. Reprinted with permission from ref (75).

Cyclodextrins (CD) are cyclic oligosaccharides of repeating1,4 linked glucose units. Their ability to form inclusion complexes with hydrophobic molecules makes them extremely useful agents for a variety of applications, from solubilization and delivery of water-insoluble drugs to environmental uses such as the capture of hydrophobic toxins within their core. An example of an ingenious application in therapeutic design is the cyclodextrin-based delivery system of CALAA-01 (Calando Pharmaceuticals-01), a unique nanoparticle assembly that has been developed for the delivery of siRNA to cells developed by the Davis group at California Institute of Technology (*75*). This formulation is made up of several components that self assemble into a truly multifunctional nanostructure (Figure 4). The "foundation" of this nanosystem is a cationic CD polymer that assembles the core of the particle and encapsulates nucleic acids thereby protecting them from degradation. Two other components, an adamantane-polyethylene glycol (AD-PEG) conjugate and a similar entity with an included targeting molecule, transferrin, (AD-PEG-Tf) complete the system. Since adamantane is encapsulated efficiently by CD, these components are displayed on the surface of the assembly and serve as both "steric stabilization" units to increase blood circulation time, and for targeting to overexpressed receptors on tumors (Tf-receptors). The complete nanoparticle is assembled from two vials at the patient's bedside, one with siRNA and the other containing the other components of the system (CDP, AD-PEG and AD-PEG-Tf, see Figure 4 for descriptions) that are admixed prior to injection to form the self-assembled particles. Homing to tumors and endocytosis causes a pH-dependent cascade that ruptures the endosome and releases the siRNA into the cytosol. Various nucleic acids (pDNA, DNAzymes, siRNA) can be delivered and the efficiency was based on fine tuning all the components of the assembly, such as CD length, nature of the cationic linker, length of the PEG chain and loading number of Tf units on the particle surface. The components of the system are biodegradable and hence very low toxicity is observed. Constructs with siRNA to silence various tumor genes (such as ribonucleotide reductase subunit 2, as is what is targeted in the formulation of CALAA-01) as well as agents that incorporate antitumor drugs like camptothecin, are in various phases of clinical trials.

Immunotherapy and Vaccines

NPs are also uniquely poised to act as platforms or delivery vehicles for various antitumor immunotherapies or vaccine components. The use of nanoparticulates and organic NPs has a very recent but already rich history in both vaccine (*76–83*) and adjuvant design (*84*, *85*). The use of solid, inorganic, magnetic or metallic NPs as carriers for antigens or adjuvants is less mature, but still not without evidence of potential usefulness in specific settings (*86–89*). As was stated for other anticancer modalities, the use of glyconanoparticles for manipulating the immune system is still in its infancy. However, the various nanoparticle platforms available may aid in the proper presentation, cellular uptake and increased circulation time of nano-antigens for higher magnitude and specificity of responses.

There are unique challenges in developing vaccines against cancer. Choosing the correct antigen is one challenge, as there can be a high degree of heterogeneity between various tumor types. The expression of what may be considered a "tumor-associated antigen" may also not be consistent among tumors of the same type as well as within a specific patient population. Probably the greatest obstacle to surmount is the simple fact that cell-surface tumor-associated antigens are part of "self", i.e., molecules (proteins, carbohydrates, and combinations) that are naturally occurring often in normal tissue along with the tumor, and thus our immune systems have developed a tolerance toward immune-surveillance of these entities. Often, it is simply the overexpression (proteins) or unique aberrant expression (carbohydrates) of these antigens that make them appear "non-self". Although our systems may produce a response against these antigens, the response is usually weak and non-neutralizing. Breaking tolerance is a major hurdle to surmount when attempting to design an effective antitumor vaccine. The situation is exacerbated for carbohydrate antigens (TACAs) since these are T-cell independent: "Aberrant" carbohydrates are not processed or presented by major histocompatibility type II pathways, necessitating addition of T-cell epitopes or molecules that will activate CD4+ T-cells and the adaptive immune response (A subversion of this paradigm has recently been discovered where certain zwitterionic bacterial polysaccharides are presented by MHC molecules in a T-cell dependent fashion (*90–93*)). Thus, the majority of vaccines directed toward TACAs have the antigen conjugated to highly immunogenic carrier proteins such as keyhole limpet hemocyanin (KLH) (*94*, *95*) or tetanus toxoid (TT) (*96*).

Although there are now increasing examples of synthesizing and presenting various antigens on NPs, virtually no reports deal with TACA conjugates. AuNPs have been used for antigen conjugation of several different peptides and protein antigens (*60*, *79*, *86*, *88*, *97*), as have other NP platforms (*81*, *82*, *98–120*).

Regarding glyconanoparticles for vaccine design against bacteria, an AuNP coated with units that structurally resembled the repeating units of cell surface carbohydrates from *Neisseria meningitides* strain Men A, showed a size- and density-dependent binding to polyclonal antibodies specific for the bacterium. The goal is to use the particles for immune-stimulation or protection against *N. meningitides*. Work from Deshong's group has shown that catanionic surfactant vesicles could be prepared and carbohydrates embedded in the surface of the NPs for drug delivery (*121*). Plans are to use these particles as vaccines against bacteria such as *N. meningitides*.

Glyconanoparticle reports for antitumor vaccine development are sparse. The Boons group has recently led the way in the preparation of fully synthetic multicomponent vaccine conjugates bearing a the TACA Tn covalently attached to a MUC1 peptide sequence as the antigen, along with a T-helper cell epitope and a TLR2 agonist and found that immunization could elicit a high titer of IgG antibodies that can recognize cancer cells expressing the tumor-associated carbohydrate (*122*). Although not a nanoparticle, the synthetic vaccine is highly insoluble and needed to be incorporated into very specific liposomes for delivery to animals. This is an example of one of the advantages of nanotechnology (resolving solubility issues) in antitumor research. Penades has published on the preparation of multi-ligand gold nanoparticles coated with tumor-associated carbohydrates as a potential vaccine platform (*123*). The group incorporated varying proportions of sialyl-Tn and Lewis^{y} TACA antigens, T-cell helper peptides and glucose on defined linkers and in different densities on the particles (Figure 5). The synthesis and characterization of these particles were described, but no immunological data has yet to be presented.

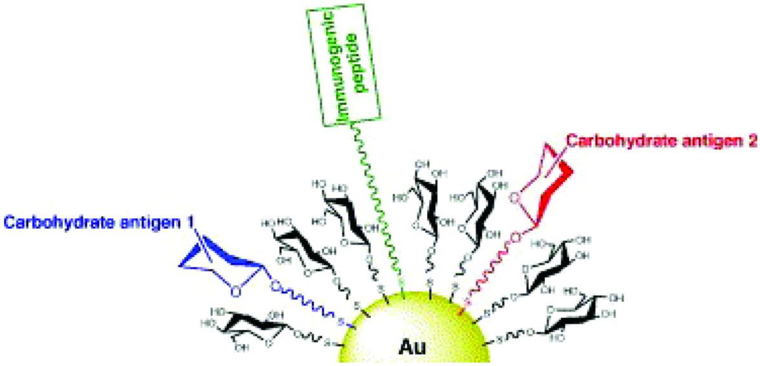

Figure 5. Schematic design of multifunctional gold nanoparticles as potential antitumor vaccines prepared by Ojeda, et al. Reprinted with permission from ref (123).

In 2004, our group set out to prepare similar type gold GNP's as antitumor vaccines. Our inspiration came from two separate reports: One was by the group of Plebanski in Melbourne who described the preparation of 50 nM carboxy styrene beads coated with MHC-1 and/or MHC-2 peptide epitopes from ovalbumin elicited CD8+ cells that could recognize tumors displaying theses antigens and inhibit growth *in vivo* (*124*). That same year, Dykman, et al., reported the remarkable immunogenic properties of colloidal gold nanoparticles when used as carriers for immunization with various antigens including proteins, peptides and small antibiotic or natural product haptens (spanning molecular weights from 700-42,000). The authors seemed as surprised as the readers at the supposed adjuvant activity of gold NPs. Our interest in tumor-associated glycopeptides antigens, i.e., mucin-derived repeating units that are conjugated at various potential glycosylation sites with TACAs, and in preparing multivalent scaffolds based on nanoparticle platforms for the presentation of these antigens, prompted us to design gold-coated TACAs for either inhibition of cell adhesion or use as potential tumor vaccines. Our strategy was to attempt, as Dykman et al. did, to elicit a response with simply attaching either TACAs or TACA-glycopeptides to gold NPs and testing for an immune response. We decided to synthesize the 16-residue repeating unit from MUC4, a tumor associated mucin that is aberrantly expressed in pancreatic adenocarcinoma's and a biomarker for pancreatic cancer (PC) (*125*). This mucin is an extremely important cell-surface protein in PC and many other cancers (*126*) but has not been as well studied as an antigen for immunological studies as the more prevalent prostate and breast cancer biomarker MUC1.

Our original synthesis of the simple TF antigen coated on gold (*56*) (Figure 6) initially proved to be a useful tool for *in vivo* treatment of 4T1 breast cancer metastasis to the lung by strongly inhibiting this process. However, reproduction was difficult as batch-to-batch reproducibility was unexpectedly difficult. Testing for immunity to TF antigen in these animals resulted in no measureable response. Progression to MUC4 glycopeptides similarly showed little to no immune response to the putative antigen. Further refinement of reducing the density of the glycopeptide GNP's by "doping" interstitial linker molecules into the self assembly process improved the monodispersity of the constructs (*127*). At that time, based on the suggestion by our colleague (Professor Rittenhouse-Olsen, University of Buffalo) it was decided to add a "molecular adjuvant" in the form of peptide from the d-subunit of complement protein 3 (C3d peptide). This 28-residue peptide was shown to act in a similar fashion as the full length protein in activating B-cells to immunoglobulin production (*128*). Thus our design consisted of 3-5 nm gold GNP's conjugated with MUC4 glycopeptides, C3d and interstitial linker in a 1:1:3 ratio (Figure 7). The linker used was a variation on the one depicted in Figure 6, containing a more complex mix of functional groups that allowed 1) ease of coupling to the glycopeptide backbone, 2) a longer hydrophobic tail for efficient packing on the surface of the particle and 3) amide linkages that could be employed for expansion of the construct and for peptide coupling on a solid support. Immunization into mice resulted in a statistically significant response to the glycopeptides with some response to the linker. Both IgG and IgM antibodies were produced. Further refinement is in progress to optimize this response as well as to test many different antigen coated particles for cytokine responses *ex vivo* to pre-screen for size and density dependent immune-stimulating properties of the particles, is currently underway.

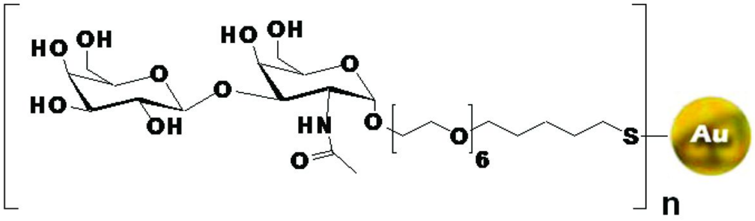

Figure 6. TF antigen gold GNP structure (56).

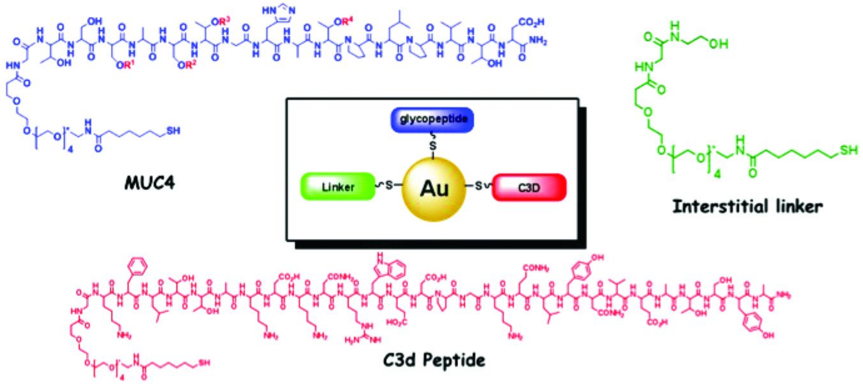

Figure 7. Schematic of gold GNP MUC4 glycopeptide vaccine particle design.

Conclusions

Research in the past decade strongly indicates that the future of glyconanoparticles in translational medicine is very bright. The progress in optimizing the synthesis, surface chemistry and biological compatibility of an array of different nano-platforms, bode well for the development of novel glyco-nanoparticles to intervene at practically every stage in the process of anticancer diagnosis, detection, therapy, prognosis and prevention. We are already well on our way to achieving success in some of these selected areas of research, and advancement to the clinic is only a matter of time as nanotoxicology and regulatory issues catch up with the rapid pace of nano-technological developments. There is good reason to predict that a follow up to this review will contain references to clinically useful glyconanoparticles for various solid and blood-borne cancers.

References

1. Issaq, H. J.; Waybright, T. J.; Veenstra, T. D. *Electrophoresis* **2011**, *32*, 967–975.
2. Morse, D. L.; Gillies, R. J. *Biochem. Pharmacol.* **2010**, *80*, 731–738.
3. Cheever, M. A.; Higano, C. S. *Clin. Cancer Res.* **2011**, *17*, 3520–3526.
4. Bawarski, W. E.; Chidlowsky, E.; Bharali, D. J.; Mousa, S. A. *Nanomed.: Nanotechnol., Biol., Med.* **2008**, *4*, 273–282.
5. McNeil, S. E. *J. Leukocyte Biol.* **2005**, *78*, 585–594.
6. McNeil, S. E. *Wiley Interdiscip. Rev.: Nanomed. Nanobiotechnol.* **2009**, *1*, 264–271.
7. Varki, A. *Glycobiology* **1993**, *3*, 97–130.
8. El-Boubbou, K.; Huang, X. F. *Curr. Med. Chem.* **2011**, *18*, 2060–2078.
9. Dong, C. M. *Comb. Chem. High Throughput Screening* **2011**, *14*, 173–181.
10. Marradi, M.; Martin-Lomas, M.; Penades, S. *Adv. Carbohydr. Chem. Biochem.* **2010**, *64*, 211–290.
11. Wang, X.; Ramstrom, O.; Yan, M. D. *Adv. Mater.* **2010**, *22*, 1946–1953.
12. De la Fuente, J. M.; Penades, S. *Biochim. Biophys. Acta, Gen. Subj.* **2006**, *1760*, 636–651.
13. Garcia, I.; Marradi, M.; Penades, S. *Nanomedicine* **2010**, *5*, 777–792.
14. HuiHui, B. U.; Yu, G.; YaPing, L. I. *Sci. China: Chem.* **2010**, *53*, 2226–2232.
15. Liang, X. J.; Chen, C.; Zhao, Y.; Wang, P. C. *Methods Mol. Biol.* **2010**, *596*, 467–88.
16. Hakomori, S. I. *Adv. Cancer Res.* **1989**, *52*, 257–331.
17. Lau, K. S.; Dennis, J. W. *Glycobiology* **2008**, *18*, 750–760.
18. Dennis, J. W.; Granovsky, M.; Warren, C. E. *Biochim. Biophys. Acta, Gen. Subj.* **1999**, *1473*, 21–34.
19. Taniguchi, N.; Gu, J. G.; Takahashi, M.; Miyoshi, E. *Proc. Jpn Acad., Ser. B* **2004**, *80*, 82–91.
20. Xu, Y. F.; Sette, A.; Sidney, J.; Gendler, S. J.; Franco, A. *Immunol. Cell Biol.* **2005**, *83*, 440–448.
21. Zhao, Q.; Barclay, M.; Hilkens, J.; Rhodes, J. M.; Yu, L. G. *Gut* **2008**, *57*, A27–A27.
22. Xiang, M. H.; Xu, X.; Liu, F.; Li, N.; Li, K. A. *J. Phys. Chem. B* **2009**, *113*, 2734–2738.
23. Pieters, R. J. *Org. Biomol. Chem.* **2009**, *7*, 2013–2025.
24. Reynolds, M.; Perez, S. *C. R. Chim.* **2011**, *14*, 74–95.
25. Fuss, M.; Luna, M.; Alcantara, D.; de la Fuente, J. M.; Enriquez-Navas, P. M.; Angulo, J.; Penades, S.; Briones, F. *J. Phys. Chem. B* **2008**, *112*, 11595–11600.
26. De Souza, A. C.; Kamerling, J. P. *Funct. Glycomics* **2006**, *417*, 221–243.
27. de la Fuente, J. M.; Penades, S. *Glycoconjugate J.* **2004**, *21*, 149–163.
28. Sacchettini, J. C.; Baum, L. G.; Brewer, C. F. *Biochemistry (Moscow)* **2001**, *40*, 3009–3015.
29. Yu, L. G.; Andrews, N.; Zhao, Q.; McKean, D.; Williams, J. F.; Connor, L. J.; Gerasimenko, O. V.; Hilkens, J.; Hirabayashi, J.; Kasai, K.; Rhodes, J. M. *J. Biol. Chem.* **2007**, *282*, 773–781.
30. Rosch, M.; Herzner, H.; Dippold, W.; Wild, M.; Vestweber, D.; Kunz, H. *Angew. Chem., Int. Ed.* **2001**, *40*, 3836–3839.

31. Toderas, F.; Baia, M.; Maniu, D.; Astilean, S. *J. Optoelectron. Adv. Mater.* **2008**, *10*, 2282–2284.
32. Guo, R.; Wang, H.; Peng, C.; Shen, M. W.; Pan, M. J.; Cao, X. Y.; Zhang, G. X.; Shi, X. Y. *J. Phys. Chem. C* **2010**, *114*, 50–56.
33. Wang, H.; Zheng, L. F.; Peng, C.; Guo, R.; Shen, M. W.; Shi, X. Y.; Zhang, G. X. *Biomaterials* **2011**, *32*, 2979–2988.
34. Guo, R.; Wang, H.; Peng, C.; Shen, M. W.; Zheng, L. F.; Zhang, G. X.; Shi, X. Y. *J. Mater. Chem.* **2011**, *21*, 5120–5127.
35. Peng, C.; Wang, H.; Guo, R.; Shen, M. W.; Cao, X. Y.; Zhu, M. F.; Zhang, G. X.; Shi, X. Y. *J. Appl. Polym. Sci.* **2011**, *119*, 1673–1682.
36. Xiao, M.; Nyagilo, J.; Arora, V.; Kulkarni, P.; Xu, D. S.; Sun, X. K.; Dave, D. P., *Nanotechnology* 2010**,** *21*, -.
37. Popovtzer, R.; Agrawal, A.; Kotov, N. A.; Popovtzer, A.; Balter, J.; Carey, T. E.; Kopelman, R. *Nano Lett.* **2008**, *8*, 4593–4596.
38. Kim, D.; Park, S.; Lee, J. H.; Jeong, Y. Y.; Jon, S. *J. Am. Chem. Soc.* **2007**, *129*, 7661–7665.
39. Kojima, C.; Umeda, Y.; Ogawa, M.; Harada, A.; Magata, Y.; Kono, K. *Nanotechnology* **2010**, *21*, 245104.
40. Chithrani, D. B.; Jelveh, S.; Jalali, F.; van Prooijen, M.; Allen, C.; Bristow, R. G.; Hill, R. P.; Jaffray, D. A. *Radiat. Res.* **2010**, *173*, 719–728.
41. Yen, H. J.; Hsu, S. H.; Tsai, C. L. *Small* **2009**, *5*, 1553–1561.
42. Shukla, R.; Bansal, V.; Chaudhary, M.; Basu, A.; Bhonde, R. R.; Sastry, M. *Langmuir* **2005**, *21*, 10644–10654.
43. Hainfeld, J. F. *Scanning Microsc.* **1995**, *9*, 239–256.
44. Kong, T.; Zeng, J.; Wang, X.; Yang, X.; Yang, J.; McQuarrie, S.; McEwan, A.; Roa, W.; Chen, J.; Xing, J. Z. *Small* **2008**, *4*, 1537–43.
45. Geng, F.; Song, K.; Xing, J. Z.; Yuan, C. Z.; Yan, S.; Yang, Q. F.; Chen, J.; Kong, B. H. *Nanotechnology* **2011**, *22*.
46. Marradi, M.; Alcantara, D.; de la Fuente, J. M.; Garcia-Martin, M. L.; Cerdan, S.; Penades, S. *Chem. Commun.* **2009**, 3922–3924.
47. Chance, R. R.; Prock, A.; Silbey, R. Molecular Fluorescence and Energy Transfer Near Interfaces. *Adv. Chem. Phys.* **2007**, *37*, 1−65.
48. Wang, Y.; Chen, L., *Nanomed. Nanotechnol. Biol. Med.* **2011**, in press.
49. de la Fuente, J. M.; Alcantara, D.; Penades, S. *IEEE Trans. NanoBiosci.* **2007**, *6*, 275–281.
50. Rojo, J.; Diaz, V.; de la Fuente, J. M.; Segura, I.; Barrientos, A. G.; Riese, H. H.; Bernade, A.; Penades, S. *ChemBioChem* **2004**, *5*, 291–297.
51. de la Fuente, J. M.; Barrientos, A. G.; Rojas, T. C.; Rojo, J.; Canada, J.; Fernandez, A.; Penades, S. *Angew. Chem., Int. Ed.* **2001**, *40*, 2258–2261.
52. Garcia, I.; Gallo, J.; Genicio, N.; Padro, D.; Penades, S. *Bioconjugate Chem.* **2011**, *22*, 264–273.
53. El-Boubbou, K.; Zhu, D. C.; Vasileiou, C.; Borhan, B.; Prosperi, D.; Li, W.; Huang, X. F. *J. Am. Chem. Soc.* **2010**, *132*, 4490–4499.
54. Fattal, E. *J. Drug Delivery Sci. Technol.* **2011**, *21*, 1–1.
55. Puri, A.; Loomis, K.; Smith, B.; Lee, J. H.; Yavlovich, A.; Heldman, E.; Blumenthal, R. *Crit. Rev. Ther. Drug Carrier Syst.* **2009**, *26*, 523–580.

56. Svarovsky, S. A.; Szekely, Z.; Barchi, J. J. *Tetrahedron: Asymmetry* **2005**, *16*, 587–598.

57. Agnihotri, S. A.; Mallikarjuna, N. N.; Aminabhavi, T. M. *J. Controlled Release* **2004**, *100*, 5–28.

58. Nam, T.; Park, S.; Lee, S. Y.; Park, K.; Choi, K.; Song, I. C.; Han, M. H.; Leary, J. J.; Yuk, S. A.; Kwon, I. C.; Kim, K.; Jeong, S. Y. *Bioconjugate Chem.* **2010**, *21*, 578–582.

59. Ahmed, M.; Deng, Z. C.; Liu, S. Y.; Lafrenie, R.; Kumar, A.; Narain, R. *Bioconjugate Chem.* **2009**, *20*, 2169–2176.

60. Zhou, X. F.; Zhang, X. H.; Yu, X. H.; Zha, X.; Fu, Q.; Liu, B.; Wan, X.; Chen, Y.; Chen, Y.; Shan, Y. M.; Jin, Y. H.; Wu, Y. G.; Liu, J. Q.; Kong, W.; Shen, J. C. *Biomaterials* **2008**, *29*, 111–117.

61. Leong, K. W. *MRS Bull.* **2005**, *30*, 640–646.

62. Dass, C. R.; Choong, P. F. M. *J. Microencapsulation* **2008**, *25*, 275–279.

63. Li, F.; Li, J. N.; Wen, X. J.; Zhou, S. H.; Tong, X. W.; Su, P. P.; Li, H.; Shi, D. L. *Mater. Sci. Eng., C* **2009**, *29*, 2392–2397.

64. Yuk, S. H.; Oh, K. S.; Cho, S. H.; Lee, B. S.; Kim, S. Y.; Kwak, B. K.; Kim, K.; Kwon, I. C. *Biomacromolecules* **2011**, *12*, 2335–2343.

65. Hong, G. Y.; Jeong, Y. I.; Lee, S. J.; Lee, E.; Oh, J. S.; Lee, H. C. *Arch. Pharm. Res.* **2011**, *34*, 407–417.

66. Liu, J.; Li, H. X.; Jiang, X. Q.; Zhang, C.; Ping, Q. N. *Carbohydr. Polym.* **2010**, *82*, 432–439.

67. Lee, J. Y.; Kim, K. S.; Kang, Y. M.; Kim, E. S.; Hwang, S. J.; Lee, H. B.; Min, B. H.; Kim, J. H.; Kim, M. S. *Int. J. Pharm.* **2010**, *392*, 51–56.

68. Saravanakumar, G.; Min, K. H.; Min, D. S.; Kim, A. Y.; Lee, C. M.; Cho, Y. W.; Lee, S. C.; Kim, K.; Jeong, S. Y.; Park, K.; Park, J. H.; Kwon, I. C. *J. Controlled Release* **2009**, *140*, 210–217.

69. Cao, Y.; Gu, Y.; Liu, L. N.; Yang, Y.; Zhao, P. G.; Su, P.; Liu, L. Y.; Qi, C.; Lei, X.; Yang, C. J. *Lett. Drug Des. Discovery* **2010**, *7*, 500–506.

70. Qi, J. N.; Yao, P.; He, F.; Yu, C. L.; Huang, C. O. *Int. J. Pharm.* **2010**, *393*, 176–184.

71. Jeong, Y. I.; Jin, S. G.; Kim, I. Y.; Pei, J.; Wen, M.; Jung, T. Y.; Moon, K. S.; Jung, S. *Colloids Surf., B* **2010**, *79*, 149–155.

72. Tan, M. L.; Friedhuber, A. M.; Dunstan, D. E.; Choong, P. F. M.; Dass, C. R. *Biomaterials* **2010**, *31*, 541–551.

73. Bisht, S.; Maitra, A. *Wiley Interdiscip. Rev.: Nanomed. Nanobiotechnol.* **2009**, *1*, 415–425.

74. Tan, M. L.; Choong, P. F. M.; Dass, C. R. *J. Pharm. Pharmacol.* **2009**, *61*, 131–142.

75. Davis, M. E. *Mol. Pharm.* **2009**, *6*, 659–668.

76. Parveen, S.; Misra, R.; Sahoo, S. K. *Nanomed.: Nanotechnol., Biol., Med.* **2011**In Press.

77. Cruz, L. J.; Rueda, F.; Cordobilla, B.; Simon, L.; Hosta, L.; Albericio, F.; Domingo, J. C. *Mol. Pharm.* **2011**, *8*, 104–116.

78. Sheng, W. Y.; Huang, L. *Pharm. Res.* **2011**, *28*, 200–214.

79. Pokharkar, V.; Bhumkar, D.; Suresh, K.; Shinde, Y.; Gairola, S.; Jadhav, S. S. *J. Biomed. Nanotechnol.* **2011**, *7*, 57–59.

80. Oyarzun-Ampuero, F. A.; Garcia-Fuentes, M.; Torres, D.; Alonso, M. J. *J. Drug Delivery Sci. Technol.* **2010**, *20*, 259–265.
81. Klippstein, R.; Pozo, D. *Nanomed.: Nanotechnol., Biol., Med.* **2010**, *6*, 523–529.
82. Xiang, S. D.; Scalzo-Inguanti, K.; Minigo, G.; Park, A.; Hardy, C. L.; Plebanski, M. *Expert Rev. Vaccines* **2008**, *7*, 1103–1119.
83. Nahar, M.; Dutta, T.; Murugesan, S.; Asthana, A.; Mishra, D.; Rajkumar, V.; Tare, M.; Saraf, S.; Jain, N. K. *Crit. Rev. Ther. Drug Carrier Syst.* **2006**, *23*, 259–318.
84. Bolhassani, A.; Safaiyan, S.; Rafati, S. *Mol. Cancer* **2011**, *10*, 3.
85. Lu, F. L.; He, F. C. *Prog. Biochem. Biophys.* **2001**, *28*, 832–835.
86. Parween, S.; Gupta, P. K.; Chauhan, V. S. *Vaccine* **2011**, *29*, 2451–2460.
87. Yue, H.; Wei, W.; Yue, Z. G.; Lv, P. P.; Wang, L. Y.; Ma, G. H.; Su, Z. G. *Eur. J. Pharm. Sci.* **2010**, *41*, 650–657.
88. Bastus, N. G.; Sanchez-Tillo, E.; Pujals, S.; Farrera, C.; Kogan, M. J.; Giralt, E.; Celada, A.; Lloberas, J.; Puntes, V. *Mol. Immunol.* **2009**, *46*, 743–748.
89. Drogoz, A.; Munier, S.; Verrier, B.; David, L.; Dornard, A.; Delair, T. *Biomacromolecules* **2008**, *9*, 583–591.
90. Kalka-Moll, W. M.; Tzianabos, A. O.; Bryant, P. W.; Niemeyer, M.; Ploegh, H. L.; Kasper, D. L. *J. Immunol.* **2002**, *169*, 6149–6153.
91. Kasper, D. L.; Cobb, B. A. *Cell. Microbiol.* **2005**, *7*, 1398–1403.
92. Cobb, B. A.; Kasper, D. L. *Glycobiology* **2008**, *18*, 707–718.
93. Avci, F. Y.; Kasper, D. L. *Annu. Rev. Immunol.* **2010**, *28*, 107–130.
94. Freire, T.; Bay, S.; Vichier-Guerre, S.; Lo-Man, R.; Leclerc, C. *Mini-Rev. Med. Chem.* **2006**, *6*, 1357–1373.
95. Livingston, P. O.; Ragupathi, G. *Hum. Vaccines* **2006**, *2*, 137–143.
96. Vichier-Guerre, S.; Lo-Man, R.; Bay, S.; Deriaud, E.; Nakada, H.; Leclerc, C.; Cantacuzene, D. *J. Pept. Res.* **2000**, *55*, 173–180.
97. Pokorski, J. K.; Steinmetz, N. F. *Mol. Pharm.* **2011**, *8*, 29–43.
98. Ma, W.; Smith, T.; Bogin, V.; Zhang, Y.; Ozkan, C.; Ozkan, M.; Hayden, M.; Schroter, S.; Carrier, E.; Messmer, D.; Kumar, V.; Minev, B. *J. Transl. Med.* **2011**, *9*, 34.
99. Crownover, E. F.; Convertine, A. J.; Stayton, P. S. *Polym. Chem.* **2011**, *2*, 1499–1504.
100. Tan, G.; Wang, Z. Y.; Zhang, X.; Cai, Z. G.; Zhang, J. K. *Oncol. Rep.* **2011**, *26*, 215–221.
101. Su, X. F.; Fricke, J.; Kavanagh, D. G.; Irvine, D. J. *Mol. Pharm.* **2011**, *8*, 774–787.
102. Ryu, M.; Nakazawa, T.; Akagi, T.; Tanaka, T.; Watanabe, R.; Yasuda, M.; Himori, N.; Maruyama, K.; Yamashita, T.; Abe, T.; Akashi, M.; Nishida, K. *J. Controlled Release* **2011**, *151*, 65–73.
103. Li, X. R.; Sloat, B. R.; Yanasarn, N.; Cui, Z. R. *Eur. J. Pharm. Biopharm.* **2011**, *78*, 107–116.
104. Hanlon, D. J.; Aldo, P. B.; Devine, L.; Alvero, A. B.; Engberg, A. K.; Edelson, R.; Mor, G. *Am. J. Reprod. Immunol.* **2011**, *65*, 597–609.
105. Perche, F.; Benvegnu, T.; Berchel, M.; Lebegue, L.; Pichon, C.; Jaffrès, P.-A.; Midoux, P. *Nanomed.: Nanotechnol., Biol., Med.* **2011**, in press.

106. Foster, S.; Duvall, C. L.; Crownover, E. F.; Hoffman, A. S.; Stayton, P. S. *Bioconjugate Chem.* **2010**, *21*, 2205–2212.
107. Dominguez, A. L.; Lustgarten, J. *Vaccine* **2010**, *28*, 1383–1390.
108. Liu, H.; Zhang, D. S.; Du, Y. Q. *J. Nanosci. Nanotechnol.* **2010**, *10*, 514–519.
109. Ge, W.; Hu, P. Z.; Huang, Y.; Wang, X. M.; Zhang, X. M.; Sun, Y. J.; Li, Z. S.; Si, S. Y.; Sui, Y. F. *Oncol. Rep.* **2009**, *22*, 915–920.
110. Ge, W.; Li, Y.; Li, Z. S.; Zhang, S. H.; Sun, Y. J.; Hu, P. Z.; Wang, X. M.; Huang, Y.; Si, S. Y.; Zhang, X. M.; Sui, Y. F. *Cancer Immunol. Immunother.* **2009**, *58*, 201–208.
111. Hamdy, S.; Molavi, O.; Ma, Z. S.; Haddadi, A.; Alshamsan, A.; Gobti, Z.; Elhasi, S.; Samuel, J.; Lavasanifar, A. *Vaccine* **2008**, *26*, 5046–5057.
112. Yoshikawa, T.; Okada, N.; Oda, A.; Matsuo, K.; Matsuo, K.; Kayamuro, H.; Ishii, Y.; Yoshinaga, T.; Akagi, T.; Akashi, M.; Nakagawa, S. *Vaccine* **2008**, *26*, 1303–1313.
113. Akagi, T.; Wang, X.; Uto, T.; Baba, M.; Akashi, M. *Biomaterials* **2007**, *28*, 3427–3436.
114. Uto, T.; Wang, X.; Sato, K.; Haraguchi, M.; Akagi, T.; Akashi, M.; Baba, M. *J. Immunol.* **2007**, *178*, 2979–2986.
115. Jiang, H. L.; Park, I. K.; Kang, M. L.; Yoo, H. S.; Choi, Y. J.; Akaike, T.; Cho, C. S. *Polym. Adv. Technol.* **2007**, *18*, 220–225.
116. Har-el, Y. E.; Kato, Y. *Curr. Nanosci.* **2007**, *3*, 329–338.
117. Solbrig, C. M.; Saucier-Sawyer, J. K.; Cody, V.; Saltzman, W. M.; Hanlon, D. J. *Mol. Pharm.* **2007**, *4*, 47–57.
118. de Jong, S.; Chikh, G.; Sekirov, L.; Raney, S.; Semple, S.; Klimuk, S.; Yuan, N.; Hope, M.; Cullis, P.; Tam, Y. *Cancer Immunol. Immunother.* **2007**, *56*, 1251–1264.
119. Hanlon, D. J.; Ackerman, A.; Shen, H.; Edelson, R.; Cresswell, P.; Saltzman, M. *J. Invest. Dermatol.* **2005**, *124*, A121–A121.
120. Standley, S. M.; Kwon, Y. J.; Murthy, N.; Kunisawa, J.; Shastri, N.; Guillaudeu, S. J.; Lau, L.; Frechet, J. M. J. *Bioconjugate Chem.* **2004**, *15*, 1281–1288.
121. Thomas, G. B.; Rader, L. H.; Park, J.; Abezgauz, L.; Danino, D.; DeShong, P.; English, D. S. *J. Am. Chem. Soc.* **2009**, *131*, 5471–5477.
122. Ingale, S.; AWolfert, M.; Gaekwad, J.; Buskas, T.; Boons, G. J. *Nat. Chem. Biol.* **2007**, *3*, 663–667.
123. Ojeda, R.; de Paz, J. L.; Barrientos, A. G.; Martin-Lomas, M.; Penades, S. *Carbohydr. Res.* **2007**, *342*, 448–459.
124. Fifis, T.; Mottram, P.; Bogdanoska, V.; Hanley, J.; Plebanski, M. *Vaccine* **2004**, *23*, 258–266.
125. Moniaux, N.; Andrianifahanana, M.; Brand, R. E.; Batra, S. K. *Br. J. Cancer* **2004**, *91*, 1633–1638.
126. Singh, A. P.; Chaturvedi, P.; Batra, S. K. *Cancer Res.* **2007**, *67*, 433–436.
127. Sundgren, A.; Barchi, J. J. *Carbohydr. Res.* **2008**, *343*, 1594–1604.
128. Toapanta, F. R.; Ross, T. M. *Immunol. Res.* **2006**, *36*, 197–210.

Downloaded by OHIO STATE UNIV LIBRARIES on June 3, 2012 | http://pubs.acs.org
Publication Date (Web): December 13, 2011 | doi: 10.1021/bk-2011-1091.ch011

Chapter 11

Biological Applications of Hyaluronic Acid Functionalized Nanomaterials

Mohammad El-Dakdouki and Xuefei Huang*

Department of Chemistry, Michigan State University,
East Lansing, Michigan 48824, U.S.A.
***Tel: (517) 355-9715, ext. 329. Fax: (517) 353-1793.**
E-mail: xuefei@chemistry.msu.edu.

The area of nanotechnology has greatly expanded over the past two decades with applications in a diverse range of fields. The physical properties and therapeutic window of many drugs can be tuned by loading them into biocompatible nanocarriers that can help them reach the desired destinations. Hyaluronic acid (HA) is a 'biologically green' multifunctional polysaccharide that has been used as/with drug delivery vehicles. In this chapter, we will summarize the recent research (2000-2011) on the biological applications of HA-nanomaterials, where HA guided nanocarriers with therapeutic and diagnostic potentials to HA-receptor expressing diseased sites. The highly anionic character of HA extended the systemic circulation time of nanocarriers, while its mucoadhesive properties and specific binding to receptors enabled extended contact with the target tissues and offered a platform for molecular imaging, drug delivery, tissue repair and regeneration.

Introduction

HA is a naturally occurring anionic glycosaminoglycan composed of a repeating disaccharide of β-1,4-D-glucuronic acid-β-1,3-D-*N*-acetylglucosamine with a molecular weight ranging from 10^5-10^7 Da (2000-25000 repeating units) (*1*). It is an essential component of the extracellular matrix and synovial fluid, and plays an important role in wound healing, cell differentiation, proliferation, and migration (*2*, *3*). HA exerts its biological functions through interactions with

In Petite and Sweet: Glyco-Nanotechnology as a Bridge to New Medicines; Huang, X., et al.;
ACS Symposium Series; American Chemical Society: Washington, DC, 2011.

a variety of HA receptors, also known as hyaladherins. These include cluster of differentiation 44 (CD44), HA receptor for endocytosis (HARE), receptor for hyaluronan-mediated motility (RHAMM), the lymphatic vessel endothelial HA receptor (LYVE-1), and the tumor necrosis factor-stimulated gene-6 protein (TSG6) (*4–6*). Of all HA receptors, the transmembrane glycoprotein CD44 is one of the most studied (*4*). CD44 exists as a standard form (CD44s) or variant isoforms (CD44v) due to alternative splicing, which can undergo further post-translational modification such as sulfation to regulate interactions with HA (*7*, *8*). In addition, the sizes of HA fragments play an important role in regulating the responses resulting from HA-CD44 interactions. CD44 requires at least a HA hexasaccharide sequence for binding, and only a decasaccharide or higher can effectively compete with polymeric HA (*9*). The binding of HA oligomers to CD44 has been shown to induce angiogenesis, while high molecular weight HA polymers are anti-angiogenic (*1*). Owing to its biocompatibility and multifaceted biological functions, HA has been exploited as a carrier or a homing moiety to deliver drugs, and for tissue engineering/repair. With the recent emergence of nanotechnology, HA has been extensively interfaced with nanosciences (*10*). In this chapter, we will review the advances in the synthesis and biological applications of diverse HA-functionalized nanomaterials. We will first discuss the methods for incorporating HA into nanoparticles (NPs), which will be followed by biological applications of the nanomaterials according to their core compositions. For the sake of completion, we include all HA related materials with sizes in the nanometer regime, i.e., below 1 μm.

Downloaded by OHIO STATE UNIV LIBRARIES on June 3, 2012 | http://pubs.acs.org
Publication Date (Web): December 13, 2011 | doi: 10.1021/bk-2011-1091.ch011

Synthesis of HA-Functionalized Nanomaterials

The method of choice for introducing HA onto nanomaterials is determined by several variables such as the core being utilized or created, the functional groups on the surface of NPs, the surface charge of NPs, the overall stability of the construct during assembly, and the desired size and applications. Both native HA and modified HA can be immobilized. The native unmodified HA can be conjugated directly to the surfaces of amine-functionalized NPs using traditional amide coupling reagents such as 1-ethyl-3-(*N*,*N*-dimethylaminopropyl)carbodiimide (EDCI) and 2,4-dichloro-6-methoxy-1,3,5-triazine (CDMT) (Figure 1a). Alternatively, HA can be attached onto NPs by direct chelation with metal NP surface (Figure 1b) or through electrostatic interactions with positively charged NPs (Figure 1c). HA-coated silver NPs were synthesized by reducing silver nitrate using HA as both the reducing agent and the passivating agent (Figure 1d). Besides native HA, HA can be functionalized first, which is then attached onto NPs. As it contains many copies of carboxylic acid groups, HA derivatization can be performed up to 35% of the disaccharide units to facilitate NP coating without significantly affecting its abilities towards receptor binding (*11*). For example, catechol moieties can be introduced onto HA, which exhibited strong chelation to iron oxide NP surfaces (Figure 1e). In addition, thiol-functionalized HA has been used to coat gold NPs as well as to form hydrogels under UV irradiation (Figure 1f, 1g). Chemical ligation of HA to a hydrophobic chain or drug resulted

Downloaded by OHIO STATE UNIV LIBRARIES on June 3, 2012 | http://pubs.acs.org
Publication Date (Web): December 13, 2011 | doi: 10.1021/bk-2011-1091.ch011

in the self-assembly of the amphiphilic conjugates in aqueous media into HA NPs with a compact hydrophobic core and hydrophilic HA outer coating (Figure 1h). These synthetic strategies are summarized in Figure 1 and will be explained in more detail when specific materials are discussed.

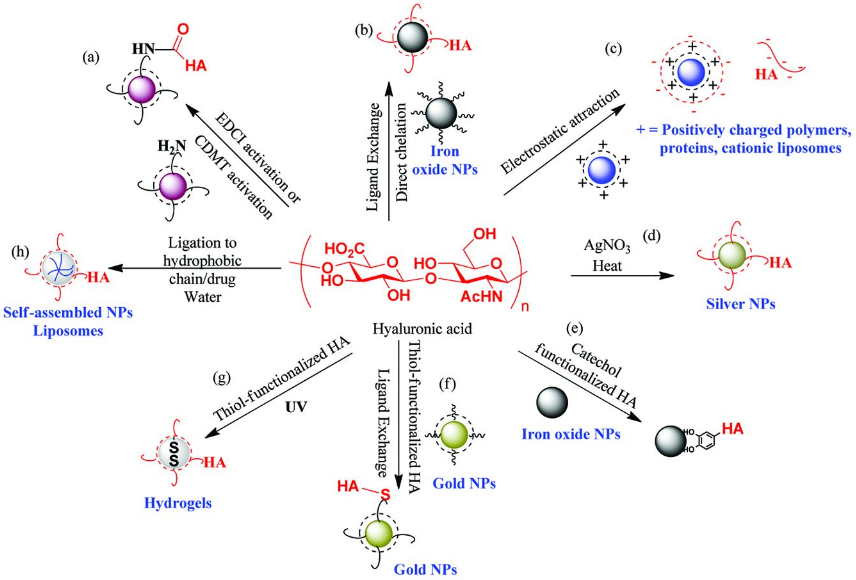
(a)
HN
O
HA
EDCI activation or
CDMT activation
H_2N
(b)
HA
Ligand Exchange
Direct chelation
Iron oxide NPs
(c)
HA
Electrostatic attraction
+ = Positively charged polymers, proteins, cationic liposomes
(h)
HA
Self-assembled NPs
Liposomes
Ligation to hydrophobic chain/drug
Water
HO_2C
O
HO
OH
AcHN
n
Hyaluronic acid
$AgNO_3$
Heat
(d)
HA
Silver NPs
(g)
Thiol-functionalized HA
UV
S
S
HA
Hydrogels
Ligand Exchange
Thiol-functionalized HA
(f)
Gold NPs
HA
S
Gold NPs
(e)
Catechol functionalized HA
Iron oxide NPs
HO
HO
HA

Figure 1. Various methods for functionalizing NPs with HA.

HA-Coated Iron Oxide NPs

Iron oxide NPs are a class of NPs with super-paramagnetic properties, which can serve as excellent contrast agents for magnetic resonance imaging (MRI) for *in vitro* and *in vivo* tracking (*12–14*). Furthermore, the large surface area of the NPs allows the co-immobilization of targeting agents with fluorophores and therapeutic drugs, enabling attractive applications in many areas such as cell labeling, pathogen separation, drug targeting, and molecular imaging (*14–17*). Another advantage of iron oxide NPs is that they are bio-compatible *in vivo* as they can be metabolized and incorporated into the body's iron pool (*18*).

It is known that one of the mechanisms for inflammatory cell recruitment to sites of pathogen infection, injury and inflammation is through the binding of CD44 and HA (*19*, *20*). To take advantage of this interaction for monitoring diseases such as atherosclerosis, we reported the preparation of iron oxide magnetite NPs coated with HA and labeled with FITC as a model drug to target CD44-expressing activated macrophages (*21*). The HA-NPs were monodispersed, colloidally stable in Fetal Bovine Serum (FBS) containing media for days with no noticeable toxicity against cells. Although many cells such as vascular endothelial cell line EA.hy926 express CD44, they do not bind HA significantly. In contrast, in the presence of inflammatory signals such as lipopolysaccharide (LPS), CD44 on human macrophage cell line THP-1 cells was transformed from the quiescent state to an activated sulfated form (*7*, *8*) displaying much enhanced affinity with HA-NP. The uptake of the HA-coated NPs by activated macrophages, through an energy-dependent CD44 receptor mediated endocytosis process, was five-fold higher than the control NPs without HA coating. This enabled the detection of activated macrophages by MRI (Figure 2), which bodes well for future detection of inflammatory diseases such as atherosclerosis.

Downloaded by OHIO STATE UNIV LIBRARIES on June 3, 2012 | http://pubs.acs.org
Publication Date (Web): December 13, 2011 | doi: 10.1021/bk-2011-1091.ch011

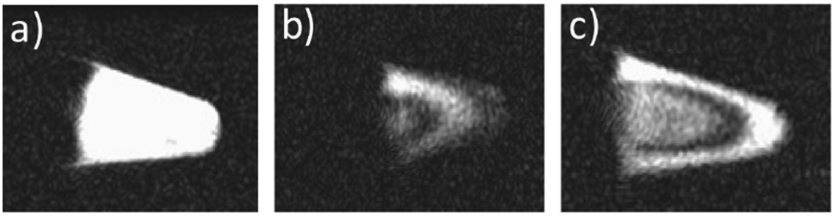

Figure 2. T2 weighted MR images of activated macrophage THP-1 cells a) before incubation with HA-NPs, b) 2 h and c) 4 h after incubation. The sign ificant T2* contrast changes upon nanoparticle incubation suggested HA-NPs can be used to monitor macrophages by MRI. (Copyright American Chemical Society. Reproduced with permission.)*

Park and coworkers developed a mussel-inspired method to immobilize HA on the surface of iron oxide NPs and evaluated its potential application as MRI T2 contrast agents for targeted cancer imaging (*22*). They derivatized HA polymer with dopamine (DN), an analog of the mussel's 3,4-dihydroxy-L-phenylalanine adhesive protein, *via* EDCI coupling (Figure 3). The catechol moiety of DN is known to form strong bonds with various inorganic surfaces. The oleic acid-coated iron oxide NPs were modified with cetyltrimethylammonium bromide (CTAB) creating a positively charged surface to facilitate the interaction with the negatively charged HA-DN conjugate and anchoring of HA through catechol chelation. This led to the instantaneous HA surface coating forming HA iron oxide NPs. These monodispersed NPs had excellent colloidal stability in aqueous media (no precipitation after 4 days). To test the role of CD44 in mediating cellular uptake, both CD44+ cell line (HCT116 human colon carcinoma cells) and CD44- (NIH-3T3 mouse fibroblast cells) were incubated with the HA-NPs. HCT116 cells showed more significant signal loss in MRI before and after NP incubation as compared to 3T3 cells (Figure 3b). The important role of CD44-HA interactions in cellular uptake was further confirmed by conducting competitive cellular uptake experiments in the presence of HA polymer in the culture media, which led to greatly suppressed uptake of the HA-NPs by HCT116 cells.

Downloaded by OHIO STATE UNIV LIBRARIES on June 3, 2012 | http://pubs.acs.org
Publication Date (Web): December 13, 2011 | doi: 10.1021/bk-2011-1091.ch011

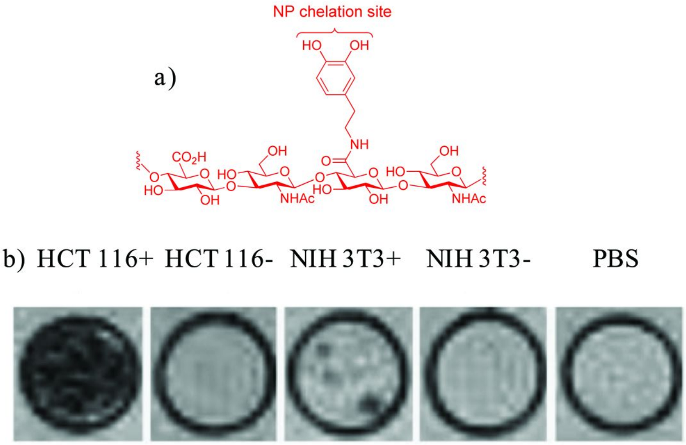

Figure 3. a) Structure of the catechol functionalized HA. b) T2 weighted MR images for HCT116 and NIH3T3 cells (HCT116+ and NIH3T3+: HA-NP treated cells; HCT116- and NIH3T3-: cells without NP treatment; PBS: buffer control). (Copyright John Wiley and Sons. Reproduced with permission.)

As discussed above, a significant advantage of NPs is that multiple agents can be co-immobilized. Kumar et al. reported a method for the preparation of HA-coated Fe_2O_3 NPs (diameters ranging from 80-160 nm) by mixing dihydrazide-crosslinked HA with a colloidal solution of iron oxide NPs (*23*). They examined drug delivery applications by encapsulating the powerful vasodilator atrial natriuretic peptide (ANP) in the HA-Fe_2O_3 NPs and monitoring its uptake by HEK293 and A549 cells. Whereas these cells lines did not uptake free ANP, HA-Fe_2O_3 NPs delivered the peptide to the nucleus of cells. This is also corroborated by our results where FITC attached to HA-magnetite NP was found to be delivered to the nucleus of THP-1 cells (Figure 4) (*21*), suggesting this may be an interesting approach for nuclear drug delivery.

Recently, we reported the development of multi-functional HA-coated iron oxide NPs for both MRI imaging of tumor cells and targeted drug delivery (*24*). Doxorubicin (DOX) was conjugated to the surface of the NPs *via* an acid sensitive hydrazone linkage that can be hydrolyzed in the acidic environments encountered inside endosomes and late lysosomes releasing DOX inside cancer cells. Competitive enzyme linked immunosorbent assays (ELISA) indicated that anchoring HA on the surface of the NPs did not alter the biological recognition with its receptor CD44. The HA-NPs were taken up by CD44 expressing cancer cells one order of magnitude higher than the control NPs without HA as demonstrated by flow cytometry and MRI. Preincubating cancer cells with anti-CD44 mAb resulted in much reduced uptake of the HA-NPs but not the control NPs validating the CD44-dependent specific uptake. After ascertaining that DOX can be selectively released from the surface of NPs under acidic conditions, we tested the cytotoxicity of DOX-HA-NPs. These particles were found to be much more potent than free DOX in cell viability assays killing not only drug sensitive SKOV-3 ovarian cancer cells but also the multidrug resistant

Downloaded by OHIO STATE UNIV LIBRARIES on June 3, 2012 | http://pubs.acs.org
Publication Date (Web): December 13, 2011 | doi: 10.1021/bk-2011-1091.ch011

NCI/ADR-RES cells. This highlighted the potential of HA-NPs in imaging and therapeutic applications towards cancer.

In addition to *in vitro* applications, HA-iron oxide NPs have been applied for *in vivo* cellular tracking. The Park group investigated the utility of amine-modified polyethylene glycol (PEG) as dispersion agents to solubilize oleic-acid coated iron-oxide NPs in aqueous media followed by chemical ligation of HA to PEG (*15*). The HA-PEG coated NPs (75 nm in size) were stable in PBS, various salt concentrations, and extreme pHs (*4–10*), and exhibited high magnetic relaxivity. The NPs were readily taken up by CD44-expressing mesenchymal stem cells, which allowed their detection in live mice by MRI following subcutaneous injection of NP loaded stem cells.

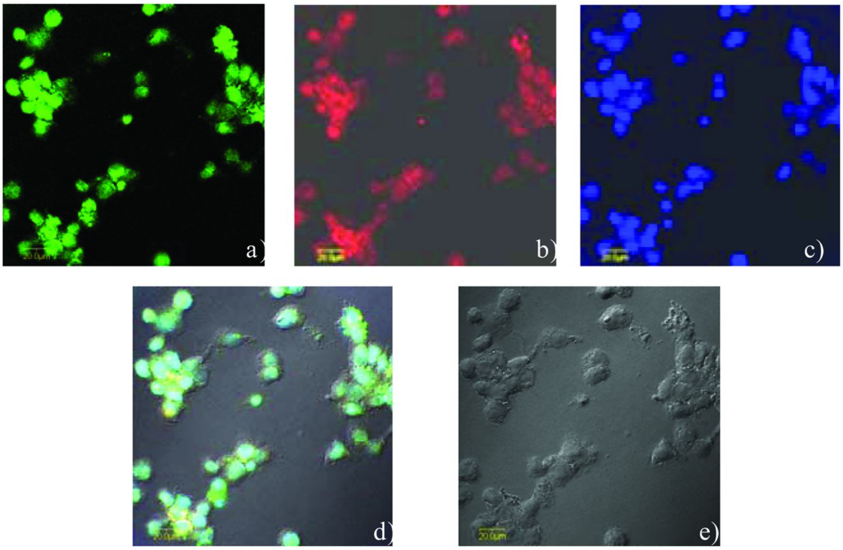

Figure 4. Confocal microscopy images of LPS activated THP-1 cells 1 hour after incubation with FITC-HA-NPs. a) Fluorescein channel; b) Lysotracker channel showing location of lysosomes; c) DAPI channel showing location of nucleus; d) overlay of a-c; e) laser image of the cells. The image overlay indicated that fluorescein was concentrated in the cell nuclei. (Copyright American Chemical Society. Reproduced with permission.) (see color insert)

HA Quantum Dots

Quantum dots (QDs) are fluorescent semiconductors with nanometer dimensions. Compared with organic dyes and fluorescent proteins, QDs have broad absorption spectra, size-tunable emission maxima, high quantum yield, and superior photostability (*25*, *26*). These unique properties render them well suited for fluorescence imaging of biological systems.

Downloaded by OHIO STATE UNIV LIBRARIES on June 3, 2012 | http://pubs.acs.org
Publication Date (Web): December 13, 2011 | doi: 10.1021/bk-2011-1091.ch011

Kim and coworkers fabricated colloidally stable HA-coated CdSe/CdS/ZnS (core/shell/shell) quantum dots as a tool for real time *in vivo* imaging of lymphatic vessels (*27*). The positively charged surface of the QDs, created through the functionalization of the QDs with amine-modified lipoic acid, was coated with the negatively charged HA polymer through electrostatic attraction resulting in HA-QDs with various sizes based on the HA/QD ratio. The HA-QDs were targeted to lymphatic endothelial cells (LEC) that over-express HA receptor LYVE-1. *In vitro* uptake studies demonstrated that HA-QDs were selectively taken up by HeLa cancer cells overexpressing LYVE-1 receptor over the LYVE-1 negative human dermal fibroblast (4-fold enhancement). Compared to the cells treated with the control unconjugated QDs, cells treated with HA-QDs showed dramatically reduced apoptosis, which was attributed to the HA layer on the surface of the QD limiting the leakage of the toxic metal ions from the core. The potential application of the HA-QD as lymphogenesis imaging agents was assessed *in vivo* by fluorescently visualizing and tracking the HA- and unconjugated QD in the lymphatic vessels (Figure 5). HA-QD was found to bind to the inner endothelial surface of the vessels with the fluorescence lasting several days. On the other hand, no signal was detected following the injection of HA-free QD. Immunohistological studies conducted on mice ear tissues injected with HA-QD confirmed the colocalization of HA-QD and LYVE-1.

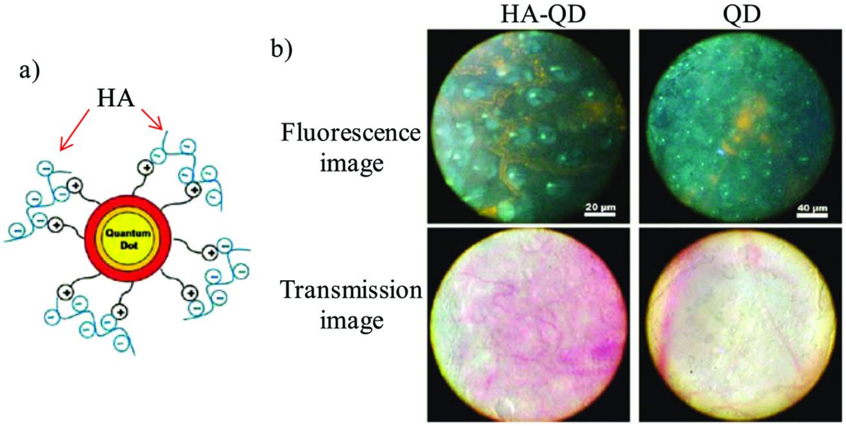

Figure 5. a) Schematic representation of the HA-QD structures; b) Upon subcutaneous injection of HA-QDs into mouse ears, fluorescence imaging clearly showed the presence of lymphatic vessels in the yellow color, while QDs were not as effective. (Copyright American Chemical Society. Reproduced with permission.) (see color insert)

Hahn and coworkers designed HA-QDs (*28*) as targeted drug delivery carriers for treatment of liver disease (*29*). In this study, hydrazide-functionalized HA was covalently conjugated to the QD surface using EDCI chemistry. Previously, the authors found that HA-QDs with degree of HA modification less than 25% accumulated mainly in the liver, whereas higher degree of modification resulted in even distribution of QD in the body. Images collected from confocal microscopy revealed that HA-QDs, not the unmodified QDs, were taken up by the normal hepatocytes (FL83B), the liver disease model cells of hepatic stellate cells (HSC-T6), and the hepatoma cells (HepG2), all of which express HA receptors on cell surfaces. Interestingly, the diseased cells (HSC-T6 and HEPG2) were much more efficient in taking up the HA-QD than the normal FL83B cells. Building on the promising *in vitro* data, the authors conducted *in vivo* real-time bioimaging of HA-QD in normal and cirrhotic model mice. Fluorescent images indicated that HA-QD was retained in the cirrhotic mice even after 8 days post injection (Figure 6). In contrast, HA-QD was cleared from the normal mice livers within 3 days. The authors hypothesized that the efficient uptake and the slow clearance/enhanced retention of the HA-QD by cirrhotic livers resembles the enhanced permeability and retention (EPR) effect observed in cancer cells (*30*) in addition to the higher concentrations of hyaluronidase around inflamed tissue (*31*) as well as the presence of HA receptors in the liver.

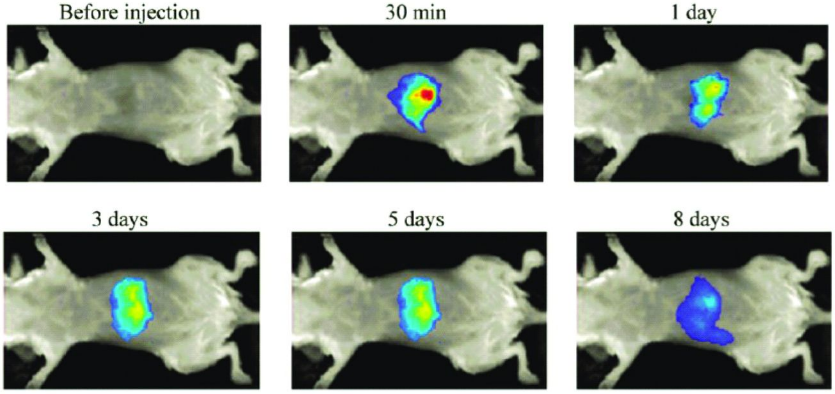

Figure 6. Fluorescent imaging of cirrhotic mice showed accumulation of HA-QDs in liver up to 8 days after tail-vein injections of the NPs. (Copyright American Chemical Society. Reproduced with permission.) (see color insert)

There has been an increasing interest in using layer-by-layer (LbL) assembly of polyelectrolytes to create functional thin films loaded with different therapeutic materials for applications such as tissue engineering and drug and gene therapy (*32*, *33*). This concept has been extended to construct LbL NPs for the controlled release of therapeutic agents *in vivo*. In theory, different drugs can be physically encapsulated in separate layers of the nanoconstruct, while being segregated by barrier layers allowing for their ordered and timed release. Recently, LbL NPs were fabricated by depositing polymers, i.e., the positively charged poly-L-lysine (PLL) or polyethyleneimine (PEI) and the negatively charged dextran sulfate (DXS) or HA, on the surface of the gold NPs and quantum dots (*34*, *35*). Hammond and coworkers were interested in establishing the basic design criteria for optimal *in vivo* pharmacokinetics such as stability, biodistribution and tissue interaction (*35*). They found that the number of layers and the terminal layer of the LbL NPs are key variables governing the stability and the biodistribution of the NPs. For example, the DXS coated-NPs accumulated largely in the liver

Downloaded by OHIO STATE UNIV LIBRARIES on June 3, 2012 | http://pubs.acs.org
Publication Date (Web): December 13, 2011 | doi: 10.1021/bk-2011-1091.ch011

Downloaded by OHIO STATE UNIV LIBRARIES on June 3, 2012 | http://pubs.acs.org
Publication Date (Web): December 13, 2011 | doi: 10.1021/bk-2011-1091.ch011

due to the high affinity of DXS to the liver sinusoidal endothelial cells receptors (LSEC). In contrast, HA coating significantly attenuated the accumulation of NPs in the liver due to the lower affinity of HA to liver cells as compared to DXS. The prolonged residence of the HA-coated LbL NPs in the bloodstream resulted in an enhanced time-dependent accumulation of the NPs in subcutaneously induced tumors (Figure 7).

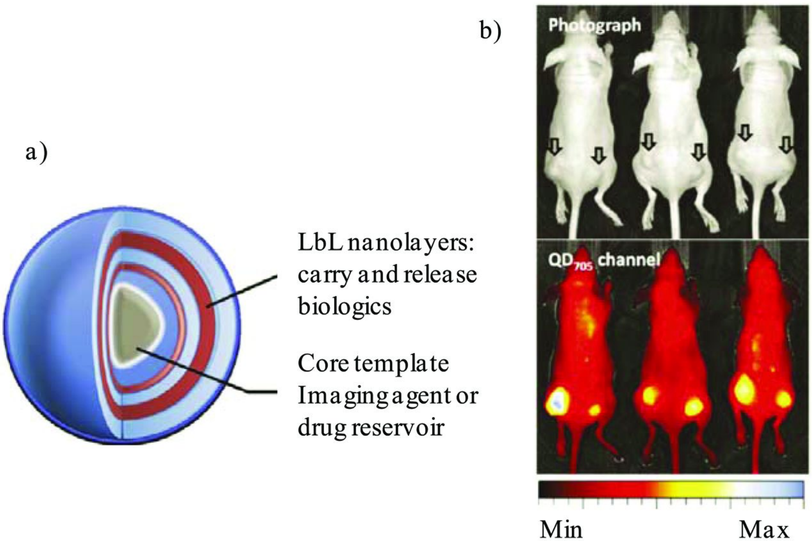
a)
LbL nanolayers: carry and release biologics
Core template Imaging agent or drug reservoir
b)
Photograph
QD705 channel
Min
Max

Figure 7. a) Schematic of a LbL-based NP delivery system. b) Fluorescence imaging of mice with KB tumors 24 hours after administering a HA coated LbL-QD. Arrows indicate locations of the tumors. (Copyright American Chemical Society. Reproduced with permission.) (see color insert)

HA Functionalized Gold NPs and Nanorods

Gold (Au) nanocomposites including nanospheres, nanorods, and nanoshells have unique optical properties. Due to their strong plasmon resonance, light absorption and scattering by such nanocomposites are strongly enhanced (*36*). Park and coworkers published an elegant study reporting the development of Au-NPs functionalized with near infrared fluorophore (NIRF) HiLyte Fluor 647 labeled HA (HHAuNPs) as ultra sensitive nanoprobes for the optical detection of reactive oxygen species (ROS) and hyaluronidase (HAdase) usually encountered in diseases such as rheumatoid arthritis (RA) and tumors (*31*). As Au-NPs have broad optical absorption, the fluorescence of the NIRF was quenched by the NP surface energy transfer (NSET) when it was attached on NPs. The fluorescence could be recovered once the HA linker was degraded by ROS or HAdase, thus releasing the NIRF from the NPs. The data collected from *in vitro* and *in vivo* experiments were promising. Activated macrophage THP-1 cells generated ROS resulting in an intense fluorescence signal when they were coincubated with

HHAuNPs. Addition of HHAuNPs to HAdase rich CD44+ cells (HCT-116 and OVCAR-3) also produced high fluorescence signals. *In vivo* fluorescence imaging of RA inflammation following systemic administration of HHAuNPs showed clearly detectable NIRF signals in arthritic joints but not in healthy ones. Similar results were observed for tumor imaging with pronounced fluorescence signals detected as early as 6 hours post injection (Figure 8). *Ex vivo* imaging of various tissues showed that HHAuNPs accumulated in the tumor more than any other organs presumably due to the EPR effect and receptor mediated endocytosis.

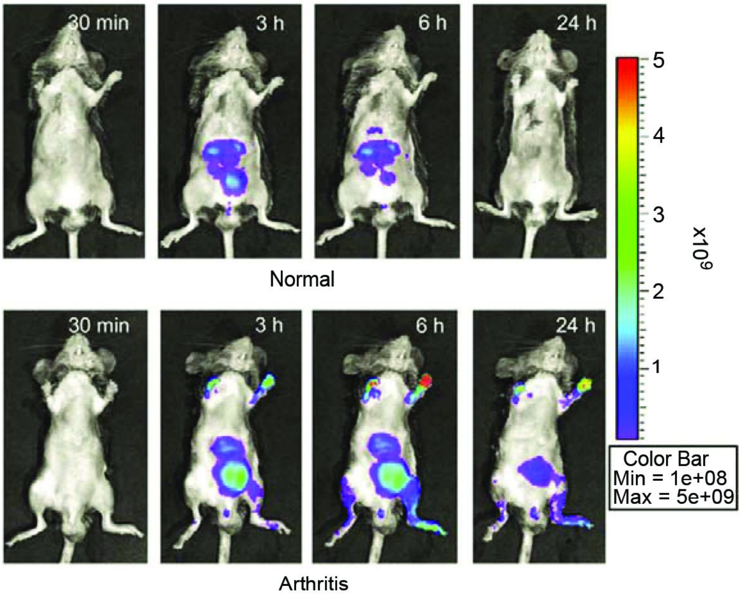

Figure 8. In vivo fluorescence images of collagen-induced RA mice upon tail vein injection of HHAuNPs in normal and arthritis mice showed significant fluorescence enhancement at diseased sites. (Copyright Elsevier. Reproduced with permission.) (see color insert)

Bioprinting is a computer aided method for LbL three dimensional (3D) deposition of cells and biomaterials to create synthetic human tissues with precise structure and architecture (*37–39*). The goal of the field is to repair and regenerate tissues and organs *in vivo*, thus providing an approach to overcome inadequate organ donor supply. Prestwich and coworkers reported an elegant study in which fibroblast cells, the “bio-ink”, and hydrogels, the “bio-paper” were printed into 3D tube-like structures using a 3D printer (*40*). In this study, the unique properties of Au-NPs, such as multivalency and thiophilicity, were exploited to crosslink thiol-modified HA and gelatin generating printable, extrudable, biocompatible, and biodegradable materials. After optimizing the mechanical properties for successful bioprinting, tubular tissue constructs were assembled using the vertical ring-stacking printing approach. The cells were cultured for four weeks during

Downloaded by OHIO STATE UNIV LIBRARIES on June 3, 2012 | http://pubs.acs.org
Publication Date (Web): December 13, 2011 | doi: 10.1021/bk-2011-1091.ch011

Downloaded by OHIO STATE UNIV LIBRARIES on June 3, 2012 | http://pubs.acs.org
Publication Date (Web): December 13, 2011 | doi: 10.1021/bk-2011-1091.ch011

which it started to produce collagen to replace the semi-synthetic extracellular matrix.

Laser soldering is a photothermal induced welding of wounds mediated by a laser activated material (solder) that can absorb laser light and convert it into heat. Near-infrared radiation (NIR) has been used in conjugation with organic dyes to weld/solder internal tissues owing to the deep penetration capability of NIR (*41*, *42*). However, this approach has been limited by the organic dye's lack of selectivity and poor solution photostability. Appreciating the excellent optical absorption and superior stability of gold nanorods (AuNR), Matteini et al. developed HA-coated AuNR that can absorb in the NIR window and tested its utility as a solder in the *in vivo* closure of a rabbit carotid artery (*43*). HA-AuNR were placed on pre-executed longitudinal incisions along the artery and subjected to NIR laser radiation. Unlike free HA that did not induce any detectable photothermal effect or wound closure, using HA-AuNR resulted in complete wound healing and full re-endothelization. HA on the NRs helped to reduce the host immune reactions to the foreign AuNR, increase the stability of the AuNR, and decrease the diffusivity of the NR thus minimizing collateral overheating. The photothermal effects can also be utilized for drug release. Wu et al. exploited silver-gold bimetallic NPs coated with PEG as a thermo-responsive polymer and HA as a targeting ligand for targeted drug delivery and imaging of cancer cells (*44*). NIR significantly enhanced the rate of drug release and the therapeutic efficacy of the drug loaded NPs.

HA-Coated Silver NPs

Silver ions (Ag^+) have long been deployed as antibacterial and antimicrobial agents (*45*). The mechanism of silver ions is not yet fully understood, but it has been reported that the positively charged silver ions bind to the negatively charged bacterial cell wall, and permeate into the cell, which would interact with thiol-bearing proteins indispensible for bacterial and microbial growth, thus inducing cell death (*46*). However, the systemic administration of silver ions to combat bacteria and viruses is concentration-restricted as it can interact with anions such as the chloride ions in the circulatory systems leading to insoluble precipitates. Silver (Ag^0) NPs arose as an alternative with potential antibacterial and antimicrobial applications against various strains especially the ones that have developed resistances against available antibiotics (*47*). The silver NPs can act as controlled Ag^+ producing machinery, where Ag^0 metal is slowly oxidized to Ag^+ ions in the presence of cellular oxidants (*48*). Interestingly, the antibacterial activity was found to be size dependent with the smaller particles bearing larger surface area to volume ratio showing the most activity (*46*).

In an attempt to synthesize "green silver NPs" (*49*, *50*) eliminating the use of conventional reducing agents such as borohydrides, Linhardt and coworkers developed HA-coated silver NPs and evaluated their anti-inflammatory and antimicrobial activities (*48*). This synthesis involved heating an aqueous solution of silver nitrate and HA. Besides acting as a stabilizing agent, as HA contains a hemiacetal moiety at its reducing end, it can reduce silver ion to Ag^0, which

Downloaded by OHIO STATE UNIV LIBRARIES on June 3, 2012 | http://pubs.acs.org
Publication Date (Web): December 13, 2011 | doi: 10.1021/bk-2011-1091.ch011

aggregates leading to silver NPs. Although the HA silver NPs had a large size distribution (5-30 nm), they exhibited high stability at physiologic salt concentrations. In an antimicrobial assay, these NPs showed high activities against *Staphylococcus aureus* [minimum inhibitory concentration (MIC)= 0.025 μM] and *Escherichia coli* [MIC= 0.1 μM]. On the other hand, the control Ag-glucose NPs and HA polymer lacked any significant activities.

Polymer Based HA-NPs

So far, we have discussed HA-NPs containing inorganic cores. HA can be conjugated to hydrophobic organic polymers including poly(lactide-co-glycolide) (PLGA) and poly(butylcyanoacrylate) (PBCA). Such amphiphilic constructs can self-assemble into NPs in aqueous media (Figure 9). Compounds such as DOX and paclitaxel (PTX) can be incorporated into these HA-NPs through either covalent ligation or the non-covalent hydrophobic-hydrophobic interactions (nanoprecipitation), thus presenting a convenient platform for drug delivery. In addition, HA-NPs could also be prepared by coupling HA to polymers such as α,β-polyaspartylhydrazide (*51*).

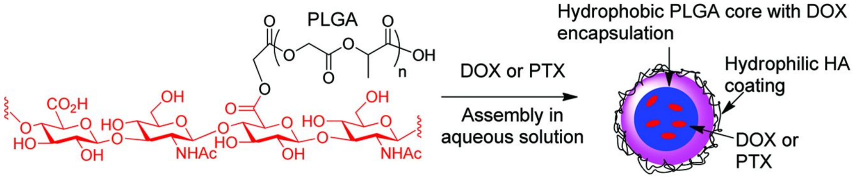
PLGA
OH
n
CO$_2$H
HO
OH
NHAc
DOX or PTX
Assembly in aqueous solution
Hydrophobic PLGA core with DOX encapsulation
Hydrophilic HA coating
DOX or PTX

Figure 9. Self assembly of PLGA grafted HA in water encapsulates hydrophobic drugs to form drug containing NPs.

Due to its high hydrophilicity, HA has poor solubility in most organic solvents hindering its direct conjugation to hydrophobic drugs. Enhancing the solubility of HA in organic solvents has been achieved by forming quaternary ammonium salts of HA (*52*, *53*). Other approaches involve reacting pre-activated hydrophobic drugs with functionalized HA polymers in a mixture of water and an organic solvent. Although this approach proved to be successful, it requires multiple activation and functionalization steps. To address these limitations, Park and coworkers employed PEG as a nano-complex forming agent by mixing HA with dimethoxy PEG (dmPEG) (*54*, *55*). The HA/dmPEG complexes could be coupled with PLGA generating HA-PLGA NPs, which then encapsulated DOX through nanoprecipitation. Alternatively, PTX could be directly conjugated with HA/dmPEG *via* formation of carboxylic esters, which then self assembled in water to form 200 nm sized micelles. Monitoring of cellular uptake of free DOX and DOX-HA-PLGA NPs by laser confocal microscopy showed that free DOX accumulated solely in the nuclei of the CD44-overexpressing HCT-116 cells, while DOX-HA-PLGA NPs appeared scattered in the cytoplasm as well as in the nuclei. When the cellular uptake was evaluated at 4 °C, only free DOX accumulated in the nuclei, with no detectable presence of DOX-HA-PLGA NPs in the cells indicating that the uptake of the NPs was mediated *via* the energy dependent endocytosis pathway. Cellular uptake of DOX-HA-PLGA was much higher than that of DOX-PLGA devoid of HA, suggesting the important roles of HA in mediating the uptake. This is further supported by the observations that the incubation of free HA together with DOX-HA-PLGA substantially reduced the uptake and the DOX-HA-PLGA NPs were 5-fold more potent than free DOX in killing HCT-116 cells. Similar to the DOX-HA-PLGA NPs, the HA-PTX micelles were more effective than PTX against the CD44 expressing cancer cells but not against the CD44 deficient cancer cells.

Hyung et al. prepared HA-coated PLGA drug carriers loaded with DOX using both the covalent and nanoprecipitation methods (*56*). Whereas the mean sizes of the NPs were comparable (~80 nm), the covalent ligation method afforded narrower size distribution, better colloidal stability, and higher amounts of HA on the surface of the NPs, which were used in further studies. 80% of total DOX was released from the HA-PLGA NPs over several weeks. Flow cytometry showed that HA-PLGA NPs were uptaken 2.5-4 folds more by the CD44-expressing MDA-MB-231 breast cancer cell line as compared to the CD44-deficient ZR-75-1 breast cancer cell line, suggesting the CD44 dependence of cellular uptake. This conclusion was further supported by cytotoxicity of the NPs. When tested against MDA-MB-231 cells, DOX-HA-PLGA NPs exhibited similar cytotoxic activities as free DOX (IC_{50} ~ 0.045 μg/mL), while the NPs were far less potent than free DOX against ZR-75-1 cells. Interestingly, the high cytotoxicity of DOX-HA-PLGA was observed only after 6 days of incubation, which was attributed to the sustained release of DOX from the NPs.

Agrawal and coworkers developed DOX loaded HA-poly(ethylene glycol)-PLGA (DOX-HA-PLGA) NPs to target tumor cells overexpressing HA receptors (*57*). The HA-PLGA amphiphilic copolymer was synthesized by reacting PEG diamine with *N*-hydroxysuccinimide (NHS)-activated PLGA to generate amine-modified PLGA-PEG, which in turn was coupled to HA using EDCI. Monomethoxy(polyethyleneglycol) (MPEG)-PLGA NPs were used as a control. The nanoprecipitation method was utilized to load DOX into HA-PEG-PLGA and MPEG-PLGA nanocarriers. The average size of the NPs varied from 100 to 200 nm depending on the amounts of polymer used, with 1:1 drug-to-polymer ratio as the optimum with high DOX entrapment efficiency. *In vivo* hematological studies were conducted to assess the safety of the nanocarriers. Neither DOX-HA-PLGA nor MPEG-PLGA NPs showed any detectable hemolytic activity on red blood cells, highlighting their hemocompatibility for drug delivery applications. The biodistribution of NPs in tissues was evaluated on Balb/C mice bearing Ehrlich ascites tumor (EAT) cells using ^{99m}Tc-labeled DOX. The ^{99m}Tc-labeled DOX-loaded HA-PLGA and MPEG-PLGA accumulated at least four folds and two folds higher, respectively, in the tumor as compared to the free DOX. However, the majority of radioactivity was detected in the liver 1 hour post injection. Disappointingly, tumor growth inhibition studies showed no statistically significant tumor size reduction in treated mice compared to control group. To improve on these results, the same group used the HA-PLGA NPs to selectively deliver 5-fluorouracil (5-FU) to tumor cells. Similar to the aforementioned DOX-HA-PLGA NPs, 5-FU-HA-PLGA-FU NPs were found to

Downloaded by OHIO STATE UNIV LIBRARIES on June 3, 2012 | http://pubs.acs.org
Publication Date (Web): December 13, 2011 | doi: 10.1021/bk-2011-1091.ch011

Downloaded by OHIO STATE UNIV LIBRARIES on June 3, 2012 | http://pubs.acs.org
Publication Date (Web): December 13, 2011 | doi: 10.1021/bk-2011-1091.ch011

be more cytotoxic to EAT cells *in vitro* and more hemocompatible than 5-FU with higher accumulation in tumor. Importantly, the 5-FU-HA-PLGA reduced the tumor volume by 19.8%, while the same dose of 5-FU caused tumor reduction of only 4.3 %.

Besides DOX and 5-FU, PTX was evaluated by the Yin group using a HA-PBCA NP system to target tumor cells *in vitro* and *in vivo* (*58*). The amphiphilic copolymer HA/PBCA (hydrophilic/hydrophobic) was constructed *via* cerium (IV) ion (Ce^{4+})-initiated radical polymerization reaction (*58*, *59*) between HA and butylcyanoacrylate (BCA) monomer. In the aqueous medium, the copolymer self-assembled into spherical NPs around 300 nm in size. Biocompatibility assays involving hemolysis and MTT cytotoxicity showed that the HA-PBCA NPs were more biocompatible and less toxic than the control PBCA NPs, which was attributed to the presence of HA chain on the surface of the PBCA NPs. Sonication of HA-PBCA NPs with PTX encapsulated the drug with 90% efficiency. The NPs released accumulatively 50-60% of the drug in PBS (pH 7.4) over 188 hours with the amount released inversely proportional to the PBCA content. After demonstrating that the HA-PBCA NPs were taken up 9.5-fold more than the plain NPs by S-180 cells, the authors evaluated the *in vivo* antitumor effect of the PTX-HA-PBCA and PTX-PBCA NPs on mice inoculated subcutaneously with S-180 tumor. The targeted PTX-HA-PBCA NPs led to an impressive 70% reduction of tumor volume. The enhanced antitumor activity of the targeted NPs was explained by the prolonged circulation of the HA-NPs in the blood and the improved uptake by tumor cells.

With its high biocompatibility, HA can be used to mask the cytotoxicity of chemotherapeutic drugs using a prodrug strategy. It is known that the concentration of HAdase can be several orders of magnitude higher in tumor sites compared to normal tissues (*60*, *61*). Thus HA functionalized prodrug can be selectively converted to the active form at diseased sites *via* HAdase mediated cleavage. Na and coworkers synthesized PEI linked all-trans retinoic acid (PRA) as a drug against P-glycoprotein (P-gp) overexpressing cancer cells (*62*). However, PEI is well known to non-selectively disrupt cell membrane resulting in cell death. To increase tumor selectivity, HA was coated on PRA complex through electrostatic interactions. The PRA-HA NPs were 143 nm in diameter with low polydispersity and good colloidal stability. The cytotoxicity of PRA-HA NPs was evaluated against HCT-8 human cancer cell line and SNU-484 human stomach cancer cell lines both of which intrinsically express P-gp. Whereas PRA was highly cytotoxic against the cells, more than 85% of the cells remained viable when incubated with PRA-HA NPs indicating the potentially low systemic toxicity. Addition of HAdase led to significantly enhanced cytotoxicity of PRA-HA NPs against the tumor cells.

In addition to drug delivery to cancer, HA-polymer NPs can be used for targeted delivery to other sites. Yenice et al. developed HA-coated poly-ε-caprolactone (PCL) nanospheres to deliver high concentrations of cyclosporine A (Cy A) into the cornea (*63*). Cy A is a neutral, hydrophobic cyclic peptide that inhibits the activation of T-helper cells by blocking the production of interleukin-2 (IL-2) cytokine. It has been used for the treatment of various ocular immune disorders such as keratoconjunctivitis and Behçet's syndrome.

The systemic administration of Cy A caused adverse side effects such as nephrotoxicity and heptatoxicity, and therapeutic levels used in the ocular tissues were limited to significantly inflamed eyes. Cy A was typically formulated with vegetable oils such as castor oil to improve its water solubility and permit topical administration. Although this formulation was non toxic, only negligible ocular penetration was observed due to the rapid clearance of castor oil from the ocular surface. The authors hypothesized that developing a nanosphere coated with mucoadhesive polymer such as HA would increase the ocular residence time of ophthalmic medications. The nanoprecipitation method was utilized to synthesize nanospheres from HA, PCL, and benzalkonium chloride (BKC), a cationic surfactant used in eye drops as a preservative. Three types of formulations, i.e., Cy A in castor oil, Cy A loaded PCL/BKC, and Cy A loaded HA/PCL/BKC NPs, were evaluated using male albino New Zealand rabbits. Following topical administration of the different formulations, the corneal Cy A concentrations of HA functionalized nanospheres were found to be 10-15-fold higher than the castor oil formulation, with the Cy A from the nanosphere cleared slower from the cornea. Thus, the HA/PCL/BKC NPs have the potential to be employed for local treatment of immune-mediated corneal diseases.

HA can improve the adhesion ability and proliferative activity of articular cells such as chondrocytes known to express CD44 on its surface (*64*). The Dellacherie group synthesized HA-coated polylactide (PLA) NPs (700 nm in size) loaded with HA or chondroitin sulfate as active molecules (*65*). The HA-coated NPs did not show toxicity against chondrocytes and synoviocytes. The uptake of the NPs was receptor mediated where NPs were found to accumulate in the cytoplasm of the cells. Gillet and coworkers published a study evaluating the toxicity of HA-coated PLA or PLGA as potential biopolymeric nanocarriers for drugs used for the treatment of RA and/or osteoarthritis (OA) (*66*). Preliminary *in vitro* and *in vivo* evaluations demonstrated that the HA-NPs were internalized by chondrocytes and synoviocytes cells without stimulating the expression of pre-inflammatory mediators such as TNF-α and IL-1β or inducing cell death. Further studies are necessary to demonstrate the beneficial use of targeted HA-loaded NPs for articular cells and arthritis treatment.

Lin et al. exploited the wound healing and angiogenic properties of HA oligomers to improve the overall performance of the naturally derived bioscafold small intestinal submucosa (SIS) in tissue regeneration (*67*). SIS has been used for tissue repair and reconstitution, however, the outcome was inconsistent. The authors hypothesized that modifying SIS with HA-coated PLGA NPs should improve its regenerative properties through enhanced angiogenesis and limit the permeability to urea allowing sustainable cell growth. The HA-PLGA-SIS NPs were spherical in shape with average diameter of 517 nm, zeta potential of +7.8 mV, and 26% HA loading efficiency. *In vitro* experiments showed that 81% of the electrostatically attached HA was released after 28 days, and the HA-PLGA NPs promoted the proliferation of endothelial cells on SIS more than the control uncoated NPs. Chicken embryo chorioallantoic membrane (CAM) vascular assay demonstrated that the HA-PLGA-SIS induced the formation of significantly more blood vessels compared to the unmodified commercial SIS or the PLGA-modified SIS (Figure 10a). This observation was supported by the data collected from an *in*

Downloaded by OHIO STATE UNIV LIBRARIES on June 3, 2012 | http://pubs.acs.org
Publication Date (Web): December 13, 2011 | doi: 10.1021/bk-2011-1091.ch011

Downloaded by OHIO STATE UNIV LIBRARIES on June 3, 2012 | http://pubs.acs.org
Publication Date (Web): December 13, 2011 | doi: 10.1021/bk-2011-1091.ch011

vivo canine bladder augmentation model, which revealed enhanced angiogenesis and better overall bladder regeneration quality (Figure 10b).

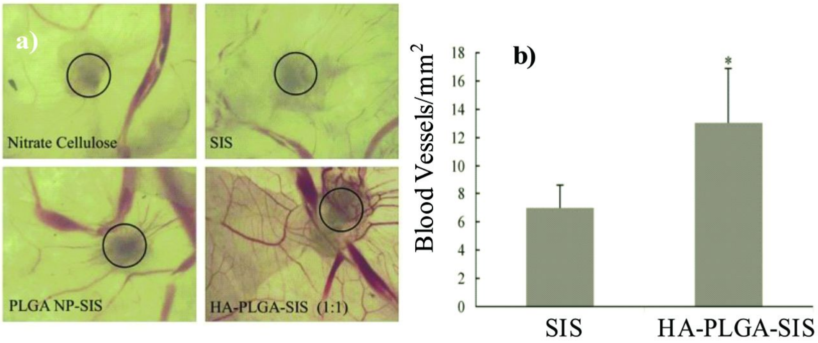

Figure 10. a) Chicken embryo CAM angiogenesis assay. Images of chicken embryo treated with nitrate cellulose, commercial SIS, PLGA-SIS, and HA-PLGA-SIS. The circles indicate where the biomaterials were implanted. b) Numbers of blood vessels with lumens in a canine bladder augmentation model treated with SIS or HA-PLGA-SIS. These results clearly suggested the superior angiogenic properties of the HA-PLGA-SIS formulation. (Copyright John Wiley and Sons. Reproduced with permission.)

Self-Assembled HA-NPs

In addition to conjugation with hydrophobic polymers, HA can be derivatized with small hydrophobic molecules to self assemble into NPs. Choi et al. published a series of reports studying NP assembly from amphiphilic HA derivatives and their potential applications in hydrophobic cancer drug delivery (*68*, *69*). The hydrophilic HA was covalently modified with the hydrophobic 5β-cholanic acid (CA) with the degree of substitution (DS) varying between 2 and 10%. Under aqueous conditions, the NPs assembled with HA exposed on the surface and CA forming the hydrophobic core for encapsulating anticancer drugs. TEM images revealed that the NPs were spherical in shape with the mean diameter varying between 237-424 nm with higher degree of substitution (DS) leading to smaller NPs. Confocal microscopy images showed that the Cy5.5-labeled HA-NPs were internalized efficiently by the CD44 expressing SCC7 cells but not by CD44-deficient CV-1 normal fibroblast cells. *In vivo* investigations demonstrated that significant amounts of HA-NPs circulated in the blood for two days and were selectively accumulated in tumor in a mouse xenograft tumor model (Figure 11). The smaller 237 nm HA-NPs were able to reach the tumor site more effectively than larger HA-NPs. An *in vivo* competitive inhibition study was carried out where the mice were pre-injected with free HA polymer prior to HA-NPs intravenous administration. The HA-NPs levels in the tumor were found to be reduced by two-fold supporting the role of HA in tumor uptake *in vivo*. PEGylation of the HA-NPs improved the percentage of the NPs reaching the tumor while reducing liver uptake (*69*).

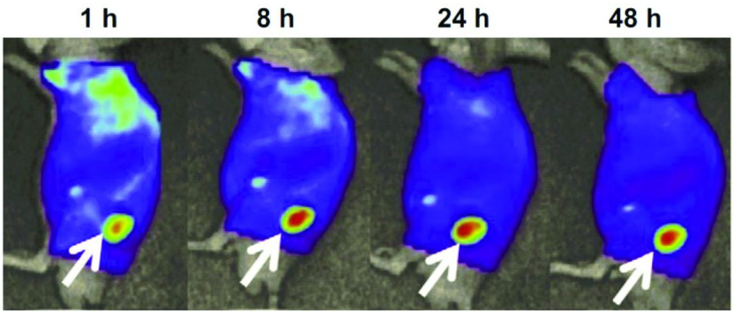

Figure 11. Time dependent in vivo whole body fluorescence imaging of a SCC7 tumor bearingmouse after injection of HA-NPs. (Copyright Elsevier. Reproduced with permission.) (see color insert)

Building on this success, the same group reported the synthesis of hydrotropic HA-NPs encapsulating PTX as the antitumor agent, and investigated their cytotoxicity *in vitro* (*70*). The authors proposed that the aqueous solubility of hydrophobic drugs should be enhanced using hydrotropic agents, such as nicotinamide-based hydrotropes as the hydrophobic chain during construction of the amphiphilic conjugates. The amine-terminated hydrotropic 2-(4-(vinylbenzyloxy)-*N*,*N*-diethylnicotinamide) oligomer (oligo(VBO-DENA)) was prepared by radical telomerization of the corresponding monomers. The HydroHA conjugate, formed by the conjugation of oligo(VBO-DENA) to HA, self-assembled in aqueous solution to generate spherical HydroHA NPs ranging in size between 274-356 nm. PTX release studies from the PTX-loaded HydroHA NPs interestingly indicated that higher loadings of PTX resulted in slower release of drug probably due to the increased hydrophobicity of the NP core. The HydroHA-PTX was taken up by SCC7 cells but very little by the CV-1 cells. The uptake profile correlated nicely with cytotoxicity data that showed a dose-dependent enhanced cytotoxic activity against SCC7 cells compared to CV-1 cells. The cytotoxicity of PTX-loaded HydroHA NPs against SCC7 was comparable to that of Cremophor-PTX, suggesting that biocompatible HydroHA NPs can potentially replace the hypersensitivity-inducing Cremophor formulation for PTX delivery.

The Xiang group linked PTX to HA using hydrophobic amino acids as linkers (valine, leucine, and phenyl alanine), resulting in an amphiphilic conjugate that self-assembled in aqueous media to form spherical NPs around 280 nm in size (*71*). The authors reported (*72*) that compared to the direct ester bond between HA and drug, the usage of an amino acid linker led to enhanced release under physiological and enzymatic conditions. *In vitro* release studies showed that PTX was released under physiological conditions (PBS, pH 7.4) with $t_{1/2}$=47-63 h, and the release rate was enhanced when HAdase was added to PBS ($t_{1/2}$ ~ 17h). Cell viability assay showed that the conjugates were more cytotoxic than free PTX, with HA-Leu-PTX showing 3-fold better activity. The authors also proved that the conjugates exerted its cytotoxic activity by arresting cell cycle at G2/M phase, which is characteristic of PTX.

Downloaded by OHIO STATE UNIV LIBRARIES on June 3, 2012 | http://pubs.acs.org
Publication Date (Web): December 13, 2011 | doi: 10.1021/bk-2011-1091.ch011

Many proteins that exhibit therapeutic potential encounter hurdles such as the short half-lives due to degradation by plasma proteases or eradication by the immune system when applied *in vivo*. One such protein is the tumor necrosis factor-related apoptosis inducing ligand (TRAIL) that binds to death receptors (DR4 and DR5) overexpressed on cancer cells, thus inducing apoptosis. The half-life of TRAIL is less than 30 minutes *in vivo*, requiring frequent redosing to maintain therapeutic levels in blood (*73*). The most common approach to prolong the half-life of proteins in circulation is through PEG ligation, which can drastically reduce the protein's therapeutic activity in addition to the generation of antibodies against PEG leading to rapid clearance of the protein from the blood (*74*). Park, Jeong and coworkers proposed that the association of the positively charged TRAIL to the negatively charged HA should protect TRAIL against enzymatic digestion and extend its systemic circulation time without affecting its biological activity (*75*). The size of the formed ionic nanoplexes was controlled by varying the feed ratio of HA/TRAIL, with higher HA ratios resulting in smaller more compact complexes. MTT cell viability assays demonstrated that TRAIL in the nanocomplexes retained its biological activity even after storage at 4 °C for 6 days, while TRAIL lost more than 90% of its bioactivity after 3 days. This is probably due to the ability of HA polymer to shield the surface of the protein and protect it against aggregation induced activity loss. The pharmacokinetic profiles of TRAIL and HA/TRAIL formulations were evaluated following subcutaneous administration in SD rats. Although native TRAIL was rapidly absorbed into blood (T_{max}= 30 minutes), the concentration returned to basal level after 3 hours. On the other hand, HA/TRAIL nanocomplexes delivered a much longer half-life in blood with a T_{max} of 7.2 hours. This was attributed to significantly delayed elimination, ensuring prolonged systemic circulation and enhanced bioavailability.

It is known that glioma cells, and not normal brian cells, express high levels of CD44 and secrete HAdase that assists in tumor invasion and metastasis (*76–79*). To target glioma cells, the Jung group developed cisplatin-incorporated HA-NPs as drug carriers (*80*). Although cisplatin has been used for the treatment of various types of tumors such as sarcomas and lymphomas, it has serious side effects such as acute nephrotoxicity and chronic neurotoxicity. To address this, HA was mixed with cisplatin resulting in NPs with 100 – 200 nm sizes and cisplatin loading efficiency between 67-81%. Drug release kinectics showed an initial burst (12 h) followed by sustained release over 4 days. Adding commercially available HAdase or HAdase secreted by U343MG human glioblastoma cells to the culture medium increased the release rate of cisplatin highlighting the importance of HAdase in enhancing the release of the drug.

The first *in vivo* study of cisplatin-HA complexes designed to examine lymphatic deposition and retention was reported by Forrest and coworkers (*81*). They aimed at targeting early breast cancer metasteses that spread to the draining lymphatic basin prior to systemic dissemination. The essence of this strategy stems from the fact that HA is primarily cleared from the body through the lymaphatic system where it is catabolized by receptor-mediated endocytosis and lysosomal degradation. Cisplatin-HA complexes with 0.25 w/w cisplatin/complex were utilized in the study. The cisplatin release half-life in

Downloaded by OHIO STATE UNIV LIBRARIES on June 3, 2012 | http://pubs.acs.org
Publication Date (Web): December 13, 2011 | doi: 10.1021/bk-2011-1091.ch011

PBS was 10 h. Free cisplatin and cisplatin-HA NP exhibited similar toxicities against the metastatic breast cancer cell lines MCF7 and MDA-MB-231 (IC_{50}= 7 µg/ml-cisplatin) indicating that the bioactivity of cisplatin was not affected upon conjuagtion to HA. Following a subcutaneous injection of cisplatin-HA into the mammary fat pad of female rats, the drug was delivered to tumor sites as well as in the draining lymph nodes of tumor (Figure 12). Whereas a burst release of free cisplatin appeared in the plasma after injection, cisplatin–HA demonstrated a longer, sustained release into the plasma suggesting this strategy can be applied to treat both loco-regional recurrence and distant metastasis. 1 out of 5 mice receiving cisplatin-HA showed complete response to treatment, with no complete responders in the group receiving cisplatin. Importantly, no significant renal or hepatic toxicities were observed in the group treated with cisplatin-HA (*82*). In contrast, animals receiving cisplatin suffered kidney damage as well as necrotizing lesions and hepatitis in the livers.

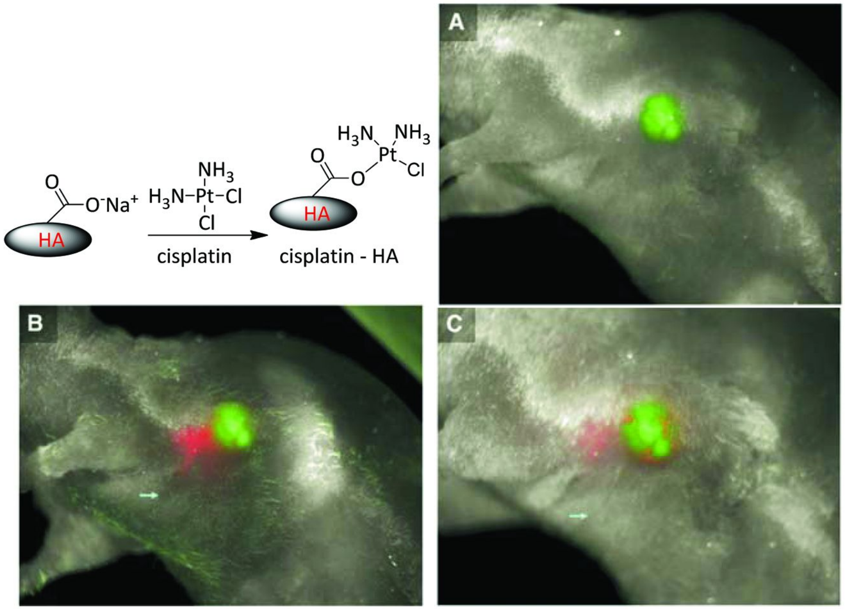

Figure 12. Formation of cisplatin-HA. A) Nude mouse bearing GFP modified MDA-MB-468 breast tumor. 5 and 18 h after injection of Texas red-HA (B and C, respectively), significant amounts of HA localized at the tumor and in the draining lymph nodes (GFP channel in green and HA in red). (Copyright Elsevier. Reproduced with permission.) (see color insert)

Small interfering RNA (siRNA) is a promising technology to selectively silence undesired genes once inside cells. However, to avoid off target side effects, it is crucial to be able to deliver siRNA to target sites and facilitate the cellular uptake of siRNA. The Park group utilized an inverse water-in-oil emulsion method to fabricate a degradable HA nanogel for target-specific intracellular delivery of siRNA (*83*). The thiol-functionalized HA polymer was crosslinked

Downloaded by OHIO STATE UNIV LIBRARIES on June 3, 2012 | http://pubs.acs.org
Publication Date (Web): December 13, 2011 | doi: 10.1021/bk-2011-1091.ch011

Downloaded by OHIO STATE UNIV LIBRARIES on June 3, 2012 | http://pubs.acs.org
Publication Date (Web): December 13, 2011 | doi: 10.1021/bk-2011-1091.ch011

through the formation of disulfide linkages upon irradiation by ultrasound waves, resulting in 200 nm sized nanogels. The anti-GFP siRNA was physically encapsulated inside the nanogels during the emulsion/crosslinking process. The release of siRNA was studied by incubating the nanogels with glutathione (GSH) at concentrations varying from 0 to 10 mM to mimic the intracellular GSH levels. With 10 mM GSH, 100% of siRNA was released in 1 hour, while minimal release was detected in the absence of GSH. The anti-GFP-siRNA/HA nanogels were effective in silencing GFP expression in CD44 expressing HCT116 cells. Adding excess amount of free HA polymer to the transfection medium resulted in decreased gene silencing efficiency. The biologically safe HA nanogels protected the siRNA from non-specific protein absorption when incubated with serum containing medium while retaining its gene silencing power.

The Huang group tested the utility of protamine-HA NPs for siRNA delivery both *in vitro* and *in vivo* (*84*). Protamine is a small arginine rich protein, which can complex with HA through electrostatic interactions and encapsulate siRNA. The surface of NPs was then modified with a PEGylated anisamide that can selectively bind to the sigma receptors over-expressed on B16F10 murine melanoma cancer cells. The size of the NP was around 115 nm, and the siRNA encapsulation efficiency was more than 90%. The *in vitro* uptake of the sigma receptor targeting NPs was 2-3 folds higher than that of control NPs without the targeting anisamide. The uptake was only modestly reduced (~25% reduction) upon co-incubation with haloperidol that binds to sigma receptors, which was possibly due to the interaction of HA in the NP with CD44 overexpressed on B16F10 cells. *In vivo* gene silencing experiments showed that the anisamide bearing NPs loaded with control siRNA and non-targeted NPs containing anti-luciferase siRNA did not affect the luciferase activity in a B16F10 mouse lung metastasis model. On the other hand, the anti-luciferase siRNA formulated in anisamide-HA-NPs silenced 80% luciferase activity. In a similar manner, the Huang group prepared protamine-HA NPs modified with tumor-targeting single chain antibody fragment (scFv) that binds with B16F10 melanoma cells (*85*). Combined siRNAs against c-Myc, MDM2 and vascular endothelial growth factor (VEGF), and a microRNA miR-34a that is known to trigger apoptosis in various cancer cells were then incorporated into these NPs. Impressively, these NPs were able to suppress tumor growth and reduce the tumor load by 80% (Figure 13). In a separate study, instead of anisamide or scFv, the Wang group explored the utility of cyclicRGD (cRGD) modified protamine-HA NPs to target the neovasculature in tumor sites (*86*). Anti growth factor antisense oligonucleotides (AMOs) were loaded into the NPs. The AMOs delivered by cRGD-LPH NPs but not the non-targeted formulation significantly reduced blood vessel growth *in vivo*.

The Hahn group explored the utility of directly targeting HA receptors on cancer cells for siRNA delivery. Nanocomplexes were formed between HA and PEI (*87*). After demonstrating that HA modification less than 25mol % did not affect HA binding with its receptors, the authors prepared siRNA/PEI-HA complex with 24% PEI, a hydrated size of 42 nm and slightly negative zeta potential. The siRNA/PEI-HA complex was less toxic to cells than the control siRNA/PEI particles probably due to the presence of the biocompatible HA that neutralizes the toxicity induced by the positively charged PEI. The antiangiogenic

In Petite and Sweet: Glyco-Nanotechnology as a Bridge to New Medicines; Huang, X., et al.;
ACS Symposium Series; American Chemical Society: Washington, DC, 2011.

Downloaded by OHIO STATE UNIV LIBRARIES on June 3, 2012 | http://pubs.acs.org
Publication Date (Web): December 13, 2011 | doi: 10.1021/bk-2011-1091.ch011

potential of antivascular endothelial growth factor siRNA (siVEGF) /PEI-HA complex was assessed for tumor treatment. Following intratumoral injection in a mouse tumor model, siVEGF/PEI-HA complex significantly suppressed tumor growth compared to the scrambled siVEFG/PEI-HA complex and the non targeted siVEGF/PEI complex (Figure 14). The levels of VEGF in the tumor tissues following NP treatment were significantly reduced, thus supporting the tumor growth suppression results.

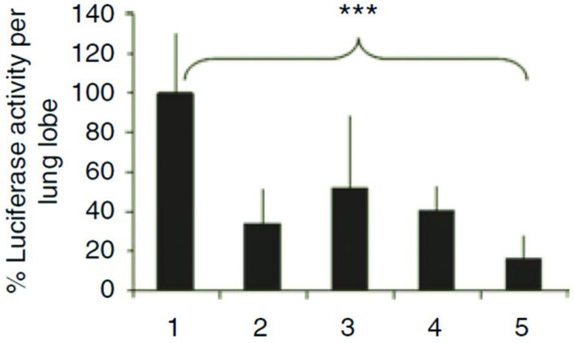

Figure 13. Growth inhibition luciferase expressing B16F10 tumor by siRNA and miRNA delivered by NPs. Formulations: untreated control (1), combined siRNAs and control miRNA in targeted NP (2), control siRNA and miR-34a in targeted NP (3), combined siRNAs and miR-34a in non-targeted control NP (4), and combined siRNAs and miR-34a in targeted NP (5). (Copyright Nature Publishing Group. Reproduced with permission.)

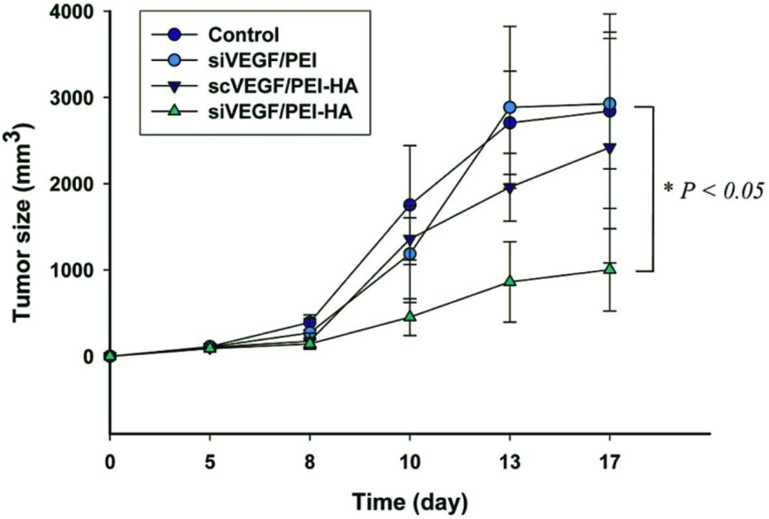

Figure 14. Tumor volume change in tumor bearing mice after intratumor injection of a control of 5% glucose solution, siVEGF/PEI complex, control siRNA (scVEGF)/PEI-HA complex, and siVEGF/PEI-HA complex. (Copyright American Chemical Society. Reproduced with permission.)

Downloaded by OHIO STATE UNIV LIBRARIES on June 3, 2012 | http://pubs.acs.org
Publication Date (Web): December 13, 2011 | doi: 10.1021/bk-2011-1091.ch011

HA-Chitosan NPs

Chitosan (CS) is a naturally existing positively charged polysaccharide, which can form NPs with HA through electrostatic interactions. Alonso and coworkers extensively explored the usage of these HA-CS NPs for gene and siRNA delivery. They loaded two model reporter gene plasmids, green fluorescent protein-encoding plasmid (pGFP) or β-galactosidase encoding plasmid, into HA-CS NPs for ocular gene therapy (*88*). The CD44-dependent uptake and transfection efficiency was evaluated on human corneal epithelial (HCE) and normal human conjunctival (IOBA-NHC) cells, both of which expressed high levels of CD44 on their surface. The transfection of pGFP was successful and the expression levels of GFP increased with higher HA content in the NPs. The uptake was shown to be through CD44 mediated endocytosis. It is important to note that the transfection efficiency is influenced by multiple factors. In addition to the amount of gene incorporated in the nanocarrier, the molecular weight of the CS and HA, pH of the cell culture experiment, and incubation time are other factors that can contribute to the overall outcome. For example, HA-CS NPs made of ultra low molecular weight CS (5 kDa) resulted in higher transfection efficiencies allowing for better DNA release from the carrier (*89*). In an analogous manner, anti-Snail 1 RNA delivered by HA-CS NP silenced the expression of the Snail 1 transcription factor, an important mediator in tumor progression (*90*).

Besides nucleic acids, the Alonso group explored the utility of HA-CS NPs to deliver heparin, which can prevent acute bronchoconstrictor response and inhibit the proliferation of smooth muscle cells. Mast cells play an important role in inflammatory events. When degranulated, the mast cells produce heparin to limit inflammation and airway remodeling (*91*, *92*). Alonso and coworkers fabricated mucoadhesive heparin-loaded HA-CS NPs for the treatment of asthma (*93*). Unfractionated and low molecular weight heparin (UFH and LMWH) were encapsulated in the NPs. *In vitro* heparin release studies revealed that only 10% of UFH was released to PBS after 12 h, compared to 80% release observed for LMWH. The authors confirmed that fluorescently labeled heparin-loaded HA-CS NPs were internalized by mast cells. This was important as heparin is thought to prevent degranulation of mast cells *via* an intracellular receptor. The ability of the heparin loaded-HA-CS NPs to prevent histamine release was assessed *ex vivo* on rat mast cells. Although a dose dependent effect was maintained, no noticeable difference between heparin solution and heparin loaded NPs was detected. However, the authors argued that, when used *in vivo*, the NP formulation would assist heparin in escaping physiological barrier in airways such as mucociliary clearance and enzymatic activity. In addition, the slow controlled release of heparin from the nanocarrier will result in prolonged antihistamine effect. In another application, the Alonso group entrapped the proangiogenic growth factors vascular endothelial growth factor (VEGF) and platelet derived growth factor (PDGF-BB) in HA-CS NPs (*94*). These NPs have potential applications in bioregenerative medicine such as tissue engineering.

Targeting colon cancer represents a challenge in cancer chemotherapy as the orally administered therapeutic agents should overcome several gastrointestinal tract (GIT) barriers such as pH variations and the premature release in the upper

Downloaded by OHIO STATE UNIV LIBRARIES on June 3, 2012 | http://pubs.acs.org
Publication Date (Web): December 13, 2011 | doi: 10.1021/bk-2011-1091.ch011

GIT (stomach and small intestine) before arriving to its target in the lower GIT (colon) (*95*). To overcome those limitations, Jain et al. encapsulated HA-CS NPs containing oxalipatin (L-OHP) in Eudragit S100-coated pellets (*96*). After validating the *in vitro* drug release profile in simulated GIT fluids, the authors conducted γ-scintigraphic study to assess the *in vivo* release pattern of the drug in Balb/c mice using ^{99m}Tc-labeled NPs. The recorded scintigraphs indicated that no ^{99m}Tc was detected in the stomach highlighting the enteric coating stability at acidic pHs. Little amounts of the tracer were released during the NP residence in the small intestine. Prominent disintegration of the pellet started upon its arrival in the ascending colon (pH 7.0) where high intensity of the tracer was clearly visible in the scintigraphs. The released radioactivity was detected in the ascending, transverse, and descending colon 15 hours post administration. In contrast to the uncoated NPs that released the tracer through the entire GIT, the pH dependent Eudragit coated NPs presented a promising tool for targeting colon diseases. In addition, the HA conjugated NPs delivered higher dose of L-OHP to tumor, delayed tumor growth and increased life span compared to free L-OHP or HA-free NPs.

Glaucoma, the leading cause of blindness in the United States, is an optic neuropathy where the optic nerve is damaged due to the increase of fluid pressure inside the eye (*97*). Conventional therapy involves using the β-adrenergic receptor blocker timolol maleate (TM) alone or in combination with the carbonic anhydrase inhibitor dorzolamide hydrochloride (DH). However, this approach does not have high therapeutic efficacy due to the poor ocular bioavailability, in addition to the cardiovascular and respiratory side effects suffered from the use of TM (*98*). Wadhwa et al. developed an HA-CS NP carrying the TM and DH for the treatment of glaucoma (*99*). The authors confirmed that enhanced permeation effect offered by CS and the extra mucoadhesiveness resulting from the binding of HA to CD44 receptors expressed on the ocular tissue. These effects increased the drugs' corneal residency time and led to multiple fold increase in drug permeation using the NPs as compared to the marketed solution formulation. Tolerance studies performed on male Albino rabbits following administration of the NPs showed no signs of discomfort, redness, mucus discharge, or corneal and conjunctival edema and hemorrhage. Glaucoma inhibition studies demonstrated considerable reduction in the intraocular pressure when CS-HA-NPs were instilled (- 9.9 mm-Hg) vs. the marketed formulation (- 5.8 mm-Hg) (*99*).

HA-Liposomes

Liposomes are artificial vesicles made of lipid bilayers. Owing to their low immunogenicity and toxicity, the Fattal group (*100*) designed liposomes coated with HA as specific delivery vehicles of nonviral vectors. HA was conjugated to a lipid moeity, L-alpha-dioleoylphosphatidyl-ethanolamine (DOPE), and inserted into the formulation during the liposome formation. The HA-coated cationic liposomes showed a positive zeta potential with a mean diameter ranging from 450 nm to 900 nm and high polydispersity index (PDI) depending on the amount of HA-DOPE conjugate introduced. Interestingly, adding pCMV-luc plasmid

DNA reorganized the lipoplexes morphology, rendering it more compact with reduced mean size and PDI. The lipoplexes protected the associated DNA against DNase I digestion by sterically hindering enzymatic access to bound DNA. Transfection was found to be more efficient against MDA-MB-231 cells (CD44 high) than MCF-7 (CD44 low). The targeted liposomes showed 7-fold increase in transfection efficiency compared to the plain liposomes, which increased further with larger amounts of HA-DOPE incorporated in the liposomes, validating the importance of HA in uptake. Preincubating the MDA-MB-231 cells with the anti-CD44 mAb Hermes-1 reduced the transfection efficiency by 70% compared to untreated cells, whereas a nonspecific anti-ErbB2 antibody had no effect on transfection. In addition, HA physically mixed with the cationic liposomes were less efficient than HA-DOPE lipoplexes highlighting the importance of the liposomal formulation.

Recently, there are increasing interests in tracking cells *in vivo* for stem cell therapy. MRI is an excellent non-invasive technique for this purpose due to its deep tissue imaging capability, superb anatomical resolution and good safety profile without the usage of ionizing radiation. Cell tracking by MRI requires labeling cells with high concentration of MRI contrast agents such as Gd^{3+}. This can be accomplished by incubating the cells with high concentrations of Gd^{3+} for long periods of time or by subjecting the cells to electroporation in the presence the Gd^{3+} salt. However, both of these methods can result in cell damage and death (*101*, *102*). Aime and coworkers reported a new method to enable rapid and efficient internalization of Gd^{3+} by CD44 expressing cells (*103*). The Gd^{3+} complex was entrapped inside cationic liposomes and HA was attached electrostatically to the surface of these liposomes generating negatively charged liposomes 175 nm in size at negative/positive charge ratio of 4:1. Evaluation of the uptake of the HA-coated liposomes by cancer cell lines with different CD44 expression levels indicated that the MRI signal enhancement was proportional to the level of receptor expression. The uptake of the targeted liposomes reached saturation typically encountered with receptor mediated endocytosis, which was 4-5 folds higher than that of the nontargeted ones.

Another important area of HA liposome applications is drug delivery to cancer cells expressing HA receptors. The Szoka group published detailed *in vitro* studies employing HA coated liposomes to target CD44-expressing tumor cells (e.g. B16F10) (*104–106*). HA oligomers rather than high molecular weight HA polymer were selected in constructing the liposomes. This was due to the consideration that minimum required length of HA to bind with CD44 was a hexamer, while HARE in liver interacts with longer HA. Using HA oligosaccharides long enough to bind to CD44 but too short to significantly interact with HARE could lead to a carrier with reduced elimination by liver while maintaining the desired binding with CD44 expressing cells (*107*). DOX was encapsulated in the targeted HA-liposomes (HA-DOX) as well as the nontargeted control liposomes without HA. The two types of liposomes displayed similar mean diameters (~130 nm) and zeta potential (~ -10 mV). The cellular uptake of HA liposomes by B16F10 cells was critically dependent on the density of HA, with higher densities resulting in enhanced cellular association. The uptake of HA liposomes by B16F10 was dose- and temperature-dependent, exhibiting a

Downloaded by OHIO STATE UNIV LIBRARIES on June 3, 2012 | http://pubs.acs.org
Publication Date (Web): December 13, 2011 | doi: 10.1021/bk-2011-1091.ch011

Downloaded by OHIO STATE UNIV LIBRARIES on June 3, 2012 | http://pubs.acs.org
Publication Date (Web): December 13, 2011 | doi: 10.1021/bk-2011-1091.ch011

saturation binding profile characteristic of specific binding. Co-incubation with excess free HA, pre-incubation with anti-CD44 antibody, and low temperature (4 °C) reduced the uptake and cytotoxicity of HA-DOX liposomes but not that of the control liposomes. The HA-DOX liposomes were about 9 folds more potent against B16F10 as compared to free DOX in a transient-exposure protocol.

Instead of using cultured tumor cells, the Peer group targeted primary head and neck cancer with the cancerous cells and the adjacent normal cells obtained directly from patients (*108*). This serves as a better mimic of *in vivo* cell behavior compared to cell culture, as culturing and passaging cells can lead to artificial transformations to cells. Although both cancer and normal cells expressed similar levels of CD44 on its surface, the authors showed that mitomycin C (MMC) loaded HA liposomes bound significantly only to cancerous cells. The binding profile correlated well with cell viability results, where the MMC-HA liposomes were cytotoxic against the cancerous cells with no effects on normal cells. These findings were significant as it demonstrated that not all CD44 expressed on cell surface bind HA. This can be due to either post-translational modification of CD44 as discussed earlier and/or the existence of different splicing variants on cancer cells vs normal cells.

These promising *in vitro* results bode well for *in vivo* studies. The Maraglit group published an elegant evaluation of the therapeutic effect of MMC loaded HA-coated liposomes *in vitro* and *in vivo* (*109*). High molecular weight HA polymer was anchored covalently to the surface of amine functionalized liposomes. The authors expected that the HA polymer offered higher binding affinity to CD44 and would promote longer systemic circulation times due to its hydrophilic nature. The targeted HA liposomes (tHA-LIP) and the nontargeted ones (nt-LIP) were 75 and 55 nm in diameter with MMC encapsulation levels of 38% and 53% respectively. Confocal microscopy demonstrated that FITC-labeled tHA-LIP bound to the surface of cancer cells, while no significant fluorescence was detected upon incubation with the control NPs. While MMC-free nt-LIP and tHA-LIP were not toxic against six cancer cell lines, MMC-tHA-LIP exhibited 50-200-fold increase in cytotoxic activity against CD44 expressing cells compared to free MMC. *In vivo* subacute toxicity studies showed that the MMC-tHA-LIPs were better tolerated than free MMC with less body weight loss. Furthermore, tHA-LIP formulation significantly prolonged the circulation of MMC in blood. Drug biodistribution was determined in healthy and B16F10.9 tumor bearing mice. Interestingly, although liver cells have HA receptors, HA coating of the liposomes decreased accumulation of MMC-tHA-LIP in the liver by 40% as compared to free MMC. The MMC-tHA-LIP accumulated in lung tumors 4-fold and 30-fold more than MMC-nt-LIP and free MMC, whereas negligible amounts of any drug was detected in the lungs of healthy animals. MMC-tHA-LIP was much more effective in a mouse lung tumor metastasis model, where significant increase in mouse survival and reduction in tumor burden were observed in the treatment group (Figure 15). The authors also tested the encapsulation of DOX using the tHA-LIP formulation (*110*). The results from potency evaluation in syngeneic and human xenograft mouse models mirrored those observed in the MMC-tHA-LIP studies demonstrating the generality of this approach.

Downloaded by OHIO STATE UNIV LIBRARIES on June 3, 2012 | http://pubs.acs.org
Publication Date (Web): December 13, 2011 | doi: 10.1021/bk-2011-1091.ch011

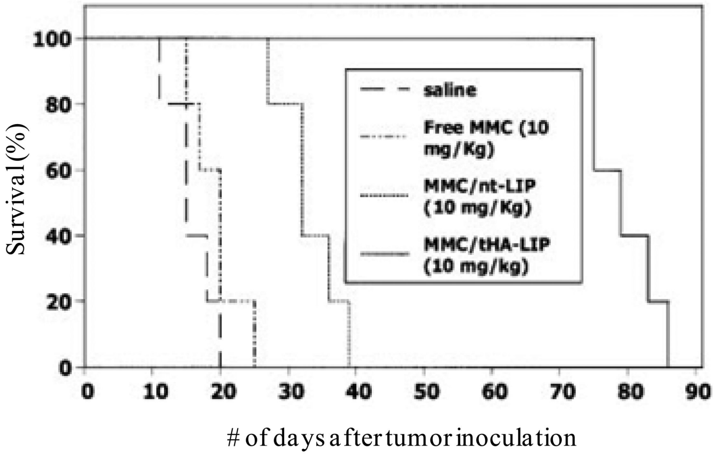

Figure 15. Survival of mice bearing B16F10.9 metastatic melanoma after administerin g saline, free MMC, MMC encapsulated non-targeted NP (MMC/nt-LIP) and MMC encapsulated HA-NP (MMC/tHA-LIP). Mice receiving MMC/tHA-LIP showed significantly enhanced survival. (Copyright John Wiley and Sons. Reproduced with permission.)

Peer, Margalit and coworkers prepared NP-like PTX clusters coated with HA for selective tumor targeting (*111*). Lipid molecules were allowed to self-assemble in the presence of PTX yielding clusters to which HA was covalently attached (PTX-HA) (Figure 16a). PTX-HA NPs were 300 nm in diameter with PTX encapsulation efficiency approaching 100%. Encapsulating PTX in HA-liposomes did not alter the cytotoxicity of the drug in cell viability assays. Unlike PTX encapsulated in Cremophor®EL (PTX-Cre, FDA approved formulation) which has serious side effects, PTX-HA liposomes were much more biocompatible as it did not cause liver damage or significant weight loss, or induce interferon or pro-inflammatory cytokine responses. In an *in vivo* tumor model, PTX-HA enabled longer systemic circulation compared to PTX-Cre resulting in 10-fold higher PTX accumulation in the tumor with concomitant decrease of PTX concentrations in liver and spleen. The therapeutic efficacy measured by tumor regression after administering PTX-HA was higher than not only PTX-Cre, but also Abraxane, a liposomal formulation used in the clinic for passive tumor targeting (Figure 16b). This highlights the advantage of active targeting of receptors expressed on tumor for drug delivery.

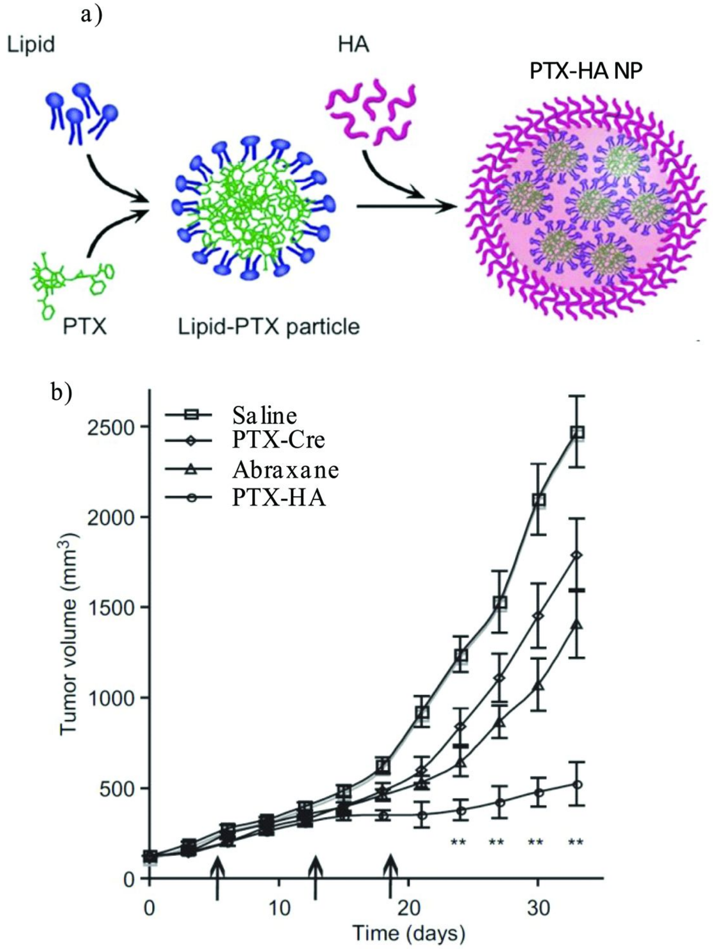

Figure 16. a) Schematic demonstration of PTX-HA NP assembly. b) Volume of tumor in mice bearing CT-26 tumor after administering saline, PTX-Cre, Abraxane and PTX-HA at the equivalent dose of PTX. Mice receiving PTX-HA showed significantly reduced tumor volume. Three injections of therapeutics were given as indicated by arrows. (Copyright Elsevier. Reproduced with permission.) (see color insert)

Future Outlook and Conclusions

In this review, we summarized the recent development of HA nanomaterials, from magnetic nanoparticle, gold nanoparticles, silver nanoparticles, quantum dots, to polymer nanoparticles, self-assembled organic based nanoparticles and liposomes. As a targeting ligand, HA has been exploited to achieve selective accumulation of therapeutic and diagnostic entities in diseased areas overexpressing HA receptors. As a carrier, HA assembles into biologically safe nanoconstructs that can encapsulate hydrophobic drugs and protect

Downloaded by OHIO STATE UNIV LIBRARIES on June 3, 2012 | http://pubs.acs.org
Publication Date (Web): December 13, 2011 | doi: 10.1021/bk-2011-1091.ch011

fragile moieties such as nucleic acids. Due to its high hydrophilicity and biocompatibility, HA helps to enhance aqueous solubility of hydrophobic drugs, change the biodistribution and reduce the toxicities of therapeutic compounds. The nanocarriers provide a powerful and versatile platform that can accommodate multiple cargos within one carrier system, enabling multi-functional applications.

Whereas the merits of using HA nanomaterials have been established, several aspects in constructing such materials have to be addressed. As there are no universal designs, the structure, composition and the core of the nanomaterials need to be tailored to suit each specific biological application. The size, shape, surface coating, as well as surface charge of nanomaterials all play important roles in determining their circulation time, final destination, binding to the receptors, and cellular uptake by cells. Another important issue is the selectivity of HA binding. HA receptors such as CD44 are expressed on many cell types, not just limited to inflammatory cells or malignant cells. However, as having been demonstrated already, not all CD44 receptors bind HA equally. This would require further study and understanding of CD44 structures and regulation factors to selectively target CD44 in diseased sites and avoid those expressed in normal tissues. Furthermore, besides CD44, there are multiple types of HA receptors, in particular HARE expressed in liver. It is important to minimize liver uptake of HA nanomaterials to avoid liver toxicity if liver is not the targeted site. This has been explored by taking advantage of the differential binding preference towards various length of HA as well as other glycosaminoglycans such as chondroitin sulfate (*31*). Further improvement in this area will perhaps come from designing more specific HA analogs with much enhanced CD44 affinities. The availability of the co-crystal structures of CD44 and a HA octasaccharide (*112*) can provide the critical insights guiding such studies.

In closing, during the past decade, many interesting applications of HA nanomaterials have emerged for a variety of biological applications from tissue engineering, molecular imaging to targeted drug delivery. In the future, we expect that the intense interests HA associated nanomaterials will continue. We are looking forward to many innovative applications of this fascinating class of structures.

Downloaded by OHIO STATE UNIV LIBRARIES on June 3, 2012 | http://pubs.acs.org
Publication Date (Web): December 13, 2011 | doi: 10.1021/bk-2011-1091.ch011

References

1. Toole, B. P.; Ghatak, S.; Misra, S. *Curr. Pharm. Biotechnol.* **2008**, *9*, 249–252.
2. Raman, R.; Sasisekharan, V.; Sasisekharan, R. *Chem. Biol.* **2005**, *12*, 267–277.
3. Lapcik, L., Jr.; Lapcik, L.; De Smedt, S.; Demeester, J.; Chabrecek, P. *Chem. Rev.* **1998**, *98*, 2663–2683.
4. Misra, S.; Heldin, P.; Hascall, V. C.; Karamanos, N. K.; Skandalis, S. S.; Markwald, R. R.; Ghatak, S. *FEBS J.* **2011**, *278*, 1429–1443.
5. Gaffney, J.; Matou-Nasri, S.; Grau-Olivares, M.; Slevin, M. *Mol. BioSyst.* **2010**, *6*, 437–443.
6. Day, A. J.; Prestwich, G. D. *J. Biol. Chem.* **2002**, *277*, 4585–4588.

7. Delcommenne, M.; Kannagi, R.; Johnson, P. *Glycobiology* **2002**, *12*, 613–622.
8. Maiti, A.; Maki, G.; Johnson, P. *Science* **1998**, *282*, 941–943.
9. Tammi, R.; MacCallum, D.; Hascall, V. C.; Pienimäki, J. P.; Hyttinen, M.; Tammi, M. *J. Biol. Chem.* **1998**, *273*, 28878–28888.
10. For a recent review on the applications of HA nanomaterial in cancer research, see Ossipov, D. A. *Expert Opin. Drug Delivery* **2010**, *7*, 681−703.
11. Oh, E. J.; Park, K.; Kim, K. S.; Kim, J.; Yang, J.-A.; Kong, J.-H.; Lee, M. Y.; Hoffman, A. S.; Hahn, S. K. *J. Controlled Release* **2010**, *141*, 2–12.
12. El-Boubbou, K.; Zhu, D. C.; Vasileiou, C.; Borhan, B.; Prosperi, D.; Li, W.; Huang, X. *J. Am. Chem. Soc.* **2010**, *132*, 4490–4499.
13. Jun, Y.-w.; Lee, J.-H.; Cheon, J. *Angew. Chem., Int. Ed.* **2008**, *47*, 5122–5135.
14. Yu, M. K.; Jeong, Y. Y.; Park, J.; Park, S.; Kim, J. W.; Min, J. J.; Kim, K.; Jon, S. *Angew. Chem., Int. Ed.* **2008**, *47*, 5362–5365.
15. Chung, H.-J.; Lee, H.-S.; Bae, K. H.; Lee, Y.-H.; Park, J.-N.; Cho, S.-W.; Hwang, J.-Y.; Park, H.-W.; Langer, R.; Anderson, D.; Park, T.-G. *ACS Nano* **2011**, *5*, 4329–4336.
16. El-Boubbou, K.; Gruden, C.; Huang, X. *J. Am. Chem. Soc.* **2007**, *129*, 13392–13393.
17. Corot, C.; Robert, P.; Idee, J.-M.; Port, M. *Adv. Drug Delivery Rev.* **2006**, *58*, 1471–1504.
18. Lawaczeck, R.; Menzel, M.; Pietsch, H. *Appl. Organomet. Chem.* **2004**, *18*, 506–513.
19. Cuff, C. A.; Kothapalli, D.; Azonobi, I.; Chun, S.; Zhang, Y.; Belkin, R.; Yeh, C.; Secreto, A.; Assoian, R. K.; Rader, D. J.; Pure, E. *J. Controlled Release* **2001**, *108*, 1031–1040.
20. DeGrendele, H. C.; Estess, P.; Picker, L. J.; Siegelman, M. H. *J. Exp. Med.* **1996**, *183*, 1119–1130.
21. Kamat, M.; El-Boubbou, K.; Zhu, D. C.; Lansdell, T.; Lu, X.; Li, W.; Huang, X. *Bioconjugate Chem.* **2010**, *21*, 2128–2135.
22. Lee, Y.; Lee, H.; Kim, Y. B.; Kim, J.; Hyeon, T.; Park, H.; Messersmith, P. B.; Park, T. G. *Adv. Mater.* **2008**, *20*, 4154–4157.
23. Kumar, A.; Sahoo, B.; Montpetit, A.; Behera, S.; Lockey, R. F.; Mohapatra, S. S. *Nanomedicine* **2007**, *3*, 132–137.
24. El-Dakdouki, M. H.; Zhu, D. C.; El-Boubbou, K.; Kamat, M.; Chen, J.; Li, W.; Huang, X. **2011**, submitted.
25. Chan, W. C. W.; Nie, S. *Science* **1998**, *281*, 2016–2018.
26. Gao, X.; Cui, Y.; Levenson, R. M.; Chung, L. W. K.; Nie, S. *Nat. Biotechnol.* **2004**, *22*, 969–976.
27. Bhang, S. H.; Won, N.; Lee, T.-J.; Jin, H.; Nam, J.; Park, J.; Chung, H.; Park, H.-S.; Sung, Y.-E.; Hahn Sei, K.; Kim, B.-S.; Kim, S. *ACS Nano* **2009**, *3*, 1389–1398.
28. Kim, J.; Park, K.; Hahn, S. K. *Int. J. Biol. Macrom.* **2008**, *42*, 41–45.
29. Kim, K. S.; Hur, W.; Park, S.-J.; Hong, S. W.; Choi, J. E.; Goh, E. J.; Yoon, S. K.; Hahn, S. K. *ACS Nano* **2010**, *4*, 3005–3014.
30. Maeda, H. *Bioconjugate Chem.* **2010**, *21*, 797–802.

Downloaded by OHIO STATE UNIV LIBRARIES on June 3, 2012 | http://pubs.acs.org
Publication Date (Web): December 13, 2011 | doi: 10.1021/bk-2011-1091.ch011

Downloaded by OHIO STATE UNIV LIBRARIES on June 3, 2012 | http://pubs.acs.org
Publication Date (Web): December 13, 2011 | doi: 10.1021/bk-2011-1091.ch011

31. Lee, H.; Lee, K.; Kim, I. K.; Park, T. G. *Biomaterials* **2008**, *29*, 4709–4718.
32. Srivastava, S.; Kotov, N. A. *Acc. Chem. Res.* **2008**, *41*, 1831–1841.
33. Boyer, C.; Bousquet, A.; Rondolo, J.; Whittaker, M. R.; Stenzel, M. H.; Davis, T. P. *Macromolecules* **2010**, *43*, 3775–3784.
34. Lee, M.-Y.; Park, S.-J.; Park, K.; Kim, K. S.; Lee, H.; Hahn, S. K. *ACS Nano* **2011**in press.
35. Poon, Z.; Lee, J. B.; Morton, S. W.; Hammond, P. T. *Nano Lett.* **2011**, *11*, 2096–2103.
36. Eustis, S.; El-Sayed, M. A. *Chem. Soc. Rev.* **2006**, *35*, 209–217.
37. Mironov, V.; Visconti, R. P.; Kasyanov, V.; Forgacs, G.; Drake, C. J.; Markwald, R. R. *Biomaterials* **2009**, *30*, 2164–2174.
38. Mironov, V.; Reis, N.; Derby, B. *Tissue Eng.* **2006**, *12*, 631–634.
39. Jakab, K.; Norotte, C.; Marga, F.; Murphy, K.; Vunjak-Novakovic, G.; Forgacs, G. *Biofabrication* **2010**, *2*, 022001.
40. Skardal, A.; Zhang, J.; McCoard, L.; Oottamasathien, S.; Prestwich, G. D. *Adv. Mater.* **2010**, *22*, 4736–4740.
41. DeCoste, S. D.; Farinelli, W.; Flotte, T.; Anderson, R. R. *Lasers Surg. Med.* **1992**, *12*, 25–32.
42. Rossi, F.; Pini, R.; Menabuoni, L.; Mencucci, R.; Menchini, U.; Ambrosini, S.; Vannelli, G. *J. Biomed. Opt.* **2005**, *10*, 024004.
43. Matteini, P.; Ratto, F.; Rossi, F.; Rossi, G.; Esposito, G.; Puca, A.; Albanese, A.; Maira, G.; Pini, R. *J. Biomed. Opt.* **2010**, *15*, 041508/1–041508/6.
44. Wu, W.; Shen, J.; Banerjee, P.; Zhou, S. *Biomaterials* **2010**, *31*, 7555–7566.
45. Rai, M.; Yadav, A.; Gade, A. *Biotechnol. Adv.* **2009**, *27*, 76–83.
46. Baker, C.; Pradhan, A.; Pakstis, L.; Pochan, D. J.; Shah, S. I. *J. Nanosci. Nanotechnol.* **2005**, *5*, 244–249.
47. Lara, H. H.; Ayala-Nunez, N. V.; Ixtepan Turrent, L. d. C.; Rodriguez Padilla, C. *World J. Microbiol. Biotechnol.*, *26*, 615–621.
48. Kemp, M. M.; Kumar, A.; Clement, D.; Ajayan, P.; Mousa, S.; Linhardt, R. J. *Nanomedicine* **2009**, *4*, 421–429.
49. Raveendran, P.; Fu, J.; Wallen, S. L. *J. Am. Chem. Soc.* **2003**, *125*, 13940–13941.
50. Huang, H.; Yang, X. *Carbohydr. Res.* **2004**, *339*, 2627–2631.
51. Pitarresi, G.; Craparo, E. F.; Palumbo, F. S.; Carlisi, B.; Giammona, G. *Biomacromolecules* **2007**, *8*, 1890–1898.
52. Luo, Y.; Prestwich, G. D. *Bioconjugate Chem.* **1999**, *10*, 755–763.
53. Zhang, M.; James, S. P. *Polymer* **2005**, *46*, 3639–3648.
54. Lee, H.; Ahn, C.-H.; Park, T. G. *Macromol. Biosci.* **2009**, *9*, 336–342.
55. Lee, H.; Lee, K.; Park, T. G. *Bioconjugate Chem.* **2008**, *19*, 1319–1325.
56. Hyung, W.; Ko, H.; Park, J.; Lim, E.; Park, S. B.; Park, Y.-J.; Yoon, H. G.; Suh, J. S.; Haam, S.; Huh, Y.-M. *Biotechnol. Bioeng.* **2007**, *99*, 442–454.
57. Yadav, A. K.; Mishra, P.; Mishra, A. K.; Mishra, P.; Jain, S.; Agrawal, G. P. *Nanomedicine* **2007**, *3*, 246–257.
58. He, M.; Zhao, Z.; Yin, L.; Tang, C.; Yin, C. *Int. J. Pharm.* **2009**, *373*, 165–173.

59. Yilmaz, E.; Adali, T.; Yilmaz, O.; Bengisu, M. *React. Funct. Polym.* **2007**, *67*, 10–18.
60. Lokeschwar, V. B.; Rubinowicz, d.; Schroeder, G. L.; Forgacsi, E.; Minnai, J. D.; Block, N. L.; Nadji, M.; Lokeshwar, B. L. *J. Biol. Chem.* **2001**, *276*, 11922–11932.
61. Liu, D.; Pearlman, E.; Diaconu, E.; Guo, K.; Mori, H.; Haqqi, T.; Markowitz, S.; Willson, J.; Sy, M.-S. *Proc. Natl. Acad. Sci. U.S.A.* **1996**, *93*, 7832–7837.
62. Yim, H.; Na, K. *Biomacromolecules* **2010**, *11*, 2387–2393.
63. Yenice, I.; Mocan, M. C.; Palaska, E.; Bochot, A.; Bilensoy, E.; Vural, I.; Irkec, M.; Hincal, A. A. *Exp. Eye Res.* **2008**, *87*, 162–167.
64. Patti, A. M.; Gabriele, A.; Vulcano, A.; Ramieri, M. T.; Della, R. C. *Tissue Cell* **2001**, *33*, 294–300.
65. Laroui, H.; Grossin, L.; Leonard, M.; Stoltz, J.-F.; Gillet, P.; Netter, P.; Dellacherie, E. *Biomacromolecules* **2007**, *8*, 3879–3885.
66. Zille, H.; Paquet, J.; Henrionnet, C.; Scala-Bertola, J.; Leonard, M.; Six Jean, L.; Deschamp, F.; Netter, P.; Verges, J.; Gillet, P.; Grossin, L. *Biomed. Mater. Eng.* **2010**, *20*, 235–242.
67. Mondalek, F. G.; Ashley, R. A.; Roth, C. C.; Kibar, Y.; Shakir, N.; Ihnat, M. A.; Fung, K.-M.; Grady, B. P.; Kropp, B. P.; Lin, H.-K. *J. Biomed. Mater. Res.* **2010**, *94*, 712–719.
68. Choi, K. Y.; Chung, H.; Min, K. H.; Yoon, H. Y.; Kim, K.; Park, J. H.; Kwon, I. C.; Jeong, S. Y. *Biomaterials* **2010**, *31*, 106–114.
69. Choi, K. Y.; Min, K. H.; Yoon, H. Y.; Kim, K.; Park, J. H.; Kwon, I. C.; Choi, K.; Jeong, S. Y. *Biomaterials* **2011**, *32*, 1880–1889.
70. Saravanakumar, G.; Choi, K. Y.; Yoon, H. Y.; Kim, K.; Park, J. H.; Kwon, I. C.; Park, K. *Int. J. Pharm.* **2010**, *394*, 154–161.
71. Xin, D.; Wang, Y.; Xiang, J. *Pharm. Res.* **2009**, *27*, 380–389.
72. Wang, Y.; Xin, D.; Liu, K.; Xiang, J. *Pharm. Res.* **2009**, *26*, 785–793.
73. Kelley, S. K.; Harris, L. A.; Xie, D.; Deforge, L.; Totpal, K.; Bussiere, J.; Fox, J. A. *J. Pharmacol. Exp. Ther.* **2001**, *299*, 31–38.
74. Ganson, N. J.; Kelly, S. J.; Scarlett, E.; Sundy, J. S.; Hershfield, M. S. *Arthritis Res. Ther.* **2006**, *8*, R12.
75. Na, S. J.; Chae, S. Y.; Lee, S.; Park, K.; Kim, K.; Park, J. H.; Kwon, I. C.; Jeong, S. Y.; Lee, K. C. *Int. J. Pharm.* **2008**, *363*, 149–154.
76. Delpech, B.; Laquerriere, A.; Maingonnat, C.; Bertrand, P.; Freger, P. *Anticancer Res.* **2002**, *22*, 2423–2427.
77. Junker, N.; Latini, S.; Petersen, L. N.; Kristjansen, P. E. G. *Oncol. Rep.* **2003**, *10*, 609–616.
78. Nakagawa, T.; Kubota, T.; Kabuto, M.; Kodera, T. *Anticancer Res.* **1996**, *16*, 2917–2922.
79. Koochekpour, S.; Pilkington, G. J.; Merzak, A. *Int. J. Cancer* **1995**, *63*, 450–454.
80. Jeong, Y.-I.; Kim, S.-T.; Jin, S.-G.; Ryu, H.-H.; Jin, Y.-H.; Jung, T.-Y.; Kim, I.-Y.; Jung, S. *J. Pharm. Sci.* **2008**, *97*, 1268–1276.
81. Cohen, M. S.; Cai, S.; Xie, Y.; Forrest, M. L. *Am. J. Surg.* **2009**, *198*, 781–786.

Downloaded by OHIO STATE UNIV LIBRARIES on June 3, 2012 | http://pubs.acs.org
Publication Date (Web): December 13, 2011 | doi: 10.1021/bk-2011-1091.ch011

82. Cai, S.; Xie, Y.; Bagby, T. R.; Cohen, M. S.; Forrest, M. L. *J. Surg. Res.* **2008**, *147*, 247–252.
83. Lee, H.; Mok, H.; Lee, S.; Oh, Y.-K.; Park, T. G. *J. Controlled Release* **2007**, *119*, 245–252.
84. Chono, S.; Li, S.-D.; Conwell, C. C.; Huang, L. *J. Controlled Release* **2008**, *131*, 64–69.
85. Chen, Y.; Zhu, X.; Zhang, X.; Liu, B.; Huang, L. *Mol. Ther.* **2010**, *18*, 1650–1656.
86. Liu, X.-Q.; Song, W.-J.; Sun, T.-M.; Zhang, P.-Z.; Wang, J. *Mol. Pharmaceutics* **2011**, *8*, 250–259.
87. Jiang, G.; Park, K.; Kim, J.; Kim, K. S.; Hahn, S. K. *Mol. Pharmaceutics* **2009**, *6*, 727–737.
88. de la Fuente, M.; Seijo, B.; Alonso, M. J. *Invest. Ophthalmol. Visual Sci.* **2008**, *49*, 2016–2024.
89. Duceppe, N.; Tabrizian, M. *Biomaterials* **2009**, *30*, 2625–2631.
90. Ravina, M.; Cubillo, E.; Olmeda, D.; Novoa-Carballal, R.; Fernandez-Megia, E.; Riguera, R.; Sanchez, A.; Cano, A.; Alonso, M. J. *Pharm. Res.* **2010**, *27*, 2544–2555.
91. Ahmed, T.; Ungo, J.; Zhou, M.; Campo, C. *J. Appl. Physiol.* **2000**, *88*, 1721–1729.
92. Ragazzi, E.; Chinellato, A. *Gen. Pharmacol.* **1995**, *26*, 697–701.
93. Oyarzun-Ampuero, F. A.; Brea, J.; Loza, M. I.; Torres, D.; Alonso, M. J. *Int. J. Pharm.* **2009**, *381*, 122–129.
94. Parajo, Y.; d'Angelo, I.; Welle, A.; Garcia-Fuentes, M.; Alonso, M. J. *Drug Delivery* **2010**, *17*, 596–604.
95. Ciftci, K.; Groves, M. J. *Int. J. Pharm.* **1996**, *145*, 157–164.
96. Jain, A.; Jain, S. K.; Ganesh, N.; Barve, J.; Beg, A. M. *Nanomedicine* **2010**, *6*, 179–190.
97. Morrison, J. C.; Johnson, E. C.; Cepurna, W.; Jia, L. *Prog. Retinal Eye Res.* **2005**, *24*, 217–240.
98. Sacca, S. C.; La Maestra, S.; Micale, R. T.; Larghero, P.; Travaini, G.; Baluce, B.; Izzotti, A. *Arch. Ophthalmol.* **2011**, *129*, 48–55.
99. Wadhwa, S.; Paliwal, R.; Paliwal, S. R.; Vyas, S. P. *J. Drug Targeting* **2010**, *18*, 292–302.
100. Surace, C.; Arpicco, S.; Dufay-Wojcicki, A.; Marsaud, V.; Bouclier, C.; Clay, D.; Cattel, L.; Renoir, J.-M.; Fattal, E. *Mol. Pharmaceutics* **2009**, *6*, 1062–1073.
101. Crich, S. G.; Biancone, L.; Cantaluppi, V.; Duo, D.; Esposito, G.; Russo, S.; Camusi, G.; Aime, S. *Magn. Reson. Med.* **2004**, *51*, 938–944.
102. Stacey, K. J.; Ross, I. L.; Hume, D. A. *Immunol. Cell Biol.* **1993**, *71*, 75–85.
103. Esposito, G.; Crich, S. G.; Aime, S. *ChemMedChem* **2008**, *3*, 1858–1862.
104. Eliaz, R. E.; Nir, S.; Szoka, F. C., Jr. *Methods Enzymol.* **2004**, *387*, 16–33.
105. Eliaz, R. E.; Nir, S.; Marty, C.; Szoka, F. C., Jr. *Cancer Res.* **2004**, *64*, 711–718.
106. Eliaz, R. E.; Szoka, F. C., Jr. *Cancer Res.* **2001**, *61*, 2592–2601.
107. Platt, V. M.; Szoka, F. C., Jr. *Mol. Pharmaceutics* **2008**, *5*, 474–486.

Downloaded by OHIO STATE UNIV LIBRARIES on June 3, 2012 | http://pubs.acs.org
Publication Date (Web): December 13, 2011 | doi: 10.1021/bk-2011-1091.ch011

108. Bachar, G.; Cohen, K.; Hod, R.; Feinmesser, R.; Mizrachi, A.; Shpitzer, T.; Katz, O.; Peer, D. *Biomaterials* **2011**, *32*, 4840–4848.
109. Peer, D.; Margalit, R. *Int. J. Cancer* **2004**, *108*, 780–789.
110. Peer, D.; Margalit, R. *Neoplasia* **2004**, *6*, 343–353.
111. Rivkin, I.; Cohen, K.; Koffler, J.; Melikhov, D.; Peer, D.; Margalit, R. *Biomaterials* **2010**, *31*, 7106–7114.
112. Banerji, S.; Wright, A. J.; Noble, M.; Mahoney, D. J.; Campbell, I. D.; Day, A. J.; Jackson, D. G. *Nat. Struct. Mol. Biol.* **2007**, *14*, 234–239.

Downloaded by OHIO STATE UNIV LIBRARIES on June 3, 2012 | http://pubs.acs.org
Publication Date (Web): December 13, 2011 | doi: 10.1021/bk-2011-1091.ch011

Subject Index

A

Adamantane-polyethylene glycol (AD-PEG), 170
α-D-Mannosyl [60]fullerenols, synthesis, 3
AD-PEG. *See* Adamantane-polyethylene glycol (AD-PEG)
AES. *See* Auger electron spectroscopies (AES)
AFM. *See* Atomic force microscopy (AFM)
α-GalNAc. *See* α-*N*-Acetylgalactosamine (α-GalNAc)
α-*N*-Acetylgalactosamine (α-GalNAc), 5
Aneurinibacillus thermoaerophilus, 31
ANP. *See* Atrial natriuretic peptide (ANP)
Antitumor therapeutic strategies
  drug delivery and therapy, 168
  imaging and radio-sensitization, 166
  immunotherapy and vaccines, 171
  nanotechnology, 164
  overview, 161
  sugars, 164
  tumors, 164
ASF. *See* Asialofetuin (ASF)
ASGP-R. *See* Asialoglycoprotein receptor (ASGP-R)
Asialofetuin (ASF), 21
Asialoglycoprotein receptor (ASGP-R), 25
Asparagine, 6
Atomic force microscopy (AFM), 57, 113
Atrial natriuretic peptide (ANP), 185
AT&T Bell Laboratories, 106
Auger electron spectroscopies (AES), 113
Au nano-dots (AuND), 17
AuND. *See* Au nano-dots (AuND)
AuNP. *See* Gold nanoparticles (AuNP)

B

Bacillus anthracis, 135
  high-resolution SEM image, 136*f*
Bacterial adhesion, 97
  inhibitors, 99*f*
BCBDBA. *See* *N*-(8-((+)-Biotinamido)-3,6-dioxaoctyl)-2-((2-phenyl-1-thioxo) thio)-4- cyano-pentanoate (BCBDBA)
Benzalkonium chloride (BKC), 194
Benzoyl (Bz) group, 6
B16F10.9 metastatic melanoma, 206*f*
B16F10 tumor, 201*f*
BKC. *See* Benzalkonium chloride (BKC)
Bovine serum albumin (BSA), 113
Brust-Schiffrin protocol, 41
BSA. *See* Bovine serum albumin (BSA)
B-Slt. *See* Shiga-like toxin (B-Slt)
Buckminsterfullerene, 2
Bz. *See* Benzoyl (Bz) group

C

CALA-01, 170*f*
Cancer cell
  biology, 164
  nano-therapeutic intervention, 165*t*
Carbohydrates, 38
  active enzymes, 32
  approaches to photocoupling using PFPA, 56*f*
  biological recognition, 50
  carbohydrate interactions, 38
  chemoselective reactions on nanoparticle surfaces, 43
  different linker lengths, 59*f*
  direct conjugation of underivatized, 59, 61*f*
  exploited on QD surfaces, 109
  formation of oximes, 42
    nucleophilic catalysis, 42*f*
  functional analysis, 38
  libraries, 149
  ligands for targeting, 107
  macromolecular interactions, 165
  magnetic nanoparticles via amide and click coupling, 55*f*
  microarrays produced with PFPA-coupled carbohydrate structures, 58*f*
  nanoparticle surface, 38
  PFPA conjugates, 57
  presenting surfaces based on PFPA-coupling, 59*f*
  protein interactions, 38
  reaction with reducing, 45
  reductive amination chemistry, 41
  representation of the hierarchy complexity, 110*s*
Carbon-based nanomaterials, 2
Carbon nanotubes (CNT), 2, 3
  non-covalent modification, 4
CD. *See* Cyclodextrins (CD)

Downloaded by 89.163.35.42 on June 2, 2012 | http://pubs.acs.org
Publication Date (Web): December 13, 2011 | doi: 10.1021/bk-2011-1091.ix002

Downloaded by 89.163.35.42 on June 2, 2012 | http://pubs.acs.org
Publication Date (Web): December 13, 2011 | doi: 10.1021/bk-2011-1091.ix002

CD44. *See* Cluster of differentiation 44 (CD44)
Cell trafficking, 25
Cetyltrimethylammonium bromide (CTAB), 184
Chagas' disease, 144
Chemoselectivity
  carbohydrates on nanoparticle surfaces, 43
  conjugation of carbohydrates to thiol-terminated linkers, 39
  hydrazide formation on the surface of gold nanoparticles, 46*f*
  nanoparticle surfaces via reductive amination, 45*f*
  o-glycosides, 40
  overview, 37
  oxime formation with heterobifunctional linker, 43*f*
  oxime formation with reducing carbohydrates on aminooxy-functionalized nanoparticles, 45*f*
  reaction of glycans, 41
  reducing carbohydrates, 40
    synthesis of mercaptoethylamine-terminated carbohydrates, 41*f*
  synthesis of glyconanoparticles at surface, 44*f*
  thiol-terminated neo-glycoconjugates from O-allyl glycosides via thiol-ene coupling, 40*f*
Chicken embryo, CAM angiogenesis assay, 196*f*
Chitosan, general structures, 169*f*
Cholera toxin, 96
  CTB, 10
  inhibitors, 97*f*
1,2-*cis*-Glycosylation, 147
Cluster of differentiation 44 (CD44), 181
CMP-sialic acid synthetase (CSS), 29
  MNP activity affected by immobilization method, 31*f*
CNT. *See* Carbon nanotubes (CNT)
Colorimetric assays, 17
Computed tomography (CT), 166
Con A. *See* Concanavalin A (Con A)
Concanavalin A (Con A), 17, 95
  multivalent inhibitors, 95*f*
Covalent conjugation, 53
  thiolated carbohydrates onto gold nanoparticles, 54*f*
cRGD. *See* CyclicRGD (cRGD)
CSS. *See* CMP-sialic acid synthetase (CSS)
CT. *See* Computed tomography (CT)
CTAB. *See* Cetyltrimethylammonium bromide (CTAB)
CuAAC. *See* Cu(I)-catalyzed azide-alkyne cycloaddition (CuAAC)
Cu(I)-catalyzed azide-alkyne cycloaddition (CuAAC), 3
CV-N. *See* Cyanovirin-N (CV-N)
Cyanovirin-N (CV-N), 60
CyclicRGD (cRGD), 200
Cyclodextrins (CD), 170
  general structures, 169*f*

D

DD. *See* Degrees of deacetylation (DD)
Degree of substitution (DS), 196
Degrees of deacetylation (DD), 169
Dendrimers, 100
Dendritic glycoligands, 91
D-Glucose oximes, ring-chain tautomeric equilibria, 41*f*
Diels-Alder reaction, 29
1,3-Dipolar cycloaddition strategies, 4
DLS. *See* Dynamic light scattering (DLS)
DN. *See* Dopamine (DN)
DNA hybridization, 49
DO3A. *See* Tetraazacyclododecane triacetic acid (DO3A)
Dopamine (DN), 184
DOPED. *See* L-alpha-Dioleoylphosphatidyl-ethanolamine (DOPE)
DOX. *See* Doxorubicin (DOX)
Doxorubicin (DOX), 185
DS. *See* Degree of substitution (DS)
Dynamic light scattering (DLS), 113

E

E. coli O157:H7, SEM images of Gal-SWNTs, 5, 6*f*
E. coli strain ORN178, 24*f*
EIS. *See* Electrochemical impedance spectroscopy (EIS)
Electrochemical impedance spectroscopy (EIS), 21
ELISA. *See* Enzyme linked immunosorbent assays (ELISA)
Enhanced Permeability and Retention (EPR), 164
Enzymatic sialylation
  mucin tetrasaccharide fragment, 149*s*
  trans-sialidase, 148
    substrates, 149
Enzyme linked immunosorbent assays (ELISA), 185

Downloaded by 89.163.35.42 on June 2, 2012 | http://pubs.acs.org
Publication Date (Web): December 13, 2011 | doi: 10.1021/bk-2011-1091.ix002

EPR. *See* Enhanced Permeability and Retention (EPR)
E-selectin, 148
Euler's theorem, 2

F

FBS. *See* Fetal Bovine Serum (FBS)
f-CNT. *See* Functionalized CNTs (f-CNT)
FET. *See* Fetuin (FET)
Fetal Bovine Serum (FBS), 183
Fetuin (FET), 21
Fluorescent silica NP (FSNP), 61
Fourier transform infrared spectroscopy (FTIR), 73
  iron oxide@gold nanoparticles, 74*f*
FSNP. *See* Fluorescent silica NP (FSNP)
FTIR. *See* Fourier transform infrared spectroscopy (FTIR)
[60]Fullerene, 3
  reaction mechanism of Prato reaction, 5*f*
Functionalized CNTs (f-CNT), 4

G

Galactose-binding agglutinin (PNA), 21
Gal_2-N_3, structure, 86*f*
Gal_2 SWNT
  H NMR spectra, 130*f*
  optical absorption spectra, 134*f*
  SEM images, 133*f*
Gal_4 SWNT
  H NMR spectra, 131*f*
  optical absorption spectra, 134*f*
GlcNAc. *See* *N*-Acetylglucosamine (GlcNAc)
Glucose/maltose/maltotriose, 20*f*
Glycans
  library used in SPR imaging studies with siglecs, 153*t*
  scaffolds coupled, 50
  sequences, 15
Glyco-CNT, 5
Glyco-conjugates, 2
Glycodendrimer microarray, 100, 100*f*
Glyco-functionalization, 109
  bioconjugation methods, 111
  quantum dots, 111, 112*t*
    organic shell, 114*s*
Glyco-magnetic nanoparticles, 8
Glyconanomaterial fabrication, 50
Glyco-nanomaterials
  carbon-based nanomaterials, 2
  overview, 1
  recent development, 2
Glyconanoparticles (glyco-NP)
  based mucin mimetics, 151
  bio-imaging through the use of fluorescence microscopy, 27*f*
  carbohydrate-based MRI nanoprobes, 26
  cell targeting, 22
  defined, 15
  explore cell-based expression of lectins, 155
  imaging, 22
  MRI imaging, 27*f*
  protein detection, 17
  separation, 22
  sialic acid-derived thiol, 155*f*
  thiol-terminated glycoconjugates by in situ reduction, 39*f*
Glycopolymers conjugation, gold glyconanoparticles and subsequent formation of DNA complexes, 52*f*
Glycoproteins, 6
Glyco-QD
  application, 116, 116*f*
  characterization, 113
  magnetic nanoparticles via biotin-streptavidin interactions, 52*f*
Glycosides, methods utilizing pre-modified, 44
Glyco-SWNT, synthesis, 7*f*
Glycosylation, 15
GM. *See* Guest materials (GM)
Gold nanoparticles (AuNP), 9
  analyte-induced colorimetric change, 151*f*
  MUC4 glycopeptide vaccine particle design, 174*f*
  potential antitumor vaccines, 172*f*
  TF antigen, 174*f*
Gold-plated quartz crystals, 58*f*
Guest materials (GM), 7

H

HA. *See* Hyaluronic acid (HA)
HAdase. *See* Hyaluronidase (HAdase)
HARE. *See* HA receptor for endocytosis (HARE)
HA receptor for endocytosis (HARE), 181
Hepatoma cells (HepG2), 187
HepG2. *See* Hepatoma cells (HepG2)
High-resolution magic angle spinning (HRMAS) NMR spectroscopy, 81

Downloaded by 89.163.35.42 on June 2, 2012 | http://pubs.acs.org
Publication Date (Web): December 13, 2011 | doi: 10.1021/bk-2011-1091.ix002

  - MNP3 in D_2O, 84*f*
  - solution spectra of an organic compound, 83*f*
- HOMO-LUMO promotion, 106
- Host lectins, 152
- Hot injection, 8
- HRMAS. *See* High-resolution magic angle spinning (HRMAS) NMR spectroscopy
- Hyaluronic acid (HA), 181
  - catechol functionalized, 185*f*
  - chitosan NPs, 202
  - coated iron oxide NPs, 183
    - in vitro applications, 186
  - coated silver NPs, 191
  - formation of cisplatin, 199*f*
  - functionalized gold NPs and nanorods, 189
  - liposomes, 203
  - overview, 181
  - polymer based, 192
  - PTX assembly, 207*f*
  - quantum dots, 186, 187*f*
  - self assembly of PLGA grafted, 192*f*
  - self-assembled NPs, 196
  - synthesis of nanomaterials, 182, 183*f*
  - Xiang group linked PTX, 197
- Hyaluronidase (HAdase), 189
- HydroHA conjugate, 197
- Hydrolysis, oximes, 42

L

- Lac. *See* Lactose (Lac)
- Lactose Au-NP, aggregation-dispersion behavior, 19*f*
- Lactose (Lac), 10
- L-alpha-Dioleoylphosphatidyl-ethanolamine (DOPE), 203
- Laser soldering, 191
- Layer-by-layer (LbL), 188
  - bioprinting method, 190
  - NP delivery system, 189*f*
- LbL. *See* Layer-by-layer (LbL)
- Localized surface plasmon resonance (LSPR), 9
- LSPR. *See* Localized surface plasmon resonance (LSPR)
- Lymphatic vessel endothelial HA receptor (LYVE-1), 181
- LYVE-1. *See* Lymphatic vessel endothelial HA receptor (LYVE-1)

M

- Magnetic nanoparticles (MNP), 8
  - schematic demonstration of pathogen, 24*f*
  - tetrasaccharide sialyl-Lewis X (sLe^X)-functionalized, 9
    - in vitro binding studies, 9*f*
- Magnetic resonance imaging (MRI), 8
- MALDI mass spectroscopy, 78
  - chemical glycosylation onto the surface of gold nanoparticles, 79*f*
- Mannose groups, scanometric strategy for in situ detection, 23*f*
- Man-SWNT, high-resolution SEM image, 136*f*
- Man$_2$ SWNT, optical absorption spectra, 134*f*
- Man$_4$ SWNT, optical absorption spectra, 134*f*
- Microfluidic cell sorting system, 25*f*
- Mitomycin C (MMC), 205
- MMC. *See* Mitomycin C (MMC)
- MNP. *See* Magnetic nanoparticles (MNP)
- Monosaccharide-functionalized nanotube samples, 136
- MRI. *See* Magnetic resonance imaging (MRI)
- Mucin tetrasaccharide synthesis, 148*f*
- Multi-walled carbon nanotubes (MWCNT), 3
- MWCNT. *See* Multi-walled carbon nanotubes (MWCNT)

N

- *N*-Acetylglucosamine (GlcNAc), 6
- Nanoparticle
  - biocompatibility based on data, 163*f*
  - physical characteristics, 70
- Nanotechnology, 164
  - sugars, 164
  - tumors, 164
- Nanotechnology Characterization Laboratory (NCL), 162
- Native chemical ligation (NCL), 29
- *N*-(8-((+)-Biotinamido)-3,6-dioxaoctyl)-2-((2-phenyl-1-thioxo) thio)-4-cyano-pentanoate (BCBDBA), 21
- NCL. *See* Nanotechnology Characterization Laboratory (NCL); Native chemical ligation (NCL)
- Near infrared fluorophore (NIRF), 189
- *Neisseria gonorrhoeae*, 31

Downloaded by 89.163.35.42 on June 2, 2012 | http://pubs.acs.org
Publication Date (Web): December 13, 2011 | doi: 10.1021/bk-2011-1091.ix002

NIRF. *See* Near infrared fluorophore (NIRF)
NMR. *See* Nuclear Magnetic Resonance (NMR) spectroscopy
Non-covalent conjugation, 51, 51*f*
Novel nanotechnology platforms, 162
NP surface energy transfer (NSET), 189
NSET. *See* NP surface energy transfer (NSET)
Nuclear Magnetic Resonance (NMR) spectroscopy, 79
  maltose coated gold nanoparticles, 80*f*
  sugar linked throught an hydrophobic spacer, 81*f*
Nuclear magnetic resonance spectroscopy (NMR), 113

O

O-Glycosides, 40
Oligosaccharides, 70

P

PAHO. *See* Pan American Health Organization (PAHO)
Pan American Health Organization (PAHO), 144
Pasteurella multocida, 31
PCB. *See* Printed circuit board (PCB) electrodes
PDI. *See* Polydispersity index (PDI)
Perfluorophenyl azide (PFPA), 19, 50
  dye-doped silica nanoparticles, 63*f*
  functionalization of AuNP, 20*f*
  phosphate-containing, 24
  photoconjugation techniques, 50
  preparation of magnetic glyconanoparticle, 63*f*
PFPA. *See* Perfluorophenyl azide (PFPA)
Phenylazide photochemistry, 56*f*
Photo-initiated coupling chemistry
  methods and application, 55
  overview, 49
  synthetic methods to glyconanomaterials, 51
PNA. *See* Galactose-binding agglutinin (PNA)
Polydispersity index (PDI), 203
Polyhydroxylated fullerenes, 3
Prato reaction, 4
  [60]fullerene, 5*f*
Printed circuit board (PCB) electrodes, 21
Protamine, 200
Protein carbohydrate interactions
  bacterial adhesion, 97
  cholera toxin, 96
  ConA, 95
  glycodendrimer microarray, 100
  overview, 91
  WGA, 93
Protein immobilization, 30*f*
Pseudomonas aeruginosa, 97

Q

QCM. *See* Quartz crystal microbalance (QCM)
QD. *See* Quantum dots (QD)
Quantum dots (QD), 16
  application, 105
  bound with biotin containing glycopolymer, 113*f*
  carbohydrates exploited, 109
  Cd-based, 106
  coated with surfaces, 107
  emission maxima and sizes, 108*f*
  glyco-functionalization, 111, 112*t*
    organic shell, 114*s*
  history, 105
  hyaluronic acid, 186, 187*f*
  properties, 105
  semiconductor crystals, 106
  synthesis, 105
  types of surface modifications, 109*s*
  UV-Vis and fluorescence spectroscopies, 115
Quartz crystal microbalance (QCM), 21, 57

R

RAFT. *See* Reversible addition-fragmentation chain transfer (RAFT)
Raman spectroscopy, 74
  glucosamine conjugated on the surface of silver nanoparticles, 75*f*
Reactive oxygen species (ROS), 189
Receptor for hyaluronan-mediated motility (RHAMM), 181
Regioselective β-galactosylation, 146, 147*s*
RES. *See* Reticuloendothelial system (RES)
Reticuloendothelial system (RES), 8
Reversible addition-fragmentation chain transfer (RAFT), 21

RHAMM. *See* Receptor for hyaluronan-mediated motility (RHAMM)
ROS. *See* Reactive oxygen species (ROS)

S

Saccharidic moiety in composite nanoparticles
  MALDI mass spectroscopy, 78
  nuclear magnetic resonance spectroscopy, 79
  overview, 69
  thermogravimetry, 75
  UV-vis spectroscopy, 71
  vibrational spectroscopies, 73
  X-ray photoelectron spectroscopy, 76
SCC7 tumor, 197*f*
SCM. *See* S-Cyanomethyl (SCM)
S-cyanomethyl (SCM), 26
SERS. *See* Surface enhanced Raman scattering (SERS)
Shiga-like toxin (B-Slt), 20
Sialic acid-binding agglutinin (SNA), 21
Sialic acid recognition, 152
Single walled nanotubes (SWNT), 85
Single-walled carbon nanotubes (SWCNT), 3
siRNA. *See* Small interfering RNA (siRNA)
SIS. *See* Small intestinal submucosa (SIS)
Small interfering RNA (siRNA), 199
Small intestinal submucosa (SIS), 195
SNA. *See* Sialic acid-binding agglutinin (SNA)
Solid-phase synthesis, mucin glycopeptides fragment, 150*s*
SPR. *See* Surface plasmon resonance (SPR)
SPRi. *See* Surface plasmon resonance imaging (SPRi)
Staphylococcus aureus, 29
Stereoselective α-GlcNAc-ylation, 146
  synthesis, 146
Sugar-functionalized carbon nanotubes
  bioapplications, 134
  characterization, 128
  composition samples and related parameters, 132*t*
  functionalized with Gal, Man, or their dendrons, 127*s*
  overview, 124, 125
  properties, 128
  visual comparison on aqueous dispersions of Gal_2 MWNT and Gal-MWNT, 128*f*
Sugar molecule
  SWNTs functionalized with various configurations, 138*t*
  synthesis via emulsion (dispersion) polymerization for polymeric nanoparticles, 137*s*
Sugar nucleotide synthesis, immobilized enzymes in, 29*f*
Surface enhanced Raman scattering (SERS), 74
Surface plasmon resonance imaging (SPRi), 59, 152
Surface plasmon resonance (SPR), 17
  responses after injection, 21*f*
SWCNT. *See* Single-walled carbon nanotubes (SWCNT)
SWNT. *See* Single walled nanotubes (SWNT)
Synthetic mucin glycopeptides, 150

T

TACA. *See* Tumor-associated carbohydrate antigens (TACA)
TEM. *See* Transmission electron microscopy (TEM)
Tetraazacyclododecane triacetic acid (DO3A), 26
TGA. *See* Thermogravimetry (TGA)
Thermogravimetry (TGA), 75
  Fe_3O_4 nanoparticles, 76*f*
THP-1 cells
  confocal microscopy images of LPS, 186*f*
  MR images, 184*f*
TIBA. *See* 2,3,5-Triiodobenzoic acid (TIBA)
TIBz. *See* 2,3,5-Triiodobenzoyl (TIBz) groups
TOPO. *See* Trioctylphosphine oxide (TOPO)
TRAIL. *See* Tumor necrosis factor-related apoptosis inducing ligand (TRAIL)
Transmission electron microscopy (TEM), 10, 17, 113
  Mal-AuNP and Man-AuNP with Con A, 18*f*
2,3,5-Triiodobenzoic acid (TIBA), 6
2,3,5-Triiodobenzoyl (TIBz) groups, 6
Trioctylphosphine oxide (TOPO), 106
Trypanosoma cruzi

Downloaded by 89.163.35.42 on June 2, 2012 | http://pubs.acs.org
Publication Date (Web): December 13, 2011 | doi: 10.1021/bk-2011-1091.ix002

Downloaded by 89.163.35.42 on June 2, 2012 | http://pubs.acs.org
Publication Date (Web): December 13, 2011 | doi: 10.1021/bk-2011-1091.ix002

  mucin glycan mimetics used to generate lyconanoparticles, 152*f*
  mucin *O*-glycans, 144
  nature, 145
  overview, 144
  strain mucin glycopeptide fragment, 145*f*
TSG6. *See* Tumor necrosis factor-stimulated gene-6 protein (TSG6)
Tumor necrosis factor-related apoptosis inducing ligand (TRAIL), 198
Tumor necrosis factor-stimulated gene-6 protein (TSG6), 181
Tumor-associated carbohydrate antigens (TACA), 164

U

UEA-I. *See Ulex europaeus* lectin I (UEA-I)
Ulex europaeus lectin I (UEA-I), 57
UV-vis spectroscopy, 71
  functionalization of core-shell AuNP, 72*f*

V

VAA. *See Viscum album* agglutinin (VAA)
Vascular endothelial growth factor (VEGF), 200
VEGF. *See* Vascular endothelial growth factor (VEGF)
Vibrational spectroscopies, 73
Viscum album agglutinin (VAA), 57

W

WGA. *See* Wheat germ agglutinin (WGA)
Wheat germ agglutinin (WGA), 53, 93
  structures of ligands, 94*f*

X

XPS. *See* X-ray Photoelectron Spectroscopy (XPS)
X-ray diffraction (XRD), 113
X-ray Photoelectron Spectroscopy (XPS), 59, 76, 113
  polymer coated gold nanoparticles, 77*f*
X-rays, AuNP, 166*f*
XRD. *See* X-ray diffraction (XRD)